THÈSE

En vue de l'obtention du

DOCTORAT DE L'UNIVERSITÉ DE TOULOUSE

Délivré par :

Université Toulouse III Paul Sabatier (UT3 Paul Sabatier)

Présentée et soutenue par :

M. CHANGLONG WANG

Vendredi 15 Septembre 2017

Nanomatériaux à base de métaux de transition pour la catalyse

---

ED SDM : Chimie moléculaire - CO 046

Unité de recherche

Laboratoire de Chimie de Coordination - CNRS - UPR 8241

Directeurs de thèse

Lionel SALMON et Didier ASTRUC

Membres du jury:

M. Jean-Marie BASSET	Professeur, Directeur du Centre de Catalyse, KAUST	Rapporteur
M. Jean-René HAMON	Directeur de Recherche au CNRS, RENNES	Rapporteur
M. Christophe DERAEDT	Chercheur à l'Université de Californie à Berkeley	Examinateur
Mme Montserrat GÓMEZ	Professeur à l'Université Paul Sabatier	Examinateur
M. Azzedine BOUSSEKSOU	Directeur CNRS, Directeur du LCC	Membre invité
M. Lionel SALMON	Directeur de Recherche au CNRS	Directeur de thèse
M. Didier ASTRUC	Professeur à l'Université de Bordeaux	CoDirecteur de thèse

Acknowledgement

This thesis was completed in the **Institute des Sciences Moléculaires** (ISM), UMR CNRS N° 5255, University of Bordeaux and **Laboratoire de Chimie de Coordination** (LCC) UPR CNRS N° 8241, Université Toulouse III - Paul Sabatier.

I would like to express my sincerest gratitude to my supervisors **Prof. Didier Astruc** and **Dr. Lionel Salmon** for their supports over the last four years, for supervising me and letting me take one more step towards my life long goal of becoming "a real scientist". In particular, I am very grateful of having **Prof. Didier Astruc** as my thesis director for his inspiring, patient instruction, insightful criticism and expert guidance on my thesis. He has taught me, both consciously and un-consciously, how to be a good chemist. His profound knowledge of chemistry, consistent and illuminating instructions, and his contributions of time and ideas, making my Ph.D. experience productive and stimulating.

I would like to warmly thank **Dr. Azzedine Bousseksou**, a prestigious scientist, for his precious administrative and scientific help that have greatly facilitated this thesis.

I am also greatly indebted to the two reporters for the thesis, Professor **Jean-Marie Basset** from King Abdullah University of Science & Technology (KAUST), and Dr. **Jean-René Hamon** from the Université de Rennes I, and to the jury president Professor **Montserrat Gómez** from the Université Toulouse III - Paul Sabatier and to Dr. **Christophe Deraedt** from the University of California at Berkeley for their time and energy in serving as referees and examinators of the PhD and for helpful discussions.

I am also deeply grateful to the engineer of our research group, **Dr. Jaime Ruiz**, for his patient guidance on experiment operations and helpful discussions. High tribute shall be paid to **Sergio Moya**, **Danijela Gregurec, Joseba Irigoyen**, **Luis Yate** and

Jimena Tuninetti for their excellent collaborations and analyses on samples.

My sincere gratitude also go to my former and current colleagues, including **Yanlan Wang**, **Amalia Rapakousiou**, **Haibin Gu**, **Dong Wang**, **Na Li**, **Sylvain Gatard**, **Roberto Ciganda**, **Xiang Liu**, **Fangyu Fu** and **Qi Wang**, who kindly gave me invaluable advises and help to solve various problems in both study and life.

Last but not the least, my gratitude also extends to my family who have been assisting, supporting and caring for me all of my life. Special thanks should also go to all my friends who give me continuous support and encouragement during my thesis.

Table of Content

General Introduction……...……1

Chapter 1. Overview on Metal Catalyzed Alkyne–Azide Cycloaddition and Recent Trend……...…….7

Chapter 2. An Amphiphilic Ligand for The Stabilization of Efficient Transition Metal Nanocatalysts in Aqueous Solution …….....29

2.1 Introduction……...…….……30
2.2 The design and applications of amphiphilic ligand for highly efficient transition metal nanoparticle catalysts in aqueous solutions.....32
2.3 From mono to tris-1,2,3-triazole-stabilized gold nanoparticles and their compared catalytic efficiency in 4-nitrophenol reduction……..……122
2.4 Design and applications of an efficient amphiphilic "click" Cu^{I} catalyst in water……...……..152

Chapter 3. Efficient Heterogeneous Nanoparticles Catalysts Based on Graphene Supports……...…….201

3.1 Introduction…….……202
3.2 RhAg/rGO nanocatalyst: ligand-controlled synthesis and superior catalytic performances for the reduction of 4-nitrophenol……...……204
3.3 Efficient parts-per-million *a*-Fe_2O_3 nanocluster/graphene oxide catalyst for Suzuki–Miyaura coupling reactions and 4-nitrophenol reduction in aqueous solution……...……239
3.4 Synthesis and high catalytic efficiency of transition-metal nanoparticle-graphene oxide nanocomposites……..……259

Chapter 4. Metal Organic Framworks Stabilize Efficient Non-noble Metal Nanoparticles Catalysis……...…….321

4.1 Introduction…… ……..……322
4.2 Hydrolysis of ammonia-borane over Ni/ZIF-8 nanocatalyst: high efficiency, ion effect and controlled hydrogen release. ……..……..……324

Conclusions and Perspective……...383

List of Published or Submitted Thesis Publications…….387

General introduction

Nanoscience and nanotechnology involve studying and working with matter on an ultrasmall scale and deal with the exploration, characterization and application of nanostructured materials. This area has undergone great prosperity and has become an emerging field of research for which significant studies have revolutionized the nanosystems.[1] Promises and possibilities are wide-ranging; for instance, nanomachines will transform modern medicine to the search for cancer cells or to deliver drugs.[2] Nanomaterials have stimulated great interest in optical, electrical, and mechanical applications, and among them nanocatalysts[3] have opened new routes for drug developments, clean energy conversion, environmental decontamination and green chemistry for fine chemical production.

Homogeneous catalysts are usually solubilized in the reaction media and are very efficient, selective, and industrially useful, but they suffer from lack of recovery, reusability and limited thermal stability.[4] On the other hand, heterogeneous catalysts benefit from easy recovery from reaction media and possible use of high temperatures, but they suffer from selectivity problems and lack of mechanistic explorations. Furthermore, green catalysis,[5] that is critically addressed by the principles of green chemistry, is an important issue in modern chemical processes. Features of the green catalysts ideally involve low preparation costs, high activities, good selectivities, high stabilities, efficient recovery, and good recyclability. Green catalysts should efficiently catalyze reactions in “green” solvents (e.g., neat condition, water, ethanol). Finally the design and applications of green catalysts is not only a task of great economic and environmental importance in catalysis science, but also should overcome the problems of metal contamination in products.

Nanocatalysis is defined by catalysis using nanoparticles (NP).[3] The catalytically active NPs have sizes between the order of one nanometer (nm) and several tens or hundreds of nanometers, but the most active ones in catalysis are only one or a few nanometers in diameter (containing a few tens to a few hundred atoms). They have a high surface-to-volume ratio and a large proportion of surface atoms, i.e.

predominantly edge and corner atoms that are very active for substrate activation. Since around the beginning of the 1990's, this area of catalysis has become an independent field usually called colloidal catalysis or quasi-homogenous catalysis since it was believed, at that time, to be a bridge between classical homogenous catalysis and heterogeneous catalysis. In this regard, nanocatalysis combines the positive aspects of both homogenous catalysis (high catalytic activity and selectivity, and mechanistic studies leading to catalyst improvements) and heterogeneous catalysis (easy catalyst separation from reaction media and good recyclability).[4]

In this context, transition metals based nanomaterials are of particular interest in the utilization of nanocatalysts.[6] Transition-metal-based heterogeneous nanomaterials contain the catalytic species that perform substrate activation, and the catalytic reaction proceeds on the supported metal surface thereby bringing about selectivity and efficiency. In order to obtain nano-sized catalytically active NPs, transition-metal NP size must be restricted to a few tens to several thousand metal atoms. Therefore these transition-metal NPs need be stabilized by dendrimers, polymers, ionic liquids (ILs) and inorganic solid supports such as silica, alumina, zirconia, carbon, etc. Indeed, stabilizers are playing a crucial role and eventually affect the catalytic properties.[7] For instance some strong ligands (thiolates, phosphines, phosphine oxides, etc.) inhibit the active surface sites, leading to negative catalytic effects on the catalytic reactions occuring at the NPs surface. Thus, "green" ligands that involve mild NP stabilization in water and are easy to displace and eventually provide more surface active sites in catalytic processes are searched to further improve activity. This is the case for instance with nitrogen donors (e.g. amines or 1,2,3-triazole based ligands) that leave the metal site at the metal surface in the zero oxidation state without back bonding, i.e. electron rich, which is potentially most favorable for catalysis. On the other hand, "ligand-free" supported nanocatalysts represent another promising alternative compared to traditional nanocatalysts, because the absence of ligand enables "clean" NP surfaces that mostly expose the edge and corner active atoms that usually are very efficient to activate substrates. Indeed, the rational synthesis of ligandless, ultrafine and efficient nanoparticle catalysts is an

ongoing challenge.

Before this PhD our research group has examined dendrimers and transition-metal NPs as templates for homogeneous and heterogeneous catalytic reactions.[8] We have extended the principle of dendritic templated nanocatalysis to ligand-induced nanocatalysis including the use of amphiphilic triazole (click) nanomaterials for improved nanocatalysis. Thus the present PhD thesis deals with the design and application of transition metals based nanomaterials as new nanocatalysts in a variety of chemical reactions with the aim to nano-engineer NP size and supporting environment in order to improve the catalytic activity, stability, recovery ability and to decrease the catalyst loading.

In the first chapter, a review is presented to generally introduce the mechanistic aspects and recent trends of the metal-catalyzed azide-alkyne cycloaddition reactions[9] with catalysts based on various transition metals. The copper-catalyzed alkyne-azide cycloaddition (CuAAC),[10] click reaction, forming 1,2,3-triazole based ligands, is the most used one and has revolutionized molecular engineering including applications to organic and medicinal chemistry, polymer science and materials science.

In the second chapter, a new concept based on the design of amphiphilic ligand that mimics the functions of dendrimers to stabilize various transition metal nanoparticles was firstly proposed. This tris(triazolyl)-polyethylene glycol (tris-trz-PEG) amphiphilic ligand containing three clicked triazole rings and a PEG 2000 chain is synthesized through CuAAC and a Williamson reaction. These amphiphilic ligand-transition metal nanoparticles are very efficient nanocatalysts with part per million (ppm) loadings for 4-nitrophenol reduction, click reaction, Suzuki-Miyaura reaction and transfer hydrogenation reaction.[11] Moreover, we also compared the stabilization of AuNPs by mono-, bis-, and tris-trz and their influence of the trz denticity on the 4-nitrophenol reduction by $NaBH_4$ in water also including comparison with current polyethylene glycol 2000 (PEG) and polyvinylpyrrolidone (PVP) AuNP stabilizers. Further, based on this ligand, especially the utilization of the chelation of the triazole groups, an efficient amphiphilic "click" Cu^I catalyst in water is designed. This catalyst shows high activity for CuAAC "click" reaction in water at

ambient temperature with catalyst loading at only ppm levels for the synthesis of various useful functional products with medicinal, catalytic, targeting, and labeling properties.[12]

The third chapter first reports the preparation of ultrafine and monodispersed bimetallic RhAg nanoparticles (NPs) that are uniformly supported on reduced graphene oxide nanosheets (RhAg/rGO). The bimetallic RhAg NPs involve a synergy between the two metals on rGO that improves the catalytic activity compared to both monometallic counterparts. The catalyst was recycled, and its amount was reduced to ppm level while retaining an exceptional catalytic efficiency in the 4-NP reduction by $NaBH_4$ in water at room temperature.[13] Secondly, the supramolecular H-bonding interactions between the PEG termini of the tris-trz-PEG ligand and the functional groups of the graphene oxide (GO) support enables the design of new heterogeneous α-Fe_2O_3 nanocluster/GO catalysts, which showed not only high efficiencies towards 4-nitropheol reduction and Suzuki-Miyaura reaction, but also can be recovered and reused without significantly loss of catalytically active NPs and activities.[14] More importantly, highly efficient ligand-free nanocatalysts synthesis based on the redox reaction between transition-metal cations and GO providing transition metal NP/GO nanocatalysts and their use in water under ambient conditions for a variety of reactions. The high efficiencies of such noble-metal as well as biometal composites as excellent green catalysts are exemplified for the 4-nitrophenol reduction, the hydrolysis of ammonia-borane (AB) for H_2 generation in water, the Sonogashira reaction and the click reaction. [15]

The fourth chapter demonstrates the highly dispersed ligand free Ni NPs have been successfully synthesized using zeolitic imidazolate framework as nanocatalyst template, exhibiting remarkably high catalytic activity for hydrogen generation from hydrolysis of ammonia-borane.[16] By the mechanistic studies, ion effect is further discovery the in this reaction, which allows the remarkable improvement of the catalytic performance and the controlled release of hydrogen.

At the end of the thesis, the “Conclusion and Perspectives” section summarizes the progress resulting from the research conducted during this thesis concerning the

design and application of transition metal based nanocatalysts for various chemical reactions. Thereafter, perspectives are provided, indicating that development of new heterogeneous nanocatalysts for instance the exploration of bimetallic catalysts, and earth abundant metal (so-called "biometals") catalysts, should be valuable research directions of further work along this line.

References

[1] a) G. M. Whitesides, *Small.* **2005**, *1*, 172-179; b) *Concepts of Nanochemistry*, ed. L. Cademartiri, G. A. Ozin, Wiley-VCH, Weinheim, **2009**, p. 5; c) M. V. Kovalenko, L. Manna, A. Cabot, Z. Hens, D. V. Talapin, C. R. Kagan, V. I. Kiminov, A. L. Rogach, P. Reiss, D. J. Milliron, *ACS Nano* **2015**, *2*, 1012-1057.

[2] *The Nobel Prize in Chemistry 2016–Advanced Information. Nobelprize.org. Nobel Media AB 2014. Web. October 6, 2016, http://www.nobelprize.org/nobel_prizes/chemistry/laureates/2016/advanced.html.*

[3] a) *Nanoparticles and Catalysis*, Ed. D. Astruc, Wiley-VCH, **2008**; b) *Modern Surface Organometallic Chemistry*, Eds. J.-M. Basset, R. Psaro, D. Roberto and R. Ugo, Wiley-VCH, Weiheim, **2009**; c) A. Fihri, M. Bouhrara, B. Nekoueishahraki, J.-M. Basset, V. Polshettiwar, *Chem. Soc. Rev.,* **2011**, *40*, 5181-5203; d) *Nanomaterials in Catalysis*, Eds. P. Serp and K. Philippot, Wiley-VCH, **2013**; e) S. Zhang, L. Nguyen, Y. Zhu, S. Zhan, C.-K. Tsung, F. Tao, *Acc. Chem. Res.,* **2013**, *46*, 1731-1739.

[4] a) D. Astruc. *Organometallic Chemistry and Catalysis*, Springer, Berlin, **2007**; b) D. Astruc, *Chimie organométallique et catalyse*. EDP Science, Les Ullis, **2013**.

[5] a) R. A. Sheldon, I. Arends, U. Hanefeld, *Green Chemistry and Catalysis*. Wiley-VCH, Weinheim, Germany, **2007**; b) *Handbook of Heterogeneous Catalysis*, eds G. Ertl, H. Knozinger and J. Weitkamp, Wiley-VCH, Weinheim, **1997**; c) A. Suzuki In. *Modern Arene Chemistry*, ed D. Astruc. Wiley-VCH, Weinheim, **2002**; d) G. A. Somorjai, *Introduction to Surface Chemistry and Catalysis*. Wiley, New York, **1994**.

[6] a) L. D. Pachón, G. Rothenberg, *Appl. Org. Chem.,* **2008**, *22*, 288-299; b) N. Yan, C. Xiao, Y. Kou, *Coord. Chem. Rev.,* **2010**, *254*, 1179-1218; c) J. D. A. Pelletier, J.-M. Basset, *Acc. Chem. Res*. **2016**, *49*, 664-677.

[7] a) N. Toshima, T. Yonezawa, *New J. Chem.* **1998**, *22*, 1179-1201; b) J. Durand, E. Teuma, M. Gomez, *Eur. J. Inorg. Chem*. **2008**, 3577-3586; c) V. S. Myers, M. G. Weir, E. V. Carino, D. F. Yancey, S. Pande, R. M. Crooks, *Chem. Sci.* **2011**, *2*, 1632-1646.

[8] a) D. Astruc, *Nat. Chem*. **2012**, *4*, 255-267; b) C. Deraedt, N. Pinaud, D. Astruc, *J. Am. Chem. Soc*. **2014**, *136*, 12092–12098; c) D. Wang, C. Deraedt, J. Ruiz, D. Astruc, *Acc. Chem. Res*. **2015**, *48*, 1871-1880.

[9] C. Wang, D. Ikhlef, S. Kahlal, J. Y. Saillard, D. Astruc, *Coord. Chem. Rev.,* **2016**, *316*, 1–20.

[10] a) M. Meldal, C. W. Tornoe, *Chem. Rev*. **2008**, *108*, 2952-3015; b) J. E. Hein, V. V. Fokin, *Chem. Soc. Rev*. **2010**, *39*, 1302-1315; c) M. Rodriguez-Rodriguez, P. Llanes, C. Pradel, M. A. Pericas, M. Gomez, *Chem. Eur. J*. **2016**, *22*, 18247-18253.

[11] C. Wang, R. Ciganda, L. Salmon, D. Gregurec, J. Irigoyen, S. Moya, J. Ruiz, D. Astruc, *Angew. Chem. Int. Ed*. **2016**, *55*, 3091-3095.

[12]C. Wang, D. Wang, S. Yu, T. Cornilleau, J. Ruiz, L. Salmon, D. Astruc, *ACS Catal*. **2016**, *6*, 5424–5431.

[13] C. Wang, R. Ciganda, L. Yate, S. Moya, L. Salmon, J. Ruiz, D. Astruc, *J. Mater. Sci.* **2017**, 52, 9465-9476.

[14] C. Wang, L. Salmon, R. Ciganda, L. Yates, S. Moya, J. Ruiz, D. Astruc, *Chem. Commun*. **2017**, *53*, 644 – 646.

[15] C. Wang, R. Ciganda, L. Yate, J. Tuninetti, V. Shalabaeva, L. Salmon, S. Moya, J. Ruiz, D. Astruc, submitted for publication.

[16] C. Wang, C. Zhang, Z. Wang, R. Ciganda, L. Yate, L. Salmon, S. Moya, J. Ruiz, D. Astruc, to be submitted for publication.

Chapter 1

Overview on Metal Catalyzed Alkyne–Azide Cycloaddition and Recent Trend

Introduction

This chapter consists in a review paper written in collaboration between our group and Prof. Jean-Yves Saillard from the University of Rennes on copper-catalyzed azide-alkyne cycloaddition reactions (CuAAC) and other metal-catalyzed azide-alkyne cycloaddition reactions (MAAC). It contains over 200 references disclosing the recent developments in the mechanistic aspects and recent trends of the MAAC reactions based on various metals (Cu, Ru, Ag, Au, Ir, Ni, Zn, Ln). The MAAC reactions are of considerable use in synthesis with applications in materials science and biomedicine, although CuAAC reactions remain by far the most prominent example of MAAC reactions and "click" chemistry. Various mechanisms based on theoretical calculations, characterizations of intermediates and optimization of reaction parameters have been proposed for different MAAC reactions. The theoretical calculations and experimental progress are intimately connected in order to improve the reaction efficiency, simplify procedures and apply them to industry in particular by decreasing catalytic amounts. Thus we reviewed the mechanistic advances and recent trends of this MAAC "click chemistry". These multiple new advances should inspire theoretical chemists to rationalize mechanisms of new routes. In turn, the theoretical advances could guide and lead chemists to imagine new reaction improvements.

Coordination Chemistry Reviews 316 (2016) 1–20

Contents lists available at ScienceDirect

Coordination Chemistry Reviews

journal homepage: www.elsevier.com/locate/ccr

Review

Metal-catalyzed azide-alkyne "click" reactions: Mechanistic overview and recent trends

Changlong Wang[a], Djamila Ikhlef[b,c], Samia Kahlal[b], Jean-Yves Saillard[b,*], Didier Astruc[a,*]

[a] ISM, UMR CNRS N° 5255, Univ. Bordeaux, 33405 Talence Cedex, France
[b] ISCR UMR CNRS 6226, University of Rennes 1, 35042 Rennes Cedex, France
[c] Laboratoire de Physico-Chimie Théorique et Chimie Informatique, Université des Sciences et de la Technologie Houari Boumédienne, B.P. 32, El Alia, Alger, Algeria

Contents

1. Introduction 1
2. MAAC reactions with various metal catalysts 2
   2.1. The CuAAC reactions 2
   2.2. The RuAAC reactions 4
   2.3. The AgAAC reactions 6
   2.4. The AuAAC reactions 7
   2.5. The IrAAC reactions 8
   2.6. The NiAAC reactions 9
   2.7. The ZnAAC reactions 9
   2.8. The LnAAC reactions 10
3. Recent trends 11
   3.1. CuAAC 11
   3.2. RuAAC 16
   3.3. Applications of the CuAAC "click" reactions 17
4. Conclusions and outlook 17
   Acknowledgement 18
   References 18

ARTICLE INFO

Article history:
Received 4 February 2016
Accepted 25 February 2016
Available online 3 March 2016

Keywords:
Metal-Catalyzed Alkyne-Azide
Cycloaddition
Copper
Click
Mechanism
CuAAC

ABSTRACT

This review is focused on the mechanistic aspects and recent trends of the metal-catalyzed azide-alkyne cycloaddition (MAAC) so-called "click" reactions with catalysts based on various metals (Cu, Ru, Ag, Au, Ir, Ni, Zn, Ln), although Cu (I) catalysts are still the most used ones. These MAAC reactions are by far the most common click reactions relevant to the "green chemistry" concept. First developed by the Fokin-Sharpless and Meldal group with Cu(I) in 2002, they have then been extended to Ru(II) catalysts by the Fokin group in 2005 and finally to many other metal catalysts. Mechanistic investigations are essential to reaction improvements and subsequent applications, and indeed as shown in this review the proposed mechanisms have been multiple during the last decade based on theoretical computations and experimental search of intermediates. New trends (since 2012) are also presented here often representing both exciting approaches for various applications and new challenges for further mechanistic investigations.

1. Introduction

The concept of "click chemistry" proposed by Kolb, Finn and Sharpless in 2001 [1] has revolutionized molecular engineering including applications to organic and medicinal chemistry [2–11], polymer science and materials science [12–21]. Among the various

* Corresponding authors.
E-mail addresses: saillard@univ-rennes1.fr (J.-Y. Saillard), d.astruc@ism.u-bordeaux.fr (D. Astruc).

http://dx.doi.org/10.1016/j.ccr.2016.02.010
0010-8545/

"click" reactions responding to the requirements of this concept, the most generally used one is the copper(I)-catalyzed reaction between terminal alkynes and azides (CuAAC) selectively yielding 1,4-disubstituted 1,2,3-triazoles, that was reported independently by the Sharpless-Fokin [22] and the Meldal groups in 2002 [23,24]. This reaction is the catalyzed version of the 1,3 dipolar cycloaddition, known in the former decades as the Huisgen reaction that had already been first disclosed in the XIXth century [25]. The advantages of the Cu(I) catalyzed "click" reaction are that (i) it is regioselective, whereas the non-catalyzed Huisgen reaction lacks regioselectivity, producing both the 1,4- and 1,5-disubstituted isomers, (ii) it proceeds at milder temperature than the non-catalyzed reaction (iii) it fulfills the requirements of "green chemistry" in so far as it can occur in aqueous or alcoholic medium, (iv) the catalyst reported by Sharpless and Fokin is simple and inexpensive; it consists in $CuSO_4{\cdot}5H_2O$ + sodium ascorbate, the later reagent being fine for the reduction of Cu(II) to Cu(I), but not to Cu(0) [22]. The only drawback is the need of large quantities of this catalyst mixture that is slow. Indeed, various nitrogen ligands accelerate the Cu(I) catalysis of the "click" reaction and allow using 1% or a few % Cu (I) catalyst [20,26]. Recently we reported that using a recyclable dendritic nanoreactor in water only, it was possible to decrease the Cu(I) amount using the $CuSO_4{\cdot}5H_2O$ + sodium ascorbate catalyst to 1 ppm or only a few ppm with various applications to biomedical targets [27a]. Disubstituted alkynes cannot be used for the CuAAC reaction, because deprotonation of the terminal alkyne to give Cu(alkynyl) intermediate species is mandatory in this reaction [26]. With pentamethylcyclopentadienyl-ruthenium catalysts, however, the Fokin group showed that the other isomer, i.e. 1,5-disubstituted triazole is regioselectively formed in the RuAAC reaction even with disubstituted alkynes according to a different mechanism [28]. Ruthenium catalysis is versatile, because other ruthenium catalysts reacted with terminal alkynes via a key ruthenium-acetylide species to yield the 1,4-disubstituted triazoles [29]. Since the early reports, a variety of transition-metal catalysts have been used for the reactions between mono- or disubstituted alkynes and azides (vide infra). For the Cu(I) catalyzed reaction, a variety of mechanisms involving Cu(I)-aryl intermediates have been proposed in which the key-step species contains either mononuclear [35] or binuclear copper species [30–38]. Theoretical studies of the RuAAC reaction have also been reported [28,39–41]. Given this mechanistic variety and the large number of transition-metals catalysts used for the MAAC reactions (M = transition metal), it is essential and timely to address the mechanistic problems by reviewing the state of knowledge in the literature, conduct theoretical calculations on MAAC reactions and compare these results with those reported in the literature.

2. MAAC reactions with various metal catalysts

2.1. The CuAAC reactions

With over 2000 publications in hardly more than a decade, the CuAAC reaction is illustrious and undoubtedly has been a breakthrough in organic synthesis and Cu(I) catalysis [2–24,42]. Although a large number of Cu(I) catalysts are efficient in catalyzing this reaction [21,24,26], the conventional Sharpless-Fokin catalyst ($CuSO_4$/sodium ascorbate) [22] is by far the most used one in spite of the large required catalyst amount, slow rate, difficulty to remove copper after the reaction, and sometimes the detrimental effects on rates and yield observed in the presence of chlorides, bromides and iodides [43]. For instance, low efficiency was observed for CuAAC of 2-azidopyridines [44]. Thus experimental protocols such as adding podand-like ionic liquids (ILs) [45], simple thermal heating [46], ultrasound-assistance [47], and the combination of both ultrasounds and ILs [48] were used to accelerate the reaction rates of the Sharpless-Fokin catalyst.

Concerning the optimization of "X" ligands in the Cu(I)(X) catalysts, Zhang et al. compared various Cu(I) sources (CuCl, CuBr, CuI, $CuSO_4{\cdot}5H_2O$/NaAsc and $[(CuOAc)_2]_n$) that catalyze the CuAAC reaction of 6 tetrazolo-[1,5-*a*]pyridines toward the synthesis of 1-(pyridin-2-yl)-1,2,3-triazoles, and the results showed that copper(I) acetate was the most efficient catalyst [49]. The nitrogen ("L") ligands accelerate the CuAAC reaction are amines, pyridines, and triazoles, in particular tridentate ligands [26,50–52]. *N*-heterocyclic carbenes (NHC) that were reported by Nolan's group to be excellent ligands, providing high reaction rates and yield for the CuAAC reaction (vide infra). Interestingly, internal alkynes were also successfully used, which suggested that a different mechanism than that implying copper-acetylide intermediates was involved [33,53]. Bertrand's mesoionic carbenes were also efficient [54,55] even with sterically hindered azide and alkynes [55]. With various ligands and Cu(I) catalysts, a large variety of solvents have been used, and the reaction is compatible with aqueous solvents [21,22].

Noticing the fact that the Cu(I) species accelerated the rate of the AAC reactions by 7–8 orders of magnitude compared to purely thermal cycloaddition reactions observed without metal catalysts, Sharpless and coworkers then proposed a stepwise mechanism involving a mononuclear Cu-acetylide intermediate based on DFT studies (top of Fig. 1) [31]. In a latter study, however, Fokin and Finn also pointed out the possibility that two Cu centers were involved in the transition state of the cycle [32], for which the following detailed kinetic studies confirmed the possibility of a σ,π-bimetallic Cu(I) intermediate [26,50,56]. Subsequent DFT calculations, carried out in the same group [22b,57], supported this hypothesis by showing that the complexation of the alkyne unit by a second metal center (bottom of Fig. 1) reduces the activation energy barrier by 4–6 kcal/mol, depending on the nature of the ligand on the Cu^B atom indicated in Fig. 1 [57]. The effect of π-complexation of the σ-alkynyl-Cu(I) species enhances the reactivity of the alkynyl ligand by decreasing electron density on the sp carbon atoms, thus facilitating the azide attack. In fact the μ^2 coordination mode of the alkyne to Cu^B was quite distorted and dependent on the ligand nature. Concomitantly to the DFT investigation on binuclear processes of Fokin and coworkers [57], Straub published a computational investigation on copper acetylide complexes showing the same trend, i.e., di- and tetra-nuclear species display higher reactivity in the CuAAC reaction than do their mononuclear relatives [58a]. According to this study, the complexation of a supplementary copper atom reduces the Cu=C=C double bond character and therefore the ring strain in the metallocyclic intermediate. Following previous work [58b], Straub's group also recently presented the first molecular copper acetylide complex that featured high activity in CuAAC with added acetic acid even at −5 °C. The relationship between the "click" reactivity and the aggregation of acetylide-copper species different from dinuclear intermediates contributes to the mechanistic interpretation of this reaction. Indeed, complexes with acetylide ligands that bind copper species may be resting states of the catalyst in such click reaction mixtures that are not acidic [58c].

Following these pioneering computational works, several theoretical mechanistic investigations on the CuAAC reactions have been carried out, considering various copper systems, most of them multinuclear, and leading basically to similar qualitative conclusions [34,58–62]. A recent investigation pointed out the possibility for a concerted vs. stepwise nature of the mechanism, however, depending on the ligand nature [63]. The most recent experimental mechanistic study by Fokin's group unambiguously demonstrated the participation of a dinuclear copper intermediate in the case of a CuAAC reaction in which a mixture of Cu(I)(aryl) complex and $[Cu(I)(MeCN)_4]^+$ was used (Fig. 2). Their study revealed that

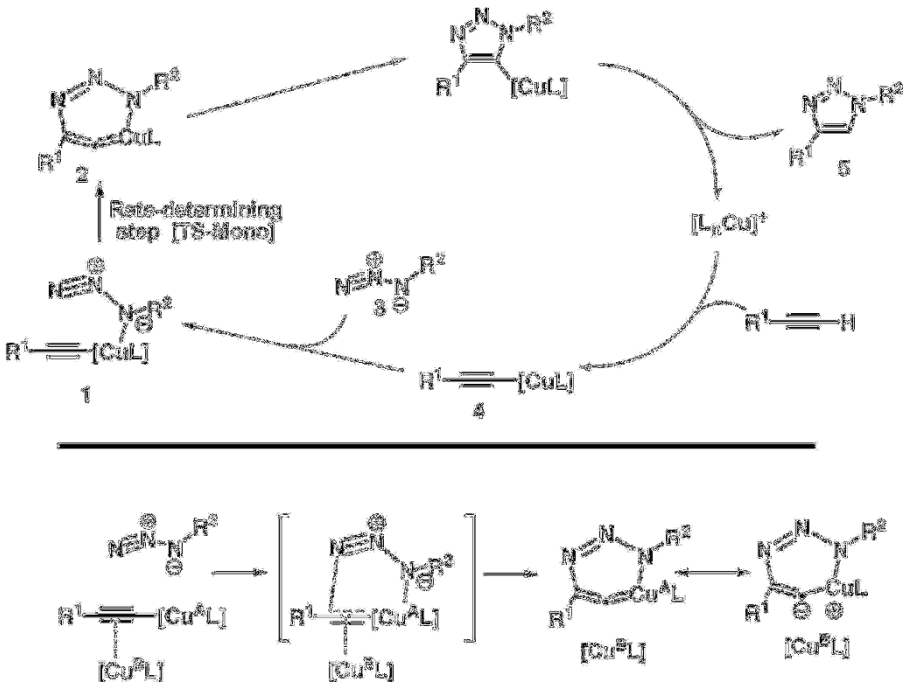

Fig. 1. The CuAAC mechanisms (Sharpless-type catalysis) proposed by Fokin and coworkers from their DFT calculations. Top: proposed mononuclear mechanism. Bottom: proposed dinuclear mechanism.
Reprinted with permission from Ref. [57]. Copyright 2007, American Chemical Society.

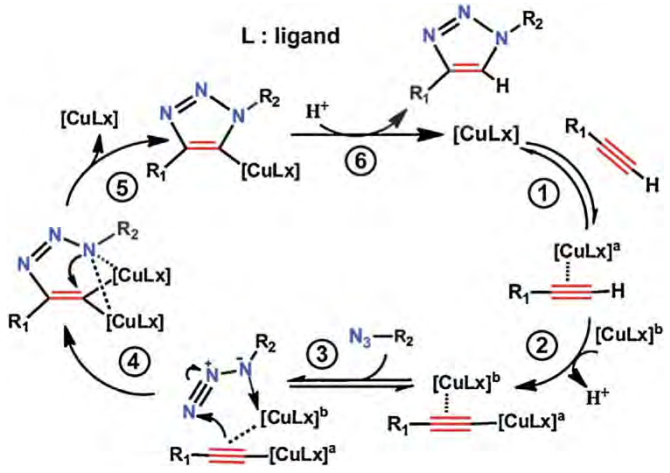

Fig. 2. Fokin's proposed mechanism for the CuAAC reaction with two copper centers.
Reproduced with permission from Ref. [38]. Copyright 2013, American Association for the Advancement of Science.

monomeric copper acetylide complexes were not reactive toward organic azides, except in the presence of exogenous copper catalyst [38]. Furthermore, direct injection by time-of-flight mass spectrometry (TOF-MS) for crossover experiments with an isotopically enriched exogenous copper source showed that two copper centers were involved within the cycloaddition process yielding the 1,4-substituted 1,2,3-triazoles. This mechanism was also recently confirmed by ESI-MS upon utilizing a mixture of an approach of neutral reactant and the strategy by Angelis's group that involves ion tagging and characterized the putative dinuclear copper intermediates [64].

The CuAAC reaction is also working well with the mononuclear mechanism as shown by efficient intradendritic catalysis that cannot accommodate two metals at the active site for obvious steric reasons. Intradendritic catalysis with the Cu catalytic center located either at the dendrimer core or activated by the triazole ligand located on the dendrimer tether is so efficient that sometimes down to a ppm amount of Cu is enough to catalyze the CuAAC reaction in water at ambient temperature [27a]. In the case of the active Cu(I)tren catalyst, a dendrimer was constructed around the tren ligand with Cu at the metallodendrimer core, emphasizing the monometallic mechanism. In such cases, the proposed mechanism based on DFT calculations [27b] involves the following intermediates (Fig. 3):

With a NHC-Cu(I) catalyst, however, DFT calculations by Nolan's group confirmed that a different mechanism was operating taking into account the reactivity of internal alkynes [33]. The following research from this group reported that, with the version of the NHC ligands bearing *N*-adamantyl substituents, the Cu-iodide catalyst was always superior to other [Cu(NHC)X] complexes in water or under neat conditions [65]. Based on the fact that the transformations involved both terminal and internal alkynes, these authors proposed a multiple mechanistic pathways for AAC reaction that suggested that the alkyne (or acetylide following deprotonation) might bind either *end on* or *side on* to Cu (Fig. 4) [66]. Moreover, the addition of aromatic nitrogen donors to the reagent mixture increased the AAC reaction activity, as reported by Gautier's group [67]. Furthermore, Nolan's group also pointed out the importance of NHC salts formation in the investigation of the cationic bis-carbene complexes for AAC. Indeed, the positive role of the second NHC ligand for the deprotonation of the terminal alkynes favors the generation of a [Cu]-acetylide species that plays a key role for AAC [68a].

Recently, the Bertrand group compared the role of the anionic ligand in each individual step of the AAC reaction catalyzed by LCuX by examining the kinetic profiles on these stoichiometric reactions [68b]. The X ligands covered a broad range of basicity (X = Cl, OAc, OPh, O*t*-Bu, OTf), and the L ligand was Bertrand's cyclic (alkyl)(amino)carbene (CAAC). In these cases, the steps are the metallation of the terminal alkyne, the formation of the σ,π-alkyne bis(copper) complex, the cycloaddition producing the metallated triazole, and the protolysis of the latter that regenerates the active

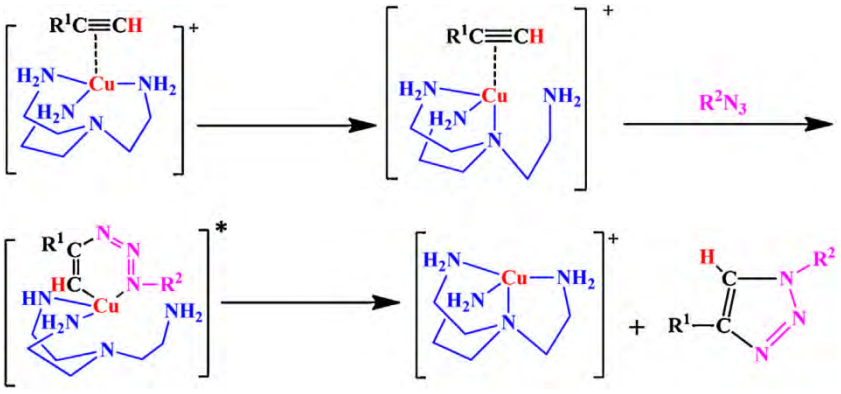

Fig. 3. Computed intermediates and transition state involved in the mechanism of Cu(I)(tren)-catalyzed CuAAC reactions.

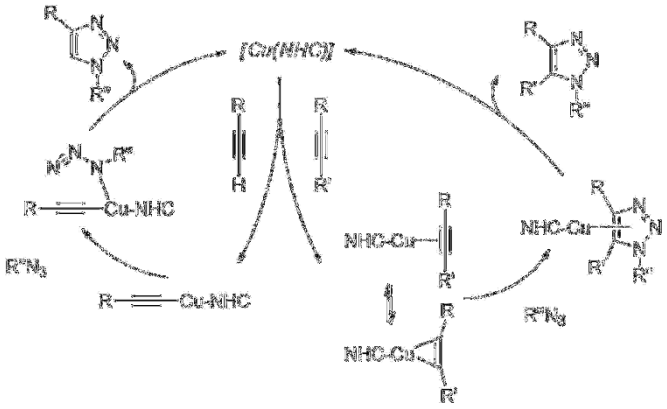

Fig. 4. Nolan's proposed multiple mechanistic pathways for the [3 + 2] cycloaddition of azides to alkynes.

Reproduced with permission from Ref. [66]. Copyright 2013, Royal Society of Chemistry.

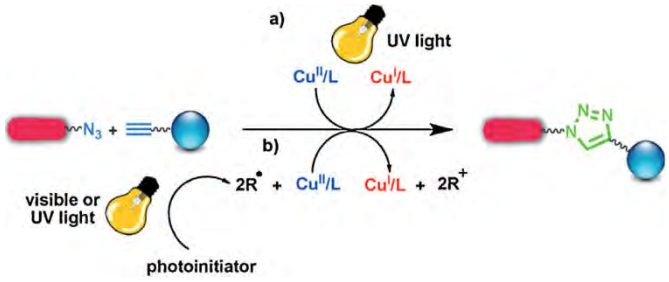

Fig. 5. Photoinduced CuAAC click reaction pathways.
Reprinted with permission from Ref. [69a]. Copyright 2013, Wiley-VCH.

catalytic species and produces the final triazole. Phenyl acetylene and benzyl azide were used as substrates. The results remarkably pointed out the Janus role of the X ligands. Basic X ligands favored the metallation, but disfavor the formation of the dinuclear intermediate, opposite to non-nucleophilic ligands. Acetate was a good compromise and very efficient for the proto-demetallation step. That the dinuclear Cu species can be disfavored in the CuAAC mechanism is also an interesting result at variance with other studies [68b].

In the CuAAC reactions, one of the interesting ways to generate Cu(I) appeared recently is by Cu(II) photoreduction simply activated using light to induce the click reactions. Tasdelen, Yagci and Ramil et al. have reviewed these applications, especially toward biomolecular systems and macromolecular syntheses [69], The mechanisms of photoinduced CuAAC "click" reactions involved the direct (i) and indirect (ii) reduction pathways of Cu(II) to Cu(I). The photo-click chemistry using visible light requires a radical-generating photoinitiator that assists photoreduction of Cu(II) to reactive Cu(I) species for the CuAAC reaction (Fig. 5, route a) as demonstrated by Bowman's group [70]. For example, upon irradiation at 350–520 nm, the presence of an additional photoinitiator is not necessary when the solvent contains at least 15 wt% of methanol that serves for the photoreduction process [71]. Another technique consists in the direct photolysis of the Cu(II) complex to generate Cu(I) by UV light irradiation, because many Cu(II) complexes such as $CuCl_2$/PMDETA [70b,70d,70e,72], $Cu(AP)_2$-PMDETA [70c], Cu(II)-PAC complex (PAC = polynuclear aromatic compound) [73], Cu(II)/carboxylate complex [74], and copper(II)-DMEDA complex [75] are sensitive to UV light or sunlight. Here the ligand is involved, i.e. it absorbs the UV light, promoting intramolecular electron transfer from the π-system of the ligand to the central Cu ion (Fig. 5, route b). During this process, Cu(II) is reduced to Cu(I) and the ligand is transformed into a radical species [76]. Interestingly, recently doping small amounts of Cu into the ZnS quantum dots (QDs) shell partially quenched the QD core (CdSe) luminescence, making QDs photoactivated vectors for the release of catalytically active Cu^+ ions for CuAAC [77]. On light irradiation, the QDs photo-oxidized with S was oxidized to SO_x^{y-}, causing Cu to form a complex with the azide that acted as a sacrificial electron acceptor allowing the click reaction to occur.

The other interesting ways to generate catalytic active species Cu(I) by using Cu(0) NPs is through comproportionation of Cu(0) and Cu(II) in the native oxide layer on the Cu surface [78]. In Alonso's proposed mechanism for the CuNP-catalyzed AAC, Cu(I) acetylides appeared as the true intermediate species [79]. The in situ generation of CuCl was postulated after acetylene deprotonation, with the concomitant formation of triethylammonium chloride (in the presence of LiCl derived from CuNPs preparation), and the action of the latter on the CuNPs. The reaction of the nascent CuCl with the acetylide species would furnish the corresponding copper(I) acetylide (Fig. 6) [80]. From this point of view, the reaction mechanism followed the original stepwise pathway that was proposed by Noodleman, Sharpless and Fokin et al. [31].

2.2. The RuAAC reactions

Apart from copper, the most frequently used catalysts for the MAAC reactions are ruthenium-based catalysts, the reaction being then abbreviated as RuAAC. Among all the Ru catalysts, the most investigated ones are the pentamethylcyclopentadienyl ruthenium chloride-based (noted [Cp*RuCl]) complexes), although Fokin's group also observed that the steric encumbrance imparted by the Cp* ligand is detrimental to the reaction [81]. These complexes catalyzed the regioselective RuAAC reaction of terminal alkynes

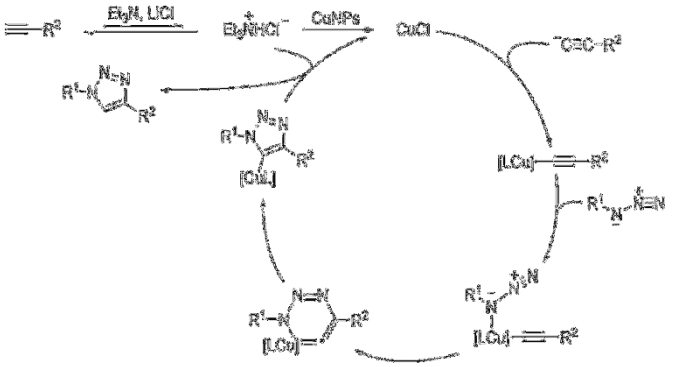

Fig. 6. Reaction mechanism proposed for the CuNPs-catalysed 1,3-dipolar cycloaddition of terminal alkynes and azides.
Reproduced with permission from Ref. [80]. Copyright 2010, WILEY-VCH.

forming, unlike CuAAC catalysts, 1,5-disubstituted 1,2,3-triazoles, and also unlike the CuAAC catalysts, they reacted with internal alkynes providing trisubstituted 1,2,3-triazoles [28,39,40,82]. The Cp*RuCl based catalysts provided multiple application that were recently developed (vide infra) [81,83–87].

The first mechanistic investigation was proposed by Lin, Jia, Fokin and coworkers based on DFT calculations [39]. The firstly formed azide-alkyne Ru complex was suggested to lead to a 6-membered ruthenacycle intermediate, followed by reductive elimination and formation of the triazole product. Subsequent calculations by Poater, Nolan and coworkers [88] found a somewhat different pathway but confirmed the key ruthenacycle intermediate. Their computed mechanism is reproduced in Fig. 7. More recently, Boz and Tüzün published a detailed DFT study in which various terminal and internal alkynes as well as Cp and Cp* ligands were considered [41]. They investigated the various possible mechanisms ensuing from the four possible configurations of the azide-alkyne Ru precursor complex. This detailed investigation allowed them to evaluate the interplay between the various electronic and steric effects. In any case the formation of a key 6-membered ruthenacycle intermediate is confirmed. Their computed regioselectivities (particularly in the case of internal alkynes) reproduce the experimental ones.

Given the richness of ruthenium catalysis, other families of ruthenium catalysts were disclosed. The Jia group first reported the RuAAC of terminal alkynes with 100% selectivity to lead to 1,4-disubstituted 1,2,3-triazoles using the catalyst $[RuH_2(CO)(PPh_3)_3]$ [29,89]. Then they compared a family of Ru catalysts that do not contain Cp ligands for the RuAAC reaction of terminal alkynes to selectively yield 1,4-disubstituted 1,2,3-triazoles [29], and the most efficient catalyst was $[RuH(\eta^2\text{-}BH_4)(CO)(PCy_3)_2]$. Both the experimental results and the DFT calculations indicated that the active species in the reactions was $[Ru(C{\equiv}CR)_2(CO)(PR'_3)_2]$ (Fig. 8). In their proposed mechanism, the authors indicated that the Ru-acetylide species **1** first formally underwent a cycloaddition reaction with an azide to give the species [Ru(triazolyl)], **2** (Fig. 8) resulting from initial coordination of the azide to the Ru center in **3** via the internal nitrogen atom (Fig. 9). Then, with a terminal alkyne metathesis of the Ru—C bond occurred via a four-centered transition state yielding the 1,4-disubstituted 1,2,3-triazole, which regenerates the starting catalyst. The complete mechanism of this catalytic cycle proposed by Jia, Lin, Fokin, and coworkers [29] from a detailed DFT analysis of the mechanism with propyne, methylazide and $[Ru(CCMe)_2(CO)(PMe)_2]$ is shown in Fig. 9. These authors showed also that the formation of the 1,5-triazole is highly disfavored. This is in line with Boz and Tüzün's theoretical work (see above) that indicated the importance of the electronic and steric effects for

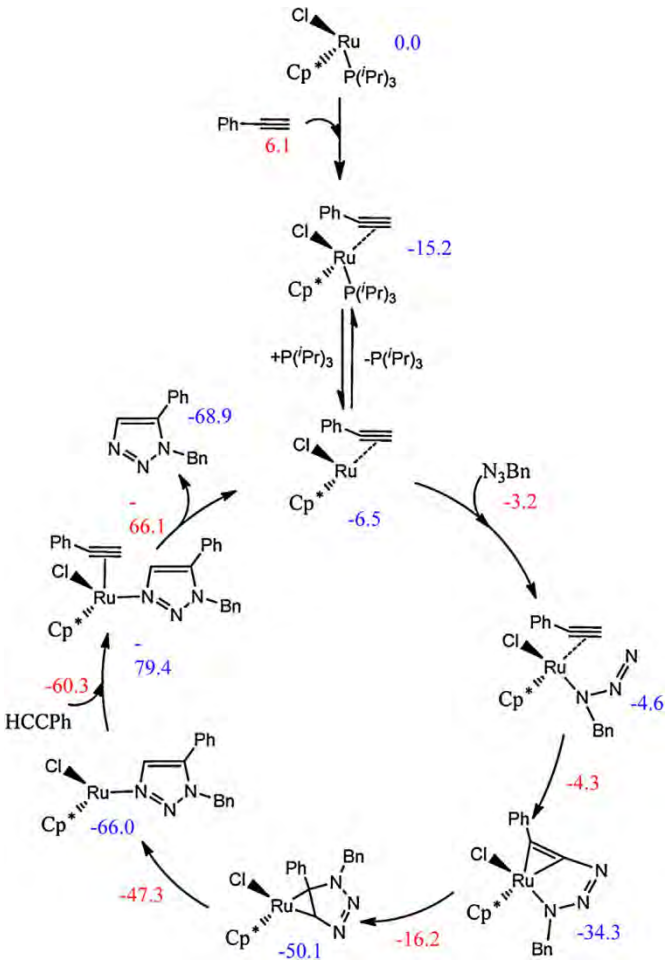

Fig. 7. Activation of the precatalyst and catalytic mechanism of the RuAAC of phenylacetylene with benzylazide. Numbers colored in blue and in red are computed relative free energies of intermediate and transition states, respectively (in kcal/mol).
Reproduced with permission from Ref. [88]. Copyright 2012, American Chemical Society.

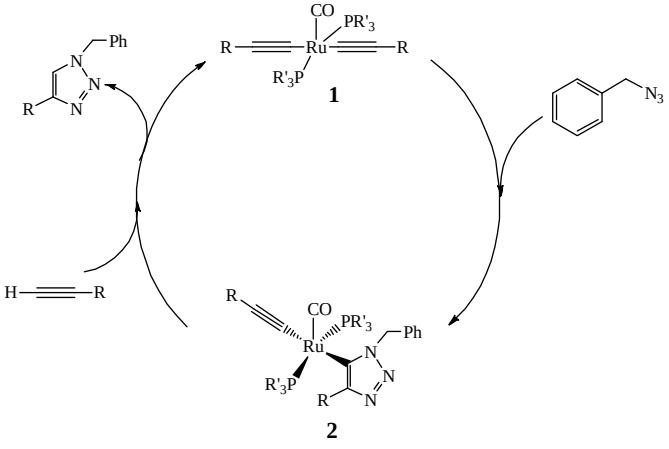

Fig. 8. Proposed catalytic cycle of RuAAC reaction catalyzed by $[RuH(\eta^2\text{-}BH_4)(CO)(PCy_3)_2]$.
Reproduced with permission from Ref. [29]. Copyright 2012, American Chemical Society.

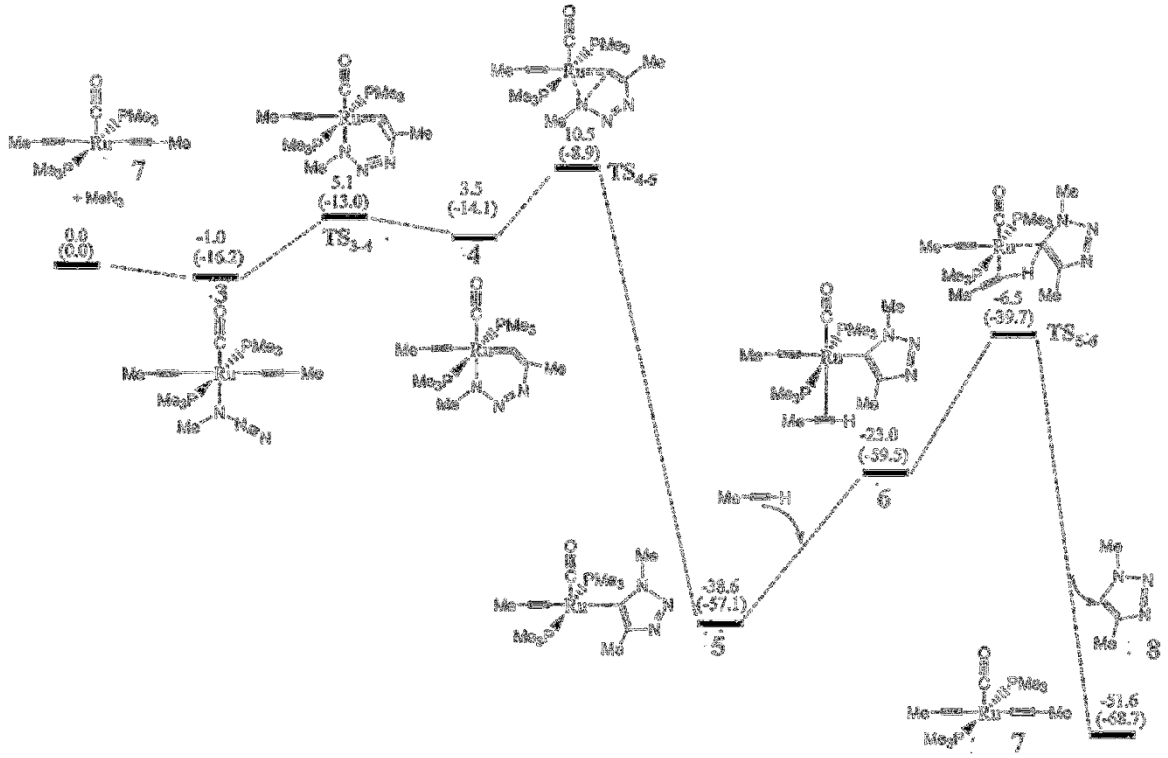

Fig. 9. DFT free energy profile (in kcal/mol) for the proposed mechanism of the formation of 1,4-triazole catalyzed by a Ru complex lacking cyclopentadienyl ligand. Reproduced with permission from Ref. [29]. Copyright 2012, American Chemical Society.

the regioselectivity, both thermodynamic and kinetic parameters playing a crucial role in the reactions [41].

Lo's group presented the first case of ruthenium azido complexes catalyzing the cycloaddition reaction of terminal alkynes with alkyl azides [90,91]. The new ruthenium azido complexes were synthesized from the mother TpRu complex [Ru(Cl)(Tp)(PPh_3)$_2$], Tp = HB(pz)$_3$, pz = pyrazolyl), yielding first [Ru(N_3)(PPh_3)[Tp(^{t}BuNC)] [90], then the amine-substituted ruthenium azido complex [Ru(N_3)(Tp(PPh_3)($EtNH_2$)] [91]. Although the detailed mechanism could not be established, the authors speculated a similar mechanism to previous proposed by Fokin et al. [28]. As shown in Fig. 10, the displacement of the spectator ligands ($EtNH_2$, PPh_3) produced the activated intermediate **A** that was then converted to the intermediate **B** via the oxidative coupling of an alkyne and an azide. After that, ligand substitution occurred in **B** leading to the release of the aromatic triazole product and regenerating the catalyst. Interestingly, in both cases, the N_3 ligand in the ruthenium azido complex did not couple the terminal alkyne in the substrate, because reaction energy for conversion of **A** to **B** is much smaller than that for conversion of **A** to **C** (DFT-computed free energies −45.9 kcal/mol vs. 34.9 kcal/mol, respectively) [91].

2.3. The AgAAC reactions

In a seminal report McNulty's group published the first example Ag(I) catalyst of the AAC reaction without copper at room-temperature (r.t.) [92]. Silver(I) salts alone were not efficient to promote the AAC reactions, but when AgOAc reacted with the P,O-ligand 2-diphenylphosphino-*N*,*N*,-diisopropylcarboxamide, the P,O ligand-silver(I) complex catalyzed the AAC reaction very well. Further experiments indicated that silver acetylide intermediate activated the formation of an acetylide–azide species toward cyclization [93]. Thus a reaction mechanism for homogeneous Ag(I)-catalyzed AAC reaction was proposed (Fig. 11). First of all, the loss of acetate from the 18-electron species **9** yield the active 14-electron catalyst **I**, forming the ligated silver(I) acetylide **II**, the electrophilicity of which is modulated by the hemilabile amide substituent. The nucleophilic reaction of the azides on **II** gives the species **IIIA**. The hemilabile ligand in **IIIA** intervenes by amide complexation generating a coordinatively saturated species that transfers the charge via the filled d orbitals to the π^* orbitals of the acetylide resulting in cyclization. The reaction occurs via the intermediate metallacycle (**IIIB**). Then the nitrogen atom migrates to carbon transporting two electrons to form the triazole **IV**, forming **3** by protonation, and the active catalyst **I** is regenerated.

Ortega-Arizmendi et al. also reported an "abnormal" NHC complex, Ag(I)-aNHC, that catalyzed the ACC reactions [94]. In this case, silver chloride by itself catalyzed the cycloaddition of various alkynes and azides in good yield, however with side reactions. Further introduction of the aNHC ligand avoided side reactions and facilitated the purification of the final products. Hybrid AgNP catalysts were also developed. For example, Salam and co-workers recently reported that the AgNP/graphene oxide (Ag/GO) based composite catalyzed multi-component reactions and one-pot click reaction (Fig. 12). In their approach, the catalysts were very stable and showed no silver leaching or aggregation, and were reused at least 5 times without loss of catalytic activity [95]. However when the AAC reaction is said to be catalyzed by Ag-based catalysts or other metal catalysts, caution is appropriate, because trace amount of copper contaminants could be enough to catalyze the AAC reactions. Indeed, Connell et al. found that the successful cycloaddition of an azide and terminal alkyne catalyzed by the isolated complex [Ag_2(**L^1**)$_2$][BF_4)$_2$] was actually catalyzed by trace amounts of copper in the catalyst [96].

Ferretti et al. recently reported that silver(I) oxide nanoparticles (Ag_2O NPs) catalyzed AAC reactions in anhydrous toluene [97]. Although the Ag_2O catalyst was less efficient than the conventional Cu^I catalyst that was generated from the Cu(0) and CuO under the same condition, the Ag_2O NPs are somewhat effective, robust and reusable, especially in the presence of a small amount

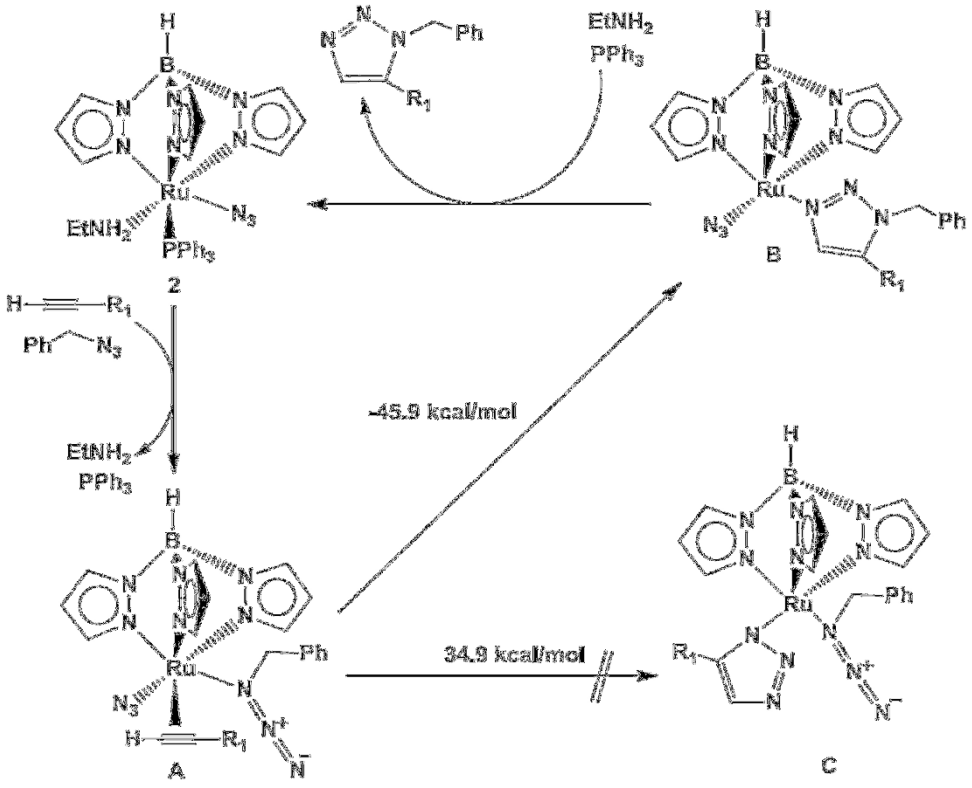

Fig. 10. Proposed mechanism of the RuAAC catalysis by ruthenium azido complexes.
Reprinted with permission from Ref. [91]. Copyright 2014, Elsevier B.V.

of water. In this case, substituent effects were noticed, and substrates containing electron-withdrawing groups onto the azide moiety gave mixtures of regioisomeric cycloadducts, which was a limitation. One should recall here that the uncatalyzed Huisgen reaction that yields such mixtures of isomeric cycloadducts works under ambient or mild conditions when substrates possess electron-withdrawing groups [25]. Sarma's group then compared various silver sources in AAC reactions conducted in H_2O/ethylene glycol (EG) under ambient conditions without exclusion of air [98]. The ligands and solvents played a critical role in their approach. Upon optimization the combinations of $AgN(CN)_2$ as a catalyst and DIPEA as a base/ligand gave the best results. It was proposed that this ligand played the same role as the tertiary amine in CuAAC reactions in the intermediate step. Various 1,4-disubstituted-1,2,3-triazoles were synthesized in high isolated yield under these very mild conditions, showing that $AgN(CN)_2$/DIPEA is a highly effective catalytic system for the AAC reactions.

2.4. The AuAAC reactions

"On-surface" chemistry was a viable method to synthesize covalent nanostructures under ambient temperature at the surface under ultra-high-vacuum (UHV) conditions [99]. This method has also been used to explore the mechanism of AAC reaction and guide the catalyst design. Bebensee et al. recently reported the fully regioselective AAC reaction on a Cu(111) surface leading to 1,4-triazoles (Fig. 13a) resulting from copper acetylide formation subsequent to C—H activation and bonding of the alkynyl group to the Cu(111) surface. The reaction proceeded with a very low yield. Therefore XPS showed that significant degradation of the azide upon adsorption occurred on the surface, though the reaction proceeded readily; especially the intact reactants were available on the surface [100]. Using on-surface chemistry under UHV, Arado et al. explored the MAAC reaction on Au(111) (Fig. 13b). By

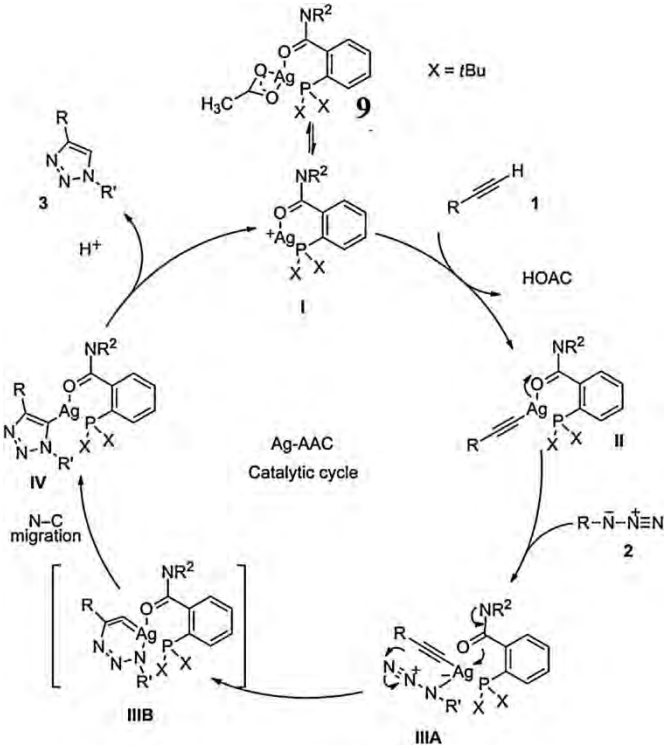

Fig. 11. Proposed catalytic cycle for the homogeneous Ag(I)-catalyzed AAC reaction.
Reproduced with permission from Ref. [93]. Copyright 2012, WILEY-VCH.

combining cryogenic scanning tunneling microscopy (STM) and DFT studies, they confirmed Bebensee's results on Cu(111) (vide supra) according which the MAAC reaction occurred on the [100] surface. However, the difference between these two examples is

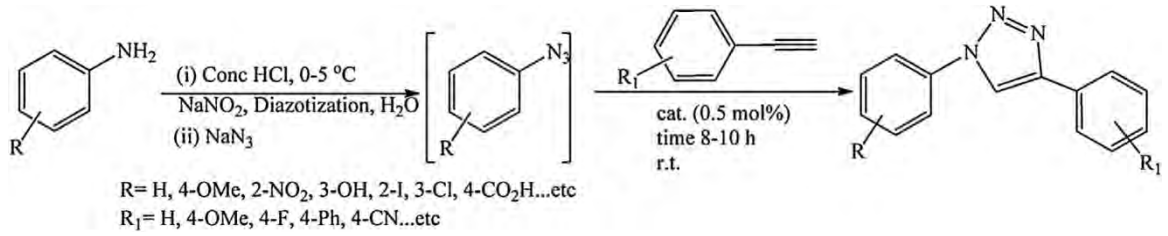

Fig. 12. One-pot AAC reaction catalyzed by Ag/GO.
Reproduced with permission from Ref. [95]. Copyright 2014, Royal Society of Chemistry.

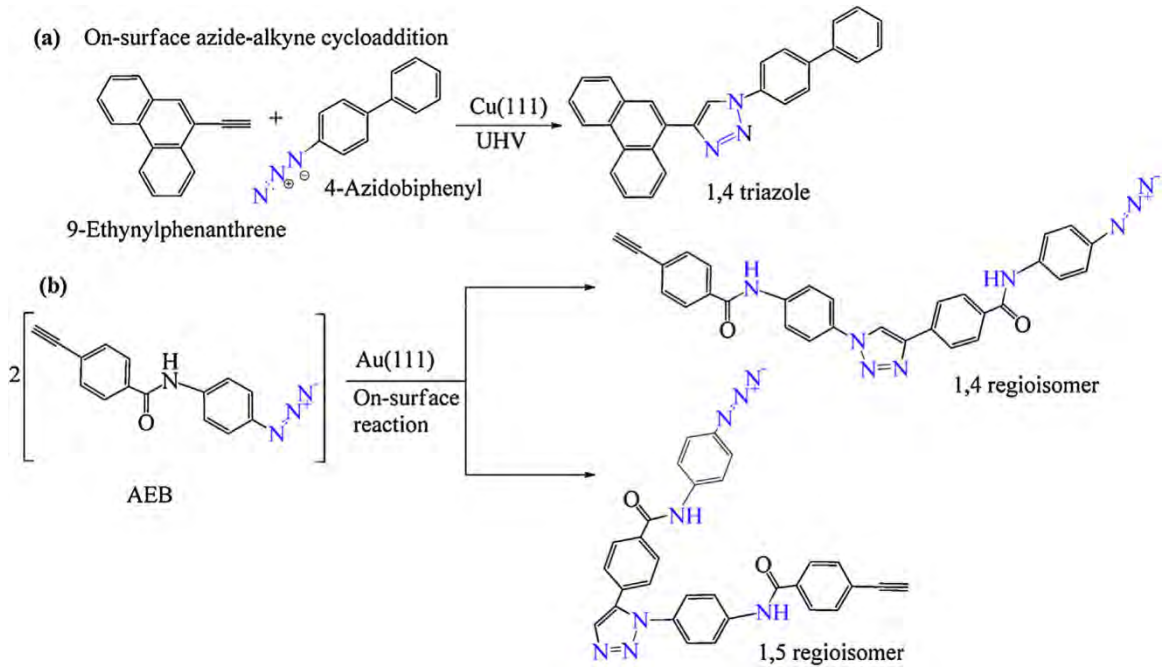

Fig. 13. (a) On Cu(111) surface catalyzed AAC. (b) Proposed on-surface AAC reaction of *N*-(4-azidophenyl)-4-ethynylbenzamide (AEB) and possible regioisomeric dimers 2 and 3.
Reproduced with permission from Refs. [100] and [101], respectively. Copyright 2013, American Chemical Society.

that Au(111) is not catalytically involved in C—H activation of alkyne. It only played a role as a two-dimensional (2D) surface to place the two partners of the reaction, which provided the observed selectivity. The successful control of the regioselectivity of the MAAC by surface constraint together with the careful design of the reactants provided the effective well-defined nanostructure without the requirement of a catalyst or additional thermal activation [101]. Recently another particular case using a heterogeneous reusable Au/TiO_2 nanostructure to efficiently catalyze the AAC reaction was highlighted (Fig. 14a). The authors proposed a mechanism in three steps (Fig. 14b): (i) a gold atom (I) reduced the electron density on the alkyne, enabling facile nucleophilic attack by the azide; (ii) a six member intermediate II, then intermediate III formed (iii) gold was removed to afford 1,4-disubstituted 1,2,3-triazoles and complete the reaction cycle [102].

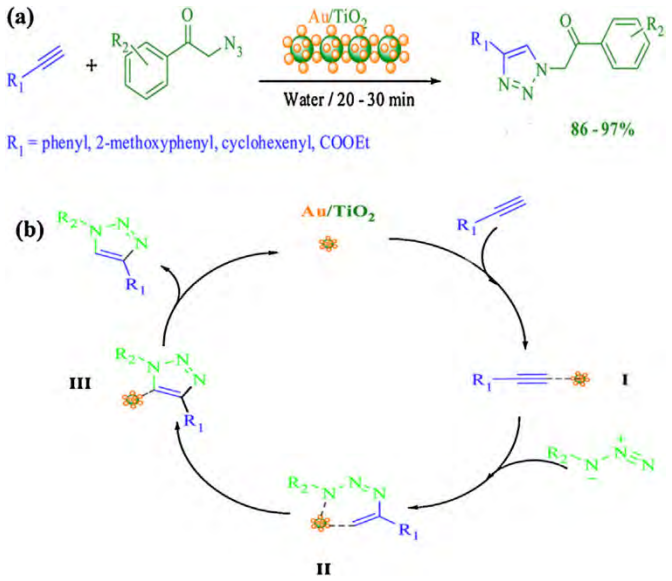

Fig. 14. (a) Titania-supported gold nanosphere-catalyzed 1,2,3-triazole synthesis. (b) Plausible mechanism for the formation of triazole.
Reproduced with permission from Ref. [102]. Copyright 2013, American Chemical Society.

2.5. The IrAAC reactions

The Iridium-catalyzed intermolecular AAC (IrAAC) has also proved to be a valuable complement to the well-known CuAAC and RuAAC reactions. The dimeric iridium complex $[Ir(cod)OMe]_2$ catalyzed the direct formation of new 1,4,5-trisubstituted triazoles [103]. $[Ir(cod)OMe]_2$ catalyzed the AAC reaction bromoalkynes producing 1,5-disubstituted 4-bromo-1,2,3-triazoles under mild conditions (Fig. 15). The electronic features of the alkyne

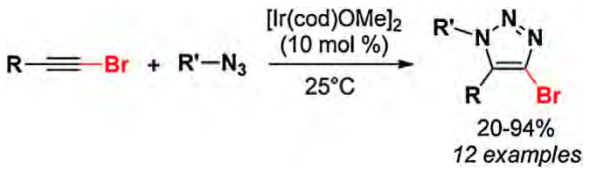

Fig. 15. Synthesis of 1,4,5-trisubstituted triazoles catalyzed by a dimeric iridium complex.

Reprinted with permission from Ref. [103]. Copyright 2013, American Chemical Society.

component strongly affected the reaction yield, i.e. the arylalkynes that are electron rich showed the optimized reactivity, while the bromoalkynes that are electron deficient provided a low yield of the corresponding 4-bromotriazoles. This catalyst was used to prepare 1,4,5-trisubstituted triazoles subsequent to Pd-catalyzed Suzuki–Miyaura reactions with appropriate arylboronic acids. Ding et al. compared various Ir complexes in the IrAAC of electron-rich internal alkynes and showed that the use of $[Ir(cod)Cl]_2$ optimized the reaction [104]. The increase of steric hindrance on the alkyne did not affect the reaction efficiency, but an electronic effect was also observed, i.e. electron-deficient alkynes led to moderate or good efficiency, while electron-rich and normal alkynes showed low reactivity except the aryloxy alkyne and selenyl alkyne.

These differences in the regioselectivities of addition of thioalkynes and bromoalkynes to azides have been elegantly rationalized through DFT calculations by Lin, Jia and coworkers [105]. Their major findings are summarized in Fig. 16. Both mechanisms start with the precoordination of the alkyne and azide on the metal center of [Ir(cod)X]. In the case of thioalkynes, a metallabicyclic Ir-carbene intermediate, stabilized by the π-donor effect of the ^{2}RS substituent is formed. In the case of bromoalkynes this π-donor effect is much weaker, and the metallabicyclic intermediate cannot be stabilized. Rather, a six-member metallacycle intermediate is formed and, depending on the π-donating ability of the R substituent, the 4- or the 5-bromotriazole is formed preferentially, as sketched in Fig. 16.

2.6. The NiAAC reactions

Rao's group recently demonstrated that the Raney Ni, without additional reducing agent, efficiently catalyzed acetylene azide cycloaddition reactions to form 1,2,3-triazoles [106]. In their methodology, the Raney nickel catalyzed combinatorial NiAAC with excellent yield. (Fig. 17a) To explore the NiAAC reaction pathway, deuteration experiments were conducted (Fig. 17b) in the presence of Ni(0) indicating that, unlike the copper-acetylide formation in CuAAC, the cycloaddition went through a metallocycle [107]. Thus in their proposed mechanism, the reaction starts on the Raney nickel surface by acetylene complexation leading to the π-complex **11** (Fig. 17b). Then the reaction proceeds AAC leading to **13** via **12**, and the Ni-acetylene species led to AAC in the orientation shown in **14**. The authors suggested that stereoelectronic features of the azide and alkyne favor the transition states **12** or **14** leading to the 1,4-product preferred to 1,5.

2.7. The ZnAAC reactions

For the ZnAAC reactions, pioneering contribution by Chen's group showed that heterogeneous zinc-on-charcoal (Zn/C) catalyzed the cycloaddition of aryl/aliphatic azides and aryl alkynes (including internal alkynes) in DMF at 50 °C without exclusion of

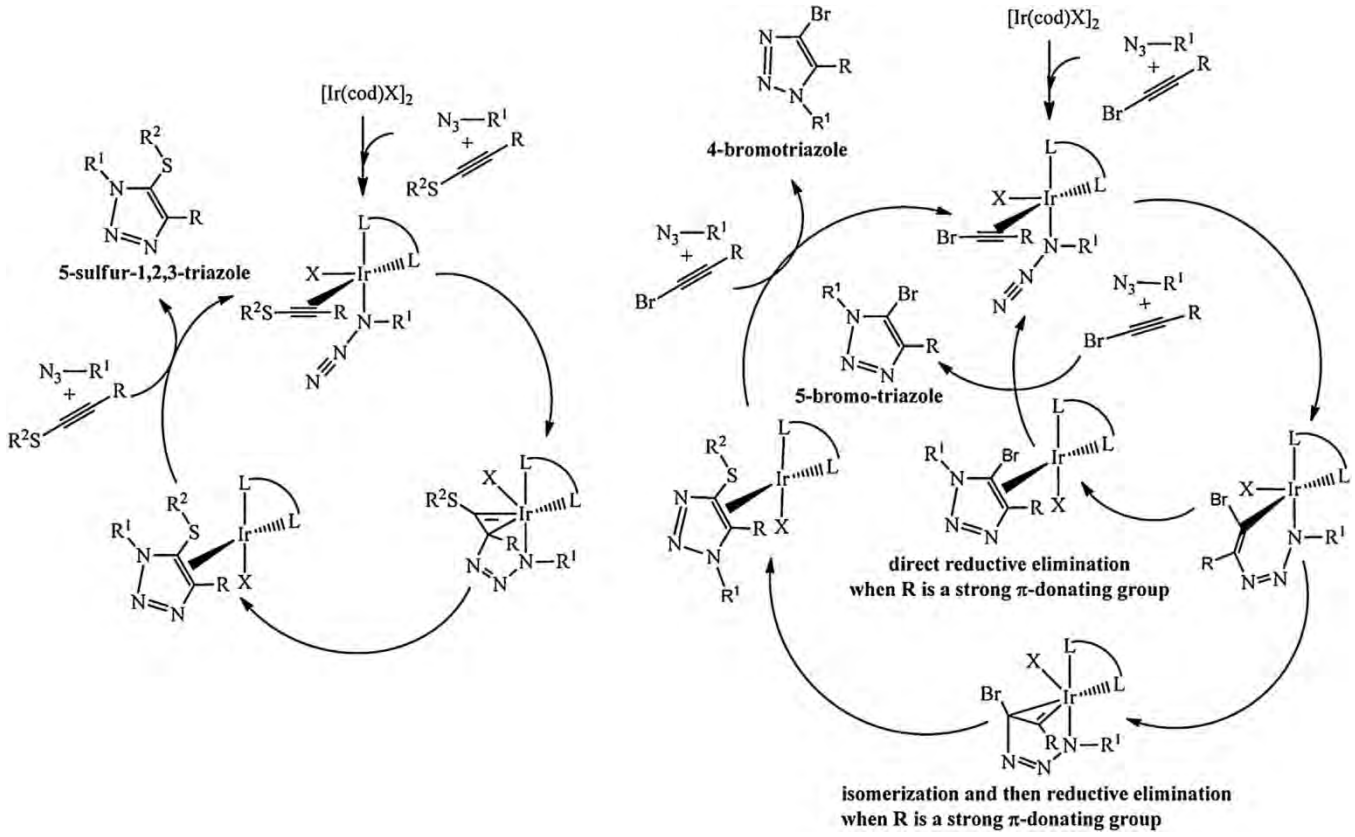

Fig. 16. The different IrAAC mechanisms proposed in the case of the addition of thioalkynes and bromoalkynes to azides in the presence of the $[Ir(cod)X]_2$ (X = Cl or OMe) dimer.

Reproduced with permission from Ref. [105]. Copyright 2014, American Chemical Society.

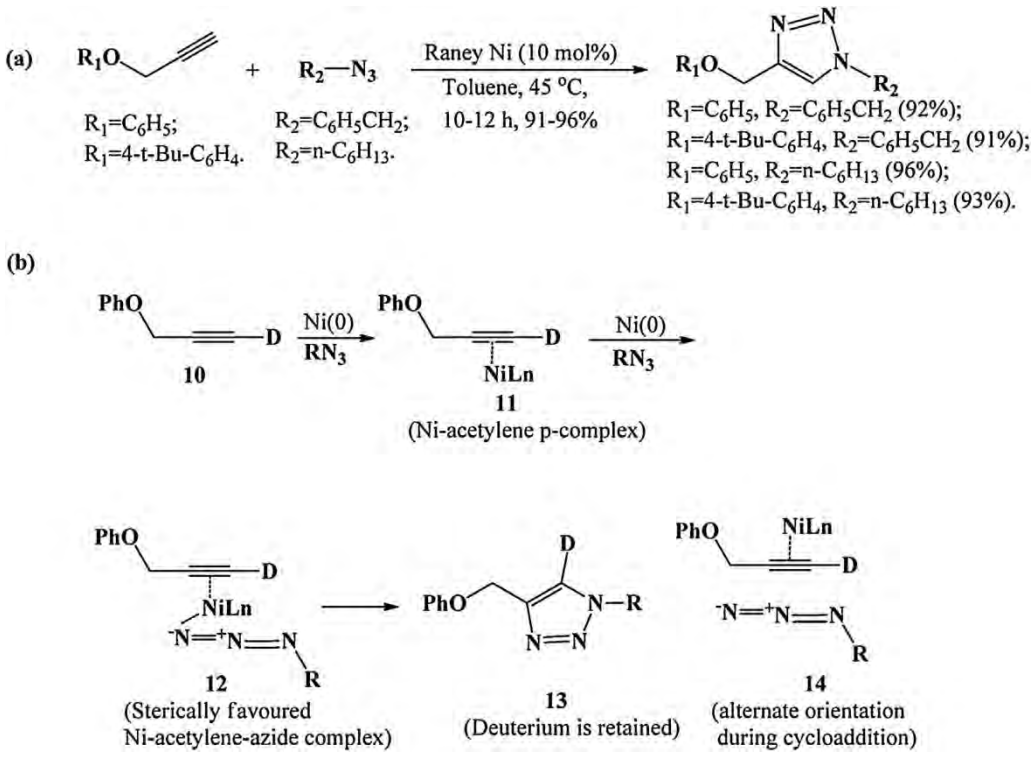

Fig. 17. (a) Combinatorial cycloaddition of two aryl propargyl ethers to benzyl and *n*-hexyl azides catalyzed by Raney Ni, and (b) Proposed mechanism for the NiAAC.
Reproduced with permission from Ref. [106]. Copyright 2014, Royal Society of Chemistry.

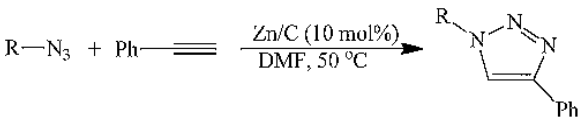

Fig. 18. Zn/C-catalyzed AAC reactions.
Reproduced with permission from Ref. [108]. Copyright 2010, WILEY-VCH.

air (63–94% yield) (Fig. 18) [108]. In this case, no electronic effect was observed, both electron-rich and electron-poor azides generating similar good reaction yield. The catalyst was recovered and reused for at least five times without significant decrease of activity. When ZnNPs were alloyed with CuNPs to form the catalysts for multicomponent 1,2,3-triazole synthesis/triazole alkynylation, the presence of Zn resisted the oxidation of Cu by sacrificial formation of ZnO that played a role in controlling the formation of alkynylated triazoles [108].

On the other hand, Greaney's group also described a mild method for the regioselective formation of 1,5-substituted 1,2,3-triazoles upon using $ZnEt_2$ at r.t [109a]. In their approach, the base *N*-methylimidazole (NMI) was needed to help the formation of the zinc acetylide species in order to promote reactivity and continue screening. The 4-position of the triazole was substituted via the aryl-zinc intermediate toward further coupling. The proposed mechanism for this reaction is summarized in Fig. 19. The initial metallation of the alkyne mediated by the amine base formed the zinc acetylide **16**. Then the reversible pre-coordination between the azide and zinc acetylide occurred before the [3 + 2]-cycloaddition, after which the aryl-zinc intermediate **15** formed, then was utilized to lead to 1,4,5-trisubstituted 1,2,3-triazoles. Based on these experimental results, Lan's group then reported their DFT calculations toward the mechanism and regioselectivity research of this ZnAAC using frontier molecular orbital (FMO) theory and distortion-interaction energy analysis [109b]. B3LYP-D3BJ calculations showed that ethynylzinc

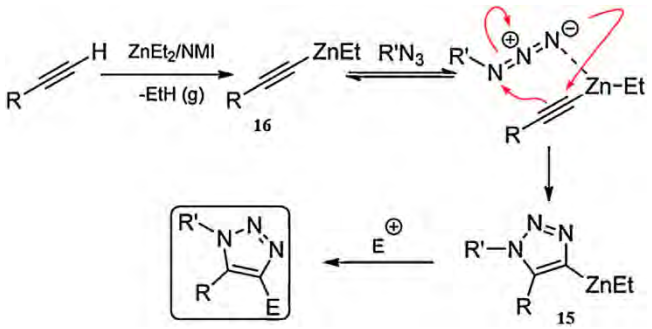

Fig. 19. Proposed mechanism explaining the reactivity in the system mediated by $ZnEt_2$.
Reproduced with permission from Ref. [109a]. Copyright 2013, American Chemical Society.

complexes bearing alkyl substituents showed a reactivity analogous to that of ethyl(phenylethynyl)zinc and a lower regioselectivity. B3LYP calculations gave a higher regioselectivity, however, because of a lower distortion energy in the transition state and led to a lower activation energy for 1,5-substituted product generation, as explained by the distortion–interaction analysis. Furthermore, the FMO analysis revealed that the binding of N-methylimidazole to zinc increased the energy of the HOMO of ethyl(phenylethynyl)zinc, which increased its reactivity.

2.8. The LnAAC reactions

Recently, a seminal example of rare earth-metal-catalyzed AAC reaction with terminal alkynes leading to 1,5-disubstituted 1,2,3-triazoles was described by Zhou's group [110]. The authors chose $[Sm\{N(SiMe_3)_2\}_3]$ as the catalyst after compared examination of the rare-earth metal catalysts $[Ln\{N(SiMe_3)_2\}_3]$, Ln = Sm, Nd, Y, Gd. Optimization of the reaction conditions showed that the presence

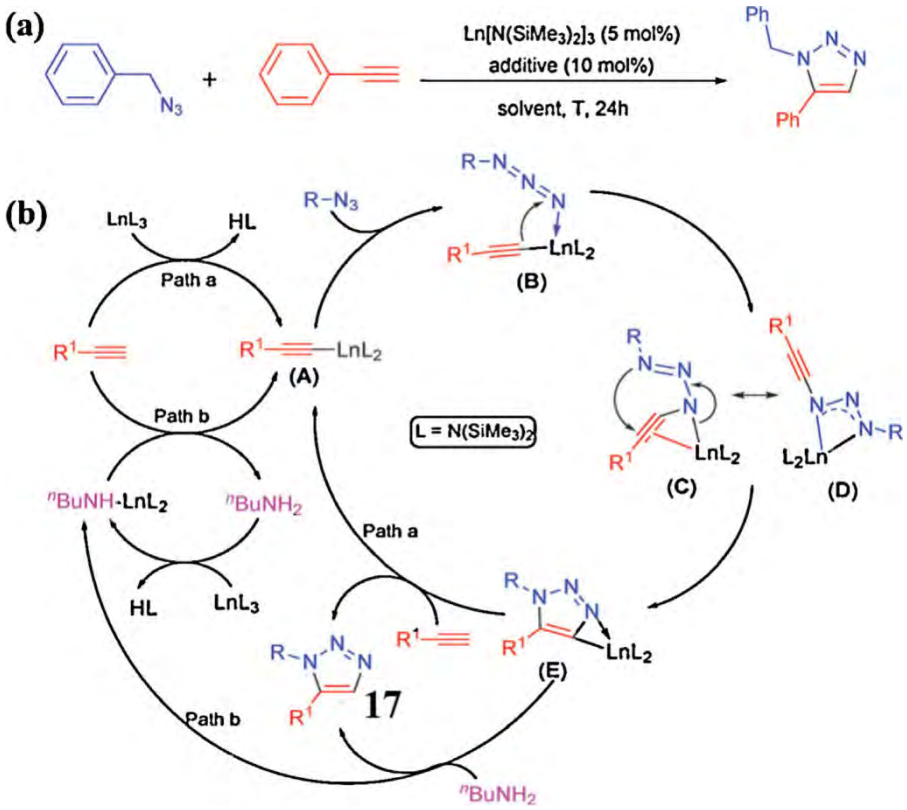

Fig. 20. (a) [Ln{N(SiMe$_3$)$_2$}$_3$]-catalyzed cycloaddition of terminal alkynes with azides (Ln = Sm, Nd, Y, Gd). (b) Reaction pathway for [Ln{N(SiMe$_3$)$_2$}$_3$]-catalyzed cycloaddition between terminal alkynes and azides.

Reproduced with permission from Ref. [110]. Copyright 2013, Royal Society of Chemistry.

of 10 mol% *n*-BuNH$_2$ improved the yield (Fig. 20a). By comparison, they suggested that the involvement of an acetylide intermediate complex was essential for the efficiency and selectivity. The proposed mechanism is shown in Fig. 20b. First activation of the C—H bond of the terminal alkyne produced the Ln acetylide **A** and HN(SiMe$_3$)$_2$. Then 1,1-insertion of the azide in the Ln—**C** bond of **A** gave the species **C** and **D**, and the anti-nucleophilic attack of the nitrogen atom to the π-coordinated alkyne led to the triazolate **E**. Then, the protonation of **E** with another alkyne molecule afforded **17** and regenerated **A** (path a). In an alternative pathway, path b was suggested based on the presence of amine additives that were favorable to the cycloaddition.

We have computationally explored this proposed mechanism by DFT calculations considering the complex [Y{N(SiH$_3$)$_2$}$_3$] (YL$_3$) as the simplified precatalyst, acetylene and hydrogen azide [27b]. The induction part of the mechanism (path **a** in the left side of Fig. 20b) that corresponds to the formation of the acetylide intermediate and a protonated ligand is computed to proceed with a rather low free energy barrier (7.0 kcal/mol). The computed **B** to **E** transit of Fig. 20b was a single step process and the rate-determining one, with a transition state that is 13.7 kcal/mol above **B** (Fig. 21). These results confirmed the proposed mechanism of Zhou's group (path a in Fig. 20b), although the pathway from **B** to **E** was computed to be a single step. Likewise, Li's group also recently computationally investigated the same catalytic process that was performed considering the pre-catalyst model [SmL$_2$S(CCPh)] (L = acetylide) and benzyl azide [111]. In their case, the observed 1,5 isomer was produced from the formation of an intermediate that resulted from the azide coordination on [SmL$_2$S(CCPh)] through its substituted nitrogen atom. This computed result was different from ours, indicating that only the 1,4-trz isomer was formed in this pathway though a similar mechanism, but with a higher energy barrier.

3. Recent trends

Following the basic features that characterize the MAAC reactions including the state of the art in the mechanistic understanding with various metals, recent trends essentially in CuAAC and RuAAC have appeared that are gathered in this section.

3.1. CuAAC

N-heterocyclic carbenes (NHCs) have become an increasingly used class of "L" ligands in organometallic chemistry and click catalysis [112]. Following the seminal work by Nolan's group [33], the Cu(I) complexes of NHC ligands were continuously very efficient catalysts for the click cycloaddition reaction between azides and alkynes [38,113]. Lal et al. compared the catalytic activity of NHC and phosphine complexes for the CuAAC formation of 5-iodo-1,2,3-triazoles (Fig. 22). The experimental/computational-DFT results suggested that iodoalkynes might be prone to dehalogenation under copper catalysis conditions. Two distinct mechanistic pathways that proceed through a copper(III) metallacycle or by direct π-activation of the starting iodoalkyne are likely to be competitive with these catalysts [112a]. Other carbene ligands that were recently used with success in catalysis of click reactions include abnormal N-heterocyclic carbenes (*a*NHCs) [55,114], mesoionic carbenes (MIC) and ring-expanded carbenes (RE-NHCs) [115]. With copper(I) complexes of triazolylidene ligands (Fig. 23a) [116] the halide-free complexes [Cu(*a*NHC)][BF$_4$], **20–23**, are more efficient than the halide-containing complexes **18** and **19** in catalyzing CuAAC reactions. The complex [CuCl(*a*NHC)] (Fig. 23b) catalyzed CuAAC reactions in excellent yield at r.t. within short reaction time under solvent-free conditions [117]. With the complex [Cu(I)(MIC)], addition of a phenanthroline derivative generated

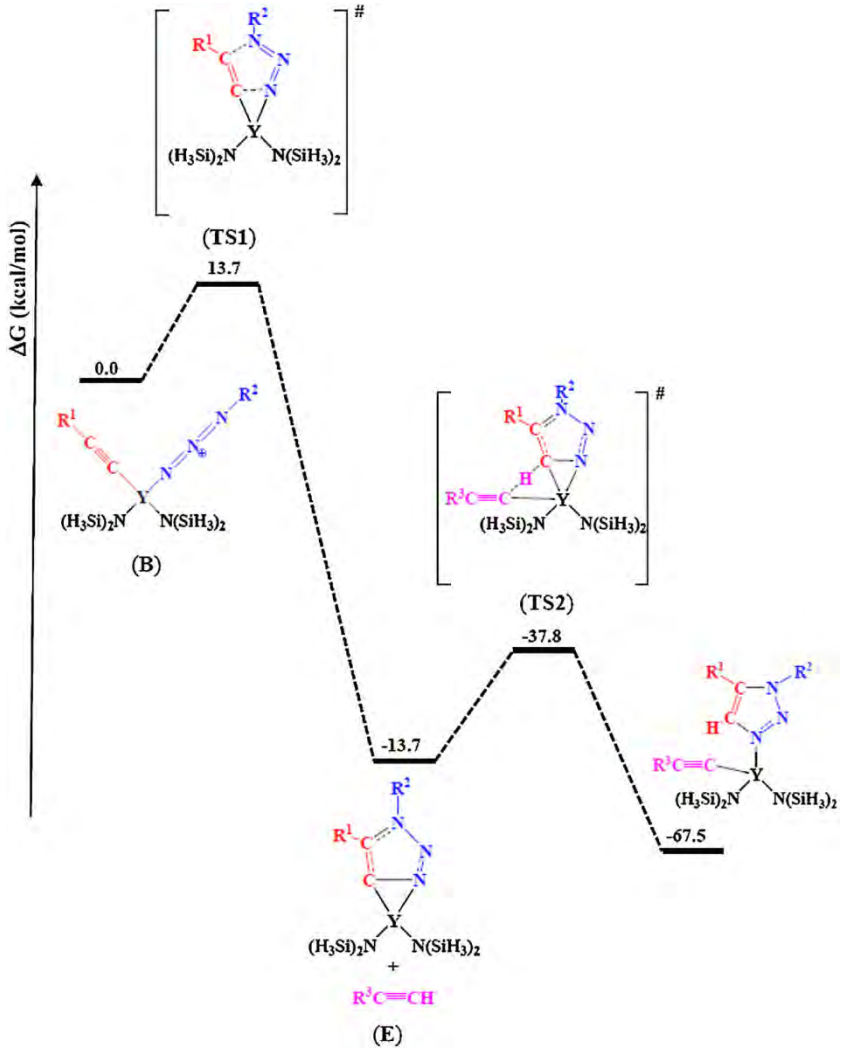

Fig. 21. DFT free energy profile (in kcal/mol) computed for the mechanism of the formation of 1,5-triazole catalyzed by a rare-earth complex reported in Ref. [110] ($R^1 = R^2 = H$; relative free energy values).

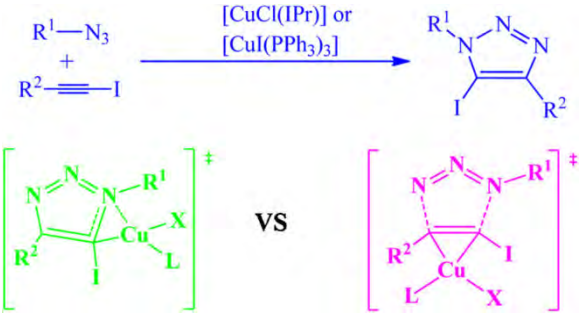

Fig. 22. NHC or phosphine-containing copper(I) complexes for the synthesis of 5-iodo-1,2,3-triazoles.

Reproduced with permission from Ref. [112a]. Copyright 2014 American Chemical Society.

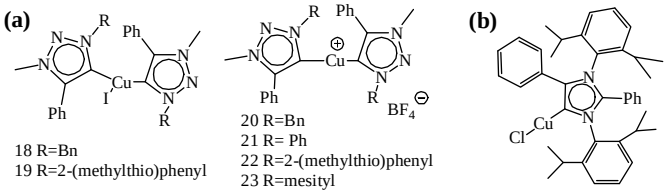

Fig. 23. (a) Copper(I)-triazolylidene complexes. (b) *a*NHC coordinated copper(I) chloro complex.

Reproduced with permission from Refs. [116] and [117], respectively. Copyright 2013, WILEY-VCH.

a highly active catalyst that surpassed the performances of a "normal" NHC complex, which was taken into account by the combination of a greater electron-donating character of the carbene ligand and a less crowded environment of the catalytic center [118]. Beside the NHC ligands, Cu(I) complexes bearing one or two α-diimine ligands [119], hybrid nitrogen–sulfur ligand-supported Cu(I)/(II) complexes [120] were also highly efficient. Other recently reported useful systems include Cu(II) complexes supported by mixed NN, NO, and NS 1,2,3-triazole based ligands utilized together with sodium ascorbate [121], Cu(I) complexes with pyridyl and thioether hybridized 1,2,3-triazole ligands [122], Cu(I) complexes containing sulfur-based ligand [123], Cu(I) complexes with new chiral phosphine ligand [124], dinuclear Cu(I) complex ($Cu_2(pip)_2$) with (2-picolyliminomethyl)pyrrole anion ligand [125], and binuclear Cu(I) complex of (*N*′1E,*N*′2E)-*N*′1,*N*′2-bis(phenyl(pyridin-2-yl)methylene)oxalohydrazide ligand [126]. On the other hand, Cu(II) species without deliberate addition of a reducing agent for CuAAC reactions have also been investigated. The mechanistic studies indicated that the real catalytic Cu(I) species were

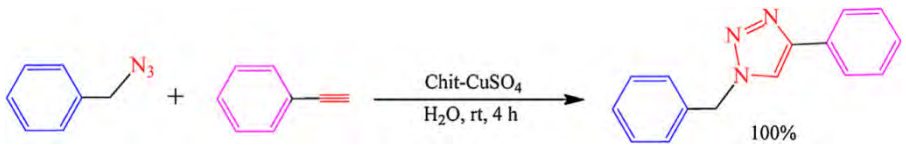

Fig. 24. Chit–$CuSO_4$ catalyzed dipolar cycloaddition of benzyl azide and phenyl acetylene (Chit = chitosan).
Reproduced with permission from Ref. [132]. Copyright 2013, Royal Society of Chemistry.

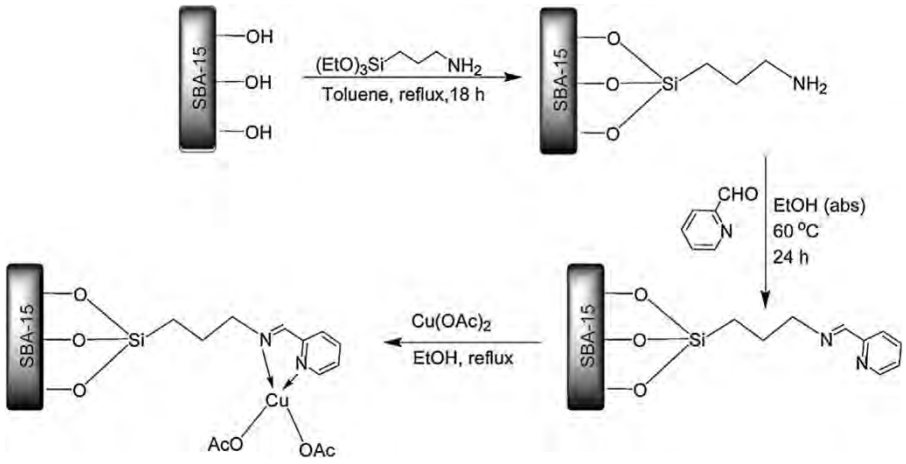

Fig. 25. Synthesis of the Cu@PyIm-SBA-15 catalyst.
Reproduced with permission from Ref. [134a]. Copyright 2014, Elsevier B.V.

generated in a short induction period via reducing Cu(II) salts by alcoholic solvents [127], sodium azide [46,128], or thiobenzanilide [129] especially in the three-component 1,3-dipolar cycloaddition for 1,4-disubstituted 1,2,3-triazoles synthesis. For instance, the recently reported 2-pyrrolecarbaldiminato-Cu(II) complexes efficiently catalyzed three-component 1,3-dipolar cycloaddition reaction of benzyl halides and sodium azide with terminal alkynes in water at r.t., leading to the synthesis of several regioselective 1,4-disubstituted 1,2,3-triazoles in 55–97% yield [130]. On the other hand, the direct use of Cu(I) complexes to catalyze three-component reactions of *N*-tosylhydrazones, terminal alkynes and azides to efficiently synthesize 1,4,5-trisubstituted 1,2,3-triazoles with good to excellent yield has also recently been explored by Wang's group [131].

From the above examples and many others, the catalysts for CuAAC reactions are usually homogeneous catalysts. Although they are often very efficient, their preparation often is tedious and/or expensive. Together with the difficulties in handling and recycling the catalysts, the applications toward the click reactions using homogeneous catalysts are somehow limited. To solve these problems, considerable interest and efforts have been devoted to develop suitable supports, especially in the field of the heterogenization of homogeneous catalysts. For example, Varma's group reported a recyclable heterogeneous copper catalyst on chitosan for CuAAC reactions in water [132]. The chitosan-supported catalyst was simply obtained by stirring an aqueous suspension of chitosan in water with copper sulfate. The catalyst was very efficient in catalyzing CuAAC in water at r.t. (Fig. 24); it was recycled and reused at least 5 times without losing its activity and changing morphology. Pourjavadi and coworkers recently reported the immobilization of copper ions ($CuSO_4$) in a graphene oxide/poly(vinyl imidazole) nanocomposite (GO/Pim/Cu) as highly efficient, robust and recyclable catalysts for one-pot three-component cycloadditions in water in the presence of NaAsc as the reductant [133]. Moreover, they also successfully reduced the amount of catalysts to 0.002% mol with 93% isolated yield of product in water at 50 °C for 20 h.

Immobilizing Cu(II) on silica-type materials, such as SBA-15, to build up heterogeneous catalysts, has also been achieved [134]. For example, Roy's group recently reported Cu(II)-anchored functionalized mesoporous SBA-15 for one-pot CuAAC reaction [134a]. In a typical synthesis procedure shown in Fig. 25, 2-pyridine-carboxaldehyde was added to a mixture of 3-amino propyl-functionalized SBA-15 in super dry ethanol. The reaction mixture was then stirred at 60 °C for 24 h to yield SBA-15 supported imine material. Then, reaction of $Cu(OAc)_2$ with SBA-15 yielded the catalyst Cu@PyIm-SBA-15. This catalyst in low amount (0.1 Cu mol%), showed a good activity and reusability for the one-pot click reaction between azides formed in situ from the corresponding amines and acetylenes in water at 0 °C to r.t., providing a wide variety of 1,4-disubstituted 1,2,3-triazoles. The electron paramagnetic resonance (EPR) spectrum of the fresh and used catalyst suggested that copper remained in +2 oxidation state throughout the reaction which was taken into account by Cu^{2+} as catalyst, though such evidence does not prove the absence of active Cu(I) species [135]. Nasr-Esfahani reported copper immobilization on nanosilica triazine dendrimer (Cu(II)-TD@nSiO_2, Fig. 26a), and excellent yield via a one-pot three-component reaction of alkynes and sodium azide with organic halides or α-bromo ketones at r.t. (Fig. 26b). Sodium ascorbate was then needed to reduce Cu(II) to Cu(I) [136], and the synthesis of 1,4-disubstituted 1,2,3-triazoles and bis- and tris-triazoles proceeded in a single-step operation. Cu(I) catalytic species were also reported upon immobilization onto solid supports for CuAAC reactions, such as silica cuprous sulfate (CDSCS) doped with Cu(I) [137], Cu(I) on modified poly(styreneco-maleic anhydride) [138], Cu(I) onto triazole functionalized Fe_3O_4 [139] and CuBr on graphene oxide/Fe_3O_4 [140].

Cu_2O, another Cu(I) source, is also used for the CuAAC reactions, though in some cases a stabilizer such as PVP was used to enable the formation of the well-defined and small copper(I) oxide [141]. Bai and Chen's group demonstrated the safe and high efficient synthesis of triazole drugs by using a Cu_2O-NP catalyst in aqueous/organic solvents (CH_3CN and H_2O) for the key AAC stage

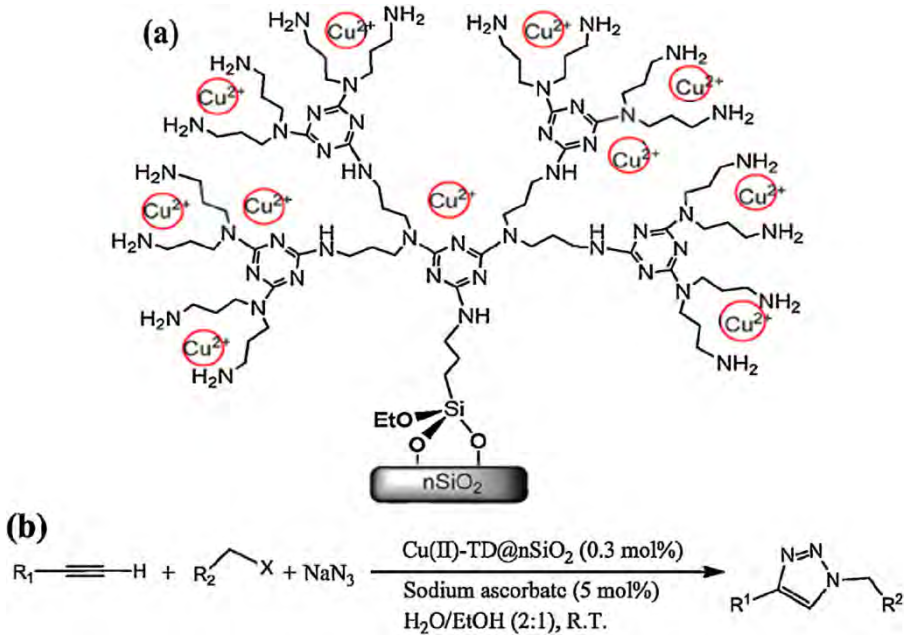

Fig. 26. (a) Structure of Cu(II)-TD@nSiO_2, (b) Cu(II)-TD@nSiO_2-catalyzed three-component synthesis of 1,4-disubstituted 1,2,3-triazoles from alkyl/benzyl halides. Reproduced with permission from Ref. [136]. Copyright 2014, American Chemical Society.

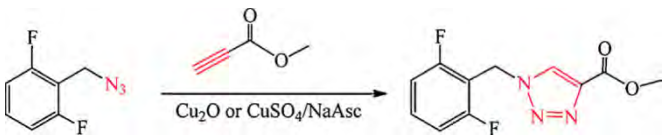

Fig. 27. AAC reactions catalyzed by Cu_2O-NP and $CuSO_4$/NaAsc. Reproduced with permission from Ref. [142]. Copyright 2013, Elsevier B.V.

(Fig. 27) [142]. In their study, Cu_2O-NP was more efficient than $CuSO_4$/NaAsc, which was explained by the fact that the Cu_2O-NP catalyst was dispensed in both organic solvent and water, while the $CuSO_4$/NaAsc system required higher ratio of water. The in situ generated Cu_2O together with HOAc exhibited better catalytic efficiency than isolated Cu_2O combined with HOAc [143]. The Cu(II) species in $Cu(OAc)_2{\cdot}H_2O$ was also reduced to Cu(I) by $NH_2NH_2{\cdot}H_2O$ that could in situ generate Cu_2O-NPs and HOAc to efficiently catalyze CuAAC reactions in water at r.t. with relatively short reaction times. However, drawbacks are obvious, because of the unrecoverable and unreusable properties of small molecular organic acids. In order to overcome these problems, the authors latter on combined Cu_2O and carboxymethylpullulan (CMP) for high-yield CuAAC reactions in water with a relatively short reaction times, and CMP still remained in water enabling easy recoverability and reusability [144]. Very recently, Cu_2O supported on graphene nanosheet [145] served as recyclable and reusable heterogeneous catalyst with excellent catalytic activity for CuAAC. More importantly, an excellent performance was also obtained for bulk CuAAC reactions via melt-rheology with trivalent azide- and alkyne-functionalized polyisobutylenes (PIB) at r.t. (Fig. 28), which was useful for designing self-healing materials. Additionally, special rhombic dodecahedra Cu_2O bounded by the {110} facets was also a promising heterogeneous catalyst for multicomponent AAC reactions [146].

Copper nanoparticles (CuNPs) have attracted interest for the CuAAC reactions due to their large surface area, tunable morphology and sustainable catalytic activities. For CuNP-catalyzed AAC, Scaiano et al. successively proved that catalysis occurred at the surface of the CuNPs by standard bench scale techniques with single-molecule spectroscopy [78a]. Following the seminal report

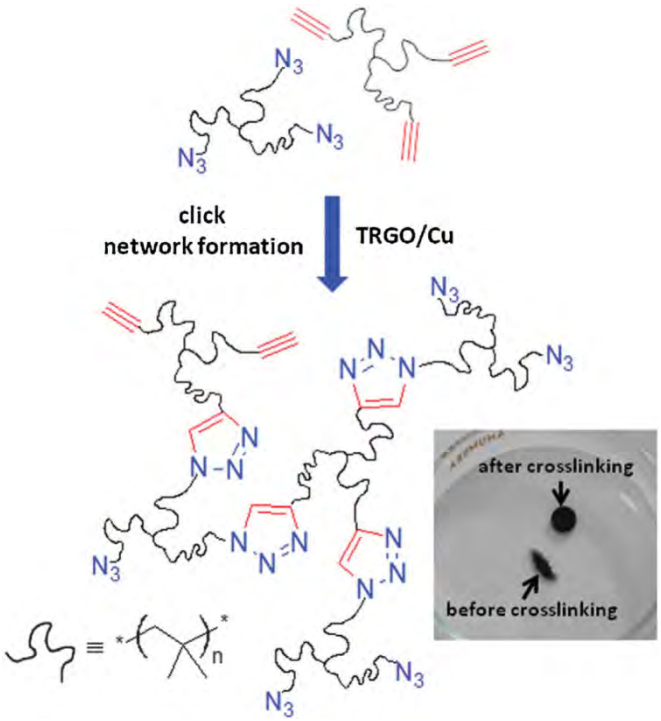

Fig. 28. Schematic illustration of the bulk CuAAC reaction of PIB-azide and PIB-alkyne with TRGO/Cu(I) at 20 °C via melt rheology.
Reprinted with permission from Ref. [145a]. Copyright 2014, Royal Society of Chemistry.

on the use of CuNPs to catalyze the CuAAC reaction by Fokin et al. [31], efforts have been devoted to design highly-efficient and low-cost heterogeneous CuNPs catalysts for this reaction. However, in most cases, strategies had to be developed in order to prevent CuNPs agglomeration [147], enabling the stability of small CuNPs and high activity toward CuAAC. For example, agarose was a cheap and degradable polysaccharide for the stabilization of active CuNP (CuNPs@agarose) in the size range of 4–8 nm in water under

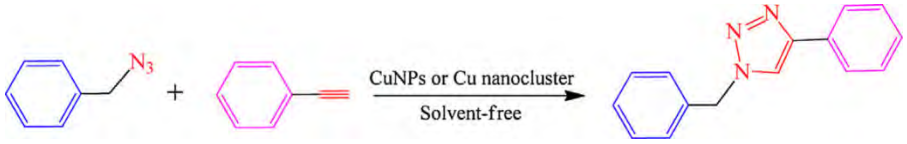

Fig. 29. CuNPs or their clusters catalyzed solvent-free AAC reaction.
Reproduced with permission from Ref. [151]. Copyright 2012, Elsevier B.V.

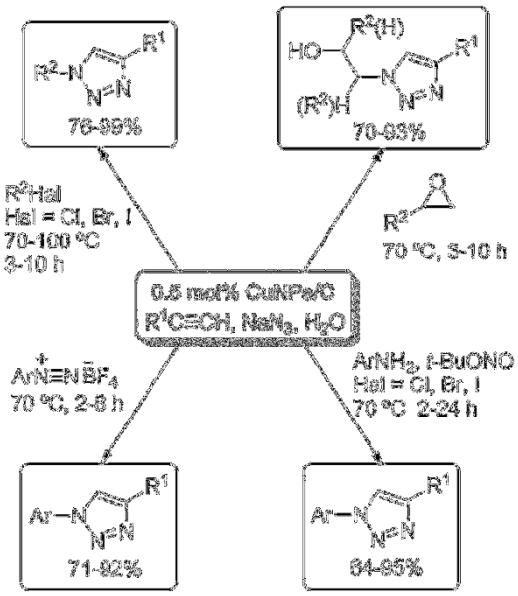

Fig. 30. Multicomponent synthesis of 1,2,3-triazoles from various azide precursors catalyzed by CuNPs/C in water.
Reproduced with permission from Ref. [153]. Copyright 2013, American Chemical Society.

low catalyst loading and mild reaction conditions [148]. The 3-aminopropylsilica support was able to stabilize smaller CuNPs with the size in the range of 1–4.5 nm, leading to very high catalytic activity (productivity up to 1689 mol/mol) in continuous-flow click reaction between phenyl acetylene and benzyl azide [149]. A more recent case showed fluorescent aggregates of hexarylbenzene derivatives serving both as reactors and stabilizers for the preparation of 9–17 nm-sized CuNPs with efficient catalysis of CuAAC reactions in excellent yield under solvent-free conditions [150].

On the other hand, Sureshan's group also successfully developed a simple methodology to generate naked CuNPs or their clusters as catalysts ($CuSO_4{\cdot}5H_2O + N_2H_4{\cdot}H_2O$) that did not require stabilizers, solid support, or special conditions for solvent-free CuAAC reactions at r.t. (Fig. 29) [151]. Interestingly, Cravotto's group successfully adopted ball-mill-based mechanochemical activation of metallic copper powder that facilitated solvent-free CuAAC reactions. This new, efficient, facile and eco-friendly procedure has afforded the corresponding 1,4-disubstituted 1,2,3-triazole derivatives in high yield and purities [152].

Alonso and Yus et al. have also investigated the use of CuNPs for multicomponent CuAAC reactions [80]. They showed that the nanostructured CuNPs supported on active carbon (CuNPs/C) catalyst displayed much higher catalytic activity than commercial bulk copper catalysts in the one-pot synthesis of 1,2,3-triazoles from inactivated alkenes. Their sequence involved two click steps including first the azidosulfenylation of the olefin, then the reaction of the in situ generated organic azide with the terminal alkyne (Fig. 30b) [153]. Other recently reported nanostructured Cu catalysts for three-component CuAAC reactions included CuNPs [154], heterogeneous porous Cu(0) [155], and CuNPs on silica coated maghemite nanoparticles (CuNPs/mag silica) [156].

Since Lipshutz's seminal study involving nickel oxide NPs in the CuAAC reaction [157], essentially Cu–M bimetallic alloys (M = metal or its oxides NPs, mainly Fe and Ni) have been explored in the AAC reaction. Among these various bimetallic alloyed nanostructures for AAC, Cu is known for its catalytic efficiency, while M is known for its magnetic nature or other catalytic efficiencies except for AAC. In the case of the CuFe system, although Nageswar's group showed the successful multicomponent synthesis of 1,4-disubstituted 1,2,3-triazoles in water at 70 °C catalyzed by magnetically separable $CuFe_2O_4$ [158], low efficiency of $CuFe_2O_4$ NP-catalyzed benzyl azide and phenylacetylene cycloaddition in water at r.t. was also observed [159]. To alleviate this limitation, they then synthesized bimetallic CuFe NPs by using presynthesized FeNP-reducted $CuSO_4$. Here, the presence of FeNPs served both as the electron source to reduce Cu(II) into Cu(I) and the support for Cu(I) species to prevent their liberation as soluble ions, enabling a heterogeneous mechanism for the CuAAC reaction. Likewise, Fulop's group also recently showed that iron powder was a readily available copper scavenger for continuous-flow CuAAC [160]. By contrast, in the case of the CuNi bimetallic alloy nanostructures, heterogeneous Cu–Ni/C catalysts have independently been reported by Lipshutz's [157] and Tang's group [161]. In the former case, Cu–Ni/C mediated both group 10 and group 11 cross-couplings [157], whereas in the latter case, transformation of waste polymer materials into valuable metal/carbon heterogeneous composites was highlighted. In this approach, the Cu/Ni molar ratios (initial catalytic substances were Ni_2O_3 and CuCl) played a crucial role in the formation of the microstructures and for the catalytic functions. Although Cu–Ni/C-0.5 was used to catalyze a CuAAC reaction with high yield (97%), the reaction time was longer compared to those of previous reports [157,162], which was attributed to the amorphous nature of carbon covering the Cu particles in Cu–Ni/C-0.5, leading to insufficient catalysis [161]. On the other hand, Mandal's group also showed that chain-like bimetallic magnetic CuNi nanoalloy in the presence of polymers (PVP or PEG) is a stabilizing/structure-directing agent for CuAAC reactions with good to excellent yield in water and in DMF at r.t. XPS and zeta potential analysis confirmed that Cu(I) on the alloyed NPs surface was responsible for the catalytic activity, while the magnetic reusability was attributed to Ni [163]. This novel unsupported Cu based nanocatalyst was highlighted for its advantages of both homogeneous and heterogeneous catalysis while avoiding their drawbacks, and it was called pseudo-homogeneous catalyst. Moreover, a new bimetallic catalyst derived from nickel and copper supported on magnetite was a good catalyst for the multicomponent reaction of terminal alkynes, sodium azide, and benzyl bromide derivatives, because of the positive and synergetic effect of the metallic species [164].

The use of microwaves was a valuable assistance in CuAAC reactions upon considerably shortening reaction times, and it improved yield [20,127c,165]. Perics's group reported the synthesis of tris(triazolyl)methane ligands [166] with CuCl for CuAAC of benzyl azide with representative alkynes. For instance with tris(aryltriazolyl)methanol–CuCl (see the ligands in Fig. 31), both **24** (R = H) and the electron-poor ligand **25** ($R = CF_3$) gave high conversions. However, the ligand **26** bearing the electron-rich

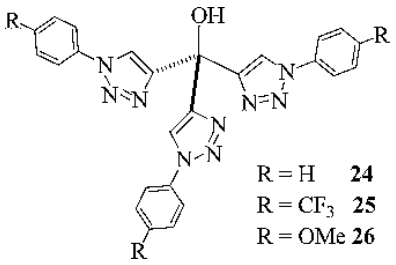

Fig. 31. Tris(aryltriazolyl)methanol ligands.
Reproduced with permission from Ref. [166c]. Copyright 2009, American Chemical Society.

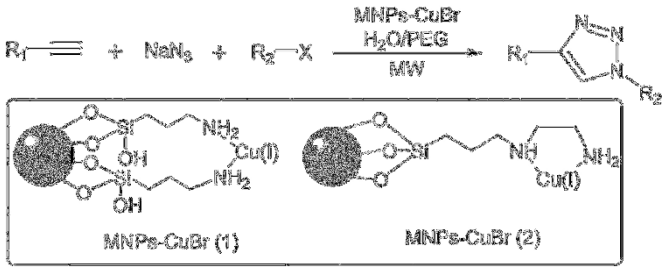

Fig. 32. MNPs–CuBr catalyzed one-pot synthesis of 1,4-disubstituted 1,2,3-triazoles in water under microwave irradiation conditions.
Reprinted with permission from Ref. [172]. Copyright 2013, Royal Society of Chemistry.

4-methoxyphenyl substituents provided a very poor catalyst in all solvents except in water. Upon taking the advantage of microwave irradiation, a quantitative reaction was observed for the CuAAC of organyl bromide and sodium azide in acetonitrile/water at 100 °C in 40 min [166c]. Other recent examples include MW-assisted of Cu–NHC-catalyzed cycloaddition of azido-disubstituted alkynes [112b], MW-assisted CuAAC of fast 2D assembling of iron oxide NPs on a self-assembled monolayer (SAM) of organic molecules [167], recoverable and recyclable Cu/SiO_2 composite for eco-friendly multicomponent synthesis of 1,2,3-triazoles [168], "copper-in-charcoal" catalyzed triazole click reactions [169], palladium and copper-supported on charcoal as heterogeneous multi-task catalysts for sequential Sonogashira-click and click-Heck reactions [170], Cu/porous glass catalyst for CuAAC in water [165c], CuNPs supported on nano-Fe_3O_4–glutathione (Cu/nano-FGT) for one-pot multicomponent synthesis of 1,2,3-triazoles [171], and Fe_3O_4-supported CuBr catalysts for one-pot and scale-up synthesis of 1,2,3-triazoles (Fig. 32) [172]. When CuNPs are used, it is indeed assumed that surface oxidation of Cu(0) to catalytically active Cu(I) species occurs upon MW irradiation.

Concerning the CuAAC reaction using the conventional Sharpless-Fokin catalyst $CuSO_4 \cdot 5H_2O$ + Na Asc. for multiple applications, the shortcoming as already mentioned above is its large quantity, together with the toxicity of copper, limiting the potential for large applications in electronics, biomedicine and biological chemistry. Thus, new Cu(I) catalysts are on the "top-wanted" list. Our group recently developed the catalyst [Cu(hexabenzyl)tren][Br] that was easily synthesized, toluene soluble, efficient, easy to separate from products and recyclable [35]. In this approach, reactions achieved TONs of the order of 10^4 reached upon recharging substrates with only 0.1 mol% amount of catalyst. The latter was active for "click" reactions between azides and alkynes in toluene or water, and the system recharged at least 10 times. A key advantage of this catalyst [35] compared to Sharpless catalyst is the tremendous ligand acceleration of the reaction.

Other recent well-defined supramolecular catalytic approaches for the CuAAC reactions such as polymer-supported catalysts of

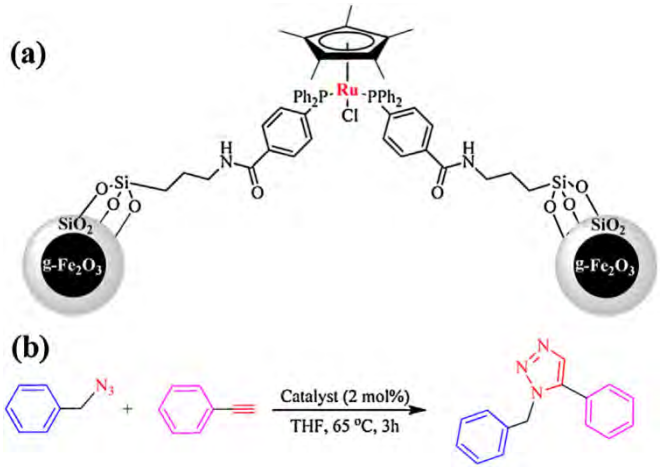

Fig. 33. (a) Magnetically recyclable $Cp^*(PPh_3)_2Ru/SiO_2/\gamma\text{-}Fe_2O_3$ catalyst. (b) Catalytic performance of magnetic catalyst in cycloaddition of phenylacetylene and benzyl azides.
Reproduced with permission from Ref. [184]. Copyright 2013, Royal Society of Chemistry.

Cu(I)-poly(styrene-*co*-maleimide) (CuI-SMI) for the one-pot three-component click synthesis of 1,4-disubstituted-1*H*-1,2,3-triazoles [138], polymer-anchored PS-C22-CuI for three-component synthesis of 1,4-disubstituted 1,2,3-triazoles under aerobic conditions in water [173], polymer-supported catalyst Amberlyst A-21-CuI for the synthesis of 1,4-disubstituted-1*H*-1,2,3-triazoles in CH_2Cl_2 at r.t. [174], Cu(I)-incorporated microporous Schiff base network polymer for CuAAC in MeCN at r.t. [175], supramolecular material of polymer supported Cu(I) catalyst, (Cu(I)-poly(2-aminobenzoic acid), Cu(I)-pABA), showed excellent yield toward AAC reactions at r.t. in aqueous media [176]. The combined use of two polymer supported reagents (polystyrene-1,5,7-triazabicyclo[4,4,0]dec-5-ene/Cu and polystyrene-2-iodoxybenzamide) enabled the reliable CuAAC in the presence of an oxidant agent [177], CuI onto dimethylamino-grafted cross-linked polystyrene (CuI@A-21) for azide-alkyne click polymerization [178], and metal–organic framework (Cu-MOF, $Cu(PTZ)(NSA)_{0.5} \cdot H_2O$) for the solvent-free CuAAC [179], were also successfully achieved.

In addition, some of the abnormal 1,2,3-triazoles, for example *N*-carbamoyl 1,2,3-triazoles [180a], and 1,4,5-trisubstituted 5-dialkylamino-1,2,3-triazole [180b] were also successfully synthesized to fill the gap.

Interestingly, the Rennes-Valparaiso groups discovered that organometallic Schiff-base copper complexes were excellent pre-catalysts for the CuAAC reactions, including with regenerated polymethylmethacrylate supports [181].

3.2. RuAAC

Recent applications of Cp*RuCl-based catalysts included the synthesis of 4-haloisoxazoles and 5-halotriazoles [81], thiolactoside glycoclusters [83], one-step synthesis of triazoles [84], palladium-based metallocene complexes [85], 1,2,3-triazole peptides [86], 5-TTF-1,2,3-triazoles [87], 1,5-substitued 1,2,3-triazole amino acids [182], 5-amino-1,2,3-triazole-4-carboxylic acid [183a], and fluorinated 1,4,5-substituted 1,2,3-triazoles [183b].

RuAAC reactions catalyzed by Ru(II) complexes and RuNPs were also reported. In the former case, our group reported the simple and efficient synthesis of magnetically recyclable magnetic NP-supported pentamethylcyclopentadienyl Ru(II) catalyst (see Fig. 33a) for RuAAC reactions to yield the fully selective construction of 1,5-disubstituted 1,2,3-triazoles [184].

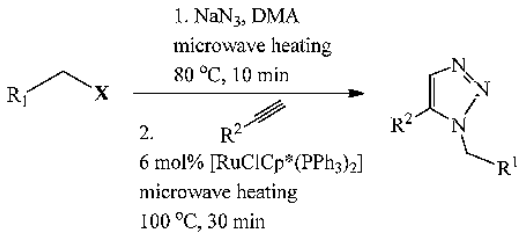

Fig. 34. Sequential one-pot RuAAC reaction under microwave heating. Reproduced with permission from Ref. [187]. Copyright 2011, American Chemical Society.

The catalyst provided excellent yield and almost 100% selectivity for the target product and was reused five times by simple magnetic separation with only a minimum decrease in catalytic activity and selectivity, (Fig. 33b) and little change in the morphology and size of the NPs.

A +3 metal oxidation state of polymer supported ruthenium complex was first demonstrated by Molla et al. who reported the synthesis of 1,4-disubstituted 1,2,3-triazoles in water with excellent yield via multicomponent coupling in aqueous medium at r.t [185]. On the other hand, Lee's group synthesized the RuNP catalyst using the co-precipitation method. The RuNP catalyst exhibited good results in terms of reactivity in the RuAAC reactions, but the size effect strongly influenced the catalytic activity of these RuNP catalysts, because the size of the catalyst was sensitive to parameters such as the pH of the medium and the type and concentration of the surfactant [186].

MW-assistance promoted RuAAC reactions [82,84,87], as recently exemplified by Johansson et al. who reported one-pot RuAAC reactions to synthesize 1,5-disubstituted 1*H*-1,2,3-triazoles involving two steps under microwave heating (Fig. 34). First of all, the organic azide was formed in situ by treating the primary alkyl halide with sodium azide in DMA under microwave heating, then the catalyst [RuClCp*$(PPh_3)_2$] was added, and a second microwave irradiation was applied to yield the cycloaddition product [187].

3.3. Applications of the CuAAC "click" reactions

The CuAAC reaction is considered as the most robust and straightforward synthetic procedure for various organic syntheses [188], especially in building novel structures, including natural products modifications [189], the synthesis of porphyrin based derivatives [190], the iterative click construction of dendrimers that are terminated with various functional groups [191], and polymers [192]. In the case of the dendrimer the "click" synthesis of a water soluble dendrimer that contained 9 intradendritic triazole rings and terminated by 27 triethylene glycol (TEG) termini was reported and used as nanoparticle stabilizer and catalyst template. This dendrimer has recently been employed as an amphiphilic micellar nanoreactor, stabilizer and activator for part-per-million Cu(I) catalyst of "click" chemistry in water under ambient conditions, due to its coordination and encapsulation abilities of Cu(I)-ions and hydrophobic Cu(I)-catalysts, respectively [27a]. The "click" synthesis of polycondensation metallopolymers containing redox-robust bis(ethynyl)biferrocene (biFc) and di(azido) poly(ethylene glycol) was also achieved [193]. This polymer showed intriguing properties; the biFc unit provided a class-II mixed-valence polyelectrolyte and electrochrome properties, while the presence of PEG in the polymer improved the water solubility and biocompatibility. The triazole linkers between biFc and PEG units facilitated redox sensing of transition-metal cations. Moreover, this easy available polymer was an excellent template for the stabilization of catalytically active AuNPs and PdNPs for 4-nitrophenol reduction and Suzuki–Miyaura reaction, respectively.

The easy accessible click approach of various material constructions has a great impact in materials science [194a,b]. The excellent reviews on click chemistry in materials science by Bowman's group [194a] and Diaz [194b] cover this area. Veige's click functionalization of inorganic complexes (inorganic click) by reaction of PPh_3AuN_3 with alkynyl- or *p*-substituted alkynyl gold complexes led to bi- and polymetallic triazoles [194c–g], and the functionalization of gold nanoparticles has also proved to be an effective method for the construction of novel nanostructures [195]. The functionalization of carbon-based nanomaterials has long attracted the interest of researchers. For example, CuAAC functionalizations of C_{60} derivatives have been achieved [196] and improved their solubility. Recent examples include the preparation of fullerene sugar balls [197], C_{60}-containing polymers [198], viral nanoparticle (VNP)-C_{60} conjugates [199], supramolecular interactions between molecular tweezers and macrocycles, functionalization of C_{70} fullerenes [200], and biotinylation of fullerene vesicle via CuAAC and conjugation with avidin [201]. Functionalized graphene and partially reduced graphene oxide (rGO) functionalized on the surface provide possibilities for improving the electrical strength recovery and utilization in devices. Functionalized rGO surface covalently immobilized with metal nanoparticles such as AuNPs and AgNPs, through the organic linkers is a good tool for achieving controllable transport in memory devices [202] and electron transfer in photocatalysis [203]. Click formation of 1,2,3-triazoles on the surface of rGO combined with localized surface plasmon resonance (LSPR) effect of the AuNPs allowed the observation of a fivefold photocurrent enhancement for triazole linkers. This showed that the triazoles linker between rGO and AuNPs were very efficient for charge separation and electron transfer [203].

In the field of biology, click chemistry has also been extensively used with various successful biological, chemical and medicinal applications [204] including nucleic acid ligation [205], bioconjugation for protein modification [206], drug design [207], gel syntheses for biomedical applications [208], chemical modification of biological molecules [209], and biomolecular labeling [210] activity-based protein profiling (ABPP) [211].

4. Conclusions and outlook

The MAAC reactions are of considerable use in synthesis with applications in materials science and biomedicine, and they remain by far the most prominent example of "click" chemistry. Therefore considerable research has been devoted to extend the variety of metal catalysts and to mechanistically understand the different MAAC reactions with the help of theoretical calculations, characterizations of intermediates and optimization of reaction parameters. In this field as in many others the theoretical calculation and experimental progress are intimately connected in order to improve the reaction efficiency, simplify procedures and apply them to industry in particular by decreasing catalytic amounts. Thus both mechanistic advances and recent trends of AAC "click chemistry" have been reviewed here. The multiple new advances are inspiring for theoretical chemists to rationalize the mechanisms of new routes. In turn, the theoretical advances guide and lead chemists to imagine new reaction improvements.

The CuAAC reaction remains the most currently used MAAC reaction, and the review has highlighted a multitude of reported improvements including the use of excellent Cu(I) ligands, copper metal and CuNPs in various forms to make this click reaction more practical and more easily applicable. The very practical initial Sharpless-Fokin catalyst $CuSO_4$ + NaAsc remains most often used, and with the use of optimized ligands researches have led to considerable decrease of the catalytic amounts down to the ppm permitting industrial applications. Some theoretical calculations have converged to the identification of a bimetallic σ, π

intermediate in a bimetallic mechanism. On the other hand, studies showed that in the presence of very low amounts of catalyst a monometallic mechanism was occurring in catalytically efficient Cu(I)-centered dendrimers with positive dendritic effect for the smaller substrates and in extraordinarily efficient dendrimer-mediated Cu(I) catalysis. The complete change of regioselectivity provided by the RuAAC reaction discovered by Fokin's group has been perfectly rationalized mechanistically, but Nolan's introduction of the NHC ligands in the RuAAC reactions showed alternative results and mechanistic features. Many more metals are active in MAAC reactions and some of them including lanthanides have been mechanistically rationalized based on theoretical calculations. Indeed, the quality of modern theoretical calculations with DFT methods now allows confident mechanistic approaches with excellent determination of reaction energetics, for both thermodynamic and kinetic sides.

In conclusion calculations and experimental research have brought MAAC at the forefront of "green chemistry" with mild, environmentally benign and useful synthetic methods that are now applicable to industry. Further work including computational and experimental research is required, however, to push MAAC toward multicomponent "one-pot" syntheses [212] for industrial production and to design multi-task catalysts based on bimetallic or multi-metallic systems for tandem reactions.

Acknowledgement

Financial support from the China Scholarship Council (CSC) of the People's Republic of China (grant to C.W.), the Universities of Bordeaux and Rennes 1 and the Centre National de la Recherche Scientifique (CNRS) are gratefully acknowledged.

References

[1] H.C. Kolb, M.G. Finn, K.B. Sharpless, Angew. Chem. Int. Ed. 40 (2001) 2004–2012.
[2] H.C. Kolb, K.B. Sharpless, Drug Discov. Today 8 (2003) 1128–1137.
[3] A.E. Speers, G.C. Adams, B.F. Cravatt, J. Am. Chem. Soc. 125 (2003) 4686–4687.
[4] H. Nandivana, X. Jiang, J. Lahann, Adv. Mater. 19 (2007) 2197–2208.
[5] J.M. Baskin, J.A. Prescher, S.T. Laughlin, N.J. Agard, P.V. Chang, I.A. Miller, A. Lo, J.A. Codelli, C.R. Bertozzi, Proc. Natl. Acad. Sci. U. S. A. 104 (2008) 16793–16797.
[6] G.C. Tron, T. Pirali, R.A. Billington, P.L. Canonico, G. Sorba, A.A. Genazzani, Med. Res. Rev. 28 (2008) 278–308.
[7] C.D. Hein, X.-M. Liu, D. Wang, Pharm. Res. 25 (2008) 2216–2230.
[8] C.A. DeForest, B.D. Polizzotti, K.S. Anseth, Nat. Mater. 8 (2009) 659–664.
[9] A.H. El-Sagheer, T. Brown, Chem. Soc. Rev. 39 (2010) 1262–1271.
[10] S.G. Agalave, S.R. Maujan, V.S. Pore, Chem. Asian J. 6 (2011) 2696–2718.
[11] N.P. Grimster, B. Stump, J.R. Fotsing, T. Weide, T.T. Talley, J.G. Yamauchi, A. Nemecz, C. Kim, K.Y. Ho, K.B. Sharpless, P. Taylor, V.V. Fokin, J. Am. Chem. Soc. 134 (2012) 6732–6740.
[12] P. Wu, A.K. Felman, A.K. Nugent, C.J. Hawker, A. Scheel, B. Voit, J. Pyun, J.M.J. Fréchet, K.B. Sharpless, V.V. Fokin, Angew. Chem. Int. Ed. 43 (2004) 3928–3932.
[13] N.V. Tsarevsky, B.S. Sumerlin, K. Matyjaszewsski, Macromolecules 38 (2005) 3558–3561.
[14] W.H. Binder, R. Sachsenhofer, Macromol. Rapid. Commun. 28 (2007) 15–54.
[15] D. Fournier, R. Hoogenboom, U.S. Schubert, Chem. Soc. Rev. 36 (2007) 1369–1380.
[16] J.-F Lutz, Angew. Chem. Int. Ed. 46 (2007) 1018–1025.
[17] W.H. Binder, R. Sachsenhofer, Macromol. Rapid. Commun. 29 (2008) 952–981.
[18] G. Franc, A. Kakkar, Chem. Commun. 42 (2008) 5267–5276.
[19] B.S. Sumerlin, A.P. Vogt, Macromolecules 43 (2010) 1–13.
[20] P.L. Golas, K. Matyjaszewski, Chem. Soc. Rev. 39 (2010) 1338–1354.
[21] L. Liang, D. Astruc, Coord. Chem. Rev. 255 (2011) 2933–2945.
[22] (a) V.V. Rostovtsev, L.G. Green, V.V. Fokin, K.B. Sharpless, Angew. Chem. Int. Ed. 41 (2002) 2596–2599;
(b) V.V. Fokin, K. Matyjaszewski, Organic Chemistry-Breakthroughs, Perspectives, Wiley-VCH Verlag GmbH & Co. KGaA, 2012, pp. 247–277.
[23] C.W. Tornøe, C. Christensen, M. Meldal, J. Org. Chem. 67 (2002) 3057–3064.
[24] M. Meldal, C.W. Tornøe, Chem. Rev. 108 (2008) 2952–3015.
[25] R. Huisgen, Angew. Chem. Int. Ed. Engl. 2 (1963) 565–598.
[26] J.E. Hein, V.V. Fokin, Chem. Soc. Rev. 39 (2010) 1302–1315.
[27] (a) C. Deraedt, N. Pinaud, D. Astruc, J. Am. Chem. Soc. 136 (2014) 12092–12098;
(b) D. Ikhlef, C. Wang, S. Kahlal, B. Maouche, D. Astruc, J.-Y. Saillard, Comput. Theor. Chem. 1073 (2015) 131–138.
[28] L. Zhang, X.G. Chen, P. Xue, H.H.Y. Sun, I.D. Williams, K.B. Sharpless, V.V. Fokin, G.C. Jia, J. Am. Chem. Soc. 127 (2005) 15998–15999.
[29] P.N. Liu, J. Li, F.H. Su, K.D. Ju, L. Zhang, C. Shi, H.H.Y. Sung, I.D. Williams, V.V. Fokin, Z.Y. Lin, G.C. Jia, Organometallics 31 (2012) 4904–4915.
[30] V.D. Bock, H. Hiemstra, J.H. van Maarseven, Eur. J. Inorg. Chem. (2005) 51–68.
[31] F. Himo, T. Lovell, R. Hilgraf, V.V. Rostovssev, L. Noodleman, K.B. Sharpless, V.V. Fokin, J. Am. Chem. Soc. 127 (2005) 210–216.
[32] V.O. Rodionov, V.V. Fokin, M.G. Finn, Angew. Chem. Int. Ed. 44 (2005) 2210–2215.
[33] S. Diez-Gonzalez, A. Correa, L. Cavallo, S.P. Nolan, Chem. Eur. J. 12 (2006) 7558–7564.
[34] D. Cantillo, M. Avalos, R. Babiano, P. Cintas, J.L. Jimenez, J.C. Placios, Org. Biomol. Chem. 9 (2011) 2952–2958.
[35] L. Liang, J. Ruiz, D. Astruc, Adv. Synth. Catal. 353 (2011) 3434–3450.
[36] D. Astruc, L. Liang, A. Rapakousiou, J. Ruiz, Acc. Chem. Res. 45 (2012) 630–640.
[37] R. Berg, B.F. Straub, Beilstein J. Org. Chem. 9 (2013) 2715–2750.
[38] B.T. Worrell, J.A. Malik, V.V. Fokin, Science 340 (2013) 457–460.
[39] B.C. Boren, S. Narayan, L.K. Rasmussen, L. Zhang, H.T. Zhao, Z.Y. Lin, G.C. Jia, V.V. Fokin, J. Am. Chem. Soc. 130 (2008) 8923–8930.
[40] D.R. Hou, T.C. Kuan, Y.K. Li, R. Lee, R.W. Luang, Tetrahedron 66 (2010) 9415–9420.
[41] E. Boz, N.S. Tuzun, J. Organomet. Chem. 724 (2013) 167–176.
[42] N.V. Sokolovaab, V.G. Nenajdenko, RSC Adv. 3 (2013) 16212–16242.
[43] R.M. Moorman, M.B. Collier, B.H. Frohock, M.D. Womble, J.M. Chalker, Org. Biomol. Chem. 13 (2015) 1974–1978.
[44] (a) B. Chattopadhyay, C.I. Rivera Vera, S. Chuprakov, V. Gevorgyan, Org. Lett. 12 (2010) 2166–2169;
(b) S. Gu, H. Xu, N. Zhang, W. Chen, Chem. Asian J. 5 (2010) 1677–1686.
[45] M. Javaherian, F. Kazemi, M. Ghaemi, Chin. Chem. Lett. 25 (2014) 1643–1647.
[46] Y. Jiang, D. Kong, J. Zhao, W. Zhang, W. Xu, W. Li, G. Xu, Tetrahedron Lett. 55 (2014) 2410–2414.
[47] M.F. Mady, G.E.A. Awad, K.B. Jørgensen, Eur. J. Med. Chem. 84 (2014) 433–443.
[48] S. Marullo, F. D'Anna, C. Rizzo, R. Noto, Ultrason. Sonochem. 23 (2015) 317–323.
[49] Q. Zhang, X. Wang, C. Cheng, R. Zhu, N. Liu, Y. Hu, Org. Biomol. Chem. 10 (2012) 2847–2854.
[50] A.N. Semakin, D.P. Agababyan, S. Kim, S. Lee, A.Y. Sukhorukov, K.G. Fedina, J. Oh, S.L. Ioffe, Tetrahedron Lett. 56 (2015) 6335–6339.
[51] D. Wang, M. Zhao, X. Liu, Y. Chen, N. Li, B. Chen, Org. Biomol. Chem. 10 (2012) 229–231.
[52] D. Wang, N. Li, M. Zhao, W. Shi, C. Ma, B. Chen, Green Chem. 12 (2010) 2120–2123.
[53] S. Diez-Gonzales, D. Edwin, S.P. Nolan, Chem. Commun. 39 (2008) 4747–4749.
[54] G. Gisado-Barrios, J. Bouffard, B. Donnadieu, G. Bertrand, Angew. Chem. Int. Ed. 49 (2010) 4759–4762.
[55] T. Nakamura, T. Terashima, K. Ogata, S. Fukusawa, Org. Lett. 13 (2011) 620–623.
[56] V.O. Rodionov, S.I. Presolski, S. Gardinier, Y.-H. Lim, M.G. Finn, J. Am. Chem. Soc. 129 (2007) 12696–12704.
[57] M. Ahlquist, V.V. Fokin, Organometallics 26 (2007) 4389–4391.
[58] (a) B.F. Straub, Chem. Commun. 37 (2007) 3868–3870;
(b) R. Berg, J. Straub, E. Schreiner, S. Mader, F. Rominger, B.F. Straub, Adv. Synth. Catal. 354 (2012) 3445–3450;
(c) A. Makarem, R. Berg, F. Rominger, B.F. Straub, Angew. Chem. Int. Ed. 54 (2015) 7431–7435.
[59] B.F. Straub, M. Bessel, R. Berg, in: P. Comba (Ed.), Modeling of Molecular Properties, Wiley-VCH, 2011, pp. 207–214.
[60] C. Özen, N.Ş. Tüzün, J. Mol. Graphics Model. 34 (2012) 101–107.
[61] E. Haldón, M. Besora, I. Cano, X.C. Cambeiro, M.A. Pericàs, F. Maseras, M.C. Nicasio, P.J. Pérez, Chem. Eur. J. 20 (2014) 1–13.
[62] S. Calvo-Losada, M.S. Pino, J.J. Quirante, J. Mol. Model. 20 (2014) 2187–2194.
[63] S. Calvo-Losada, M.S. Pino-González, J.J. Quirante, J. Phys. Chem. 119 (2014) 1243–1258.
[64] C. Iacobucci, S. Reale, J.-F. Gal, F.D. Angelis, Angew. Chem. Int. Ed. 54 (2015) 3065–3068.
[65] S. Díez-González, E.C. Escudero-Adan, J. Benet-Buchholz, E.D. Stevens, A.M.Z. Slawin, S.P. Nolan, Dalton Trans. 39 (2010) 7595–7606.
[66] J.D. Egbert, C.S.J. Cazin, S.P. Nolan, Catal. Sci. Technol. 3 (2013) 912–926.
[67] (a) M.-L. Teyssot, A. Chevry, M. Traikia, M. El-Ghozzi, D. Avignant, A. Gautier, Chem. Eur. J. 15 (2009) 6322–6326;
(b) M.-L. Teyssot, L. Nauton, J.-L. Canet, F. Cisnetti, A. Chevry, A. Gautier, Eur. J. Org. Chem. (2010) 3507–3519.
[68] (a) S. Díez-González, S.P. Nolan, Angew. Chem. Int. Ed. 47 (2008) 8881–8884;
(b) L. Jin, E.A. Romero, M. Melaimi, G. Bertrand, J. Am. Chem. Soc. 137 (2015) 15696–15698.
[69] (a) M.A. Tasdelen, Y. Yagci, Angew. Chem. Int. Ed. 52 (2013) 5930–5938;
(b) C.P. Ramil, Q. Lin, Curr. Opin. Chem. Biol. 21 (2014) 89–95;
(c) S. Dadashi-Silab, S. Doran, Y. Yagci, Chem. Rev. (2016), http://dx.doi.org/10.1021/acs.chemrev.5b00586.
[70] (a) B.J. Adzima, Y.H. Tao, C.J. Kloxin, C.A. DeForest, K.S. Anseth, C.N. Bowman, Nat. Chem. 3 (2011) 256–259;
(b) T. Gong, B.J. Adzima, N.H. Baker, C.N. Bowman, Adv. Mater. 25 (2013) 2024–2028;
(c) T. Gong, B.J. Adzima, C.N. Bowman, Chem. Commun. 49 (2013) 7950–7952;
(d) M.K. McBride, T. Gong, D.P. Nair, C.N. Bowman, Polymer 55 (2014) 5880–5884;

(e) A.A. Alzahrani, A.H. Erbse, C.N. Bowman, Polym. Chem. 5 (2014) 1874–1882.
[71] B. Sandmann, B. Happ, J. Vitz, M.D. Hager, P. Burtscher, N. Moszner, U.S. Schubert, Polym. Chem. 4 (2013) 3938–3942.
[72] (a) Y. Yagci, M.A. Tasdelen, S. Jockusch, Polymer 55 (2014) 3468–3474;
(b) S. Dadashi-Silab, B. Kiskan, M. Antoniettib, Y. Yagci, RSC Adv. 4 (2014) 52170–52173.
[73] G. Yilmaz, B. Iskin, Y. Yagci, Macromol. Chem. Phys. 215 (2014) 662–668.
[74] X. Guan, J. Zhang, Y. Wang, Chem. Lett. 43 (2014) 1073–1074.
[75] R. Beniazza, R. Lambert, L. Harmand, F. Molton, C. Duboc, S. Denisov, G. Jonusauskas, N.D. McClenaghan, D. Lastecoueres, J.-M. Vincent, Chem. Eur. J. (20) (2014) 13181–13187.
[76] M.A. Tasdelen, G. Yilmaz, B. Iskin, Y. Yagci, Macromolecules 45 (2012) 56–61.
[77] J.C. Bear, N. Hollingsworth, P.D. McNaughter, A.G. Mayes, M.B. Ward, T. Nann, G. Hogarth, I.P. Parkin, Angew. Chem. Int. Ed. 53 (2014) 1598–1601.
[78] (a) M.R. Decan, S. Impellizzeri, M.L. Marin, J.C. Scaiano, Nat. Commun. 5 (2014) 4612;
(b) T. Jin, M. Yan, Y. Yamamoto, ChemCatChem 4 (2012) 1217–1229.
[79] F. Alonso, Y. Moglie, G. Radivoy, Acc. Chem. Res. 48 (2015) 2516–2528.
[80] F. Alonso, Y. Moglie, G. Radivoy, M. Yus, Eur. J. Org. Chem. (2010) 1875–1884.
[81] J.S. Oakdale, R.K. Sit, V.V. Fokin, Chem. Eur. J. 20 (2014) 11101–11110.
[82] L.K. Rasmussen, B.C. Boren, V.V. Fokin, Org. Lett. 9 (2007) 5337–5339.
[83] A.J. Cagnoni, O. Varela, M.L. Uhrig, J. Kovensky, Eur. J. Org. Chem. (2013) 972–983.
[84] J.R. Johansson, E. Hermansson, B. Nordén, N. Kann, T. Beke-Somfai, Eur. J. Org. Chem. (2014) 2703–2713.
[85] E. Chardon, G.L. Puleo, G. Dahm, S. Fournel, G. Guichard, S. Bellemin-Laponnaz, ChemPlusChem 77 (2012) 1028–1038.
[86] D.S. Pedersen, A. Abell, Eur. J. Org. Chem. (2011) 2399–2411.
[87] T. Biet, T. Cauchy, N. Avarvari, Chem. Eur. J. 18 (2012) 16097–16103.
[88] M. Lamberti, G.C. Fortman, A. Poater, J. Broggy, A.M.Z. Slawin, L. Cavallo, S.P. Nolan, Organometallics 31 (2012) 756–767.
[89] (a) P.N. Liu, H.X. Siyang, L. Zhang, S.K.S. Tse, G. Jia, J. Org. Chem. 77 (2012) 5844–5849;
(b) H.X. Siyang, H.L. Liu, X.Y. Wu, P.N. Liu, RSC Adv. 5 (2015) 4693–4697.
[90] Y.-H. Lo, T.-H. Wang, C.-Y. Lee, Y.-H. Feng, Organometallics 31 (2012) 6887–6899.
[91] T.-H. Wang, F.-L. Wu, G.-R. Chiang, S.-T. He, Y.-H. Lo, J. Organomet. Chem. 774 (2014) 57–60.
[92] J. McNulty, K. Keskar, R. Vemula, Chem. Eur. J. 17 (2011) 14727–14730.
[93] J. McNulty, K. Keskar, Eur. J. Org. Chem. (2012) 5462–5470.
[94] A.I. Ortega-Arizmendi, E. Aldeco-Perez, E. Cuevas-Yanez, Sci. World J. (2013) 186537.
[95] N. Salam, A. Sinha, A.S. Roy, P. Mondal, N.R. Jana, S.M. Islam, RSC Adv. 4 (2014) 10001–10012.
[96] T.U. Connell, C. Schieber, I.P. Silvestri, J.M. White, S.J. Williams, P.S. Donnelly, Inorg. Chem. 53 (2014) 6503–6511.
[97] A.M. Ferretti, A. Ponti, G. Molteni, Tetrahedron Lett. 56 (2015) 5727–5730.
[98] A.A. Ali, M. Chetia, B. Saikia, P.J. Saikia, D. Sarma, Tetrahedron Lett. 56 (2015) 5892–5895.
[99] (a) A. Gourdon, Angew. Chem. Int. Ed. 47 (2008) 6950–6953;
(b) D. Perepichka, F. Rosei, Science 323 (2009) 216–217.
[100] F. Bebensee, C. Bombis, S.-R. Vadapoo, J.R. Cramer, F. Besenbacher, K.V. Gothelf, T.R. Linderoth, J. Am. Chem. Soc. 135 (2013) 2136–2139.
[101] O.D. Arado, H. Monig, H. Wagner, J.-H. Franke, G. Langewisch, P.A. Held, A. Studer, H. Fuchs, ACS Nano 7 (2013) 8509–8515.
[102] M. Boominathan, N. Pugazhenthiran, M. Nagaraj, S. Muthusubramanian, S. Murugesan, N. Bhuvanesh, ACS Sustain. Chem. Eng. 1 (2013) 1405–1411.
[103] E. Rasolofonjatovo, S. Theeramunkong, A. Bouriaud, S. Kolodych, M. Chaumontet, F. Taran, Org. Lett. 15 (2013) 4698–4701.
[104] S. Ding, G. Jia, J. Sun, Angew. Chem. Int. Ed. 53 (2014) 1877–1880.
[105] Q. Luo, G. Jia, J. Sun, Z. Lin, J. Org. Chem. 79 (2014) 11970–11980.
[106] H.S.P. Rao, G. Chakibanda, RSC Adv. 4 (2014) 46040–46048.
[107] S. Chassaing, A.S.S. Sido, A. Alix, M. Kumarraja, P. Pale, J. Sommer, Chem. Eur. J. 14 (2008) 6713–6721.
[108] X. Meng, X. Xu, T. Gao, B. Chen, Eur. J. Org. Chem. (2010) 5409–5414.
[109] (a) C.D. Smith, M.F. Greaney, Org. Lett. 15 (2013) 4826–4829;
(b) Y. Li, X. Qi, Y. Lei, Y. Lan, RSC Adv. 5 (2015) 49802–49808.
[110] L. Hong, W. Lin, F. Zhang, R. Liu, X. Zhou, Chem. Commun. 49 (2013) 5589–5591.
[111] J.M. Wang, S.B. Yu, Z.M. Li, Q.R. Wang, Z.T. Li, J. Phys. Chem. A 119 (2015) 1359–1368.
[112] (a) S. Lal, H.S. Rzepa, S. Díez-Gonzalez, ACS Catal. 4 (2014) 2274–2287;
(b) Y. Xia, L. Chen, S. Lv, Z. Sun, B. Wang, J. Org. Chem. 79 (2014) 9818–9825;
(c) J.-M. Collinson, J.D.E.T. Wilton-Ely, S. Diez-Gonzalez, Chem. Commun. 49 (2013) 11358–11360;
(d) E. Tasca, G.L. Sorella, L. Sperni, G. Struku, A. Scarso, Green Chem. 17 (2015) 1414–1422.
[113] F. Lazreg, A.M.Z. Slawin, C.J. Cazin, Organometallics 31 (2012) 7969–7975.
[114] S. Hohloch, C.-Y. Su, B. Sarkar, Eur. J. Inorg. Chem. (2011) 3067–3075.
[115] L.R. Collins, T.M. Rookes, M.F. Mahon, I.M. Riddlestone, M.K. Whittlesey, Organometallics 33 (2014) 5882–5887.
[116] S. Hohloch, D. Scheiffele, B. Sarkar, Eur. J. Inorg. Chem. (2013) 3956–3965.
[117] S.C. Sau, S.R. Roy, T.K. Sen, D. Mullangi, S.K. Mandal, Adv. Synth. Catal. 355 (2013) 2982–2991.
[118] S. Hohloch, B. Sarkar, L. Nauton, F. Cisnetti, A. Gautier, Tetrahedron Lett. 54 (2013) 1808–1812.
[119] J.M. Barta, S. Díez-González, Molecules 18 (2013) 8919–8928.
[120] S.-Q. Bai, L. Jiang, J.-L. Zuo, T.S.A. Hor, Dalton Trans. 42 (2013) 11319–11326.
[121] D. Mendoza-Espinosa, G.E. Negrón-Silva, D. Ángeles-Beltrán, A. Álvarez-Hernández, O.R. Suárez-Castillo, R. Santillán, Dalton Trans. 43 (2014) 7069–7077.
[122] L. Jiang, Z. Wang, S.-Q. Bai, T.S.A. Hor, Dalton Trans. 42 (2013) 9437–9443.
[123] B.-H. Lee, C.-C. Wu, X. Fang, C.W. Liu, J.-L. Zhu, Catal. Lett. 143 (2013) 572–577.
[124] T. Song, L. Li, W. Zhou, Z.-J. Zheng, Y. Deng, Z. Xu, L.-W. Xu, Chem. Eur. J. 21 (2015) 554–558.
[125] H.-B. Chen, N. Abeyrathna, Y. Liao, Tetrahedron Lett. 55 (2014) 6575–6576.
[126] D.P. Singh, B.K. Allam, K.N. Singh, V.P. Singh, J. Mol. Catal. A: Chem. 398 (2015) 158–163.
[127] (a) G.-C. Kuang, H.A. Michaels, J.T. Simmons, R.J. Clark, L. Zhu, J. Org. Chem. 75 (2010) 6540–6548;
(b) W.S. Brotherton, H.A. Michaels, J.T. Simmons, R.J. Clark, N.S. Dalal, L. Zhu, Org. Lett. 11 (2009) 4954–4957;
(c) P. Appukkuttan, W. Dehaen, V.V. Fokin, E. Van der Eycken, Org. Lett. 6 (2004) 4223–4225.
[128] S. Mohammed, A.K. Padala, B.A. Dar, B. Singh, B. Sreedhar, R.A. Vishwakarma, S.B. Bharate, Tetrahedron 68 (2012) 8156–8162.
[129] Z. Mirjafary, L. Ahmadi, M. Moradi, H. Saeidian, RSC Adv. 5 (2015) 78038–78046.
[130] C. Zhou, J. Zhang, P. Liu, J. Xie, B. Dai, RSC Adv. 5 (2015) 6661–6665.
[131] Z. Zhang, Q. Zhou, F. Ye, Y. Xia, G. Wu, M.L. Hossain, Y. Zhang, J. Wang, Adv. Synth. Catal. 357 (2015) 2277–2286.
[132] R.B.N. Baig, R.S. Varma, Green Chem. 15 (2013) 1839–1843.
[133] A. Pourjavadia, N. Safaiea, S.H. Hosseinia, C. Bennett, Appl. Organomet. Chem. 29 (2015) 601–607.
[134] (a) S. Roy, T. Chatterjee, M. Pramanik, A.S. Roy, A. Bhaumik, S.M. Islam, J. Mol. Catal. A: Chem. 386 (2014) 78–85;
(b) I. Jlalia, F. Gallier, N. Brodie-Linder, J. Uziel, J. Aué, N. Lubin-Germain, J. Mol. Catal. A: Chem. 393 (2014) 56–61.
[135] N. Mukherjee, S. Ahammed, S. Bhadra, B.C. Ranu, Green Chem. 15 (2013) 389–397.
[136] M. Nasr-Esfahani, I. Mohammadpoor-Baltork, A.R. Khosropour, M. Moghadam, V. Mirkhani, S. Tangestanineja, H.A. Rudbari, J. Org. Chem. 79 (2014) 1437–1443.
[137] M.N.S. Rad, S. Behrouz, M.M. Doroodmand, A. Movahediyan, Tetrahedron 68 (2012) 7812–7821.
[138] E. Hashemi, Y.S. Beheshtiha, S. Ahmadi, M.M. Heravi, Transit. Metal Chem. 39 (2014) 593–601.
[139] F.M. Moghaddam, S.E. Ayati, RSC Adv. 5 (2015) 3894–3902.
[140] X. Xiong, H. Chen, Z. Tang, Y. Jiang, RSC Adv. 4 (2014) 9830–9837.
[141] F. Chahdoura, C. Pradel, M. Gómez, ChemCatChem 6 (2014) 2929–2936.
[142] J.-H. Wang, C.-W. Pan, Y.-T. Li, F.-F. Meng, H.-G. Zhou, C. Yang, Q. Zhang, C.-G. Bai, Y. Chen, Tetrahedron Lett. 54 (2013) 3406–3409.
[143] Y. Jiang, D. Kong, J. Zhao, Q. Qi, W. Li, G. Xu, RSC Adv. 4 (2014) 1010–1014.
[144] W. Zhang, B. Ren, Y. Jiang, Z. Hu, RSC Adv. 5 (2015) 12043–12047.
[145] (a) A.S. Nia, S. Rana, D. Dohler, X. Noirfalise, A. Belfiore, W.H. Binder, Chem. Commun. 50 (2014) 15374–15377;
(b) A.S. Nia, S. Rana, D. Dohler, F. Jirsa, A. Meister, L. Guadagno, E. Koslowski, M. Bron, W.H. Binder, Chem. Eur. J. 21 (2015) 10763–10770;
(c) A.S. Nia, S. Rana, D. Dohler, W. Osim, W.H. Binder, Polymer 79 (2015) 21–28.
[146] K. Chanda, S. Rej, M.H. Huang, Chem. Eur. J. 19 (2013) 16036–16043.
[147] A. Kumar, S. Aerry, A. Saxena, A. Deb, S. Mozumdar, Green Chem. 14 (2012) 1298–1301.
[148] M. Gholinejad, N. Jeddi, ACS Sustain. Chem. Eng. 2 (2014) 2658–2665.
[149] R.P. Jumde, C. Evangelisti, A. Mandoli, N. Scotti, R. Psaro, J. Catal. 324 (2015) 25–31.
[150] S. Kaur, V. Bhalla, M. Kumar, Chem. Commun. 51 (2015) 526–529.
[151] A. Pathigoolla, R.P. Pola, K.M. Sureshan, Appl. Catal. A: Gen. 453 (2013) 151–158.
[152] L. Rinaldi, K. Martina, F. Baricco, L. Rotolo, G. Cravotto, Molecules 20 (2015) 2837–2849.
[153] F. Alonso, Y. Moglie, G. Radivoy, M. Yus, J. Org. Chem. 78 (2013) 5031–5037.
[154] L. Huang, W. Liu, J. Wu, Y. Fu, K. Wang, C. Huo, Z. Du, Tetrahedron Lett. 55 (2014) 2312–2316.
[155] (a) Y. Chen, Z.-J. Zhuo, D.-M. Cui, C. Zhang, J. Organomet. Chem. 749 (2014) 215–218;
(b) C. Zhang, B. Huang, Y. Chen, D.-M. Cui, New J. Chem. 37 (2013) 2606–2609.
[156] F. Nador, M.A. Volpe, F. Alonso, A. Feldhoff, A. Kirschning, G. Radivoy, Appl. Catal. A: Gen. 455 (2013) 39–45.
[157] B.H. Lipshutz, D.M. Nihan, E. Vinogradova, B.R. Taft, Z.V. Boskovic, Org. Lett. 10 (2008) 4279–4282.
[158] B.S.P.A. Kumar, K.H.V. Reddy, B. Madhav, K. Ramesh, Y.V.D. Nageswar, Tetrahedron Lett. 53 (2012) 4595–4599.
[159] R. Hudson, C.-J. Li, A. Moores, Green Chem. 14 (2012) 622–624.
[160] S.B. Otvos, G. Hatoss, A. Georgiades, S. Kovacs, I.M. Mandity, Z. Novakb, F. Fulop, RSC Adv. 4 (2014) 46666–46674.
[161] J. Gong, J. Liua, L. Ma, X. Wen, X. Chen, D. Wan, H. Yua, Z. Jianga, E. Borowiak-Palenc, T. Tang, Appl. Catal. B: Eng. 117 (2012) 185–193.
[162] B.H. Lipshutz, B.R. Taft, Angew. Chem. 118 (2006) 8415–8418.
[163] M. Biswas, A. Saha, M. Dule, T.K. Mandal, J. Phys. Chem. C 118 (2014) 22156–22165.

[164] J.M. Perez, R. Cano, D.J. Ramon, RSC Adv. 4 (2014) 23943–23951.
[165] (a) C.Y. Lee, R. Held, A. Sharma, R. Baral, C. Nanah, D. Dumas, S. Jenkins, S. Upadhaya, W.J. Du, J. Org. Chem. 78 (2013) 11221–11228;
(b) D. Ashok, D.M. Gandhi, G. Srinivas, A.V. Kumar, Med. Chem. Res. 23 (2014) 3005–3018;
(c) K. Jacob, A. Stolle, Synth. Commun. 44 (2014) 1251–1257;
(d) N. Mnasri, J.L. Nyalosaso, E. Colacino, G. Derrien, F. Lamaty, J. Martinez, J. Zajac, C. Charnay, ACS Sustain. Chem. Eng. 3 (2015) 2516–2525.
[166] (a) P. Etayo, C. Ayats, M.A. Pericàs, Chem. Commun. (2016), http://dx.doi.org/10.1039/C5CC08961A;
(b) E. Ozkal, S. Ozcubukcu, C. Jimeno, M.A. Pericas, Catal. Sci. Technol. 2 (2012) 195–200;
(c) E. Ozkal, P. Llanes, F. Bravo, A. Ferrali, M.A. Pericàs, Adv. Synth. Catal. 356 (2014) 857–869;
(d) L. Maestre, E. Ozkal, C. Ayats, Á. Beltrán, M.M. Díaz-Requejo, P.J. Pérez, M.A. Pericàs, Chem. Sci. 6 (2015) 1510–1515;
(e) D. Wang, L. Etienne, M.E. Igartua, S. Moya, D. Astruc, Chem. Eur. J. 20 (2014) 4047–4054.
[167] D. Toulemon, B.P. Pichon, C. Leuvrey, S. Zafeiratos, V. Papaefthimiou, X. Cattoen, S. Begin-Colin, Chem. Mater. 25 (2013) 2849–2854.
[168] C.S. Radatz, L.D.A. Soares, E.R. Vieira, D. Alves, D. Russowsky, P.H. Schneider, New J. Chem. 38 (2014) 1410–1417.
[169] B.R. Buckley, R. Butterworth, S.E. Dann, H. Heaney, E.C. Stubbs, ACS Catal. 5 (2015) 793–796.
[170] C. Rossy, J. Majimel, M.T. Delapierre, E. Fouquet, F.-X. Felpin, J. Organomet. Chem. 755 (2014) 78–85.
[171] R.B.N. Baig, R.S. Varma, Green Chem. 14 (2012) 625–632.
[172] X. Xiong, L. Cai, Catal. Sci. Technol. 3 (2013) 1301–1307.
[173] B. Movassagh, N. Rezaei, Tetrahedron 70 (2014) 8885–8892.
[174] R. Slimi, S. Kalhor-Monfared, B. Plancq, C. Girard, Tetrahedron Lett. 56 (2015) 4339–4344.
[175] O.S. Taskin, S. Dadashi-Silab, B. Kiskan, J. Weber, Y. Yagci, Macromol. Chem. Phys. 216 (2015) 1746–1753.
[176] R. Ullslam, A. Taher, M. Choudhary, M.J. Witcomb, K. Mallick, Dalton Trans. 44 (2015) 1341–1349.
[177] P.M. Diz, A. Coelho, A.E. Maatougui, J. Azuaje, O. Caamano, A. Gil, E. Sotelo, J. Org. Chem. 78 (2013) 6540–6549.
[178] H. Wu, H. Li, R.T. Kwok, E. Zhao, J.Z. Sun, A. Qin, B.Z. Tang, Sci. Rep. 4 (2014) 5107.
[179] P. Li, S. Regati, H. Huang, H.D. Arman, J.C.-G. Zhao, B. Chen, Inorg. Chem. Front. 2 (2015) 42–46.
[180] (a) E. Haldon, E. Alvarez, M.C. Nicasio, P.J. Perez, Chem. Commun. 50 (2014) 8978–8981;
(b) B. Wang, N. Liu, W. Chen, D. Huang, X. Wang, Y. Hu, Adv. Synth. Catal. 357 (2015) 401–407.
[181] X. Liu, N. Novoa, C. Manzur, D. Carrillo, J.-R. Hamon, New J. Chem. (2016), http://dx.doi.org/10.1039/c5nj02681d.
[182] N. Kann, J.R. Johansson, T. Beke-Somfai, Org. Biomol. Chem. 13 (2015) 2776–2785.
[183] (a) S. Ferrini, J.Z. Chandanshive, S. Lena, M.C. Franchini, G. Giannini, A. Tafi, M. Taddei, J. Org. Chem. 80 (2015) 2562–2572;
(b) Q. Shen, E. Han, Y. Huang, Q. Chen, Y. Guo, Synthesis 47 (2015) 3936–3946.
[184] D. Wang, L. Salmon, J. Ruiz, D. Astruc, Chem. Commun. 49 (2013) 6956–6958.
[185] R.A. Molla, A.S. Roy, K. Ghosh, N. Salam, M.A. Iqubal, K. Tuhina, S.M. Islam, J. Organomet. Chem. 776 (2015) 170–179.
[186] A.P. Kumar, M.-W. Baek, C. Sridhar, B.P. Kumar, Y.-I. Lee, Bull. Korean Chem. Soc. 35 (2014) 1144–1148.
[187] J.R. Johansson, P. Lincoln, B. Norden, N. Kann, J. Org. Chem. 76 (2011) 2355–2359.
[188] (a) B. Chattopadhyay, V. Gevorgyan, Angew. Chem. Int. Ed. 51 (2012) 862–872;
(b) M.A. Tasdelen, B. Kiskan, Y. Yagci, Prog. Polym. Sci. 52 (2016) 19–78;
(c) S. Dadashi-Silab, S. Doran, Y. Yagci, Chem. Rev. (2016), http://dx.doi.org/10.1021/acs.chemrev.5b00586.
[189] A. Sharma, J.F. Hartwig, Nature 517 (2015) 600–604.
[190] K. Ladomenou, V. Nikolaou, G. Charalambidis, A.G. Coutsolelos, Coord. Chem. Rev. 306 (2016) 1–42.
[191] N.E. Brahmi, S.E. Kazzouli, S. Mignani, M. Bousmina, J.P. Majoral, Tetrahedron 69 (2013) 3103–3133;
(b) M. Arseneault, C. Wafer, J.F. Morin, Molecules 20 (2015) 9263–9294.
[192] (a) K. Kempe, A. Krieg, C.R. Becer, U.S. Schubert, Chem. Soc. Rev. 41 (2012) 176–191;
(b) G. Delaittre, N.K. Guimard, C. Barner-Kowollik, Acc. Chem. Res. 48 (2015) 1296–1307;
(c) B. Yao, J.Z. Sun, A. Qin, B.Z. Tang, J. Inorg. Organomet. Polym. 25 (2015) 37–46.
[193] C. Deraedt, A. Rapakousiou, Y. Wang, L. Salmon, M. Bousquet, D. Astruc, Angew. Chem. Int. Ed. 53 (2014) 8445–8449.
[194] (a) W. Xi, T.F. Scott, C.J. Kloxin, C.N. Bowman, Adv. Funct. Mater. 34 (2014) 2572–2590;
(b) D.D. Diaz, Macromol. Symp. 358 (2015) 10–20;
(c) T.J. Del Castillo, S. Sarkar, K.A. Abboud, A.S. Veige, Dalton Trans. 40 (2011) 8140–8144;
(d) A.R. Powers, X. Yang, T.J. Del Castillo, I. Ghiviriga, K.A. Abboud, A.S. Veige, Dalton Trans. 42 (2013) 14963–14966;
(e) X. Yang, S. Wang, I. Ghiviriga, K.A. Abboud, A.S. Veige, Dalton Trans. 44 (2015) 11437–11443;
(f) A.R. Powers, I. Ghiviriga, K.A. Abboud, A.S. Veige, Dalton Trans. 44 (2015) 14747–14752;
(g) C.C. Beto, X. Yang, A.R. Powers, I. Ghiviriga, K.A. Abboud, A.S. Veige, Polyhedron (2015), http://dx.doi.org/10.1016/j.poly.2015.08.032.
[195] (a) N. Li, W.H. Binder, J. Mater. Chem. 21 (2011) 16717–16734;
(b) G.K. Such, A.P.R. Johnston, K. Liang, F. Caruso, Prog. Polym. Sci. 37 (2012) 985–1003.
[196] C. Constant, S. Albert, N. Zivic, K. Baczko, H. Fensterbank, E. Allard, Tetrahedron 70 (2014) 3023–3029.
[197] M. Durka, K. Buffet, J. Iehl, M. Holler, J.-F. Nierengarten, S. Vincent, Chem. Eur. J. 18 (2012) 641–651.
[198] X.-H. Dong, W.-B. Zhang, Y. Li, M. Huang, S. Zhang, R.P. Quirk, S.Z.D. Cheng, Polym. Chem. 3 (2012) 124–134.
[199] A.M. Wen, M.J. Ryan, A.C. Yang, K. Breitenkamp, J.K. Pokorski, N.F. Steinmetz, Chem. Commun. 48 (2012) 9044–9046.
[200] K. Mulla, H. Shaik, D.W. Thompson, Y. Zhao, Org. Lett. 15 (2013) 4532–4535.
[201] K. Harano, K. Minami, E. Noiri, K. Okamotob, E. Nakamura, Chem. Commun. 49 (2013) 3525–3527.
[202] P. Cui, S. Seo, J. Lee, L. Wang, E. Lee, M. Min, H. Lee, ACS Nano 5 (2011) 6826–6833.
[203] S.G. Yenchalwar, R.R. Devarapalli, A.B. Deshmukh, M.V. Shelke, Chem. Eur. J. 20 (2014) 7402–7409.
[204] (a) T. Prakasam, M. Dariusz, J. Krzysztof, Chem. Rev. 113 (2013) 4905–4979;
(b) J. Totobenazara, A.J. Burke, Tetrahedron Lett. 56 (2015) 2853–2859.
[205] A.H. El-Sagheer, T. Brown, Acc. Chem. Res. 45 (2012) 1258–1267.
[206] (a) O. Boutureira, G.J.L. Bernardes, Chem. Rev. 115 (2015) 2174–2195;
(b) W. Tang, M.L. Becker, Chem. Soc. Rev. 43 (2014) 7013–7039.
[207] (a) C.S. McKay, M.G. Finn, Chem. Biol. 21 (2014) 1075–1101;
(b) Y. Duan, Y. Ma, E. Zhang, X. Shi, M. Wang, X. Ye, H. Liu, Eur. J. Med. Chem. 62 (2013) 11–19.
[208] (a) D.Y. Ko, U.P. Shinde, B. Yeon, B. Jeong, Prog. Polym. Sci. 38 (2013) 672–701;
(b) Y. Jiang, J. Chen, C. Deng, E.J. Suuronen, Z. Zhong, Biomaterials 35 (2014) 4969–4985.
[209] A. Lauria, R. Delisi, F. Mingoia, A. Terenzi, A. Martorana, G. Barone, A. Maria Almerico, Eur. J. Org. Chem. (2014) 3289–3306.
[210] C. Uttamapinant, A. Tangpeerachaikul, S. Grecian, S. Clarke, U. Singh, P. Slade, K.R. Gee, A.Y. Ting, Angew. Chem. Int. Ed. 51 (2012) 5852–5856.
[211] J. Martell, E. Weerapana, Molecules 19 (2014) 1378–1393.
[212] S. Hassan, T.J.J. Mülle, Adv. Synth. Catal. 357 (2015) 617–666.

Summary

In the first chapter, a Review on "**Metal-Catalyzed Azide-Alkyne "Click" Reactions: Mechanistic Overview and Recent Trends**" is presented. This review is focused on the mechanistic aspects and recent trends of the metal-catalyzed azide-alkyne cycloaddition (MAAC) "click" reactions with catalysts based on various metals (Cu, Ru, Ag, Au, Ir, Ni, Zn, Ln), although Cu(I) catalysts are still the most used ones (Figure 1).

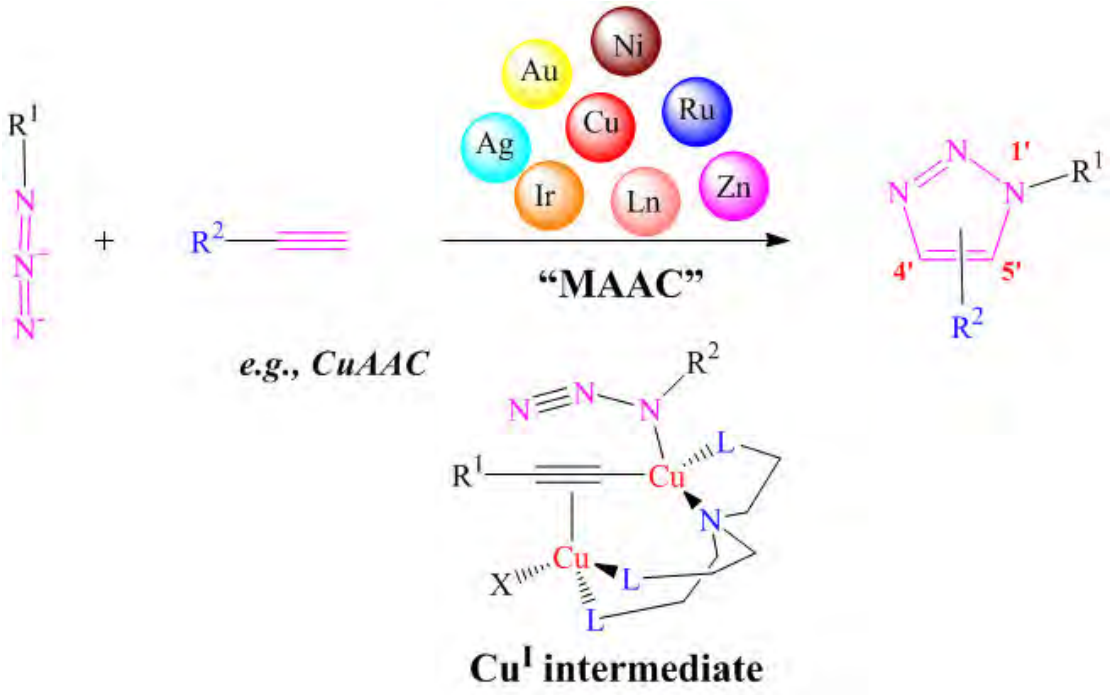

Figure 1. Metal-catalyzed azide-alkyne "click" reactions.

The concept of "click chemistry" proposed by Kolb, Finn and Sharpless in 2001[1] has revolutionized molecular engineering including applications to organic and medicinal

chemistry,[2-11] polymer science and materials science.[12-21] Among the various "click" reactions responding to the requirements of this concept, the most generally used one is the copper(I)-catalyzed reaction between terminal alkynes and azides (CuAAC) selectively yielding 1,4-disubstituted 1,2,3-triazoles, that was reported independently by the Sharpless-Fokin[22] and the Meldal groups in 2002.[23,24] This reaction is the catalyzed version of the 1,3 dipolar cycloaddition, known in the former decades as the Huisgen reaction that had already been first disclosed in the XIXth century.[25]

The advantages of the Cu(I) catalyzed "click" reaction are that:

(i) it is regioselective, whereas the non-catalyzed Huisgen reaction lacks regioselectivity, producing both the 1,4- and 1,5-disubstituted isomers;

(ii) it proceeds at milder temperature than the non-catalyzed reaction;

(iii) it fulfills the requirements of "green chemistry" in so far as it can occur in aqueous or alcoholic medium;

(iv) the catalyst reported by Sharpless and Fokin is simple and inexpensive; it consists in $CuSO_4 \cdot 5H_2O$ and sodium ascorbate.

The only drawback is the need of large quantities of this catalyst mixture that is slow. Indeed, various nitrogen ligands accelerate the Cu(I) catalysis of the "click" reaction and allow using 1% or a few % Cu (I) catalyst.[20,26] For the Cu(I) catalyzed reaction, a variety of mechanisms involving Cu(I)-aryl intermediates have been proposed in which the key-step species contains either mononuclear[27] or binuclear copper

species.[28-35]

With pentamethylcyclopentadienyl-ruthenium catalysts, however, the Fokin group showed that the other isomer, i.e. 1,5-disubstituted triazole is regioselectively formed in the RuAAC reaction even with disubstituted alkynes according to a different mechanism.[36] Ruthenium catalysis is versatile, because other ruthenium catalysts reacted with terminal alkynes via a key ruthenium-acetylide species to yield the 1,4-disubstituted triazoles.[37]

Ag(I) catalysts of the AAC reaction without copper at room-temperature (r.t.)[38] indicated that silver acetylide intermediate activated the formation of an acetylide–azide species toward cyclization.[39] An ‘‘abnormal’’ NHC complex, Ag(I)-aNHC, catalyzed the ACC reactions.[40] It showed that silver chloride by itself catalyzed the cycloaddition of various alkynes and azides in good yield, however with side reactions. Moreover, in the case of AgNP/graphene oxide (Ag/GO) catalyst, multi-component reactions and one-pot click reaction were efficiently catalyzed; the catalysts were very stable and showed no silver leaching or aggregation and were reused at least 5 times without loss of catalytic activity.[41]

For the AuAAC, X-ray photoelectron spectroscopy suggested that significant degradation of the azide upon adsorption occurred on the surface, though the reaction proceeded readily; especially the intact reactants were available on the surface.[42] On the other hand, the mechanism of heterogeneous reusable Au/TiO_2 nanostructure to efficiently catalyze the AAC reaction involves : (i) a gold atom (I) reduced the electron density on the alkyne, enabling facile nucleophilic attack by the azide; (ii) a

six member intermediate II, then intermediate III formed (iii) gold was removed to afford 1,4-disubstituted 1,2,3-triazoles and complete the reaction cycle.[43]

While in the case of iridium-catalyzed intermolecular AAC (IrAAC), the dimeric iridium complex $[Ir(cod)OMe]_2$ catalyzed the direct formation of new 1,4,5-trisubstituted triazoles.[44] The electronic features of the alkyne component strongly affected the reaction yield. Ding et al. compared various Ir complexes in the IrAAC of electron-rich internal alkynes and showed that the increase of steric hindrance on the alkyne did not affect the reaction efficiency, but an electronic effect was crucial.[45] Lin, Jia and coworkers[46] then rationalized through DFT calculations the differences in the regioselectivities of addition of thioalkynes and bromoalkynes to azides.

Raney Ni, without additional reducing agent, efficiently catalyzed acetylene azide cycloaddition reactions to form 1,2,3-triazoles with excellent yield. To explore the NiAAC reaction pathway, deuteration experiments were conducted in the presence of Ni(0) indicating that, unlike the copper-acetylide formation in CuAAC, the cycloaddition went through a metallocycle.[47]

For the ZnAAC reactions, heterogeneous zinc-on-charcoal (Zn/C) catalyzed the cycloaddition of aryl/aliphatic azides and aryl alkynes (including internal alkynes) in DMF at 50 °C without exclusion of air (63%-94% yield)[48] When ZnNPs were alloyed with CuNPs to form the catalysts for multicomponent 1,2,3-triazole synthesis/triazole alkynylation, the presence of Zn resisted the oxidation of Cu by sacrificial formation of ZnO that played a role in controlling the formation of

alkynylated triazoles.[48] On the other hand, DFT calculations towards the mechanism and regioselectivity research of this $ZnEt_2$ catalyzed regioselective formation of 1,5-substituted 1,2,3-triazoles at r.t.;[49] ethynylzinc complexes bearing alkyl substituents showed a reactivity analogous to that of ethyl(phenylethynyl)zinc and a lower regioselectivity. Higher regioselectivity was due to a lower distortion energy in the transition state and led to a lower activation energy for 1,5-disubstituted product generation.

Rare earth-metal-catalyzed AAC reaction with terminal alkynes leading to 1,5-disubstituted 1,2,3-triazoles was described by Zhou's group.[50] The authors chose $[Sm\{N(SiMe_3)_2\}_3]$ as the catalyst after compared examination of the rare-earth metal catalysts $[Ln\{N(SiMe_3)_2\}_3]$, Ln = Sm, Nd, Y, Gd. Optimization of the reaction conditions showed that the presence of 10 mol% *n*-$BuNH_2$ improved the yield. By comparison, they suggested that the involvement of an acetylide intermediate complex was essential for the efficiency and selectivity.

On the other hand, following the basic features that characterize the MAAC reactions including the state of the art in the mechanistic understanding with various metals, recent trends essentially in CuAAC and RuAAC have appeared that are gathered. The recent trends in CuAAC involve:

(i) The design of "L" ligands, well-defined supramolecular catalytic approaches in organometallic chemistry and click catalysis;

(ii) The direct use of Cu(I) complexes to catalyze three-component reactions;

(iii) Recyclable heterogeneous copper catalyst for CuAAC reactions, including the use of Cu_2O and copper nanoparticles (CuNPs) for the CuAAC reactions.

(iv) Abnormal 1,2,3-triazoles synthesis.

Moreover, recent developments of the CuAAC reaction are also reviewed in the fields of organic syntheses, materials science, and biological, chemical and medicinal applications.

The recent trends in RuAAC involve:

(i) The applications of Cp*RuCl-based catalysts to the synthesis of 1,2,3-triazoles;

(ii) The design of novel Ru(II) complexes and RuNPs catalyzed RuAAC reactions;

(iii) Physical methods promoted RuAAC reactions.

From the above short summary, considerable research has been devoted to extend the variety of metal catalysts and to mechanistically understand the different MAAC reactions with the help of theoretical calculations, characterizations of intermediates and optimization of reaction parameters. In this field as in many others the theoretical calculations and experimental progress are intimately connected in order to improve the reaction efficiency, simplify procedures and apply them to industry in particular

by decreasing catalytic amounts. Thus both mechanistic advances and recent trends of AAC "click chemistry" have been reviewed. The multiple new advances are inspiring for theoretical chemists to rationalize the mechanisms of new routes. In turn, the theoretical advances guide and lead chemists to imagine new reaction improvements.

In conclusion, calculations and experimental research have brought MAAC at the forefront of "green chemistry" with mild, environmentally benign and useful synthetic methods that are now applicable to industry. Further work including computational and experimental research is required, however, to push MAAC towards multicomponent "one-pot" syntheses[51] for industrial production and to design multi-task catalysts based on bimetallic or multi-metallic systems for tandem reactions.

Reference

[1] H. C. Kolb, M. G. Finn, K. B. Sharpless, *Angew. Chem., Int. Ed.* **2001**, *40*, 2004-2012.

[2] H. C. Kolb, K. B. Sharpless, *Drug Discov. Today* **2003**, *8*, 1128-1137.

[3] A. E. Speers, G. C Adams, B. F. Cravatt, *J. Am. Chem. Soc.* **2003**, *125*, 4686-4687.

[4] H. Nandivana, X. Jiang, J. Lahann, *Adv. Mater.* **2007**, *19*, 2197-2208.

[5] J. M. Baskin, J. A. Prescher, S. T. Laughlin, N. J. Agard, P. V. Chang, I. A. Miller, A. Lo, J. A. Codelli, C. R. Bertozzi, *Proc. Nat. Acad. Sci.* **2008**, *104*, 16793-16797.

[6] G. C. Tron, T. Pirali, R. A. Billington, P. L. Canonico, G. Sorba, A. A. Genazzani, *Med. Res. Rev.* **2008**, *28*, 278-308.

[7] C. D. Hein, X. -M. Liu, D. Wang, *Pharmaceut. Res.* **2008**, *25*, 2216-2230.

[8] C. A. DeForest, B. D. Polizzotti, K. S. Anseth, *Nat. Mater.* **2009**, *8*, 659-664.

[9] A. H. El-Sagheer, T. Brown, *Chem. Soc. Rev.* **2010**, *39*, 1262-1271.

[10] S. G. Agalave, S. R. Maujan, V. S. Pore, *Chem. Asian J.* **2011**, *6*, 2696-2718.

[11] N. P. Grimster, B. Stump, J. R. Fotsing, T. Weide, T. T. Talley, J. G. Yamauchi, A. Nemecz, C. Kim, K. Y. Ho, K. B. Sharpless, P. Taylor, V. V. Fokin, *J. Am. Chem. Soc.* **2012**, *134*, 6732-6740.

[12] P. Wu, A. K Felman, A. K. Nugent, C. J. Hawker, A. Scheel, B. Voit, J. Pyun, J. M. J. Fréchet, K. B. Sharpless, V. V. Fokin, *Angew. Chem., Int. Ed.* **2004**, *43*, 3928-3932.

[13] N. V. Tsarevsky, B. S. Sumerlin, K. Matyjaszewsski, *Macromol.* **2005**, *38*, 3558-3561.

[14] W. H. Binder, R. Sachsenhofer, *Macromol Rapid. Commun.* **2007**, *28*, 15-54.

[15] D. Fournier, R. Hoogenboom, U. S. Schubert, *Chem. Soc. Rev.* **2007**, *36*, 1369-1380.

[16] J. -F. Lutz, *Angew. Chem., Int. Ed.* **2007**, *46*, 1018-1025.

[17] W. H. Binder, R. Sachsenhofer, *Macromol. Rapid. Commun.* **2008**, *29*, 952-981.

[18] G. Franc, A. Kakkar, *Chem. Commun.* **2008**, *42*, 5267-5276.

[19] B. S. Sumerlin, A. P. Vogt, *Macromol.* **2010**, *43*, 1-13.

[20] P.L. Golas, K. Matyjaszewski, *Chem. Soc. Rev.* **2010**, *39*, 1338-1354.

[21] L. Liang, D. Astruc, *Coord. Chem. Rev.* **2011**, *255*, 2933-2945.

[22] (a) V. V. Rostovtsev, L. G. Green, V. V. Fokin,, K. B. Sharpless, *Angew. Chem.,*

Int. Ed. **2002**, *41*, 2596-2599; (b) V. V. Fokin, K. Matyjaszewski, CuAAC: the quintessential click reaction, in: Organic Chemistry-Breakthroughs, Perspectives, Wiley-VCH Verlag GmbH & Co. KGaA, **2012**, pp. 247–277.

[23] C. W. Tornøe, C. Christensen, M. Meldal, *J. Org. Chem.* **2002**, *67*, 3057-3064.

[24] M. Meldal, C. W. Tornøe, *Chem. Rev.* **2008**, *108*, 2952-3015.

[25] R. Huisgen, *Angew. Chem., Int. Ed. Engl.* **1963**, *2*, 565-598.

[26] J. E. Hein, V. V. Fokin, *Chem. Soc. Rev.* **2010**, *39*, 1302-1315.

[27] L. Liang, J. Ruiz, D. Astruc, *Adv. Syn. Catal.* **2011**, *353*, 3434-3450.

[28] V. D. Bock, H. Hiemstra, J. H. van Maarseven, *Eur. J. Inorg. Chem.* **2005**, 51-68.

[29] F. Himo, T. Lovell, R. Hilgraf, V. V. Rostovssev, L. Noodleman , K. B. Sharpless, V. V. Fokin, *J. Am. Chem. Soc.* **2005**, *127*, 210-216.

[30] V. O. Rodionov, V. V. Fokin, M. G. Finn, *Angew. Chem., Int. Ed.* **2005**, *44*, 2210-2215.

[31] S. Diez-Gonzalez, A. Correa, L. Cavallo, S. P. Nolan, *Chem. Eur. J.* **2006**, *12*, 7558-7564.

[32] D. Cantillo, M. Avalos, R. Babiano, P. Cintas, J. L. Jimenez, J. C. Placios, *Org. Biomol. Chem.* **2011**, *9*, 2952-2958.

[33] D. Astruc, L. Liang, A. Rapakousiou, J. Ruiz, *Acc. Chem. Res.* **2012**, *45*, 630-640.

[34] R. Berg, B. F. Straub, *Beilstein J. Org. Chem.* **2013**, *9*, 2715-2750.

[35] B. T. Worrell, J. A. Malik, V. V. Fokin, *Science* **2013**, *340*, 457-460.

[36] L. Zhang, X. G. Chen, P. Xue, H. H. Y. Sun, I. D. Williams, K. B. Sharpless, V. V.

Fokin, G. C. Jia, *J. Am. Chem. Soc.* **2005**, *127*, 15998-15999.

[37] P. N. Liu, J. Li, F. H. Su, K. D. Ju, L. Zhang, C. Shi, H. H. Y. Sung, I. D. Williams, V. V. Fokin, Z. Y. Lin, G. C. Jia, *Organometallics* **2012**, *31*, 4904-4915.

[38] J. McNulty, K. Keskar, R. Vemula, *Chem. Eur. J.* **2011**, *17*, 14727-14730.

[39] J. McNulty, K. Keskar, *Eur. J. Org. Chem.* **2012**, 5462–5470.

[40] A. I. Ortega-Arizmendi, E. Aldeco-Perez, E. Cuevas-Yanez, *Sci. World J.* **2013**, 186537.

[41] N. Salam, A. Sinha, A. S. Roy, P. Mondal, N. R. Jana, S. M. Islam, *RSC Adv.* **2014**, *4*, 10001-10012.

[42] F. Bebensee, C. Bombis, S.–R. Vadapoo, J. R. Cramer, Fl. Besenbacher, K. V. Gothelf, T. R. Linderoth, *J. Am. Chem. Soc.* **2013**, *135*, 2136−2139.

[43] M. Boominathan, N. Pugazhenthiran, M. Nagaraj, S. Muthusubramanian, S. Murugesan, N. Bhuvanesh, *ACS Sustainable Chem. Eng.* **2013**, *1*, 1405−1411.

[44] E. Rasolofonjatovo, S. Theeramunkong, A. Bouriaud, S. Kolodych, M. Chaumontet, F. Taran, *Org. lett.* **2013**, *15*, 4698-4701.

[45] S. Ding, G. Jia, J. Sun, *Angew. Chem., Int. Ed.* **2014**, *53*, 1877-1880.

[46] Q. Luo, G. Jia, J. Sun, Z. Lin, *J. Org. Chem.* **2014**, *79*, 11970−11980.

[47] S. Chassaing, A. S. S. Sido, A. Alix, M. Kumarraja, P. Pale, J. Sommer, *Chem.-Eur. J.* **2008**, *14*, 6713–6721.

[48] X. Meng, X. Xu, T. Gao, B. Chen, *Eur. J. Org. Chem.* **2010**, 5409–5414.

[49] C. D. Smith, M. F. Greaney, *Org. Lett.* **2013**, *15*, 4826-4829.

[50] L. Hong, W. Lin, F. Zhang, R. Liu, X. Zhou, *Chem. Commun.* **2013**, *49*,

5589-5591.

[51] S. Hassan, T. J. J. Müller, *Adv. Synth. Catal.* **2015**, *357*, 617-666.

Chapter 2

An Amphiphilic Ligand for The Stabilization of Efficient Transition Metal Nanocatalysts in Aqueous Solution

Introduction

Our group has long been engaged in the use of copper-catalyzed alkyne-azide Huisgen-type cycloaddition (CuAAC, "click" reactions) yielding weak 1,4-disubstituted 1,2,3-triazoles (trz) ligands that mildly stabilize various transition metal nanoparticles (trz-NPs) that are very efficient catalysts in water. Amphiphilic dendrimers as nanoreactors have been exploited for catalysis in water with as little as parts per million (ppm) amounts of metal amounts from TMNP catalysts.[1] The synthesis and use in catalysis of amphiphilic dendrimers as nanoreactors represents a very productive sophistication, but it is time-consuming. On the other hand, trz ligands with PEG tails were recently shown to stabilize AuNPs that catalyze 4-nitrophenol reduction in water with excellent rates.[2] We then proposed a ligand design by conceptualizing the efficient amphiphilic dendrimers with tris(triazolyl)-polyethylene glycol (tris-trz-PEG) amphiphilic ligand. The tris-trz-PEG ligand stabilized various ultrafine transition metals NPs, showing high efficiencies in the 4-nitrophenol reduction, click reaction, Suzuki-Miyaura reaction and transfer hydrogenation reaction with only part per million metal loading in water under ambient conditions.

In the second part we compare the stabilization of AuNPs by mono-, bis-, and tris-trz and their influence of the trz denticity on the 4-NP reduction by $NaBH_4$ in water also including comparison with current polyethylene glycol 2000 (PEG) and polyvinylpyrrolidone (PVP) AuNP stabilizers. We show the benefit of utilizing tris-trz-PEG amphiphilic ligand for efficient and ultrafine transition metals NPs stabilization.

In the third part, we report that the CuAAC reaction using the conventional Sharpless-Fokin catalyst that consists of $CuSO_4$ + Na ascorbate, the most well-known and used "click" reaction, is considerably accelerated by the addition of a tris(triazolyl)-polyethylene glycol (tris-trz-PEG) amphiphilic ligand in water under ambient conditions. Only parts-per-million Cu^I were necessary to reach quantitative yields with TON up to 86000 and TOF 3600 h^{-1}. The ligand was fully recycled, and

the catalyst reused at least 6 times without decomposition. Large-scale syntheses were also successfully achieved with 93 % yield. The catalyst was applied to the efficient synthesis of various useful functional products with medicinal, catalytic, targeting, and labeling properties.

[1] a) C. Deraedt, N. Pinaud, D. Astruc, *J. Am. Chem. Soc.* **2014**, *136*, 12092-12098; b) C. Deraedt, D. Astruc, *Acc. Chem. Res.* **2014**, *47*, 494-503.

[2] P. Zhao, N. Li, L. Salmon, N. Liu, J. Ruiz, D. Astruc, *Chem. Commun.,* **2013**, *49*, 3218-3220; b) N. Li, P. Zhao, N. Liu, M. Echeverria, S. Moya, L. Salmon, J. Ruiz, D. Astruc, *Chem. Eur. J.* **2014**, *20*, 8363-8369; c) N. Li, P. Zhao, M. E. Igartua, A. Rapakousiou, L. Salmon, S. Moya, J. Ruiz, D. Astruc, *Inorg. Chem.*, **2014**, *53*, 11802–11808.

Nanocatalysts

International Edition: DOI: 10.1002/anie.201511305
German Edition: DOI: 10.1002/ange.201511305

Highly Efficient Transition Metal Nanoparticle Catalysts in Aqueous Solutions

*Changlong Wang, Roberto Ciganda, Lionel Salmon, Danijela Gregurec, Joseba Irigoyen, Sergio Moya, Jaime Ruiz, and Didier Astruc**

Dedicated to Dr. Jean-René Hamon on the occasion of his 60th birthday

Abstract: *A ligand design is proposed for transition metal nanoparticle (TMNP) catalysts in aqueous solution. Thus, a tris(triazolyl)-polyethylene glycol (tris-trz-PEG) amphiphilic ligand,* ***2****, is used for the synthesis of very small TMNPs with Fe, Co, Ni, Cu, Ru, Pd, Ag, Pt, and Au. These TMNP-****2*** *catalysts were evaluated and compared for the model 4-nitrophenol reduction, and proved to be extremely efficient. High catalytic efficiencies involving the use of only a few ppm metal of PdNPs, RuNPs, and CuNPs were also exemplified in Suzuki–Miyaura, transfer hydrogenation, and click reactions, respectively.*

Since the seminal discoveries by Haruta[1] and Hutchings,[2] catalysis of chemical reactions by transition metal nanoparticles (TMNPs) has attracted considerable interest owing to its efficiency, greenness, convenient use, and improved understanding of reaction mechanisms.[3–9] The support and medium have been shown to play an essential role in TMNP catalysis, but relatively little attention has been paid to TMNP surface ligand design. Yet both TMNP formation in micelles or inverted micelles and catalysis therein are also strongly dependent on the stereoelectronic parameters of the stabilizing agents.[10–13]

Catalysis in water offers great advantages in terms of green chemistry, and has recently been actively investigated.[14–21] For instance, amphiphilic dendrimers are unimolecular micelles,[18–20] and this property has recently been exploited for catalysis in water with little as parts per million (ppm) amounts of molecular or TMNP catalysts.[21] The synthesis and use in catalysis of amphiphilic dendrimers as nanoreactors represents a very productive sophistication, but it is time-consuming, and one can conceptualize a related approach using simpler amphiphilic ligands.

Toward this goal, we suggest the design of weak, but multidentate bulky ligands that offer both easy displacement from TMNP surface by substrates for catalysis and sufficient TMNP stabilization. As a result, we report the amphiphilic tripodal ligand tris(1,2,3-triazolyl)-polyethylene glycol (tris-trz-PEG), **2**, that led to the synthesis of very small TMNPs with various transition metals (Fe, Co, Ni, Cu, Ru, Ag, Pt, Pd, and Au). These TMNP-**2** complexes are shown to be remarkably efficient catalysts of several major green reactions. First, 4-nitrophenol (4-NP) reduction by $NaBH_4$ in water was used as a model NP surface reaction to demonstrate the catalyst efficiency and compare all of these metals with one another. Then RuNP-catalyzed transfer hydrogenation of nitrobenzene with *i*-propanol as the hydrogen source in water/*i*-propanol, PdNP-catalyzed Suzuki–Miyaura cross-coupling reaction between bromobenzene and phenylboronic acid in water/EtOH, and CuNP-catalyzed azide–alkyne 1,3-cycloaddition (CuAAC, click) reaction in water were shown to work using extremely low amounts (down to a few ppm) of catalysts.

The synthesis of the tris-trz-PEG ligand **2** starts with the preparation of tris(1-benzyl-1*H*-1,2,3-triazol-4-yl)methanol,[22] **1** (Figure 1a). Three clicked trz rings of **1**, formed through CuAAC reactions,[23,24] are amphoteric π-electron-rich aromatics that are biocompatible and stable toward both oxidizing and reducing agents. They are neutral and weak ligands for TMNP core surfaces, but provide stabilization of TMNPs, owing to their bulk and compared to monodentate ligands.[25,26] This ligand is not water soluble, however, and the pursuit of green chemistry has led us to search catalysts in aqueous solution. To this end, a Williamson reaction was conducted between **1** and chlorinated PEG 2000 (mPEG2000-Cl) to form ligand **2** that contains both the tris-trz ligand and a water-solubilizing and biocompatible PEG chain. See the Supporting Information (Section 2) for the details.

The synthesis of the family of TMNP-**2** (with Fe, Co, Ni, Cu, Ru, Pd, Ag, Pt, and Au) was carried out in water at r.t. in the presence of the ligand **2** by $NaBH_4$ reduction of the transition metal salts followed by dialysis (Figure 1b; Supporting Information, Section 3). Both the trz groups of the

[*] C. Wang, Dr. R. Ciganda, Dr. J. Ruiz, Prof. D. Astruc
ISM, UMR CNRS No 5255, Univ. Bordeaux
33405 Talence Cedex (France)
E-mail: d.astruc@ism.u-bordeaux1.fr
Dr. R. Ciganda
Facultad de Quimica de San Sebastian
Universidad del Pais Vasco
Apdo. 1072, 20080 San Sebastian (Spain)
Dr. L. Salmon
Laboratoire de Chimie de Coordination, UPR CNRS No 8241
31077 Toulouse Cedex (France)
Dr. D. Gregurec, Dr. J. Irigoyen, Dr. S. Moya
CIC biomaGUNE, Unidad Biosuperficies
Paseo Miramon No 182, Edif "C"
20009 Donostia-San Sebastian (Spain)

Supporting information and ORCID(s) from the author(s) for this article are available on the WWW under http://dx.doi.org/10.1002/anie.201511305.

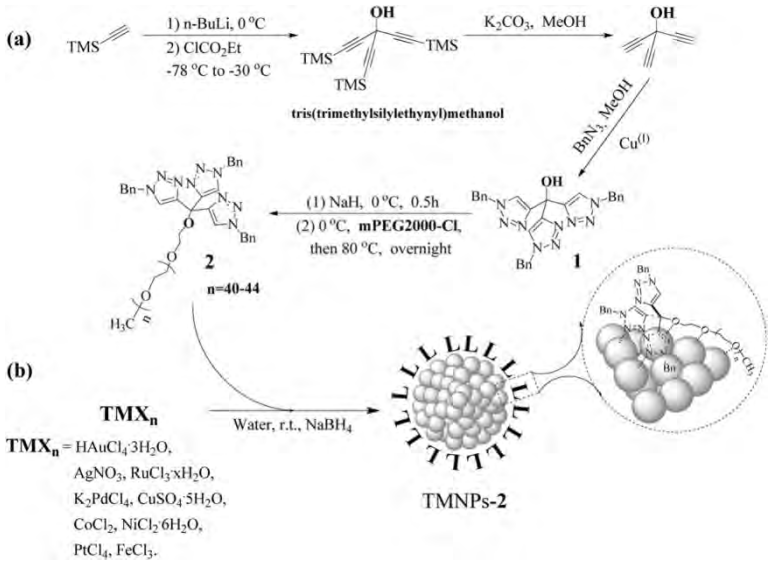

Figure 1. a) Synthesis of the amphiphilic ligand **2**. b) Synthesis of the TMNP-**2**.

tris-trz ligand and the PEG 2000 polymer are acting as weak ligands for the TMNP-**2**, whereby the synergy between weak, but multidentate, TMNP surface coordination and the overall large bulk permit the stabilization of these TMNPs (Figure 1 b). Although the neutral nitrogen ligands are known to be better ligands than the neutral oxygen ligands, the electronic delocalization within the trz ligands very much weakens the nitrogen donor ability, which should favor catalytic reactions by easy ligand substitution by substrates for surface catalysis. The thermal stability of the TMNP-**2** in water is ascertained by the lack of aggregation throughout catalytic experiments, even upon heating under inert atmosphere (see below).

For instance, with AuNP-**2**, refluxing the aqueous solution for 5 hours did not provoke aggregation or any change of the SPB at 515 nm (Figure S15). Moreover, although the large class of AuNPs with thiolate ligands contain Au^I surface atoms, in the present case the X-ray photoelectron spectroscopy (XPS) signals at 84.05 eV for Au $4f_{7/2}$ of AuNP-2 clearly show the presence of only Au^0 surface atoms (Figure 2 a and S16). We selected the 4-NP reduction to 4-AP by $NaBH_4$ in water catalyzed by TMNPs [Eq. (1)] as a standard reaction that can be used to evaluate the potential of the new ligand **2** to promote catalytic activity at the surface of TMNP-**2**. This homogeneous reaction is simple, without side paths, and easily monitored through UV/Vis spectroscopy by the decrease of the strong adsorption of the 4-NP anion at 400 nm.[27–29] The Ballauff group has shown that the mechanism (although unknown) involves rearrangement of the substrates 4-NP and $NaBH_4$ at the AuNP surface according to the Langmuir–Hinshelwood (LH) kinetic model, that is, the diffusion of the reactants is fast compared to the rate-limiting substrate rearrangement at the AuNP surface.[27]

The AuNP-**2** displays a surface plasmon band (SPB) at 515 nm in the UV/Vis spectrum, and a core size of 2.9 ± 0.3 nm in TEM (Table 1; Supporting Information). First, the 4-NP reduction in water catalyzed by AuNP-**2** was conducted [Eq. (1)], and the reaction rates show that the AuNP-**2** is one of the most efficient catalysts known ($k_{app} = 4.37 \times 10^{-2}\ s^{-1}$), compared with other catalysts from the literature (Supporting Information, Table S2). In addition, no induction times are found for the AuNP-**2**, although the latter was observed in previous studies of thiolate-AuNPs and citrate-AuNPs.[30] The very high reaction rates observed here, and the absence of induction time, reveal the successful design of AuNP-**2** as very efficient catalysts, as expected from the weak bonding ability of the trz- and PEG-coordination to AuNPs. The catalyst AuNP-**2** was recycled five times with reaction rates that decreased only overall by less than 20 %, showing good stereoelectronic stabilization by the ligand **2**, although the catalyst undergoes Ostwald ripening illustrated by the core size increase and slight variations by a few nm in the SPB. This structural change is due to catalysis at the AuNP-**2** surface, introducing the 4-AP product as a ligand. Precipitation is never observed, however. Finally, we compared 4-NP reduction catalyzed by AuNP-**2** and AuNP-**3**, the latter being stabilized by the ligand trz-PEG 2000, **3**, which contains a single trz ligand (Figure S10).

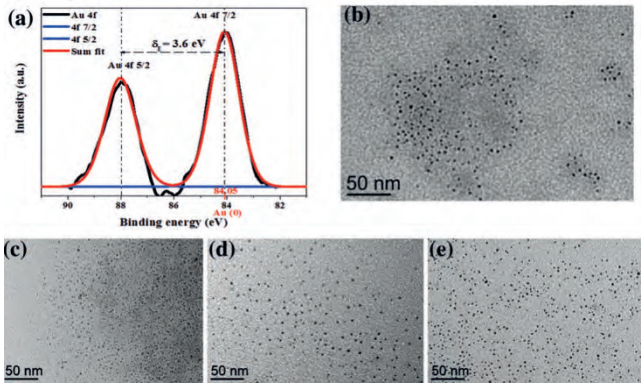

Figure 2. Characterization of TMNP-**2**. a) X-ray photoelectron spectroscopy (XPS) of Au 4f. Typical TEM images of the as-synthesized: b) AuNPs, c) PdNPs, d) AgNPs, and e) PtNPs. For additional characterization of TMNP-**2**, see the Supporting Information, Section 3.

In this way, the goal was to examine the influence of the multiplicity of the mono- versus tris-trz ligands containing the same PEG tail. The results indicate that the catalysis of 4-NP was significantly faster with AuNP-**2** ($k_1 = 0.410\ L\,s^{-1}\,m^{-2}$) than with AuNP-**3** ($k_1 = 0.253\ L\,s^{-1}\,m^{-2}$), showing the positive influence on catalysis of the tris-trz ligand bulk in **2** near the AuNP-**2** surface.

We then extended the use of **2** to the synthesis of TMNP-**2** with both cheap, abundant metals (Fe, Co, Ni, and Cu), and some other second- and third-row noble transition metals (Ru, Pd, Pt, and Ag) in the same manner as for the above-mentioned preparation of AuNP-**2** (Figure 1 b). Interestingly, most of the TMNPs were formed with **2** in their nanocluster size (< 2 nm), except the CoNPs and AgNPs which were

Table 1: 4-NP reduction by $NaBH_4$ catalyzed by TMNP-**2** in water at 20 °C.

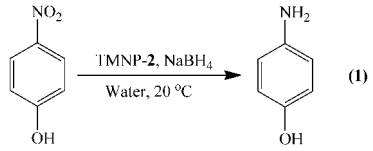

(1)

TMNP-**2**	Amount[a] [mol%]	D_{core}[b] [nm]	t_0[c] [s]	k_{app}[d] [10^{-3} s^{-1}]	k_1[e] [$L\,s^{-1}\,m^{-2}$]
FeNPs	2	1.3	780	1.88	1.21×10^{-3}
CoNPs	2	2.1	420	1.47	1.57×10^{-3}
NiNPs	2	1.6	720	0.30	2.69×10^{-4}
CuNPs	2	1.4	940	2.48	1.75×10^{-3}
AgNPs	2	2.2	520	7.85	6.07×10^{-3}
PtNPs	0.2	1.7	0	1.86	1.17×10^{-2}
RuNPs	0.2	1.0	0	3.15	1.26×10^{-2}
PdNPs	0.2	1.5	0	24.80	0.137
AuNPs	0.2	2.9	0	43.70	0.410

[a] Amount of TMNP-**2** used in the catalyzed 4-NP reduction. $NaBH_4$ is in excess. [b] Core size (TEM) of the TMNP-**2**. [c] Induction time. [d] Rate constant. [e] Surface-independent rate constant.

slightly larger than 2 nm (Table 1). This small size is advantageous for catalysis because the majority of atoms (54–70%) are located on the TMNP surface for these metals (Fe, Ni, Cu, Ru, Pd, and Pt), forming monodispersed TMNP-**2** cores with diameters smaller than 2 nm (Figure 2b–e; Supporting Information, Section 3). Thus, the catalytic properties of these TMNP-**2** were also evaluated for the model 4-NP reduction with $NaBH_4$ [Eq. (1)].

For the group of first-row NPs, the induction time was observed in all the cases, and these TMNP-**2** exhibited the reaction rate order of Cu > Co > Fe > Ni in k_1 ($k_1 = k_{app}/S$, S being the NP core surface area).[27,28] Interestingly, no SPB of CuNP-**2** was observed, whereas a SPB at 590 nm was observed for large CuNPs in the absence of **2** (Figure S18). Indeed, the SPB is absent in the UV/Vis spectra of the very small nanoclusters, in which the molecular structure dominates.[31,32] CuNP-**2**, with its small size (1.4 nm), presented no SPB, and showed a reaction rate of $k_1 = 1.75\times10^{-3}\,L\,s^{-1}\,m^{-2}$.

Other noble metal NP-**2** (Au, Pd, and Pt) catalyzed the 4-NP reduction very well, using only 0.2 mol% catalyst, and no induction time was observed. In this category, the reaction rate k_1 decreased with the order of Au > Pd > Pt > Ag. In the group 11 (Cu, Ag, and Au), from the first to the third row of transition metals, the induction time decreases, and the reaction rates greatly increase, which is best taken into account by the increased facility of oxidative addition in the catalytic mechanism for heavier late transition metals (Table 1). For RuNPs, exceptionally small sizes (1 nm) and remarkably high reaction rate constants were observed ($k_1 = 1.26\times10^{-2}\,L\,s^{-1}\,m^{-2}$), ranking third best among these TMNP-**2**. Altogether, the tris-trz-PEG amphiphilic ligand **2** stabilized very small, monodispersed TMNP-**2** with high efficiencies, as shown in the comprehensive comparisons of the recent literature for reaction rate constants of TMNP-catalyzed 4-NP reduction reactions with various stabilizers (Table S3). Note that, although the first-row transition metal NP-**2** complexes exhibited high efficiencies in the 4-NP reduction when compared to other reported catalysts, their catalytic activities were still much lower than those of the noble metal NP-**2**.

For further catalytic investigations, we then selected three of the most efficient TMNP-**2** (Cu, Pd, and Ru), AuNP-2 having already been shown to exhibit excellent catalytic activity for 4-NP reduction (see above).

CuAAC[23,24] is well established as one of the most useful reactions in organic synthesis, materials science, and biomedical sciences. Recently, it has also been shown that CuNPs are active catalysts for this reaction.[33–38] CuNP-**2** was tested here as a catalyst for AAC between benzyl azide and phenylacetylene [Eq. (2)], and found to be highly efficient. This reaction was quantitatively achieved at 35 °C for 24 h using only 20 ppm of Cu from CuNP-**2**, leading to an exceptional TON of 28 000 and TOF of 1170 h^{-1} (Table S4). This is one of the best results ever obtained using CuNP catalysts.

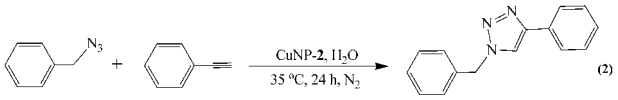

(2)

For the investigation of the actually active species, X-ray photoelectron spectroscopy (XPS) of CuNPs was conducted (Figure 3). The main Cu peak, Cu $2p_{3/2}$, is found at binding energy (BE) of 932.6 eV (Figure 3a). The very weak satellite at around 945 eV gives the first indication of Cu^{I} and the absence of Cu^{2+}. Other indications for assignment to Cu^{I} are on one hand the Cu $2p_{3/2}$ peak at a relatively high FWHM compared to the C 1 s peaks (2.3 eV vs. 1.4 eV; Figure 3a and S45), and on the other hand the modified Auger parameter calculated from the Cu LMM (Figure 3b) that is assigned to Cu^{I} (Supporting Information, Section 5). All of these data showed that the catalyst was in its classic Cu^{I} state.[23,24] It is unavoidable that the CuNPs surface is oxidized by molecular oxygen from the air, and the active Cu^{I} species is thus formed in the native oxide layer on the Cu surface through comproportionation of Cu^{0} and Cu^{II}, even if caution is taken to remove air. Recycling experiments using 100 pm of Cu from CuNP-**2** provided yields larger than 80% during at least four successive recycling experiments, showing the good stability of the catalyst CuNP-**2**.

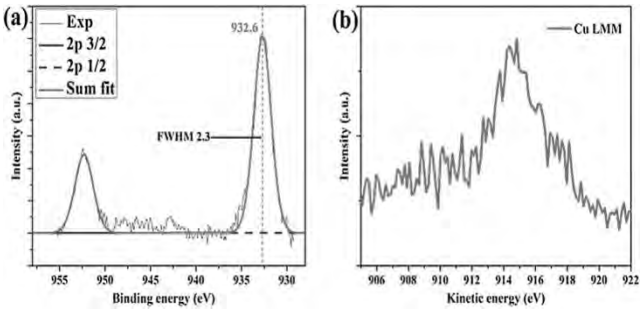

Figure 3. a) X-ray photoelectron spectroscopy of Cu 2p. b) Cu LMM Auger spectra.

The palladium-catalyzed Suzuki–Miyaura reaction is one of the common cross carbon–carbon coupling reactions.[39–42] Thus, catalysis of this reaction with ppm amounts of Pd is an ongoing challenge,[43,44] and only a few works are known to use this approach.[21,45–47] PdNPs are a valuable option, because toxic ligands that are often employed in efficient Pd catalysis are avoided with PdNP catalysts. The 1.5 nm core-sized PdNP-**2** with Pd^0 surface (from UV/Vis spectroscopy; Figure S20) catalyzed the Suzuki–Miyaura reaction between bromobenzene and phenylboronic acid using down to 10 ppm Pd per mol substrate [Eq. (3)], reaching a TON of 89 000 and a TOF of 3700 h^{-1} in 24 h at 80 °C in water/EtOH mixture (Supporting Information, Section 6). After the reaction, no aggregation of PdNPs was observed, indicating the very good thermal stability of the PdNP-**2**. In addition, recycling the PdNP-**2** catalyst in 0.1 mol % for this reaction gave yields of 87 % or above up to the 5th successive recycling run, with only a slight increase of the PdNP-**2** core size from 1.5 to 1.8 nm (Figure S54) without any aggregation.

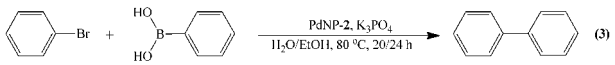

(3)

Another challenging example is the catalysis of transfer hydrogenation (TH). TH refers to the addition of hydrogen to a molecule using a non-H_2 hydrogen source (such as isopropanol). It is a convenient, powerful, and green method to access various hydrogenated compounds.[48,49]

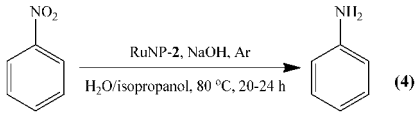

(4)

The UV/Vis spectrum of the RuNP-**2** confirms reduction to the Ru^0 surface following $NaBH_4$ reduction of $RuCl_3{\cdot}x\,H_2O$ (Figure S21). We found that the RuNP-**2** efficiently catalyzed TH of nitrobenzene using H_2O/isopropanol as the solvent at 80 °C in the presence of the base with only 0.01 mol % of catalyst at 80 °C for 24 h [Eq. (4)], leading to a TON of 2300 and TOF of 96 h^{-1} (Table S5). Recycling this catalyst with 0.1 mol % RuNP-**2** provided a product yield of 85 % or more up to the 3rd successive recycling run.

In summary, ligand design for nanoparticle catalysis with very weak but multidentate N and O ligands has been shown to apply to the stabilization and remarkable catalytic efficiency of very small, water-soluble TMNPs-**2**. The favorable effect of the tris-trz ligand **2** over the less bulky, simple mono-trz ligand **3** is illustrated by the increased reaction rate of AuNP-catalyzed 4-NP reduction observed with **2** compared to **3**. The success of the ligand design involving **2** was exemplified with the catalysis by TMNP-**2** of various major reactions that were conducted in water or aqueous media. This engineering efficiently applies to the first row transition metals, as shown with click chemistry and the reduction of the 4-nitrophenol pollutants to useful 4-aminophenol dyes. It also applies to the noble transition metals with the use of only ppm amounts of TMNP-**2** catalysts for transfer hydrogenation of nitrobenzene, reduction of 4-NP, and cross carbon–carbon coupling.

The recyclability studies were conducted using a biphasic organic/aqueous separation of products and subsequent addition of new reactants, which is a potential means to reuse the catalyst in a continuous flow-type arrangement. Many other reactions should benefit from this simple and general concept, operating under green conditions with ppm amounts of TMNP catalyst and in the absence of toxic ligands. So far, very few studies have demonstrated the possibility using only ppm amounts of metal, responding to the industrial limit of a maximum of 5 ppm of residual metal in products,[21,45–47] and this new concept should enhance trends towards this goal.

Acknowledgements

Financial support from the China Scholarship Council (CSC) of the People's Republic of China (grant to C.W.), the Universities of Bordeaux, Toulouse 3, Basque Country, and San Sebastian, the LCC (Toulouse), and the Centre National de la Recherche Scientifique (CNRS) is gratefully acknowledged.

Keywords: green chemistry · heterogeneous catalysis · ligand design · nitroarene reduction · transition metal nanoparticles

How to cite: *Angew. Chem. Int. Ed.* **2016**, *55*, 3091–3095
Angew. Chem. **2016**, *128*, 3143–3147

[1] a) M. Haruta, T. Kobayashi, H. Sano, N. Yamada, *Chem. Lett.* **1987**, 405–408; b) M. Haruta, *Angew. Chem. Int. Ed.* **2014**, *53*, 52–56; *Angew. Chem.* **2014**, *126*, 54–58.
[2] G. J. Hutchings, *J. Catal.* **1985**, *96*, 292–295.
[3] a) A. Corma, H. Garcia, *Chem. Soc. Rev.* **2008**, *37*, 2096–2126; b) A. Fihri, M. Bouhrara, B. Nekoueihahraki, J. M. Basset, V. Polhettiwar, *Chem. Soc. Rev.* **2011**, *40*, 5181–5203.
[4] a) R. M. Crooks, M. Q. Zhao, L. Sun, V. Chechik, L. K. Yeung, *Acc. Chem. Res.* **2001**, *34*, 181–190; b) V. S. Myers, M. G. Weir, E. V. Carino, D. F. Yancey, S. Pande, R. M. Crooks, *Chem. Sci.* **2011**, *2*, 1632–1646.
[5] a) E. Gross, J. H.-C. Liu, F. D. Toste, G. A. Somorjai, *Nat. Chem.* **2012**, *4*, 947–952; b) K. An, G. A. Somorjai, *Catal. Lett.* **2015**, *145*, 233–248; c) K. M. Choi, K. Na, G. A. Somorjai, O. M. Yaghi, *J. Am. Chem. Soc.* **2015**, *137*, 7810–7816.
[6] a) L. M. Bronstein, Z. B. Shifrina, *Chem. Rev.* **2011**, *111*, 5301–5344; b) L. M. Bronstein, *ChemCatChem* **2015**, *7*, 1058–1060.
[7] a) A. Balanta, C. Godart, C. Claver, *Chem. Soc. Rev.* **2011**, *40*, 4973–4985; b) J. E. Mondloch, E. Bayram, R. G. Finke, *J. Mol. Catal. A* **2012**, *355*, 1–38; c) S. Rawalekar, T. Mokari, *Adv. Energy Mater.* **2013**, *3*, 12–27; d) *Nanomaterials in Catalysis* (Eds.: P. Serp, K. Philippot), Wiley-VCH, Weinheim, **2013**; e) C. Amiens, D. Ciuculescu-Pradines, K. Philippot, *Coord. Chem. Rev.* **2016**, *308*, 409–432.
[8] P. D. Jadzinsky, G. Calero, C. J. Ackerson, D. A. Bushnell, R. D. Kornberg, *Science* **2007**, *318*, 430–433.
[9] a) G. Hutchings, *Catal. Today* **2005**, *100*, 55–61; b) N. T. S. Phan, M. Van der Sluys, C. W. Jones, *Adv. Synth. Catal.* **2006**, *348*, 609–679; c) J. Durand, E. Teuma, M. Gomez, *Eur. J. Inorg. Chem.*

2008, 3577 – 3586; d) *Nanoparticles and Catalysis* (Ed.: D. Astruc), Wiley-VCH, Weinheim, **2008**; e) P. Chen, X. Zhou, H. Shen, N. M. Andoy, E. Choudhary, K.-S. Han, G. Liu, W. Meng, *Chem. Soc. Rev.* **2010**, *39*, 4560 – 4570; f) N. Yan, C. Xiao, Y. Kou, *Coord. Chem. Rev.* **2010**, *254*, 1179 – 1218; g) V. P. Ananikov, I. Beletskaya, *Organometallics* **2012**, *31*, 1595 – 1604; h) C. Bai, M. Liu, *Nano Today* **2012**, *7*, 258 – 281; i) J. D. Scholden, B. C. Leal, J. Dupont, *ACS Catal.* **2012**, *2*, 184 – 200; j) M. Sankar, N. Dimitratos, P. J. Miedjack, P. P. Wells, C. J. Kiely, G. J. Hutchings, *Chem. Soc. Rev.* **2012**, *41*, 8099 – 8139; k) R. B. N. Baig, R. S. Varma, *Chem. Commun.* **2013**, *49*, 752 – 770.

[10] X. Pang, L. Zhao, W. Han, X. Xin, Z. Lin, *Nat. Nanotechnol.* **2013**, *8*, 426 – 431.
[11] M. Li, H. Schnalegger, S. Mann, *Nature* **1999**, *402*, 393 – 395.
[12] T. Dwars, E. Paetzold, G. Oehme, *Angew. Chem. Int. Ed.* **2005**, *44*, 7174 – 7199; *Angew. Chem.* **2005**, *117*, 7338 – 7364.
[13] X. Wang, G. Guerin, H. Wang, Y. Wang, I. Manners, M. A. Winnik, *Science* **2007**, *317*, 644 – 647.
[14] R. W. J. Scott, O. M. Wilson, R. M. Crooks, *J. Phys. Chem. B* **2005**, *109*, 692 – 704.
[15] C. J. Li, L. Chen, *Chem. Soc. Rev.* **2006**, *35*, 68 – 82.
[16] R. A. Sheldon, *Green Chem.* **2007**, *9*, 1273 – 1283.
[17] B. H. Lipshutz, S. Ghorai, *Green Chem.* **2014**, *16*, 3660 – 3679.
[18] G. R. Newkome, C. N. Moorefield, G. R. Baker, M. J. Saunders, S. H. Grossman, *Angew. Chem. Int. Ed. Engl.* **1991**, *30*, 1178 – 1180; *Angew. Chem.* **1991**, *103*, 1207 – 1209.
[19] G. R. Newkome, C. Shreiner, *Chem. Rev.* **2010**, *110*, 6338 – 6442.
[20] D. Astruc, E. Boisselier, C. Ornelas, *Chem. Rev.* **2010**, *110*, 1857 – 1959.
[21] a) C. Deraedt, N. Pinaud, D. Astruc, *J. Am. Chem. Soc.* **2014**, *136*, 12092 – 12098; b) C. Deraedt, D. Astruc, *Acc. Chem. Res.* **2014**, *47*, 494 – 503.
[22] E. Ozkal, P. Llanes, F. Bravo, A. Ferrali, M. A. Pericas, *Adv. Synth. Catal.* **2014**, *356*, 857 – 869.
[23] M. Meldal, C. W. Tornøe, *Chem. Rev.* **2008**, *108*, 2952 – 3015.
[24] J. E. Hein, V. V. Fokin, *Chem. Soc. Rev.* **2010**, *39*, 1302 – 1315.
[25] K. E. Sapsford, W. R. Algar, L. Berti, K. B. Gemmill, B. J. Casey, E. Oh, M. H. Stewart, I. L. Medintz, *Chem. Rev.* **2013**, *113*, 1904 – 2074.
[26] D. Astruc, L. Liang, A. Rapakousiou, J. Ruiz, *Acc. Chem. Res.* **2012**, *45*, 630 – 640.
[27] T. Aditya, A. Pal, T. Pal, *Chem. Commun.* **2015**, *51*, 9410 – 9431.
[28] P. Hervés, M. Pérez-Lorenzo, L. M. Liz-Marzán, J. Dzubiella, Y. Lu, M. Ballauff, *Chem. Soc. Rev.* **2012**, *41*, 5577 – 5587.
[29] P. Zhao, X. Feng, D. Huang, G. Yang, D. Astruc, *Coord. Chem. Rev.* **2015**, *287*, 114 – 136.
[30] R. Ciganda, N. Li, C. Deraedt, S. Gatard, P. Zhao, L. Salmon, R. Hernandez, J. Ruiz, D. Astruc, *Chem. Commun.* **2014**, *50*, 10126 – 10129.
[31] K. L. Kelly, E. Coronado, L. L. Zhao, G. C. Schatz, *J. Phys. Chem. B* **2003**, *107*, 668 – 677.
[32] M.-C. Daniel, D. Astruc, *Chem. Rev.* **2004**, *104*, 293 – 346.
[33] F. Alonso, Y. Moglie, G. Radivoy, *Acc. Chem. Res.* **2015**, *48*, 2516 – 2528.
[34] M. R. Decan, S. Impellizzeri, M. L. Marin, J. C. Scaiano, *Nat. Commun.* **2014**, *5*, 4612.
[35] T. Jin, M. Yan, Y. Yamamoto, *ChemCatChem* **2012**, *4*, 1217 – 1229.
[36] A. Kumar, S. Aerry, A. Saxena, A. Deb, S. Mozumdar, *Green Chem.* **2012**, *14*, 1298 – 1301.
[37] R. P. Jumde, C. Evangelisti, A. Mandoli, N. Scotti, R. Psaro, *J. Catal.* **2015**, *324*, 25 – 31.
[38] M. O'Halluin, T. Mabit, N. Fairley, V. Fernandez, M. B. Gawande, E. L. Grognec, F.-X. Felpin, *Carbon* **2015**, *93*, 974 – 983.
[39] D. Astruc, F. Lu, J. Ruiz, *Angew. Chem. Int. Ed.* **2005**, *44*, 7852 – 7872; *Angew. Chem.* **2005**, *117*, 8062 – 8083.
[40] C. C. C. Johansson Seechurn, M. O. Kitching, T. J. Colacot, V. Sniekus, *Angew. Chem. Int. Ed.* **2012**, *51*, 5062 – 5085; *Angew. Chem.* **2012**, *124*, 5150 – 5174.
[41] L. Yin, J. Liebscher, *Chem. Rev.* **2007**, *107*, 133 – 173.
[42] A. Molnar, *Chem. Rev.* **2011**, *111*, 2251 – 2320.
[43] N. Miyaura, A. Suzuki, *Chem. Rev.* **1995**, *95*, 2457 – 2483.
[44] A. J. J. Lennox, G. C. Lloyd-Jones, *Chem. Soc. Rev.* **2014**, *43*, 412 – 443.
[45] A. Alimardanov, L. Schmieder-van de Vondervoort, A. H. M. de Vries, J. G. de Vries, *Adv. Synth. Catal.* **2004**, *346*, 1812 – 1817.
[46] S. Ogasawara, S. Kato, *J. Am. Chem. Soc.* **2010**, *132*, 4608 – 4613.
[47] S. Handa, Y. Wang, F. Gallou, B. H. Lipshutz, *Science* **2015**, *349*, 1087 – 1091.
[48] A. Corma, P. Serna, *Science* **2006**, *313*, 332 – 334.
[49] D. Wang, D. Astruc, *Chem. Rev.* **2015**, *115*, 6621 – 6686.

Received: December 6, 2015
Revised: December 30, 2015
Published online: January 28, 2016

Inorganic Chemistry

Article

pubs.acs.org/IC

From Mono to Tris-1,2,3-triazole-Stabilized Gold Nanoparticles and Their Compared Catalytic Efficiency in 4-Nitrophenol Reduction

Changlong Wang,[†] Lionel Salmon,[‡] Qian Li,[†] María Echeverría Igartua,[§] Sergio Moya,[§] Roberto Ciganda,[†,∥] Jaime Ruiz,[†] and Didier Astruc*[,†]

[†]ISM, UMR CNRS 5255, University of Bordeaux, 33405 Talence Cedex, France

[‡]Laboratoire de Chimie de Coordination, UPR CNRS 8241, 31077 Toulouse Cedex, France

[§]CIC biomaGUNE, Unidad Biosuperficies, Paseo Miramon No. 182, Edif "C", 20009 Donostia-San Sebastian, Spain

[∥]Facultad de Quimica, Universidad del Pais Vasco, Apdo 1072, 20080 San Sebastian, Spain

Supporting Information

ABSTRACT: Mono-, bis-, and tris-1,2,3-triazole ligands are used for the stabilization of gold nanoparticles (AuNPs), and the catalytic activities of these AuNPs in 4-nitrophenol reduction by $NaBH_4$ in water are compared as well as with polyethylene glycol 2000 (PEG)- and polyvinylpyrrolidone (PVP)-stabilized AuNPs. The excellent catalytic results specifically obtained with the tris-triazolate ligand terminated by a PEG tail are taken into account by the synergy between the weakness of the tris-triazole-AuNP bond combined with the stabilizing ligand bulk.

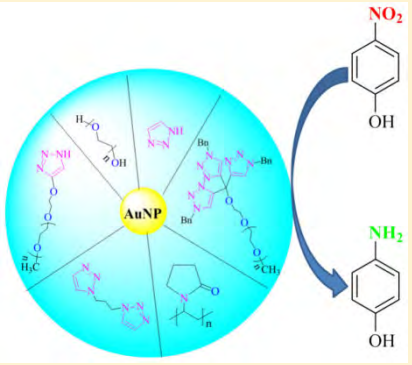

INTRODUCTION

Gold nanoparticles (AuNPs) have received considerable scientific interests and are actively investigated in the areas of nanomaterials,[1] catalysis,[2] and biomedicine.[3] In the field of heterogeneous catalysis, exceptional activity has long been disclosed with very small AuNPs, especially with metal-oxide-supported AuNPs.[2] To obtain catalytically active AuNPs, stabilizers (dendrimers, polymers, ionic liquids (ILs), inorganic solid supports) are indeed playing a crucial role and eventually affect the catalytic properties.[4] Catalytic reactions typically occur at the AuNPs surface, although some strong ligands (thiolates, phosphines, phosphine oxides, etc.) inhibit the active surface sites, leading to negative catalytic effects. Thus, "green" ligands that involve mild NP stabilization in water and are easy to displace and eventually provide more surface active sites in catalytic processes are searched to further improve activity. This is the case for nitrogen donors that leave the metal site at the metal surface in the zero oxidation state without back bonding, that is, electron rich, which is potentially most favorable for catalysis.

4-Nitrophenol (4-NP) reduction by $NaBH_4$ to 4-aminophenol (4-AP) is among the most studied AuNP-catalyzed reactions, because its kinetics is easy to follow in aqueous media.[5] It is monitored by UV−vis spectroscopy, and the C_t value represents the absorbance at 400 nm that corresponds to the nitrophenolate anion decreases with time along with the growth of a weak 4-AP band at 300 nm. This 4-NP reduction reaction catalyzed by NP catalysts is fitted with a pseudo-first-order kinetics with respect to 4-NP in the presence of excess $NaBH_4$, leading to the determination of the rate constant $k_{app} = \ln(C_t/C_0)/t$.[2f] This reaction was pioneered by Pal et al. in 2002,[6] and detailed kinetics studies by Ballauff's group have demonstrated that the mechanism involves rearrangement of the substrate fitting the Langmuir−Hinshelwood (LH) model with an induction time caused by dynamic restructuring of the NP surface.[7] This reaction provides a convenient way to examine the behavior of the stabilizing ligand at the NP metal surface including the facility of ligand displacement and catalysis on NP surface. Thus, in the present study we used this reaction in water to examine the efficiency of 4-NP reduction by $NaBH_4$ at the AuNP surface stabilized by 1,2,3-triazole ligands.

In previous reports, we already used the well-known copper(I)-catalyzed azide alkyne cycloaddition (CuAAC) reaction[8] to form weak 1,2,3-triazole (trz) ligands that mildly stabilize various AuNPs.[9] Among small transition metal NPs,[10] these trz-AuNPs have been shown to efficiently catalyze 4-NP reduction to 4-AP by $NaBH_4$ in water.[9−12] In particular, both mono- and tris-trz ligands with PEG tails were recently shown to stabilize AuNPs that catalyzed 4-NP reduction in water with excellent rates.[10] It has also been shown by Raman spectroscopy that the trz C−N and N═N bonds are much closer to the AuNP surface than other ligand atoms, suggesting that the trz

Received: May 5, 2016
Published: June 15, 2016

DOI: 10.1021/acs.inorgchem.6b01092
Inorg. Chem. 2016, 55, 6776−6780

neutral ligands stabilize the AuNPs by coordination of their nitrogen atoms to the AuNP surface.[11] AuNPs stabilized by trz ligands present reaction rates for 4-NP reduction by $NaBH_4$ that are higher than those obtained with other ligands. In addition, AuNPs stabilized by trz ligands do not show induction times for this reaction, contrary to AuNPs stabilized by citrates and thiolates.[12] These features suggested that the weak trz ligands on AuNP surface were easily displaced by the 4-NP and $NaBH_4$ substrates that directly led to high reaction rates. Therefore, it was of interest to compare the AuNP stabilization and catalytic activities of various types of trz ligands. Here we are reporting the stabilization of AuNPs by mono-, bis-, and tris-trz and the influence of the trz denticity on the 4-NP reduction by $NaBH_4$ in water, also including comparison with current polyethylene glycol 2000 (PEG) and polyvinylpyrrolidone (PVP) AuNP stabilizers. These results should be informative concerning the benefit of AuNP stabilization by multidendate nitrogen ligands and catalytic properties herewith.

RESULTS AND DISCUSSION

We started the study by the parent trz **1** (Figure 1). Indeed, the stabilization of AuNPs in water upon $NaBH_4$ reduction of

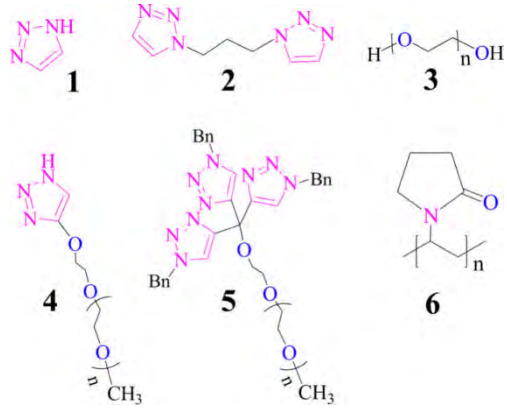

Figure 1. Ligands used in this study for AuNP stabilization.

$HAuCl_4$ in the presence of **1** very much depends on the reaction stoichiometry. With the stoichiometry 1:1 trz/$HAuCl_4$, aggregation of the formed AuNP-**1** upon adding $NaBH_4$ quickly occurs as visually observed while stirring in water at room temperature (rt). This is confirmed by the weak surface plasmon band (SPB; Figure 2a, and Supporting Information), although a reaction rate in 4-NP reduction was obtained upon ultrasonic dispersion of AuNP-**1** (Table 1). The use of 3 equiv of **1** versus $HAuCl_4$ to stabilize AuNPs resulted in considerably slowing this aggregation, and the AuNP-**1** were now stable for several hours and could thus also be used to study their catalysis of 4-NP reduction. We then turn to the use of 1,3-di(1*H*-1,2,3-triazol-1-yl)propane, **2**, as the AuNP stabilizing agent with the hope of taking advantage of the stabilizing chelation of the AuNP surface by the bis-triazole ligand. This attempt was somewhat successful, because the AuNP-**2** were stable overnight, allowing the records of AuNP-**2** SPB and catalytic 4-NP reduction process by UV−vis spectroscopy (Table 1). The SPBs of AuNP-**2** with various amounts of ligand **2** are much smaller than that of Au-**1**, while the 4-NP reaction rates are lower with AuNP-**2** than with AuNP-**1**. These results suggested that the ligand **2** is a much better AuNP stabilizer than the ligand **1**, as indicated by the smaller AuNP size and lower reaction rate of 4-NP reduction, although the main drawback is again the lack of long-term stability.

Polyethylene glycol (PEG) is a liner and green polymer that has long been recognized as an NP stabilizer and a phase transfer agent.[13] It has also been used to encapsulate some molecules for further catalytic processes, and these properties depend on the polymer chain length.[14] This typical PEG 2000 polymer (Mw = 2000, n = 44) was then used to stabilize AuNPs, and the stable PEG-stabilized AuNP-**3** obtained presented a SPB at 527 nm with a core size measured by transmission electron microscopy (TEM) of 8.3 ± 0.5 nm, similar to those of AuNP-**2** (Figure 2c, Table 1 and Supporting Information). The 4-NP reduction was then successfully conducted, yielding a reaction rate of k_{app} = 18.3 × 10^{-3} s^{-1} that is higher than some of the known published literature values (see the comparison in Table S1). In addition, an induction time was not observed, indicating that the weak Au−O bonds interactions in PEG-encapsulated AuNPs were easily displaced, favoring 4-NP reduction.

Trz with a PEG chain was then used with the idea that coordination of the triazoles on some AuNP surface atoms would leave the rest of the surface atoms only weakly stabilized by the weak ether ligand of the PEG. With this goal, the known monotrz-substituted PEG **4** was then used to encapsulate AuNPs, and under conditions identical to the above-mentioned AuNP preparations the use of 1 equiv of the monotrz-substituted PEG **4** led to the known AuNP-**4** with the SPB of 524 nm and AuNP core size measured by TEM of 5.8 ± 0.4 nm.[10] The 4-NP reduction rate catalyzed by AuNP-**4**, 20.9 × 10^{-3} s^{-1} (k_{app}), was higher than that of AuNP-**3**, but the AuNP size was larger than expected. To obtain smaller AuNPs, 3 equiv of ligand **4** versus $HAuCl_4$ was used, and the core size of AuNP-**4** was reduced to 3.1 ± 0.3 nm (Figure 2d) with a SPB of 515 nm in the UV−vis spectrum. The 4-NP reaction rate increased to 24.9 × 10^{-3} s^{-1} (k_{app}),[10] which is one of the highest records among rates of 4-NP reduction compared with the recent literature (Table S1).

Recently active studies of micellar catalysts in water (e.g., dendrimer-encapsulated NPs) were reported, and these catalysts usually showed enhanced catalytic activities and selectivities. However, NP formation in micelles or inverted micelles and catalysis therein are very dependent on the stereoelectronic parameters of the stabilizing agent.[15] Moreover with the inspiring results obtained above we then envisaged that a water-soluble amphiphilic ligand containing hydrophobic tris(1,2,3-triazolyl) on the one side and a hydrophilic PEG chain on the other side to stabilize AuNPs, forming a micellar AuNP catalyst, would further improve the catalytic efficiency. The known ligand **5** was expected to fulfill all the important features with the AuNPs including small size (3 nm) and improved reaction rates on the AuNP surface. The optimizations of Au and ligand mole ratios with variations of SPBs, TEM sizes, and 4-NP reaction rates were thus investigated, and a best result was obtained with the stoichiometry of ligand **5**: Au^{III} of 1:1 with the smallest AuNP core size and highest reaction rate.[10] The positive influence on catalysis of the tris-trz ligand bulk in **5** near the AuNP-**5** surface was also confirmed by comparison between the multiplicity of the mono- versus tris-trz ligand containing the same PEG tail (AuNP-**4** and AuNP-**5**, respectively).[10] Comparison between AuNP-**5** stabilized by the ligand **5** and AuNP-**6** stabilized by the widely used commercial polymer polyvinylpyrrolidone[16] (PVP, Mw = 10 000, 90 monomer

DOI: 10.1021/acs.inorgchem.6b01092
Inorg. Chem. 2016, 55, 6776−6780

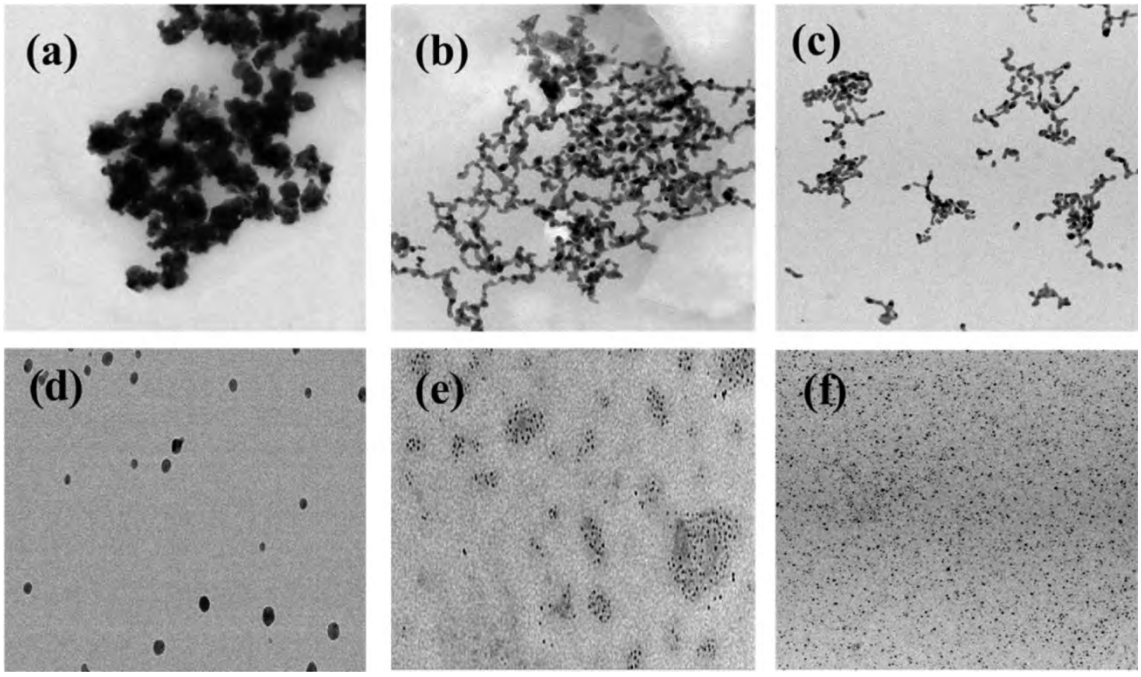

Figure 2. TEM images of various AuNP-L samples. (a) AuNP-**1**; (b) AuNP-**2**; (c) AuNP-**3**; (d) AuNP-**4**; (e) AuNP-**5**; (f) AuNP-**6**. Scale bar: 100 nm. For other TEM images and size distributions see the Supporting Information.

Table 1. 4-NP Reduction to 4-AP by $NaBH_4$ Catalyzed by Various AuNP-L (20 °C)[a]

AuNP-L	SPB (nm)	size (nm)[c]	induction time (s)	K_{app}[d] (1×10^{-3} s^{-1})
AuNP-**1**[b]			0	5.2 (3.5)
AuNP-**2**[b]	527 (537)	7.3 ± 0.5 (9.5 ± 0.7)	0	2.6 (2.3)
AuNP-**3**[b]	527	8.3 ± 0.5	0	18.4
AuNP-**4**[b]	515 (524)	3.1 ± 0.3 (5.8 ± 0.4)	0	24.9 (20.9)
AuNP-**5**	515	2.9 ± 0.3	0	43.7
AuNP-**6**	495	2.2 ± 0.4	40	15.2
AuNP-**5-THT**	556	14.5 ± 1	0	17.5
AuNP-**5**–**0**°C	538	3.4 ± 0.7	40	13.3

[a]Conditions: 4-NP (1 equiv), $NaBH_4$ (81 equiv), and AuNP-**L** catalysts (0.2 mol %). [b]Data are shown using 3 trz per AuNP; data in brackets are using 1 trz per AuNP. [c]Core size (TEM) of AuNP-**L**. [d]Rate constant.

units) showed that although AuNP-**6** was smaller than AuNP-**5** (2.2 ± 0.4 vs 2.9 ± 0.3 nm), the reaction rate was much lower with AuNP-**6** (15.2 vs 43.7 × 10^{-3} s^{-1} in k_{app}), indicating that the stronger Au–N and Au–O bonds in AuNP-**6** than in AuNP-**5** ensured smaller AuNP formation but also inhibited the surface catalytic efficiencies (induction time). Also, in the 4-NP reduction catalyzed by AuNP-**5**–**0**°C at 20 °C, a short induction time of 40 s was noticed, probably resulting from higher order in more compact ligand distribution on the AuNP surface. The lack of induction time for AuNP-**1**, AuNP-**2**, and AuNP-3 is taken into account by the very small sizes of the ligands in the two former AuNPs and for the very weak AuNP-ligand bond for the latter. These data demonstrate the successful design of this well-defined, new, green, and amphiphilic surface ligand **5**.

It was finally of interest to investigate the AuNP formation in the presence of the ligand **5** under various conditions in order to compare various key points concerning efficient nanogold catalysts preparations. Although both Au^{III} and Au^{I} compounds are well-known, AuNP precursors for AuNP syntheses are almost exclusively based on Au^{III} derivatives (e.g., $HAuCl_4 \cdot 3H_2O$ or $AuCl_3$), while less efforts have been paid to the use of Au^{I} compounds as precursors. Previously it has been reported that the intermediate Au^{I} state played a critical role in controlling the morphologies of AuNP synthesized from Au^{III} ions.[17] Indeed, some encouraging results have been obtained by using Au^{I} as precursors in the presence of ligands to form AuNPs with controlled size, shape, and crystallinity.[18] Thus, Au^{I} precursors with ligands make it possible to prepare AuNPs under mild conditions without a reducing agent. We then first investigated the use of gold(I)chloro(tetrahydrothiophene) [$AuCl(SC_4H_8)$] as a Au^{I} precursor to illustrate the effect of the nature of the Au oxidation state on the AuNP size and catalytic properties in the presence of ligand **5**. A Au(I) complex of **5** was obtained by ligand substitution in CH_2Cl_2, but this complex was not stable at rt (Scheme 1). On the one hand, after careful removal of CH_2Cl_2 instead of adding water, **AuNP-5-THT** was obtained as purple solution after dialysis. However,

Scheme 1

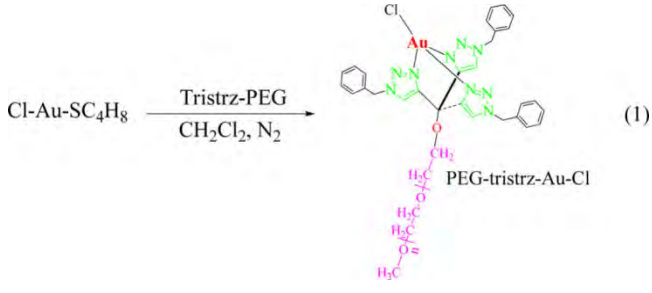

DOI: 10.1021/acs.inorgchem.6b01092
Inorg. Chem. 2016, 55, 6776–6780

at variance with previous reports, the present process led to the formations of **AuNP-5-THT** with a relatively large SPB (556 nm) and NP sizes (Table 1), and wide AuNP size distribution due to the usage of the weak ligand **5**.[18] On the other hand, although large **AuNP-5-THT** were obtained, the use of **AuNP-5-THT** to catalyze 4-NP reduction was very successful, leading to a surprising value of K_{app} = 17.5 × 10^{-3} s^{-1}. This rate constant value is higher than that obtained with small AuNPs stabilized by PVP (AuNP-**6**), and no induction time was observed, suggesting both the promoting effect ligand **5** in 4-NP reduction and the ligand weakness upon easy displacement by substrates.

We also compared AuNP-**5** synthesis at rt and 0 °C (ice−water bath), namely, AuNP-**5** and **AuNP-5−0**°C, respectively, to investigate the temperature effect in AuNP synthesis and catalytic properties in 4-NP reduction. Previously, it was established that a lower synthesis temperature favored the formation of two-dimensional-like nanostructures.[19] In the present case, AuNP-**5−0**°C shows a broad SPB (main at 538 nm) in the UV−vis spectrum, and TEM images show various shapes of anisotropic AuNPs (e.g., platelike and/or spherical particles) with a broad size distribution. The increase of temperature results in the decrease of particle size and narrows size distribution, whereas decrease in reaction temperature results in increase in particle size and broad size distribution with anisotropic AuNP nanostructures.[20] These phenomena were observed in many cases, because reactant depletions took place faster with higher reaction rates caused by high temperature, leading to the formation of smaller nanoparticles.[19,21]

■ CONCLUDING REMARKS

Simple trz ligands stabilize AuNPs, but only the increase of ligand denticity to two and especially three insures full AuNP stabilization. Such AuNPs form with small core sizes of ∼3 nm, which allows observation of the plasmonics. Interestingly, the use of amphiphilic mono- and tris-trz ligand provides micellar AuNPs in a rather similar way to amphiphilic micellar dendrimers used in efficient catalysis,[22] but of much simpler synthesis. The 4-NP reduction in water is an excellent tool to investigate the AuNP−ligand bonding in water-soluble NPs, and indeed very high rate constant values were obtained in comparison with classical PEG-AuNPs and PVP-AuNPs. This technique also highlights the privileged tris-triazole ligand **5** (and presumably other tris-trz and tris-nitrogen ligands) over other triazole-type AuNP ligands for 4-NP reduction. This study opens the route both toward investigation of various other NP stabilizers and ligands for NP surface catalysis and toward micellar-type NP catalysts.[23]

■ EXPERIMENTAL SECTION

General Data. All solvents and chemicals were used as purchased, unless elsewhere noted. Milli-Q water (18.2 MΩ) was used for all the AuNP preparations. Prior to the synthesis, the Schlenk flask was washed with a solution of aqua regia (HCl/HNO_3 = 3:1 v/v) to remove any traces of metal residue. NMR spectra were recorded at 25 °C with a Bruker 300 (300 MHz) spectrometer. All the chemical shifts are reported in parts per million (δ, ppm) with reference to Me_4Si for the ^1H and ^{13}C NMR spectra. UV−vis absorption spectra were measured with PerkinElmer Lambda 19 UV−vis spectrometer. Transmission electron microscopy (TEM) were recorded at the "Laboratoire de Chimie de Coordination" (LCC), CNRS, 205 Route de Narbonne, 31077 Toulouse Cedex, France, and at "CIC bioma GUNE, Unidad Biosuperficies, Paseo Miramon No 182, Edif "C" 20009 Donostia-San Sebastian, Spain". Size was calculated based on at least 100 NPs.

Synthesis of 1,3-Diazidopropane. A dried flask was charged with dimethyl sulfoxide (40 mL) and NaN_3 (1 g, 14.85 mol) under N_2. 1,3-Dibromopropane (1 g, 4.95 mmol) was added by syringe, and the mixture was stirred for 24 h at rt. Water was added in portions (5 × 20 mL) while allowing the reaction mixture to cool to rt between portions. The mixture was extracted with 3 × 50 mL of Et_2O. The extracts were combined and washed with water (3 × 50 mL) and brine (150 mL). The ether layer was separated and dried over $MgSO_4$. The solvent was removed in vacuo to yield a clear oil. Yield: 90%. ^1H NMR ($CDCl_3$): δ_{ppm} 3.43 (t, 4H), 1.84 (quintet, 2H).

*Synthesis of 1,3-Di(1H-1,2,3-triazol-1-yl)propane, **2**.* A dried flask was charged with 1,3-diazidopropane (850 mg, 1 equiv) and ethynyltrimethylsilane (1.65 g, 2.5 equiv) in the presence of THF under N_2. An aqueous solution of $CuSO_4$ (0.2 equiv, 10 mol % per branch) was added, and stirred for 30 min. Afterward, NaAsc (10 equiv per branch) was added dropwise. The mixture was then allowed to stir for 24 h at rt. Then, the mixture was then filtered and washed, and the solvents were removed in vacuo. Then MeOH and K_2CO_3 was added, and the mixture was stirred for 24 h at rt to yield a white solid product. Yield: 76%. ^1H NMR ($CDCl_3$): δ_{ppm} 7.68 (s, 2H), 7.63 (s, 2H), 4.39−4.32 (m, 2H), 2.57−2.48 (m, 2H).

*Synthesis of the 1,2,3-Triazole-mPEG Ligand, **3**.* In a dried flask, trimethylsilyl azide (0.2 mL, 1.5 mmol) was added to a mixed dimethylformamide/MeOH solution (3 mL, 9:1) that contained the catalyst CuI (5.8 mg, 0.03 mmol) and ethynyl-mPEG (1000 mg, 1 mmol) under N_2. The reaction mixture was stirred at 90 °C overnight. Then the mixture was cooled to rt, filtered, and the solvents were removed in vacuo. Then, the residue was dissolved in CH_2Cl_2 and washed three times with water. The organic phase was collected and dried over anhydrous sodium sulfate to yield the white solid product. Yield 65%. ^1H NMR ($CDCl_3$, 200 MHz) 7.67 (1H, *H* of triazole), 4.66 (2H, CH_2-triazole), 3.58 (176H, $-CH_2CH_2O-$), 3.32 (3H, $-OCH_3$).

*Synthesis of AuNP-**L**.* Generally, the gold precursor (1 equiv) in 1 mL of water was added to a solution that contained 1 or 3 equiv of ligand (1 or 3 triazole per Au) in 5 mL of water. The mixture was allowed to stir for 15 min. Then, a freshly prepared aqueous solution of $NaBH_4$ (10 equiv) was added to the solution dropwise, and the solution was continuously stirred for another 30 min. Dialysis was conducted for 24 h to remove the excess of ligand and $NaBH_4$. The AuNP-**L** was kept in aqueous solution for characterization and used as catalyst. The AuNPs stabilized by PEG were prepared under identical condition, except that 1 equiv of PEG per equiv of Au^{3+} was used.

Reduction of 4-NP by $NaBH_4$ (at 20 °C). The catalytic efficiencies of the catalysts AuNP-**L** were tested using the model reaction of 4-NP reduction with an 81 equiv excess of $NaBH_4$ that is fast, simple, and well-controlled. Generally, 4-NP (1 equiv) was mixed with $NaBH_4$ in water under air. The color of the solution changed from light yellow to dark yellow due to the formation of 4-nitrophenolate ion. Then a solution containing AuNP-**L** (0.2 mol %) was added to the mixture. The solution quickly lost its dark yellow color with time, and the progress of the reaction was monitored by UV−vis spectroscopy (250−550 nm, 40 s for each run).

■ ASSOCIATED CONTENT

Supporting Information

The Supporting Information is available free of charge on the ACS Publications website at DOI: 10.1021/acs.inorgchem.6b01092.

Characterizations and data of compounds and AuNPs. TEM images and size distributions, and UV−vis spectra. (PDF)

■ AUTHOR INFORMATION

Corresponding Author

*E-mail: d.astruc@ism.u-bordeaux1.fr.

DOI: 10.1021/acs.inorgchem.6b01092
Inorg. Chem. 2016, 55, 6776−6780

Notes

The authors declare no competing financial interest.

■ ACKNOWLEDGMENTS

Financial support from the China Scholarship Council (CSC) of the People's Republic of China (grant to C.W.), the Universities of Bordeaux, Toulouse 3, the LCC (Toulouse), and the Centre National de la Recherche Scientifique (CNRS) is gratefully acknowledged.

■ REFERENCES

(1) (a) Xia, Y.; Xiong, Y.; Lim, B.; Skrabalak, S. E. *Angew. Chem., Int. Ed.* **2009**, *48*, 60−103. (b) Sardar, R.; Funston; Alison, M.; Mulvaney, P.; Murray, R. *Langmuir* **2009**, *25*, 13840−13851. (c) Chen, H. J.; Shao, L.; Li, Q.; Wang, J. F. *Chem. Soc. Rev.* **2013**, *42*, 2679−2724. (d) Schluecker, S. *Angew. Chem., Int. Ed.* **2014**, *53*, 4756−4795. (e) Li, N.; Zhao, P.; Astruc, D. *Angew. Chem., Int. Ed.* **2014**, *53*, 1756−1789.

(2) (a) Haruta, M.; Date, M. *Appl. Catal., A* **2001**, *222*, 427−437. (b) Haruta, M. *Angew. Chem., Int. Ed.* **2014**, *53*, 52−56. (c) Herzing, A. A.; Kiely, C. J.; Carley, A. F.; Landon, P.; Hutchings, G. J. *Science* **2008**, *321*, 1331−1335. (d) Corma, A.; Leyva-Perez, A.; Sabater, J. M. *Chem. Rev.* **2011**, *111*, 1657−1712. (e) Dimitratos, N.; Lopez-Sanchez, J. A.; Hutchings, G. J. *Chem. Sci.* **2012**, *3*, 20−44. (f) Herves, P.; Perez-Lorenzo, M.; Liz-Marzàn, L. M.; Dzubiella, J.; Lu, Y.; Ballauff, M. *Chem. Soc. Rev.* **2012**, *41*, 5577−5587. (g) Stratakis, M.; Garcia, H. *Chem. Rev.* **2012**, *112*, 4469−4506. (h) Li, G.; Jin, R. *Acc. Chem. Res.* **2013**, *46*, 1749−1758. (i) Lang, X.; Chen, X.; Zhao, J. *Chem. Soc. Rev.* **2014**, *43*, 473−486. (j) Wang, C.; Astruc, D. *Chem. Soc. Rev.* **2014**, *43*, 7188−7216.

(3) (a) Rosi, N. L.; Mirkin, C. A. *Chem. Rev.* **2005**, *105*, 1547−1562. (b) Nel, A. E.; Madler, L.; Velegol, D.; Xia, T.; Hoek, E. M. V.; Somasundaran, P.; Klaessig, F.; Castranova, V.; Thompson, M. *Nat. Mater.* **2009**, *8*, 543−557. (c) Bardhan, R.; Lal, S.; Joshi, A.; Halas, N. J. *Acc. Chem. Res.* **2011**, *44*, 936−946. (d) Saha, K.; Agasti, S. S.; Kim, C.; Li, X. N.; Rotello, V. M. *Chem. Rev.* **2012**, *112*, 2739−2779. (e) Dreaden, E. C.; Alkilany, A. M.; Huang, X. H.; Murphy, C. J.; El-Sayed, M. A. *Chem. Soc. Rev.* **2012**, *41*, 2740−2779. (f) Yang, X.; Yang, M.; Pang, B.; Vara, M.; Xia, Y. *Chem. Rev.* **2015**, *115*, 10410−10488.

(4) (a) Toshima, N.; Yonezawa, T. *New J. Chem.* **1998**, *22*, 1179−1201. (b) Crooks, R. M.; Zhao, M.; Sun, L.; Chechik, V.; Yeung, L. K. *Acc. Chem. Res.* **2001**, *34*, 181−190. (c) Crooks, R. M.; Lemon, B. I.; Sun, L.; Yeung, L. K.; Zhao, M. *Top. Curr. Chem.* **2001**, *212*, 81−135. (d) Niu, Y.; Crooks, R. M. *C. R. Chim.* **2003**, *6*, 1049−1059. (e) Myers, V. S.; Weir, M. G.; Carino, E. V.; Yancey, D. F.; Pande, S.; Crooks, R. M. *Chem. Sci.* **2011**, *2*, 1632−1646. (f) Daniel, M.; Astruc, D. *Chem. Rev.* **2004**, *104*, 293−346. (g) Astruc, D.; Lu, F.; Ruiz, J. *Angew. Chem., Int. Ed.* **2005**, *44*, 7852−7872. (h) Corma, A.; Garcia, H. *Chem. Soc. Rev.* **2008**, *37*, 2096−2126. (i) Bronstein, L. M.; Shifrina, Z. B. *Chem. Rev.* **2011**, *111*, 5301−5344. (j) Cuenya, B. R. *Thin Solid Films* **2010**, *518*, 3127−3150.

(5) (a) Sau, T. K.; Pal, A.; Pal, T. *J. Phys. Chem. B* **2001**, *105*, 9266−9272. (b) Saha, S.; Pal, A.; Kundu, S.; Basu, S.; Pal, T. *Langmuir* **2010**, *26*, 2885−2893. (c) Kuroda, K.; Ishida, T.; Haruta, M. *J. Mol. Catal. A: Chem.* **2009**, *298*, 7−11. (d) Aditya, T.; Pal, A.; Pal, T. *Chem. Commun.* **2015**, *51*, 9410−9431. (e) Zhao, P.; Feng, X.; Huang, D.; Yang, G.; Astruc, D. *Coord. Chem. Rev.* **2015**, *287*, 114−136.

(6) Pradhan, N.; Pal, A.; Pal, T. *Colloids Surf., A* **2002**, *196*, 247−257.

(7) (a) Mei, Y.; Sharma, G.; Lu, Y.; Drechsler, M.; Irrgang, T.; Kempe, R.; Ballauff, M. *Langmuir* **2005**, *21*, 12229−12234. (b) Wunder, S.; Polzer, F.; Lu, Y.; Ballauff, M. *J. Phys. Chem. C* **2010**, *114*, 8814−8820. (c) Wunder, S.; Lu, Y.; Albrecht, M.; Ballauff, M. *ACS Catal.* **2011**, *1*, 908−916. (d) Gu, S.; Lu, Y.; Kaiser, J.; Albrecht, M.; Ballauff, M. *Phys. Chem. Chem. Phys.* **2015**, *17*, 28137−28143.

(8) (a) Meldal, M.; Tornøe, C. W. *Chem. Rev.* **2008**, *108*, 2952−3015. (b) Hein, J. E.; Fokin, V. V. *Chem. Soc. Rev.* **2010**, *39*, 1302−1315.

(9) (a) Astruc, D.; Liang, L.; Rapakousiou, A.; Ruiz, J. *Acc. Chem. Res.* **2012**, *45*, 630−640. (b) Zhao, P.; Li, N.; Salmon, L.; Liu, N.; Ruiz, J.; Astruc, D. *Chem. Commun.* **2013**, *49*, 3218−3220.

(10) Wang, C.; Ciganda, R.; Salmon, L.; Gregurec, D.; Irigoyen, J.; Moya, S.; Ruiz, J.; Astruc, D. *Angew. Chem., Int. Ed.* **2016**, *55*, 3091−3095.

(11) Li, N.; Zhao, P.; Liu, N.; Echeverria, M.; Moya, S.; Salmon, L.; Ruiz, J.; Astruc, D. *Chem. - Eur. J.* **2014**, *20*, 8363−8369.

(12) Ciganda, R.; Li, N.; Deraedt, C.; Gatard, S.; Zhao, P.; Salmon, L.; Hernández, R.; Ruiz, J.; Astruc, D. *Chem. Commun.* **2014**, *50*, 10126−10129.

(13) (a) Muller, J.; Klankermayer, J.; Leitner, W. *Chem. Commun.* **2007**, 1939−1941. (b) Chen, Y.; Yang, F.; Dai, Y.; Wang, W.; Chen, S. *J. Phys. Chem. C* **2008**, *112*, 1645−1649. (c) Biswas, M.; Saha, A.; Dule, M.; Mandal, T. K. *J. Phys. Chem. C* **2014**, *118*, 22156−22165.

(14) Gillich, T.; Acikgöz, C.; Isa, L.; Schlüter, A. D.; Spencer, N. D.; Textor, M. *ACS Nano* **2013**, *7*, 316−329.

(15) (a) Mann, S.; Schnablegger, H.; Li, M. *Nature* **1999**, *402*, 393−395. (b) Dwars, T.; Paetzold, E.; Oehme, G. *Angew. Chem., Int. Ed.* **2005**, *44*, 7174−7199. (c) Wang, X.; Guerin, G.; Wang, H.; Wang, Y.; Manners, I.; Winnik, M. A. *Science* **2007**, *317*, 644−647. (d) Pang, X.; Zhao, L.; Han, W.; Xin, X.; Lin, Z. *Nat. Nanotechnol.* **2013**, *8*, 426−431.

(16) Koczkur, K. M.; Mourdikoudis, S.; Polavarapu, L.; Skrabalak, S. E. *Dalton Trans.* **2015**, *44*, 17883−17905.

(17) (a) Rodríguez-Fernández, J.; Pérez-Juste, J.; Mulvaney, P.; Liz-Marzán, L. M. *J. Phys. Chem. B* **2005**, *109*, 14257−14261. (b) Zheng, N.; Fan, J.; Stucky, G. D. *J. Am. Chem. Soc.* **2006**, *128*, 6550−6551. (c) Halder, A.; Ravishankar, N. *J. Phys. Chem. B* **2006**, *110*, 6595−6600. (d) Li, C.; Shuford, K. L.; Park, Q.-H.; Cai, W.; Li, Y.; Lee, E. J.; Cho, S. O. *Angew. Chem., Int. Ed.* **2007**, *46*, 3264−3268. (e) Lu, X.; Tuan, H.; Korgel, B. A.; Xia, Y. *Chem. - Eur. J.* **2008**, *14*, 1584−1591. (f) Gu, H.; Ciganda, R.; Castel, P.; Vax, A.; Gregurec, D.; Irigoyen, J.; Moya, S.; Salmon, L.; Zhao, P.; Ruiz, J.; Hernández, R.; Astruc, D. *Chem. - Eur. J.* **2015**, *21*, 18177−18186.

(18) (a) Tao, A. R.; Habas, S.; Yang, P. *Small* **2008**, *4*, 310−325. (b) Briñas, R. P.; Hu, M.; Qian, L.; Lymar, E. S.; Hainfeld, J. F. *J. Am. Chem. Soc.* **2008**, *130*, 975−982. (c) Grzelczak, M.; Pérez-Juste, J.; Mulvaney, P.; Liz-Marzán, L. M. *Chem. Soc. Rev.* **2008**, *37*, 1783−1791.

(19) Chen, S.; Carroll, D. L. *J. Phys. Chem. B* **2004**, *108*, 5500−5506.

(20) Park, J.; Joo, J.; Kwon, G. S.; Jang, Y.; Hyeon, T. *Angew. Chem., Int. Ed.* **2007**, *46*, 4630−4660.

(21) (a) Lee, G.; Shin, S.; Kim, Y.; Oh, S. *Mater. Chem. Phys.* **2004**, *84*, 197−204. (b) Park, J.; Joo, J.; Kwon, G. S.; Jang, Y.; Hyeon, T. *Angew. Chem., Int. Ed.* **2007**, *46*, 4630−4660.

(22) Deraedt, C.; Pinaud, N.; Astruc, D. *J. Am. Chem. Soc.* **2014**, *136*, 12092−12098.

(23) Xia, Y.; Xia, X.; Peng, H. *J. Am. Chem. Soc.* **2015**, *137*, 7947−7966.

DOI: 10.1021/acs.inorgchem.6b01092
Inorg. Chem. 2016, 55, 6776−6780

ACS Catalysis

Research Article

pubs.acs.org/acscatalysis

Design and Applications of an Efficient Amphiphilic "Click" Cu^{I} Catalyst in Water

Changlong Wang,[†] Dong Wang,[†] Shilin Yu,[†] Thomas Cornilleau,[†] Jaime Ruiz,[†] Lionel Salmon,[‡] and Didier Astruc*[,†]

[†]ISM, UMR CNRS No. 5255, Univ. Bordeaux, 33405 Talence, France

[‡]Laboratoire de Chimie de Coordination, UPR CNRS No. 8241, 31077 Toulouse, France

Supporting Information

ABSTRACT: The copper(I)-catalyzed azide alkyne cycloaddition (CuAAC) using the conventional Sharpless–Fokin catalyst that consists of $CuSO_4$ + Na ascorbate, the most well-known and used "click" reaction, is considerably accelerated by the addition of a tris(triazolyl)-poly(ethylene glycol) (tris-trz-PEG) amphiphilic ligand in water under ambient conditions. Only parts per million amount of Cu^{I} were necessary to reach quantitative yields with TONs up to 86000 and TOFs of 3600 h^{-1}. The ligand was fully recycled, and the catalyst was reused at least six times without decomposition. Large-scale syntheses were also successfully achieved with 93% yield. The catalyst was applied to the efficient synthesis of various useful functional products with medicinal, catalytic, targeting, and labeling properties.

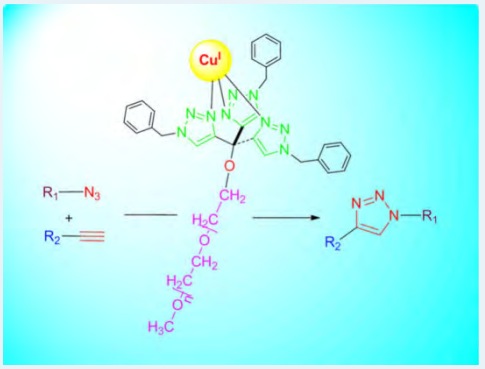

KEYWORDS: *"click" reaction, CuAAC, tris-trz-PEG, Cu^{I}, parts per million, catalyst, triazole*

INTRODUCTION

The concept of "click chemistry" proposed by Kolb, Finn, and Sharpless in 2001[1] has undoubtedly revolutionized molecular engineering science. Following the seminal and independent report by the Sharpless–Fokin[2] and Meldal[3] groups in 2002 of copper(I)-catalyzed azide alkyne cycloaddition (CuAAC) selectively yielding 1,4-disubstituted 1,2,3-triazoles, CuAAC has been applied to an enormous range of new syntheses and applications to macromolecules and nanomaterials.[4−7] For such CuAAC reactions, the catalytically active Cu^{I} species was usually generated from the cheap and easily available mixture of $CuSO_4$ and sodium ascorbate (NaAsc), known as the Sharpless–Fokin catalyst. The CuAAC reaction rate is low if the catalyst is not presented in high concentration and in the presence of activating ligand, however. For practical reaction processes, in most of the cases the Sharpless–Fokin catalyst is used in relatively large quantities in order to avoid the formation of the 1,5-isomer[8a] and to keep an acceptable reaction rate.[8b,c] The problem then remains to remove the copper ions, which limits this "click" chemistry in electronics and biomedicine.[9] To overcome these difficulties, some ligands have been shown to considerably accelerate the reactions and reduce the catalyst amounts. Among them, nitrogen-based ligands such as polytriazoles[10,11] and tris(2-aminoethyl)amine derivatives (tren)[12−14] have been found to be excellent, reducing the amount of Cu^{I} catalyst to an order of 1% or less. Recently it was reported that a recyclable dendritic nanoreactor containing intradendritic triazoles[9] and the poly(*N*-isopropylacrylamide-*co*-*N*-vinylimidazole) polymer[15] promoted CuAAC reactions in water and in *t*-BuOH/H_2O, respectively, down to the remarkable parts per million level of Cu^{I} catalyst under the conditions of in situ Cu^{2+} reduction using NaAsc. With such low amounts of catalysts and exceptional efficiencies, CuAAC reactions in aqueous solution under mild reaction conditions have effectively contributed to the pursuit of "green chemistry" with potential industrial applications. Nevertheless, only very few useful examples of synthetic applications under such conditions are known. In addition, in the case of the dendrimer,[9] such efficiency is associated with the complicated and time-consuming synthetic procedure of the catalyst. In this context we now address the utilization of an amphiphilic tripodal ligand, tris(triazolyl)-poly(ethylene glycol) (tris-trz-PEG),[16] the synthesis of which is simple, "green", and biocompatible. Its catalytic efficiency is similar to that of the dendrimer,[9] promoting the use of the conventional Sharpless–Fokin catalyst to the high efficiency of parts per million of Cu^{I} in water for various organic syntheses of medicinal, catalytic, targeting, and labeling interests.

RESULTS AND DISCUSSION

The preparation of the new "click" catalyst involves addition of $CuSO_4 \cdot 5H_2O$ under nitrogen to an aqueous solution containing the amphiphilic tris-trz-PEG ligand and then in situ reduction of the precatalyst PEG-tris-trz-Cu^{2+} to the PEG-tris-trz-Cu^{I} catalyst by dropwise addition of NaAsc (Scheme 1 and Supporting Information).

Received: May 18, 2016
Revised: June 22, 2016

DOI: 10.1021/acscatal.6b01389
ACS Catal. 2016, 6, 5424−5431

Scheme 1. Synthesis of the PEG-tris-trz-Cu^{I} "Click" Catalyst

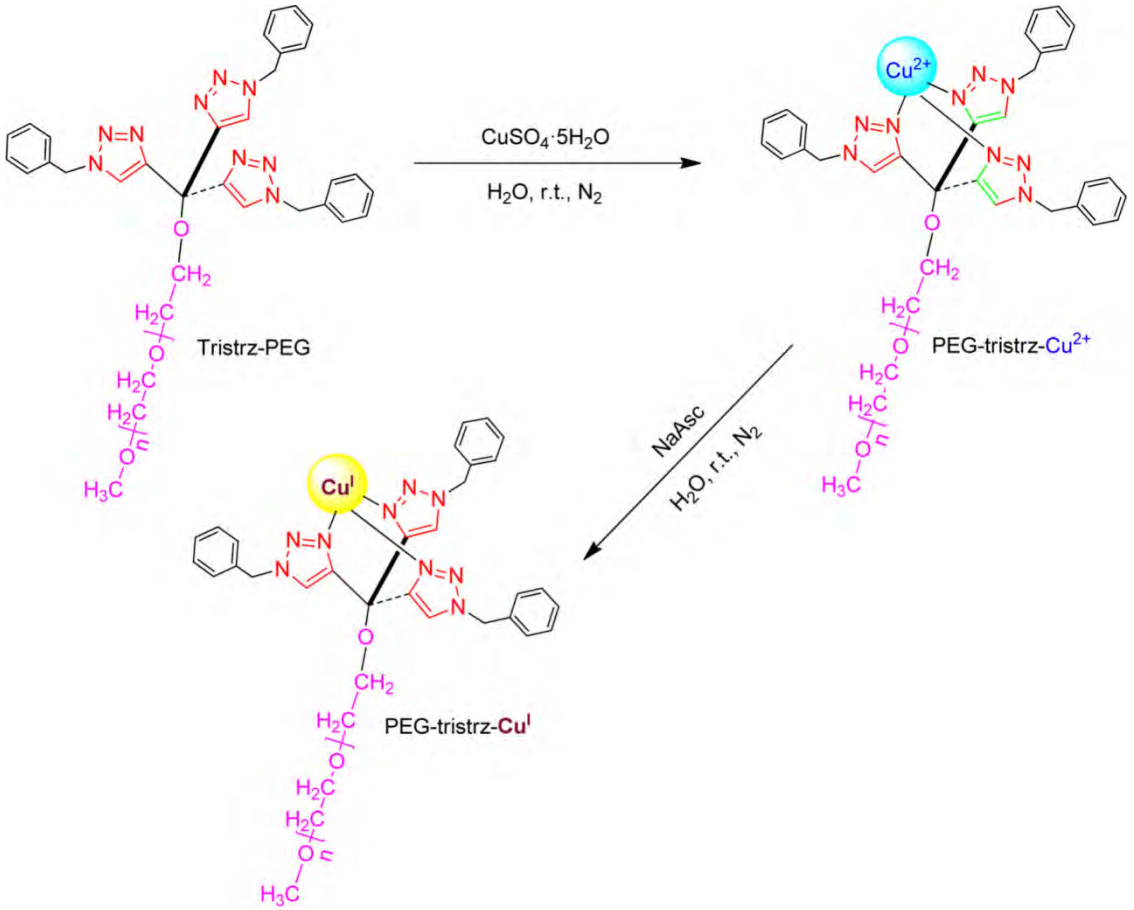

The synthetic procedure has been monitored by UV−vis (Figure 1) and ^{1}H NMR spectroscopy (Supporting Information). In UV−vis spectroscopy, an aqueous solution of $CuSO_4 \cdot 5H_2O$ has an absorption in the range of 700−800 nm (Figure 1, insert), which is attributed to the Cu^{2+} d−d transition.[17] Upon coordination of Cu^{2+} to the triazole rings this absorption disappears. After further reduction by NaAsc (10 equiv/mol of $CuSO_4$), the PEG-tris-trz-Cu^{I} complex exhibits a moderately intense band in the range between 300 and 400 nm (main absorption at 370 nm, Figure 1) which is assigned to a metal to ligand charge transfer (MLCT) transition.[18] These phenomena have also been confirmed by ^{1}H NMR spectroscopy using D_2O as the solvent (Figure S1 in the Supporting Information). After addition of Cu^{2+}, the NMR signal of the triazole proton of the tris-trz-PEG ligand vanishes due to the paramagnetism of the Cu^{2+} species, suggesting complexation.[9] When NaAsc is added, the NMR signal of the triazole proton of the tris-trz-PEG ligand reappears, but it is shifted to 8.19 ppm in comparison to the initial proton signal at 8.04 ppm (Figure S1), indicating that the triazole rings are coordinated to Cu^{I}.[9,19]

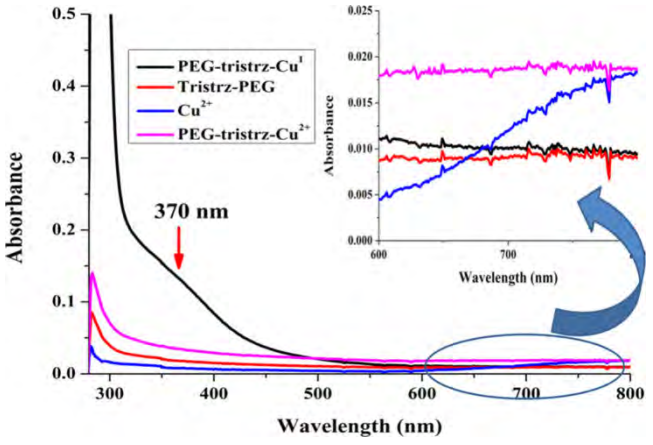

Figure 1. Synthetic process for the PEG-tris-trz-Cu^{I} catalyst monitored by UV−vis spectroscopy.

The efficiency of this new CuAAC catalyst was then tested using the standard "click" reaction between benzyl azide and phenylacetylene with various amounts of catalyst in neat water as the solvent (eq 1 and Table 1). When these reactions were performed in the presence of 2000, 200, and 100 ppm of PEG-tris-trz-Cu^{I} catalyst, respectively, in water at 35 or 30 °C, the crude reaction yields after 20 h were quantitative, and the desired 1,2,3-triazole was obtained in 97% yields (entries 1−3). A decrease in the catalyst amount to 50 ppm also resulted in quantitative conversion and 95% isolated yield at 35 °C (entry 4). Although the catalyst amount has been successfully decreased to 20 or 10 ppm (entries 5 and 6) without quantitative conversions, excellent yields are obtained, leading to TONs up to 86000 and TOFs up to 3600 h^{-1}. When the catalyst was reduced to 4 ppm (entry 7), the yield decreased but resulted in TON and TOF values that were still higher than those obtained with 20 ppm. The best conditions for this CuAAC catalytic system are at 50 ppm and 35 °C for 20 h, leading to full conversions and high isolated yields. A large-scale reaction under these conditions was

DOI: 10.1021/acscatal.6b01389
ACS Catal. 2016, 6, 5424−5431

Table 1. CuAAC Reactions between Benzyl Azide and Phenylacetylene using Various Amounts of PEG-tris-trz-Cu^{I} Catalyst[a]

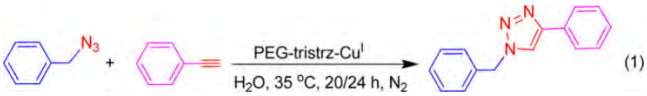

(1)

entry	temp (°C)	Cu^{I} (ppm)	time (h)	conversion[b]/ yield[c] (%)	TON	TOF (h^{-1})
1[d]	35	2000	20	100/97	485	24.25
2[d]	35	200	20	100/97	4850	242.5
3[d]	35	100	20	100/97	9700	485
4[e,f]	35	50	20	100/95	19000	950
5	35	20	20	95/90	45000	2250
6	35	10	24	90/86	86000	3600
7	35	4	24	37/30	75000	3125
8	35	0	24	0		

[a]Reaction conditions: 0.1 mmol of benzyl azide, 0.105 mmol of phenylacetylene, and 1 mL of water. [b]^{1}H NMR conversion. [c]Isolated yield. [d]Similar yields were also obtained at 30 °C. [e]A similar yield (93%) was also obtained when large amounts of benzyl azide (10 mmol) and phenylacetylene (10.5 mmol) were used in 10 mL of H_2O. [f]The catalyst was recycled six times under these conditions.

also successfully conducted, and a similar isolated yield (93%) was obtained (entry 4). Moreover, recycling the catalyst was also successful, because the amphiphilic tris-trz-PEG ligand is insoluble in cold diethyl ether, allowing complete extraction of the "click" products from the aqueous solution while the catalyst remained in the water phase. In this way, the catalyst was recycled at least six times without change of ligand structure during the CuAAC reactions (Figure S2 in the Supporting Information). However, a slight decrease in the yields was observed (Table S2 in the Supporting Information), which was due to the unavoidable lost of copper ions that were stoichiometrically trapped inside the product through interaction with the trz group (before being extracted with an ammonia solution).[20]

It was then of interest to investigate the underlying reason(s) for such an efficiency in the CuAAC reactions in water using such low amounts of PEG-tris-trz-Cu^{I} catalyst. To this end, Cu^{I} stabilized by PEG 2000 (**B**), monotrz-PEG (1 and 3 equiv for **C** and **D**, respectively), and tris-trz-PEG (**E**) were compared with the original neat Cu^{I} ($CuSO_4$ + NaAsc, **A**) catalyst for the CuAAC of benzyl azide and phenylacetylene in water under identical conditions. First, the original Cu^{I} and PEG-stabilized Cu^{I} species were compared, because the tris-trz-PEG has a PEG tail. The water-soluble and eco-friendly PEG is used extensively as a solvent or cosolvent in water for a variety of purposes due to its phase-transfer catalytic nature that is efficient in organic synthesis.[21] Previously, it was shown that "click" synthesis of 1,4-disubstituted 1,2,3-triazoles proceeded in good yields using $CuSO_4$ + NaAsc in PEG 400/water under mild conditions for a short time, due to very efficient activation by PEG 400.[22−25] However, this effect is not observed in the present study, because similar yields were obtained on comparison of **A** and **B** with different catalyst loadings. It appears that the concentration of PEG played a key role in the previous studies (PEG 400/water = 1/1, v/v).[22−25] Here the present PEG concentration is too low to provide such an effect, and therefore the PEG ligand does not lead to a good yield. When the monofunctional 1,2,3-triazole terminated with PEG 2000 (PEG-monotrz-Cu^{I}, 1 equiv, **C**),[26] was introduced, the yields increased, especially with low catalyst amounts (i.e., 26.5% vs 5% at 100 ppm). This confirmed that the nitrogen-based ligand served as a rate accelerator in this Cu^{I} catalysis, resulting in increased yields.[4−7] When a stoichiometric amount of monotrz-PEG vs Cu^{2+} was used in the synthetic procedure (3 equiv, **D**), the yields also greatly increased in comparison to those of the reactions catalyzed by **A** with various catalyst loadings (i.e., 66.7% vs 5% at 100 ppm; 34.0% vs 0% at 50 ppm). Surprisingly, quantitative conversions with excellent isolated yields were generally obtained at 2000, 200, 100, and 50 ppm using the PEG-tris-trz-Cu^{I} catalyst (**E**) under the present conditions. It thus appears that a strong chelation effect becomes more and more important as the concentration decreases.[4−7,10,11] In the cases of Cu^{2+} in neat water and Cu^{2+} in water in the presence of PEG and 1 equiv of monotrz-PEG, when NaAsc was added, the color of the aqueous solution changed very quickly from colorless to light yellow. This was not the case for Cu^{2+} in water in the presence of the ligands that are in a stoichiometric ratio of trz to Cu^{2+} (3 equiv of monotrz-PEG and 1 equiv of tris-trz-PEG). In these cases 1/2 h or more was required to change from colorless to light yellow. The differences in Cu^{2+} reduction rates are seemingly due to the increased electron density brought about on Cu^{2+} upon complexation by all trz ligands, making reduction of Cu^{2+} thermodynamically and subsequently kinetically more difficult. Altogether, as depicted in Figure 2, the high efficiency of these "click" reactions catalyzed by very low amounts of PEG-tris-trz-Cu^{I} catalysts benefit from (i) the chelation effect, (ii) the amphiphilicity of the tris-trz-PEG ligand containing a tris-triazole tripod that increases the electron density on the metal center, and (iii) a PEG chain allowing homogeneous "click" reactions in water.

Encouraged by the success of the initial efforts, the scope of applicability of this very low level amount of PEG-tris-trz-Cu^{I} catalyst was explored with CuAAC reactions between various alkynes and organic azides in water (Table 2). As an inspection of Table 2 reveals, excellent yields were generally obtained in the CuAAC of a wide variety of alkynes with organic azides. In addition, in most of the studied cases, purifications of the products by silica chromatography were not necessary, because most of the "click" products are water-insoluble solids, and the excess alkyne was removed by simple solvent washing and eventually by recycling. Thus, these "click" products were obtained by a simple extraction−washing−filtration process, revealing the advantages of this low level of PEG-tris-trz-Cu^{I} catalyst for CuAAC reactions in neat water.

As shown in Scheme 2, the catalyst PEG-tris-trz-Cu^{I} was also successfully used to prepare functional materials, namely "click"-triazole-functionalized 1-ethynylcyclohexanol (**1**; eq 3), 6-monodeoxy-6-monoazido-β-CD (**2**; eq 4), *p*-bis(ferrocenyl-1,2,3-triazolylmethyl)benzene (**3**; eq 5), "click"-triazole functionalized 7-(propargyloxy)coumarin (**4**; eq 6), two kinds of 9-triazolyl dendrimers (**5** and **6**; eq 7), "click"-triazole functionalized moxestrol (**7**; eq 8), and 3′-deoxy-3-azidothymidine (**8**; eq 9).

First, 1-ethynylcyclohexanol was chosen, because it has a simple structure, and it is known as an active metabolite of the old central nervous system depressant drug ethinamate. The "click" reaction with benzyl azide was achieved in excellent isolated yield (93%) using only 200 ppm at 35 °C for 20 h (Scheme 2, eq 3).

Cyclodextrin (CD) has been largely dominated by its unique ability to form inclusion complexes with guests fitting in their hydrophobic activity,[27,28] and its functionalizations have been a powerful means to improve its applications toward drug delivery, sensing or enzyme mimicking, pharmaceuticals, and biomedicine and also as catalysts of aqueous-phase metal-catalyzed organic

DOI: 10.1021/acscatal.6b01389
ACS Catal. 2016, 6, 5424−5431

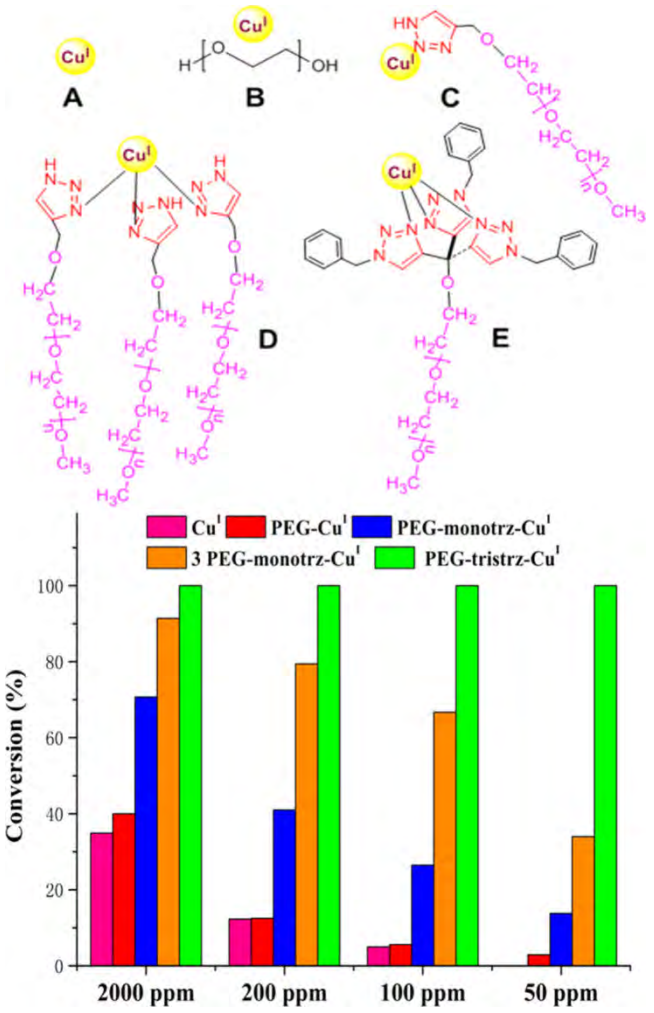

Figure 2. Comparison studies among Cu^I, PEG-Cu^I, PEG-monotrz-Cu^I, and PEG-tris-trz-Cu^I catalysts in the CuAAC reaction between benzyl azide and phenylacetylene.

reactions.[29−36] Previously, it has been shown by Ding's group that a water-soluble palladium complex based on **2** exhibited extremely high TONs and TOFs for Suzuki−Miyaura cross-coupling reactions in neat water. This was mainly attributed to the β-CD-fragment enhanced water solubility of the catalyst and accommodated the substrate through a recognition process, although the Sharpless−Fokin catalyst was used in high amount (10 mol %).[37] Now with the promotion of the amphiphilic tris-trz-PEG ligand, only 300 ppm of the Sharpless−Fokin catalyst efficiently catalyzed the "click" reaction with **2** in 85% isolated yield (Scheme 2, eq 4). Furthermore, host−guest molecular interactions between β-CD and ferrocene derivatives[38] for nanoparticle catalysts in aqueous solution are also known, and recently this host−guest system was utilized in AuNP assembly for photothermal therapy.[39] Now the "click" synthesis of one of these host−guest system precursors, *p*-bis(ferrocenyl-1,2,3-triazolylmethyl)benzene (**3**), was achieved using only 100 ppm per branch at 35 °C for 24 h with 83% isolated yield (Scheme 2, eq 5). It is expected that this material will be useful to complex β-CD in a host−guest assembly to stabilize metal nanoparticles for catalysis in aqueous solvents[38] and develop smart nanocarriers for intracellular diagnosis and therapy.

"Click"-triazole functionalized 7-(propargyloxy)coumarin (**4**) was also tested in the CuAAC "click" reaction with PEG-tris-trz-Cu^I in water (Scheme 2, eq 6). Coumarin derivatives are often used for their antioedematous properties, and their flavor properties have rendered this family famous in the perfume industry. Moreover, coumarins are also known as fluorescence dyes. With 300 ppm of PEG-tris-trz-Cu^I catalyst, this "click" product was isolated in 89% yield.

The CuAAC "click" reaction is a superb synthetic tool that has also been usefully and successfully applied to the synthesis of "click" dendrimers.[7,40] Following our original report of the first "click" synthesis of metallodendrimers,[19,41] iterative "click" constructions of metallodendrimers terminated by redox ferrocenyl groups and pyridyltriazole ligands were achieved.[42] Subsequently the use of these trz-metallodendrimers in redox sensing[20] and catalysis of carbon−carbon cross-coupling reactions[42,43] attracted increasing attention. However, the constructions of multiple and pure 1,4-regioisomers of 1,2,3-triazole-terminated "click" dendrimers are rather difficult, unless specific Cu^I catalysts are designed or/and used with high catalyst loading in organic solvents at relatively high temperature. In addition, "click" dendrimers tend to trap organic solvents and other impurities such as Cu ions that are more or less difficult to remove. The present study using the PEG-tris-trz-Cu^I catalyst allows "click" synthesis of 9-ferrocenyltriazole dendrimer **5** and 9-pyridyltriazole dendrimer **6** in excellent yields with 100 ppm of Cu^I per azido branch of catalyst under ambient conditions in water (Scheme 2, eq 7). Moreover, the purification of the dendrimers was achieved by straightforward solid/liquid phase separation. After the reaction, dendrimers **5** and **6** were separated from water as light yellow waxy solids sticking to the wall of the glass vessel and magnetic stirring bar by simply removing the liquid water phase and washing with pentane.

Moxestrol is known as a synthetic steroidal estrogen for the treatment of menopausal symptoms, and it is one of the most potent estrogens known. The natural alkyne of moxestrol has afforded easy functional ability for various medicinal applications. Herein we use the easily accessible "click" means to functionalize this useful material, with 500 ppm of PEG-tris-trz-Cu^I in only water at 35 °C for 48 h with 100% conversion and 93% isolated yield to the desired product **7** (Scheme 2, eq 8). Another key important natural product, 3′-deoxy-3-azidothymidine (AZT, zidovudine), a nucleoside-analogue reverse transcriptase inhibitor, was the first approved antiviral product for the treatment of human immunodeficiency virus (HIV). The 3′-azido group of AZT has afforded its potential application to HIV RT binding,[43] and its "click" functionalization has shown to be a convenient tool for the synthesis of novel nucleoside inhibitors with low to submicromolar potencies against HIV-1,[44,45] novel fluorescent markers, and cytostatic agents.[46,47] Moreover "click" functionalization of AZT to form nucleoside-based bioconjugates has also recently been employed as a biological CO tracer.[48] Herein, we quote an example of these useful AZT-derived 1,2,3-triazoles by synthesizing **8** using 500 ppm of PEG-tris-trz-Cu^I in only water at 45 °C for 48 h with 100% conversion and 89% isolated yield (Scheme 2, eq 9). To the best of our knowledge, the AZT-derived 1,2,3-triazoles have never been synthesized using such a low amount of Cu^I catalyst under ambient conditions in water. This successful attempt not only opens the way to efficiently synthesize clean AZT-derived 1,2,3-triazoles for drug design (especially for anti-HIV) but also contributes to the development of new classes of potential biological tracers/labels for various applications.

DOI: 10.1021/acscatal.6b01389
ACS Catal. 2016, 6, 5424−5431

Table 2. Substrate Scope of CuAAC Reactions between Various Azides and Alkynes using the PEG-tris-trz-Cu^{I} Catalyst[a]

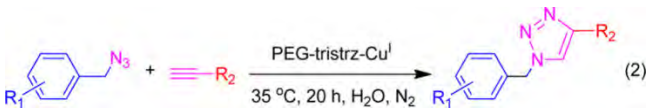

Entry	Azide	Alkyne	Cu^{I} (ppm)	Conversion[b] (%)	Yield[c] (%)
9	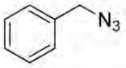	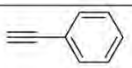	20	95	90
10	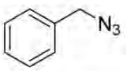	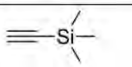	50	100	90
11	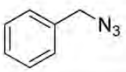	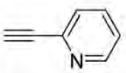	50	100	93
12	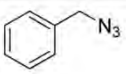	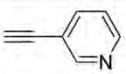	50	100	94
13	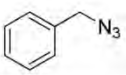	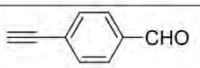	50	100	91
14	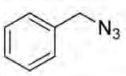	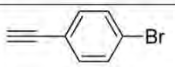	50(20)	100(72)	95(66)
15	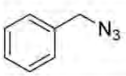	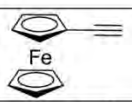	50	100	93
16	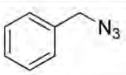	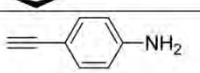	50	100	93
17	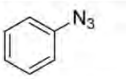	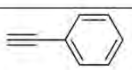	50	100	92
18	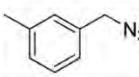	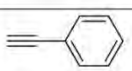	50	100	91
19	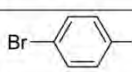	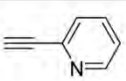	50	100	93
20	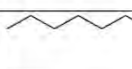	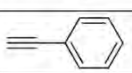	100	100	93
21	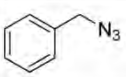	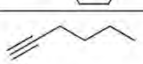	200	100	88
22	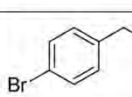	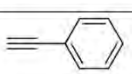	200	100	87
23	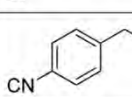	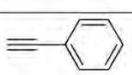	200	98	90

[a]Reaction conditions: 0.1 mmol of azide, 0.105 mmol of alkyne, and 1 mL of water. [b]^{1}H NMR conversion. [c]Isolated yield.

CONCLUSION

The family of nitrogen-based ligands that accelerate the CuAAC reactions has been extended here with the utilization of the amphiphilic tris-trz-PEG ligand. This recyclable ligand has now been shown to promote the conventional Sharpless−Fokin catalyst as a highly efficient Cu^{I} "click" catalyst in water for various organic syntheses. Comparative catalytic studies indicate that the tris-trz-PEG ligand is more efficient than the monotrz-PEG ligand, and reduction of Cu^{II} to Cu^{I} is considerably slower with the former ligand than with the latter. These trends confirm

DOI: 10.1021/acscatal.6b01389
ACS Catal. 2016, 6, 5424−5431

Scheme 2. Application of the PEG-tris-trz-Cu^{I} Catalyst to the Synthesis of Functional Materials

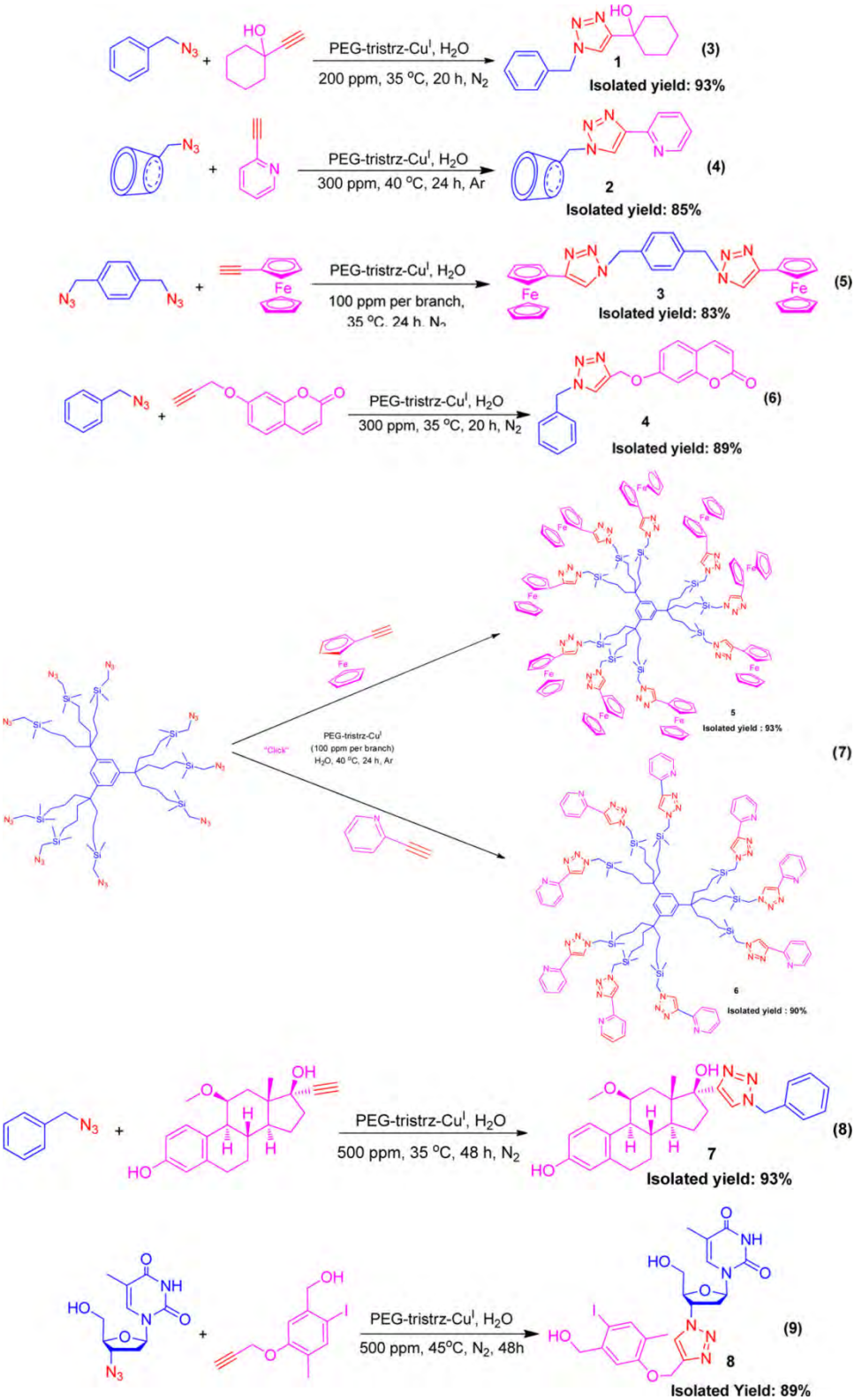

the favorable effect of the chelation in tris-trz-PEG concerning the catalytic properties. This study should contribute to the more effective synthesis of click compounds that are useful in current organic reactions and in various fields with the use of the copper catalyst in minute quantities down to industrially tolerable amounts.

EXPERIMENTAL SECTION

Synthesis of the Cu^{I}-L Catalysts. Generally, in a dried Schlenk flask, 1 mL of degassed aqueous solution of ligand (**L**) and $CuSO_4 \cdot 5H_2O$ (0.8 mg, 3.20×10^{-6} mol) solubilized in 1 mL of degassed water were successively added. A 12 mL portion of degassed water was placed in the Schlenk flask, and the solution

DOI: 10.1021/acscatal.6b01389
ACS Catal. 2016, 6, 5424−5431

was stirred at room temperature for 30 min under N_2. Sodium ascorbate (NaAsc, 10 equiv per Cu^{2+}) solubilized in 2 mL of degassed water was added dropwise to the solution of **Cu^{2+}-L**. After the mixture was stirred for another 30 min under N_2, the **Cu^{I}-L** solution was ready for use. The details of the syntheses of these catalysts are described in the Supporting Information.

General Procedure for the CuAAC Reactions. A glass vessel equipped with a magnetic stir bar was charged with 0.1 mmol of organic azide and 0.105 mmol of alkyne under a nitrogen atmosphere. Catalytic amounts of catalyst were placed in the vessel under N_2, and degassed water was added in order to obtain 1 mL as the total volume of water. The reaction mixture was stirred for 20 h at 35 °C under N_2. After the reaction, the mixture was filtered and then extracted using CH_2Cl_2 (3 × 10 mL). The organic layer was dried over Na_2SO_4 and filtered, and the solvent was removed in vacuo to give the corresponding 1,2,3-triazoles. The product was then purified by silica chromatography when necessary.

■ ASSOCIATED CONTENT

Supporting Information

The Supporting Information is available free of charge on the ACS Publications website at DOI: 10.1021/acscatal.6b01389.

General data, syntheses and characterizations of the catalysts, detailed experimental procedures for CuAAC reactions and their recycling, and spectra for all compounds (PDF)

■ AUTHOR INFORMATION

Corresponding Author

*E-mail for D.A.: didier.astruc@u-bordeaux.fr.

Notes

The authors declare no competing financial interest.

■ ACKNOWLEDGMENTS

Financial support from the China Scholarship Council (CSC) of the People's Republic of China (grant to C.W.), the Universities of Bordeaux and Toulouse 3, the LCC (Toulouse), and the Centre National de la Recherche Scientifique (CNRS) is gratefully acknowledged.

■ REFERENCES

(1) Kolb, H. C.; Finn, M. G.; Sharpless, K. B. *Angew. Chem., Int. Ed.* **2001**, *40*, 2004−2021.

(2) Rostovtsev, V. V.; Green, L. G.; Fokin, V. V.; Sharpless, K. B. *Angew. Chem., Int. Ed.* **2002**, *41*, 2596−2599.

(3) Tornøe, C. W.; Christensen, C.; Meldal, M. *J. Org. Chem.* **2002**, *67*, 3057−3064.

(4) Wu, P.; Feldman, A. K.; Nugent, A. K.; Hawker, C. J.; Scheel, A.; Voit, B.; Pyun, J.; Fréchet, J. M. J.; Sharpless, K. B.; Fokin, V. V. *Angew. Chem., Int. Ed.* **2004**, *43*, 3928−3932.

(5) Grimster, N. P.; Stump, B.; Fotsing, J. R.; Weide, T.; Talley, T. T.; Yamauchi, J. G.; Nemecz, A.; Kim, C.; Ho, K. Y.; Sharpless, K. B.; Taylor, P.; Fokin, V. V. *J. Am. Chem. Soc.* **2012**, *134*, 6732−6740.

(6) For selected reviews, see: (a) Meldal, M.; Tornøe, C. W. *Chem. Rev.* **2008**, *108*, 2952−3015. (b) Hein, J. E.; Fokin, V. V. *Chem. Soc. Rev.* **2010**, *39*, 1302−1315. (c) Liang, L.; Astruc, D. *Coord. Chem. Rev.* **2011**, *255*, 2933−2945. (d) Alonso, F.; Moglie, Y.; Radivoy, G. *Acc. Chem. Res.* **2015**, *48*, 2516−2528. (e) Haldón, E.; Nicasio, M. C.; Pérez, P. J. *Org. Biomol. Chem.* **2015**, *13*, 9528−9550. (f) Castro, V.; Rodríguez, H.; Albericio, F. *ACS Comb. Sci.* **2016**, *18*, 1−14. (g) Wang, C.; Ikhlef, D.; Kahlal, S.; Saillard, J.; Astruc, D. *Coord. Chem. Rev.* **2016**, *316*, 1−20.

(7) Astruc, D.; Liang, L.; Rapakousiou, A.; Ruiz, J. *Acc. Chem. Res.* **2012**, *45*, 630−640.

(8) (a) Liang, L.; Ruiz, J.; Astruc, D. *Adv. Synth. Catal.* **2011**, *353*, 3434−3450. (b) Murphy, A. R.; Fréchet, J M. J.; Chang, P.; Lee, J.; Subramanian, V. *J. Am. Chem. Soc.* **2004**, *126*, 1596−1597. (c) Gupta, S. S.; Kuzelka, J.; Singh, P.; Lewis, W. G.; Manchester, M.; Finn, M. G. *Bioconjugate Chem.* **2005**, *16*, 1572−1579.

(9) Deraedt, C.; Pinaud, N.; Astruc, D. *J. Am. Chem. Soc.* **2014**, *136*, 12092−12098.

(10) Chan, T. R.; Hilgraf, R.; Sharpless, K. B.; Fokin, V. V. *Org. Lett.* **2004**, *6*, 2853−2855.

(11) (a) Hong, V.; Presolski, S. I.; Ma, C.; Finn, M. G. *Angew. Chem., Int. Ed.* **2009**, *48*, 9879−9883. (b) Özçubukçu, S.; Ozkal, E.; Jimeno, C.; Pericàs, M. A. *Org. Lett.* **2009**, *11*, 4680−4683. (c) Etayo, P.; Ayats, C.; Pericàs, M. A. *Chem. Commun.* **2016**, *52*, 1997−2010.

(12) Golas, P. L.; Tsarevsky, N. V.; Sumerlin, B. S.; Matyjaszewski, K. *Macromolecules* **2006**, *39*, 6451−6457.

(13) Golas, P. L.; Tsarevsky, N. V.; Matyjaszewski, K. *Macromol. Rapid Commun.* **2008**, *29*, 1167−1171.

(14) Candelon, N.; Lastecouere, D.; Diallo, A. K.; Ruiz, J.; Astruc, D.; Vincent, J.-M. *Chem. Commun.* **2008**, *6*, 741−743.

(15) Yamada, Y. M. A.; Sarkar, S. M.; Uozumi, Y. *J. Am. Chem. Soc.* **2012**, *134*, 9285−9290.

(16) Wang, C.; Ciganda, R.; Salmon, L.; Gregurec, D.; Irigoyen, J.; Moya, S.; Ruiz, J.; Astruc, D. *Angew. Chem., Int. Ed.* **2016**, *55*, 3091−3095.

(17) Irie, H.; Kamiya, K.; Shibanuma, T.; Miura, S.; Tryk, D. A.; Yokoyama, T.; Hashimoto, K. *J. Phys. Chem. C* **2009**, *113*, 10761−10766.

(18) Su, C.; Liao, S.; Wanner, M.; Fiedler, J.; Zhang, C.; Kang, B.; Kaim, W. *Dalton Trans.* **2003**, 189−202.

(19) Badeche, S.; Daran, J.-C.; Ruiz, J.; Astruc, D. *Inorg. Chem.* **2008**, *47*, 4903−4908.

(20) Ornelas, C.; Ruiz, J.; Cloutet, E.; Alves, S.; Astruc, D. *Angew. Chem., Int. Ed.* **2007**, *46*, 872−877.

(21) Colacino, E.; Martinez, J.; Lamaty, F.; Patrikeeva, L. S.; Khemchyan, L. L.; Ananikov, V. P.; Beletskaya, I. P. *Coord. Chem. Rev.* **2012**, *256*, 2893−2920.

(22) Kumar, D.; Reddy, V. B.; Varma, R. S. *Tetrahedron Lett.* **2009**, *50*, 2065−2068.

(23) Kumar, D.; Reddy, V. B.; Kumar, A.; Mandal, D.; Tiwari, R.; Parang, K. *Bioorg. Med. Chem. Lett.* **2011**, *21*, 449−452.

(24) Keshavarz, M.; Badri, R. *Mol. Diversity* **2011**, *15*, 957−962.

(25) Pericherla, K.; Khedar, P.; Khungar, B.; Kumar, A. *Tetrahedron Lett.* **2012**, *53*, 6761−6764.

(26) Zhao, P.; Li, N.; Salmon, L.; Liu, N.; Ruiz, J.; Astruc, D. *Chem. Commun.* **2013**, *49*, 3218−3220.

(27) Chen, G.; Jiang, M. *Chem. Soc. Rev.* **2011**, *40*, 2254−2266.

(28) Harada, A.; Takashima, Y.; Nakahata, M. *Acc. Chem. Res.* **2014**, *47*, 2128−2140.

(29) Liang, L.; Diallo, A. K.; Salmon, L.; Ruiz, J.; Astruc, D. *Eur. J. Inorg. Chem.* **2012**, *2012*, 2950−2958.

(30) Shin, J.; Lim, Y.; Lee, K. *J. Org. Chem.* **2012**, *77*, 4117−4122.

(31) Kairouz, V.; Schmitzer, A. R. *Green Chem.* **2014**, *16*, 3117−3124.

(32) Doyagüez, E. G.; Rodríguez-Hernández, J.; Corrales, G.; Fernández-Mayoralas, A.; Gallardo, A. *Macromolecules* **2012**, *45*, 7676−7683.

(33) Noël, S.; Léger, B.; Ponchel, A.; Philippot, K.; Denicourt-Nowicki, A.; Roucoux, A.; Monflier, E. *Catal. Today* **2014**, *235*, 20−32.

(34) Hapiot, F.; Bricout, H.; Menuel, S.; Tilloy, S.; Monflier, E. *Catal. Sci. Technol.* **2014**, *4*, 1899−1908.

(35) Zaborova, E.; Deschamp, J.; Guieu, S.; Blériot, Y.; Poli, G.; Ménand, M.; Madec, D.; Prestat, G.; Sollogoub, M. *Chem. Commun.* **2011**, *47*, 9206−9208.

(36) Chau, N. T. T.; Handjani, S.; Guegan, J.; Guerrero, M.; Monflier, E.; Philippot, K.; Denicourt-Nowicki, A.; Roucoux, A. *ChemCatChem* **2013**, *5*, 1497−1503.

(37) Zhang, G.; Luan, Y.; Han, X.; Wang, Y.; Wen, X.; Ding, C.; Gao, J. *Green Chem.* **2013**, *15*, 2081−2085.

(38) Liu, J.; Mendoza, S.; Román, E.; Lynn, M. J.; Xu, R.; Kaifer, A. E. *J. Am. Chem. Soc.* **1999**, *121*, 4304−4305.

DOI: 10.1021/acscatal.6b01389
ACS Catal. 2016, 6, 5424−5431

(39) Wang, Y.; Li, H.; Jin, Q.; Ji, J. *Chem. Commun.* **2016**, *52*, 582−585.
(40) Astruc, D.; Boisselier, E.; Ornelas, C. *Chem. Rev.* **2010**, *110*, 1857−1959.
(41) Diallo, A. K.; Ornelas, C.; Salmon, L.; Aranzaes, J. R.; Astruc, D. *Angew. Chem., Int. Ed.* **2007**, *46*, 8644−8648.
(42) Wang, D.; Denux, D.; Ruiz, J.; Astruc, D. *Adv. Synth. Catal.* **2013**, *355*, 129−142.
(43) Thirumurugan, P.; Matosiuk, D.; Jozwiak, K. *Chem. Rev.* **2013**, *113*, 4905−4979.
(44) Zhou, L.; Amer, A.; Korn, M.; Burda, R.; Balzarini, J.; Clercq, E. D.; Kern, E. R.; Torrence, P. F. *Antiviral Chem. Chemother.* **2005**, *16*, 375−383.
(45) Sirivolu, V. R.; Vernekar, S. K. V.; Ilina, T.; Myshakina, N. S.; Parniak, M. A.; Wang, Z. *J. Med. Chem.* **2013**, *56*, 8765−8780.
(46) Baraniak, D.; Kacprzak, K.; Celewicz, L. *Bioorg. Med. Chem. Lett.* **2011**, *21*, 723−726.
(47) Szafrański, P. W.; Kasza, P.; Kępczyński, M.; Cegła, M. T. *Heterocycl. Commun.* **2015**, *21*, 263−267.
(48) Cornilleau, T.; Audrain, H.; Guillemet, A.; Hermange, P.; Fouquet, E. *Org. Lett.* **2015**, *17*, 354−357.

DOI: 10.1021/acscatal.6b01389
ACS Catal. 2016, 6, 5424−5431

Summary

In the second chapter, we proposed a new concept based on the design of amphiphilic ligand that mimics the functions of dendrimers to stabilize various transition metal nanoparticles in water, which are very efficient nanocatalysts with part per million (ppm) loadings for 4-nitrophenol (4-NP) reduction, "click" reaction, Suzuki-Miyaura reaction and transfer hydrogenation reaction. Moreover, we compared the stabilization of AuNPs by mono-, bis-, and tris-trz and their influence of the triazole denticity on the 4-NP reduction by $NaBH_4$ in water also including comparison with current polyethylene glycol 2000 (PEG) and polyvinylpyrrolidone (PVP) AuNP stabilizers. Further, based on this tris-trz-PEG amphiphilic ligand, especially the utilization of the chelation of the triazole groups, an efficient amphiphilic "click" Cu^I catalyst in water is designed. This catalyst shows high activity for CuAAC "click" reaction in water at ambient temperature with catalyst loading at only ppm levels for the synthesis of various useful functional products with medicinal, catalytic, targeting, and labeling properties.

Highly Efficient Transition Metal Nanoparticle Catalysts in Aqueous Solutions

In this first paper, we proposed a ligand design by conceptualizing the efficient amphiphilic dendrimers with tris-trz-PEG amphiphilic ligand. This tris-trz-PEG amphiphilic ligand containing three clicked triazole rings and a PEG 2000 chain is

synthesized through CuAAC and a Williamson reaction.

Firstly, tris(1-benzyl-1H-1,2,3-triazol-4-yl)methanol was synthesized by three steps (Scheme 1): In a flask, tris(trimethylsilylethynyl)methanol (1.5 g) was dissolved in methanol (15 mL) and stirred in the presence of K_2CO_3 (8.0 g) at r.t. for 4 h. The solution was then filtered to remove excess K_2CO_3 and added to a solution of benzyl azide (1.9 g) in methanol (15 mL). The general "click" reaction was conducted for 72 h by using $CuSO_4 \cdot 5H_2O$ (60 mg) and sodium ascorbate (150 mg) as the catalyst. After the reaction, the solvent was removed *in vacuo*. The residue was dissolved in dichloromethane (100 mL) and washed with a saturated Na_2CO_3 solution (5×50 mL) until the aqueous phase was no longer blue (the color of the copper salts). The organic phase was then collected and dried over Na_2SO_4, and the solvent was removed *in vacuo*. The product was obtained and purified by precipitation three times from an ethyl acetate with pentane. Yield: 63.5%, 1.47 g. ^{1}H NMR (300 MHz, $CDCl_3$): δ_{ppm}=7.63 (s, 3H), 7.37-7.39 (m, 9 H), 7.26-7.30 (m, 6H), 5.50 (s, 6 H), 4.62 ppm (s, 1 H).

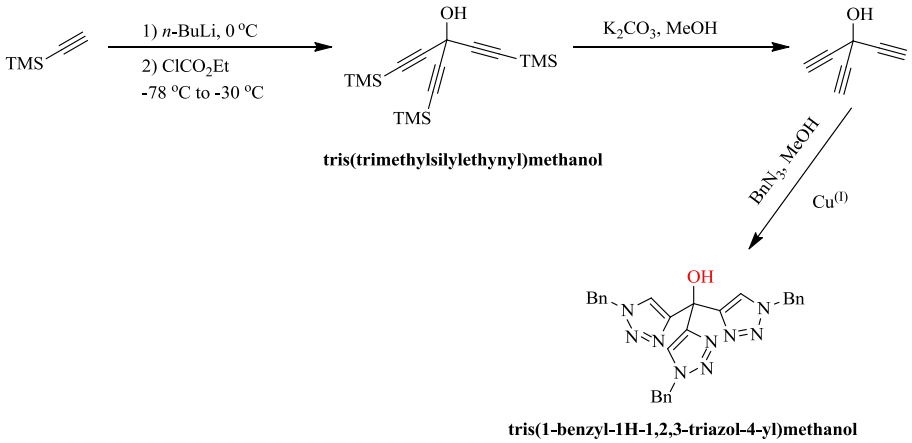

Scheme 1. Synthesis of tris(1-benzyl-1H-1,2,3-triazol-4-yl)methanol.

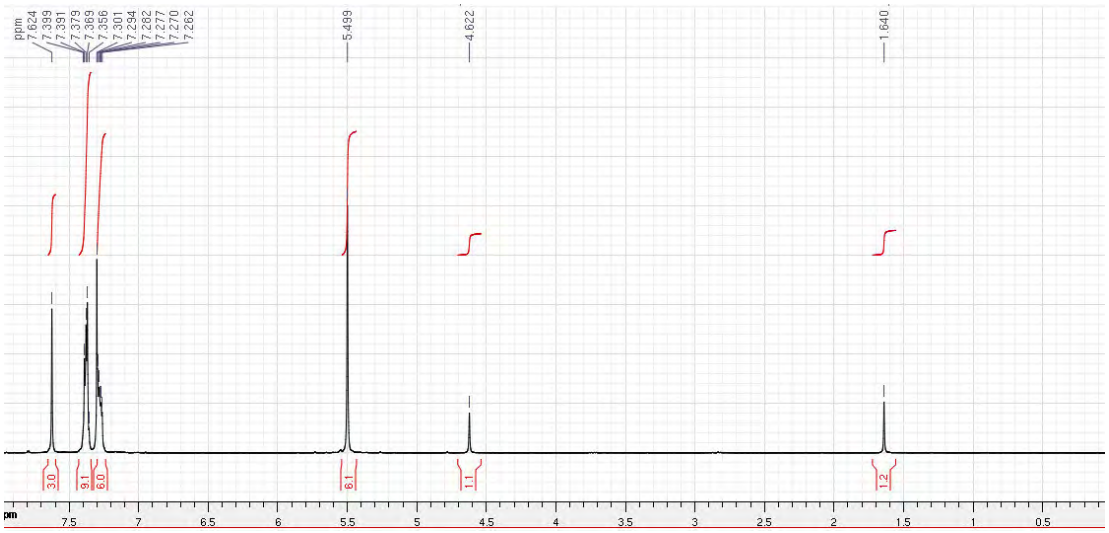

Figure 1. ^{1}H NMR ($CDCl_3$, 300 MHz) spectrum of tris(1-benzyl-1H-1,2,3-triazol-4-yl)methanol, **1**.

Then, a Williamson reaction was conducted between tris(1-benzyl-1H-1,2,3-triazol-4-yl)methanol and chlorinated mPEG2000 (Figure 2). The ligand has been fully characterized by ^{1}H NMR, ^{13}C NMR, MS, elemental analysis and IR.

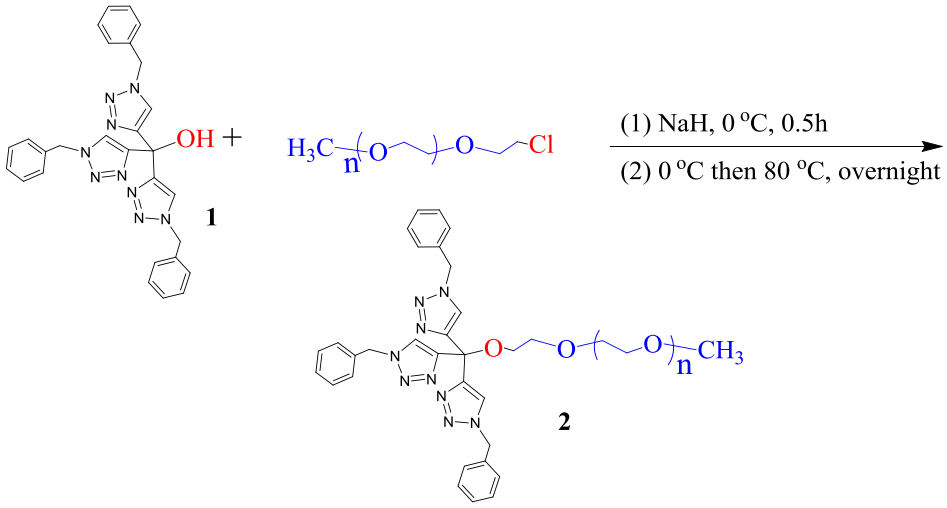

Figure 2. Synthesis of the new amphiphilic ligand **2**(n = 40-44).

Transition metal nanoparticles (TMNPs) are synthesized in the presence of the amphiphilic ligand in water upon external reduction by $NaBH_4$: Generally, the transition metal precursor (1 equiv.) in 1 mL water was added to a solution that contained **2** (1 equiv.) in 5 mL water. The mixture was allowed to stir for 15 min. Then, the freshly prepared aqueous $NaBH_4$ (10 equiv.) solution was added to the solution dropwise, and the solution was continuously stirred for another 30 min. Then, dialysis was conducted for 24 hours to remove the excess of ligand and $NaBH_4$. The TMNPs-**2** were kept in aqueous solution for characterization and used as the catalysts. Most of the TMNPs were formed with tris-trz-PEG amphiphilic ligand in their nanocluster size (i.e. very small, $<$ 2 nm), except CoNPs and AgNPs that are slightly larger than 2 nm. This small size is advantageous for catalysis, because the majority of atoms (between 54% and 70%) are located on the TMNP surface for these metals (here Fe, Ni, Cu, Ru, Pd, and Pt) forming monodispersed TMNP-tris-trz-PEG amphiphilic ligand cores with diameters smaller than 2 nm. It is suggested that both the trz groups of the tris-trz ligand and the PEG 2000 polymer are acting as weak ligands for the TMNP-**2** whereby the synergy between weak, but multidentate TMNP surface coordination and the overall large bulk permit the stabilization of these TMNPs.

All the TMNPs have been fully characterized by UV-vis spectroscopy, XPS, TEM, HRTEM techniques. For example, in the case of AuNPs, TEM showed the size of 2.9 nm, and a surface plasmon band of 515 nm. The XPS showed the only Au(0) surface atoms. While in the case of the amphiphilic ligand stabilized CuNPs, no SPB was

observed, because of the very small size of the CuNPs. However, CuNPs prepared in the absence of ligand, the CuNPs color was totally different and presented a SPB of 590 nm (Figure 3).

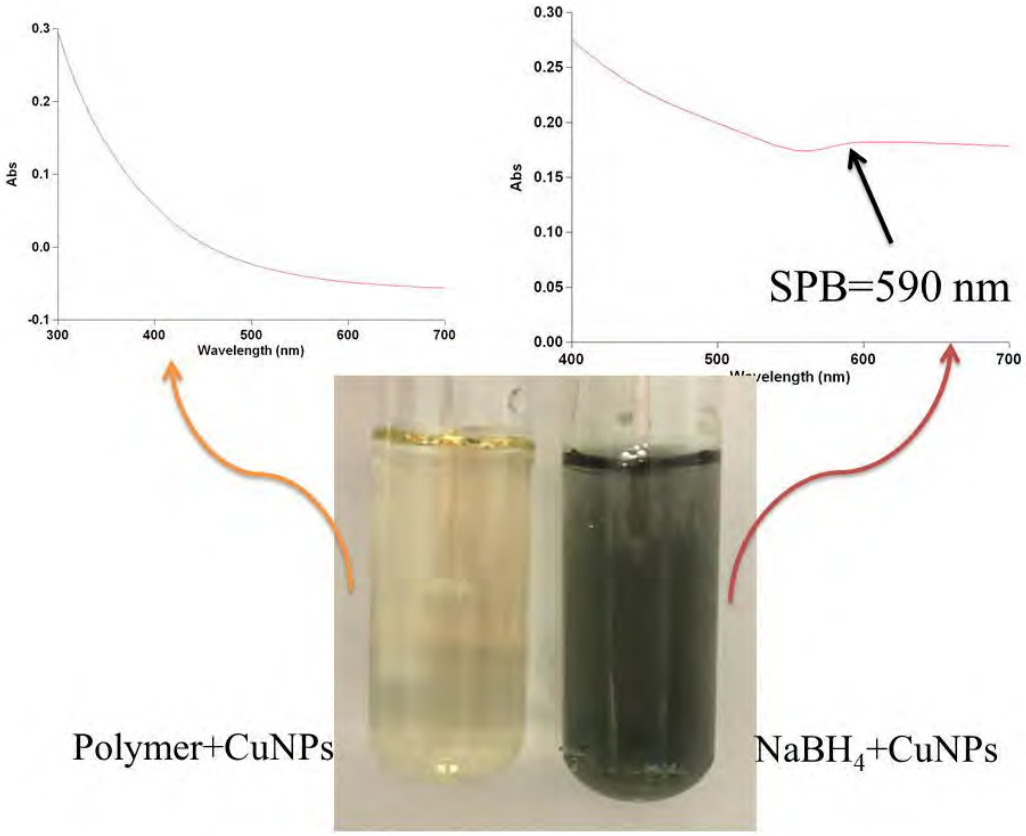

Figure 3. UV-vis. spectra of the CuNPs-**2** (top left) and the CuNPs without **2** (top-right), and their colors.

To compare the catalytic efficiencies of those TMNPs, we used 4-nitrophenol reduction reaction. 4-NP reduction by $NaBH_4$ to 4-aminophenol (4-AP) is among the most studied reactions, because its kinetics is easy to follow in aqueous media. It is monitored by UV-vis. spectroscopy, and the C_t value represents the absorbance at 400

nm that corresponds to the nitrophenolate anion decreases with time along with the growth of a weak 4-AP band at 300 nm. This 4-NP reduction reaction catalyzed by NP catalysts is fitted with a pseudo-first-order kinetics with respect to 4-NP in the presence of excess $NaBH_4$, leading to the determination of the rate constant $k_{app} = \ln(C_t/C_0)/t$.[1] This reaction was pioneered by Pal et al. in 2002,[2] and detailed kinetic studies by Ballauff's group have demonstrated that the mechanism involves rearrangement of the substrate fitting the Langmuir–Hinshelwood (LH) model with an induction time caused by dynamic restructuring of the NP surface (Scheme 2).[3]

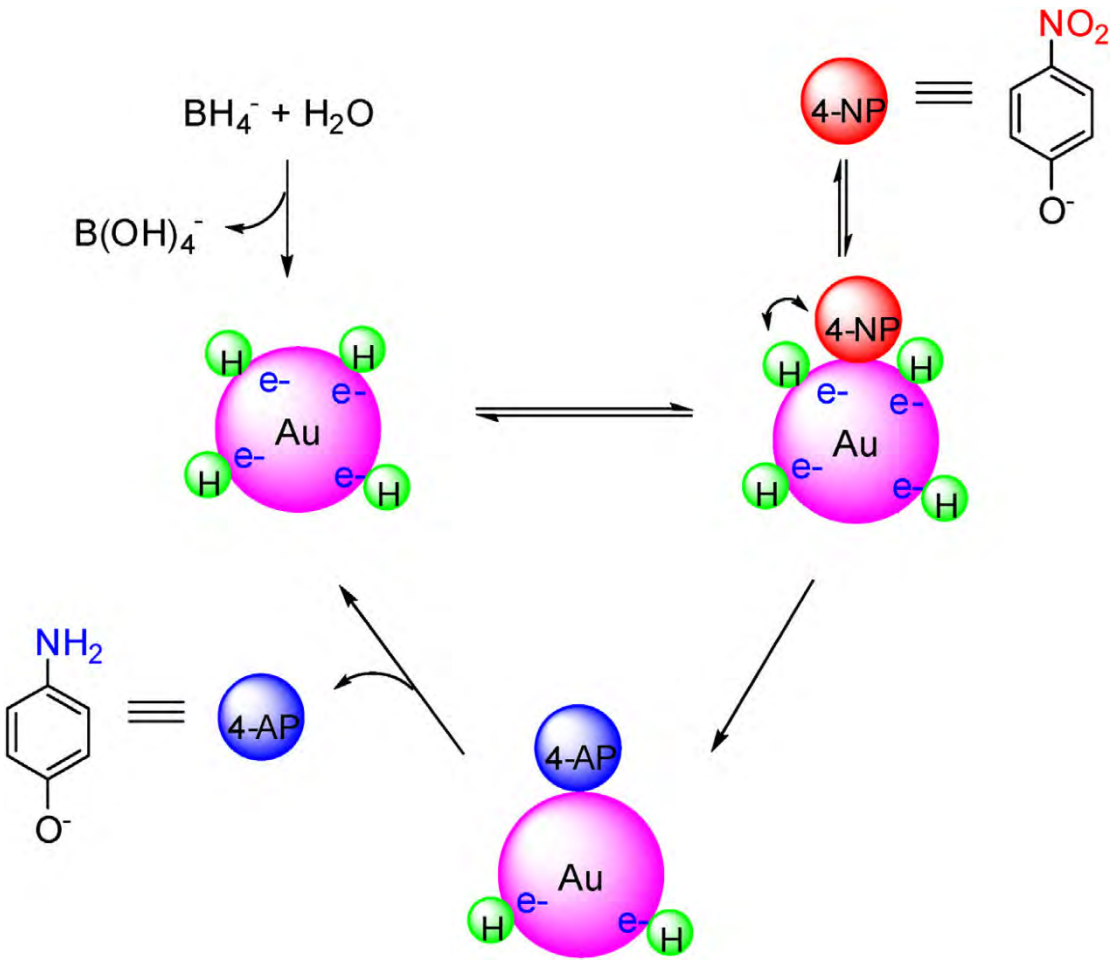

Scheme 2. Langmuir–Hinshelwood mechanism for the reduction of 4-NP to 4-AP catalyzed by nano-gold in the presence of $NaBH_4$.[4]

We compared the efficiencies of amphiphilic ligand-transition metal nanoparticles nanocatalysts in the 4-NP reduction reaction (Table 1). We selected the most efficient four NPs, namely AuNPs, PdNPs, RuNPs, and CuNPs. The later three were then utilized for their well-known reactions such as the Suzuki-Miyaura reaction, transfer hydrogenation and "click" reaction, respectively.

Table 1: 4-NP reduction by $NaBH_4$ catalyzed by TMNP-**2** in water at 20 ℃.

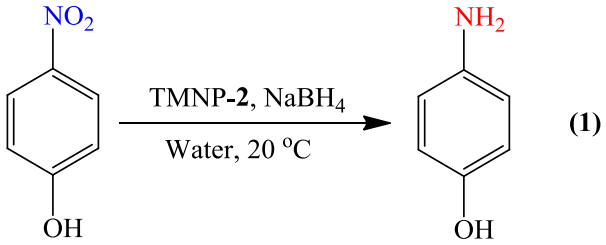

(1)

TMNP-**2**	Amount[a] [mol%]	D_{core}[b] [nm]	t_0[c] [s]	k_{app}[d] [10^{-3} s^{-1}]	k_1[e] [L s^{-1} m^{-2}]
FeNPs	2	1.3	780	1.88	1.21×10^{-3}
CoNPs	2	2.1	420	1.47	1.57×10^{-3}
NiNPs	2	1.6	720	0.30	2.69×10^{-4}
CuNPs	2	1.4	940	2.48	1.75×10^{-3}
AgNPs	2	2.2	520	7.85	6.07×10^{-3}
PtNPs	0.2	1.7	0	1.86	1.17×10^{-2}
RuNPs	0.2	1.0	0	3.15	1.26×10^{-2}

PdNPs	0.2	1.5	0	24.80	0.137
AuNPs	0.2	2.9	0	43.70	0.410

[a] Amount of TMNP-**2** used in the catalyzed 4-NP reduction. $NaBH_4$ is in excess. [b] Core size (TEM) of the TMNP-**2**. [c] Induction time. [d] Rate constant. [e] Surface-independent rate constant.

These nanocatalysts are surprisingly efficient with only parts-per-million (ppm) metal loadings, and recyclable. For instance, the 1.5 nm-core-sized PdNP-**2** with Pd(0) surface catalyzed the Suzuki-Miyaura reaction between bromobenzene and phenylboronic acid using down to 10 ppm Pd per mol substrate (Scheme 3 and Figure 4), reaching a TON of 89000 and a TOF of 3700 h^{-1} in 24 h at 80 ℃ in water/EtOH mixture. Recycling the PdNP-**2** catalyst in 0.1 mol% for this reaction gave yields of 87% or above up to the 5th successive recycling run with only a slight increase of the PdNP-**2** core size from 1.5 to 1.8 nm without any aggregation (Table 2).

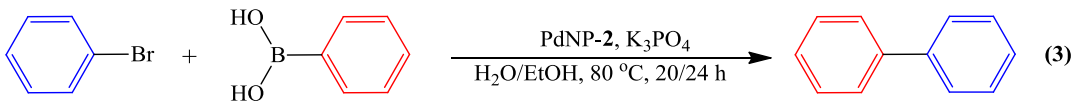

(3)

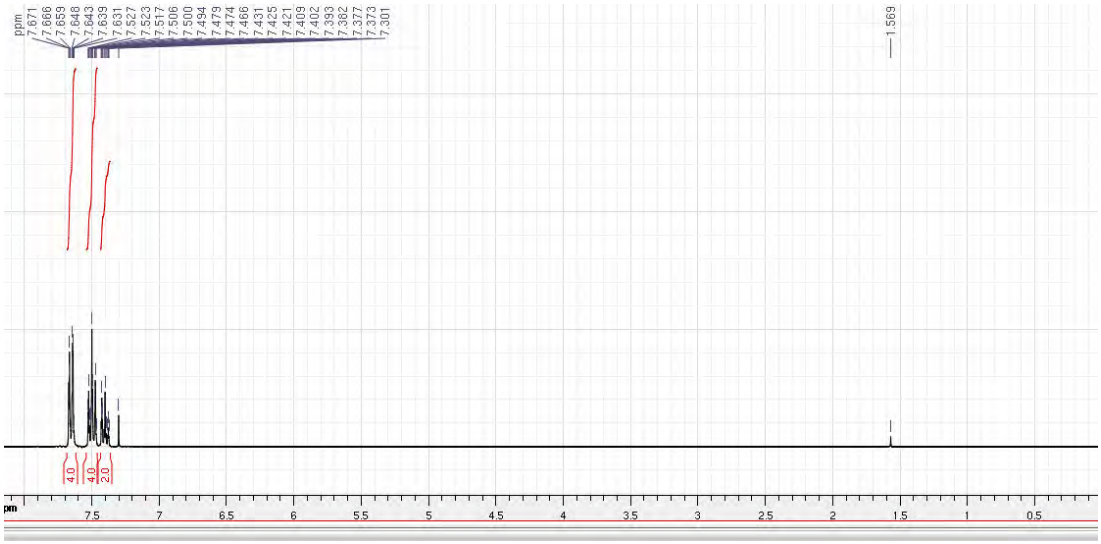

Figure 4. ^{1}H NMR ($CDCl_3$, 300 MHz) spectrum of biphenyl, δ_{ppm}: 7.37-7.43 (m, 2H), 7.46-7.52 (m, 4H), 7.63-7.67 (d, 4H).

Table 2. Recycling results of Suzuki-Miyaura reactions between bromobenzene and phenylboronic acid using 0.1 mol% of PdNPs-**2**.

Catalytic runs	1st	2nd	3rd	4th	5th	6th
Yield	93%	91%	88%	87%	87%	63.6%

RuNP-**2** efficiently catalyzes transfer hydrogenation of nitrobenzene using H_2O / *i*-propanol as the solvent at 80 ℃ in the presence of the base with only 0.01 mol% of catalyst at 80 ℃ for 24 h (Scheme 4 and Figure 5), leading to a TON of 2300 and TOF of 96 h^{-1}. Recycling this catalyst with 0.1 mol % RuNP-**2** provides a product yield of 85% or more up to the 3rd successive recycling run (Table 3).

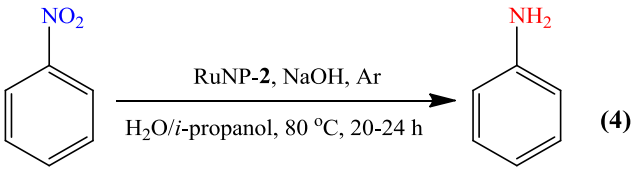

(4)

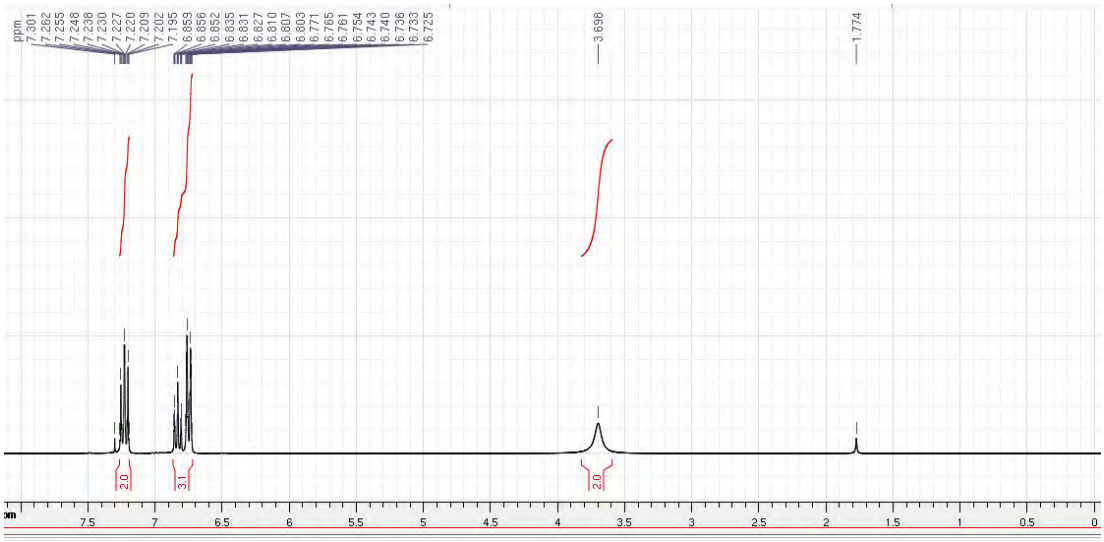

Figure 5. ^{1}H NMR spectrum (300 MHz, $CDCl_3$) of aniline. δ_{ppm}: 3.69 (s, 2H), 6.72-6.89 (m, 3H), 7.19-7.26 (m, 2H).

Table 3. Recycling results of the transfer hydrogenation of nitrobenzene using 0.1 mol% of RuNPs-**2**.

Catalytic Runs	1st	2nd	3rd	4th
Yield	90%	85%	85%	70%

CuNP tested as catalyst for click reaction between benzyl azide and phenylacetylene (Scheme 5 and Figure 6), and found to be extremely efficient. This reaction is indeed quantitatively achieved at 35℃ for 24 h using only 20 ppm of Cu from CuNP-**2**

leading to an exceptional TON of 28000 and TOF of 1170 h^{-1}; this is one of the very best results ever obtained using CuNP catalysts. Moreover, recycling experiments using 100 pm of CuNP provided yields larger than 80% during at least four successive recycling experiments, showing the good stability of the catalyst (Table 4).

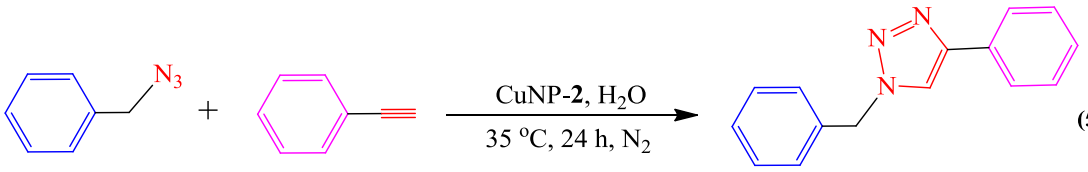

(5)

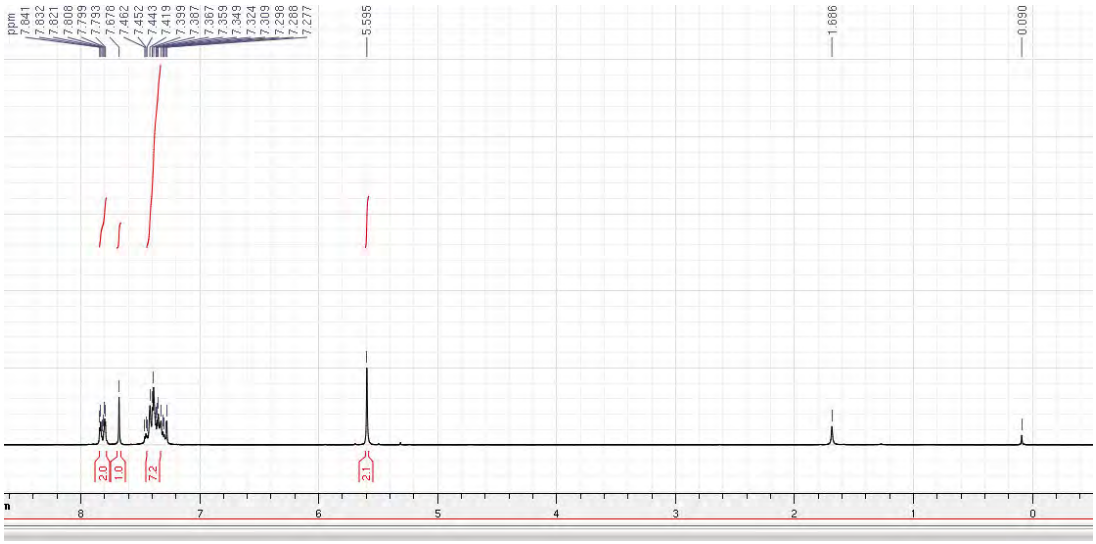

Figure 6. ^{1}H NMR spectrum of 1-benzyl-4-phenyl-1H-[1,2,3]triazole.

^{1}H NMR (200 MHz, $CDCl_3$) δ_{ppm}: 7.84-7.79 (m, 2H), 7.67 (s, 1H), 7.41-7.67 (m, 7H), 5.59 (s, 2H).

Table 4. Recycling results of CuAAC reactions between benzyl azide and phenylacetylene using 100 ppm of CuNPs-**2**.

Catalytic Runs	1st	2nd	3rd	4th	5th *a*
Yield	96%	86%	85%	83%	50%

a Reaction for 48 h.

We used X-ray photoelectron spectroscopy (XPS) to investigate the actually active species in this "click" reaction, and found that the catalyst was in its classic Cu(I) state. It is unavoidable that the CuNPs surface is oxidized by molecular oxygen from air, and the active Cu^{I} species is thus formed in the native oxide layer on the Cu surface through comproportionation of Cu^{0} and Cu^{II}, even if caution is taken to remove air.

Further study has then been shown that the weak surface ligand coordination and easy ligand substitution by substrates played a critical role in determining the high efficiencies of the nanocatalysts (Figure 7).

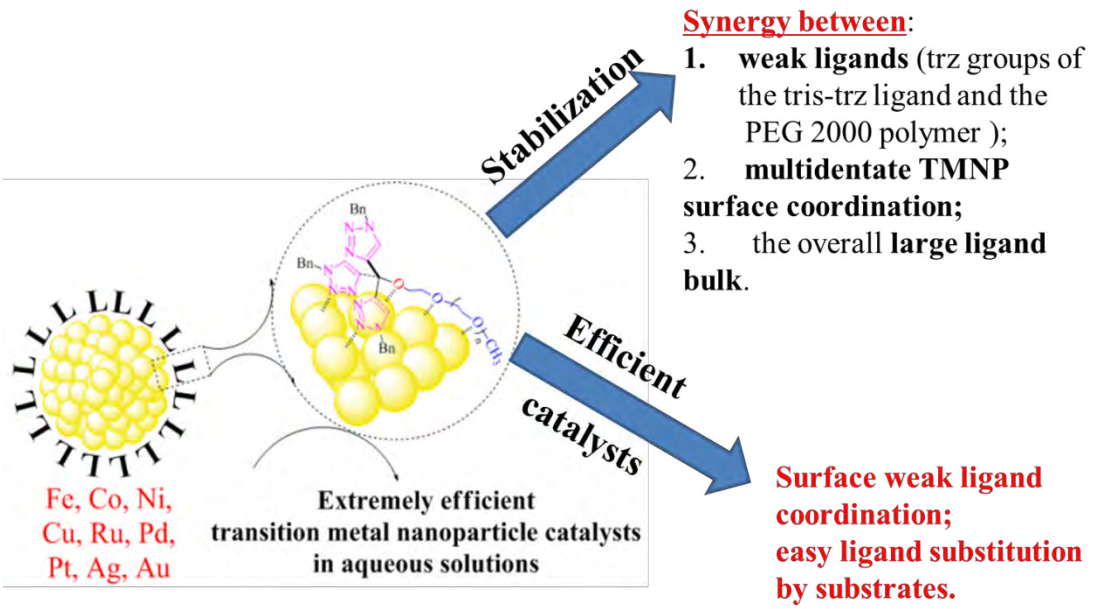

Figure 7. The summary of the working principles of tristrz-PEG ligand in both effective TMNPs stabilizations and efficient catalysts.

From Mono-to Tris-1,2,3-triazole-Stabilized Gold Nanoparticles and their Compared Catalytic Efficiency in 4-Nitrophenol Reduction

In this paper, we compared the stabilization of AuNPs by mono-, bis-, and tris-trz and their influence of the trz denticity on the 4-NP reduction by $NaBH_4$ in water also including comparison with current polyethylene glycol 2000 (PEG) and polyvinylpyrrolidone (PVP) AuNP stabilizers (Figure 8 and Table 5).

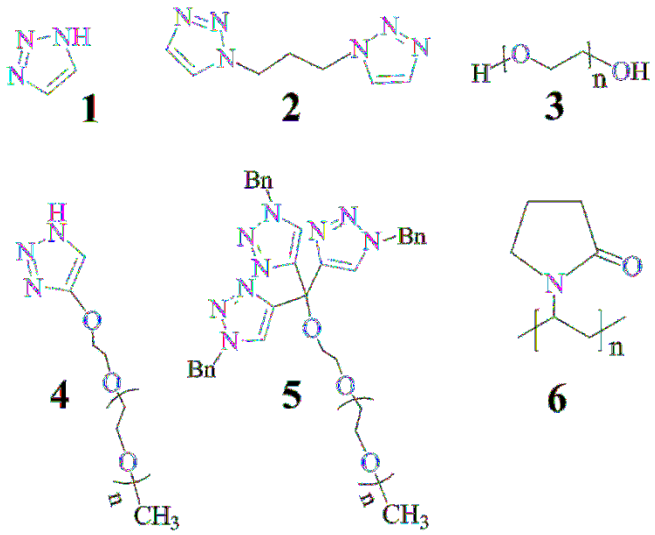

Figure 8. Ligands used for AuNP stabilization. **1** 1.2.3, triazole; **2** bis-triazole; **3** PEG 2000; **4** mono-triazole-PEG; **5** Tris-triazole-PEG; **6** PVP (Mw=10,000).

The synthesis of 1,3-di(1H-1,2,3-triazol-1-yl)propane, **2**, followed the published procedures (Scheme 6). Briefly, A dried flask was charged with 1,3-diazidopropane (850 mg, 1 equiv.) and ethynyltrimethylsilane (1.65 g, 2.5 equiv.) in the presence of THF under N_2. An aqueous solution of $CuSO_4$ (0.2 equiv., 10 mol% per branch) was added, and stirred for 30 min. Afterward, NaAsc (10 equiv. per branch) was added drop wised. The mixture was then allowed to stir for 24 h at rt. Then, the mixture was then filtered, washed and the solvents were removed *in vacuo*. Then MeOH and K_2CO_3 were added, and the mixture was stirred for 24 h at rt to yield a white solid product. This product is characterized by ^{1}H NMR (Figure 9).

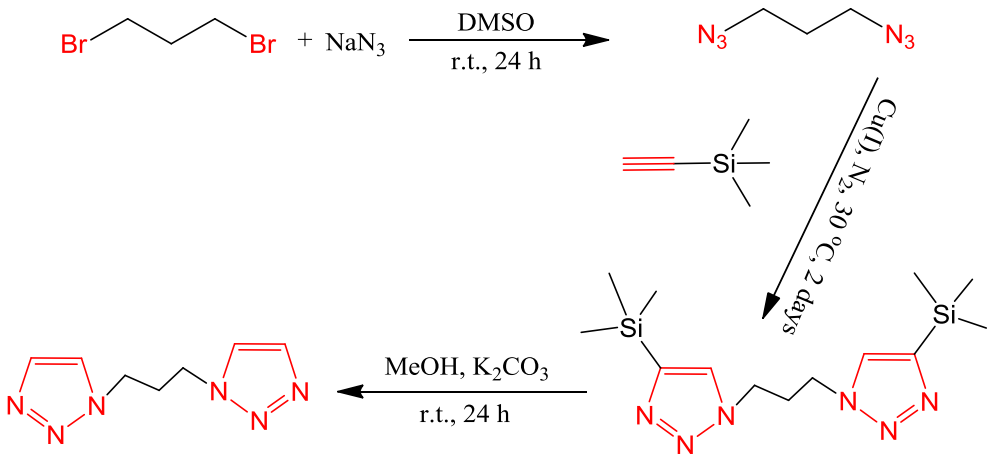

Scheme 6. Synthesis of 1,3-di(1H-1,2,3-triazol-1-yl)propane, **2.**

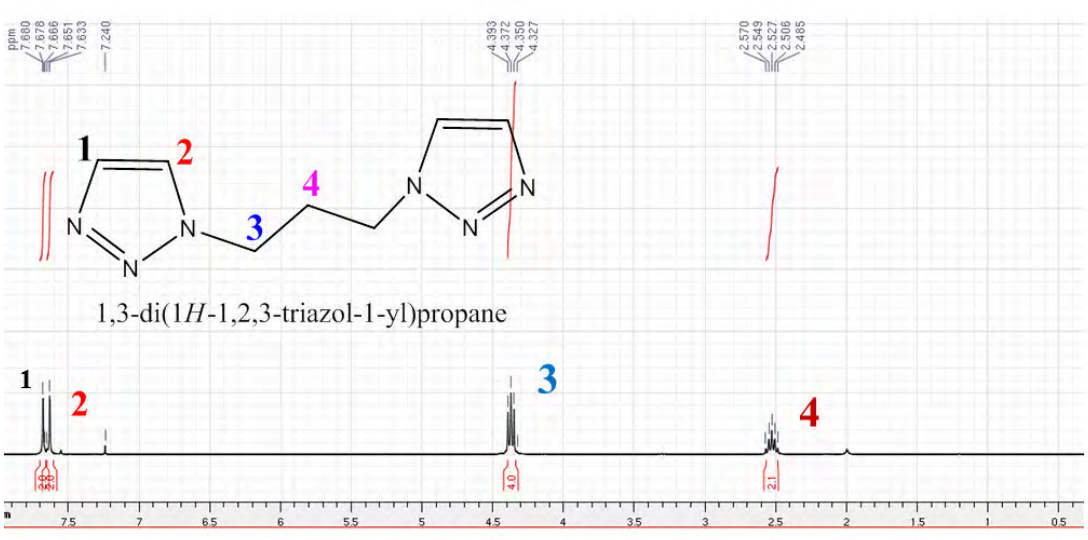

Figure 9. ^{1}H NMR ($CDCl_3$, 300 MHz) spectrum of 1,3-di(1H-1,2,3-triazol-1-yl)propane, **2.** (δ_{ppm}=7.68 (2H), 7.63 (2H), (δ_{ppm}=4.73, *J*=6.3 Hz, 2H), (δ_{ppm}=2.53 *J*=6.3 Hz, 2H).

On the other hand, the synthesis of the 1,2,3-triazole-mPEG ligand, **3**: trimethylsilyl azide (0.2 mL, 1.5 mmol) was added to a mixed DMF/MeOH solution (3 mL, 9:1) that contained the catalyst CuI (5.8 mg, 0.03 mmol) and ethynyl-mPEG (1000 mg, 1 mmol) under N_2. The reaction mixture was stirred at 90 °C overnight. Then the mixture was cooled to rt, filtered, and the solvents were removed *in vacuo*. Then, the

residue was dissolved in CH_2Cl_2 and washed three times with water. The organic phase was collected and dried over anhydrous sodium sulfate to yield the white solid product.

The synthesis of AuNP-L was used the gold precursor (1 equiv.) in 1 mL water was added to a solution that contained 1 or 3 equiv. ligand (1 or 3 triazole per Au) in 5 mL water. The mixture was allowed to stir for 15 min. Then, a freshly prepared aqueous solution of $NaBH_4$ (10 equiv.) was added to the solution dropwise, and the solution was continuously stirred for another 30 min. Dialysis was conducted for 24 hours to remove the excess of ligand and $NaBH_4$. The AuNP-**L** was kept in aqueous solution for characterization and used as catalyst. The AuNPs stabilized by PEG were prepared under identical conditions, except that 1 equiv. PEG per equiv. Au^{3+} was used.

Table 5: 4-NP reduction to 4-AP by $NaBH_4$ catalyzed by various AuNP-**L** (20 ℃).[a]

AuNP-**L**	SPB (nm)	Size (nm)[c]	Induction time (*S*)	K_{app} [d] ($\times 10^{-3}$ S^{-1})
AuNP-**1**[b]	-- (--)	**--**	0	5.2 (3.5)
AuNP-**2**[b]	527 (537)	7.3±0.5 (9.5±0.7)	0	2.6 (2.3)
AuNP-**3**[b]	527	8.3±0.5	0	18.4
AuNP-**4**[b]	515 (524)	3.1±0.3 (5.8±0.4)	0	24.9 (20.9)

AuNP-**5**	515	2.9±0.3	0	43.7
AuNP-**6**	495	2.2±0.4	40	15.2
AuNP-**5-THT**	556	14.5±1	0	17.5
AuNP-**5-0℃**	538	3.4±0.7	40	13.3

[a] Conditions: 4-NP (1 equiv.), $NaBH_4$ (81 equiv.) and AuNP-**L** catalysts (0.2 mol%). [b] Data are shown using 3 trz per AuNP; data in brackets are using 1 trz per AuNP. [c] Core size (TEM) of AuNP-**L**. [d] Rate constant.

Thus, from the comparisons, simple trz ligands stabilize AuNPs, but only the increase of ligand denticity to two and especially three insures full AuNP stabilization. Such AuNPs form with small core sizes around 3 nm, which allows observation of the plasmonics. Interestingly, the use of amphiphilic mono- and tris-trz ligand provides micellar AuNPs in a rather similar way to amphiphilic micellar dendrimers used in efficient catalysis, but of much simpler synthesis. The 4-NP reduction in water is an excellent tool to investigate the AuNP-ligand bonding in water-soluble NPs, and indeed very high rate constant values were obtained in comparison with classical PEG-AuNPs and PVP-AuNPs.

With this ligand, on the other band, we also showed the influence of AuNP precursors (gold(I)chloro(tetrahydrothiophene) [$AuCl(SC_4H_8)$]) for both AuNP morphologies and catalytic efficiencies. The direct synthesis of Au(I)-ligand complex was not stable, however, and it soon decomposed, resulting in the formation of AuNPs with a relative

large SPB (556 nm) and NP size (Figure 10 amd Table 5). On the other hand, 4-NP reduction was very successful, leading to a surprising value of k_{app} =17.5×10^{-3} s^{-1}.

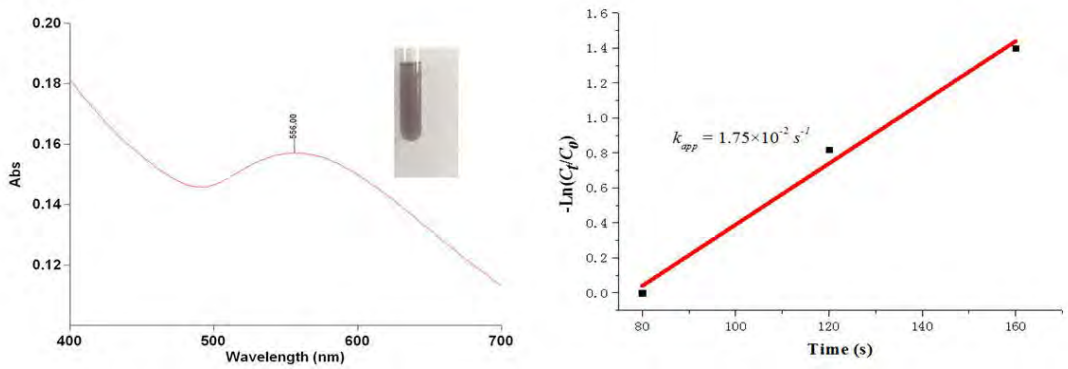

Figure 10. UV-vis. absorption spectrum of the **AuNP-5-THT** (left); Consumption rate of 4-NP: -ln(C_t/C_0) *vs.* reaction time (right, R^2 = 0.9807).

Furthermore, we also compared AuNP-**5** synthesis at rt and 0 ℃ (ice-water bath), namely AuNP-**5** and **AuNP-5-0℃**, respectively, to investigate the temperature effect in AuNP synthesis and catalytic properties in 4-NP reduction. AuNP-**5-0℃** shows a broad SPB (main at 538 nm) in the UV-vis. spectrum, and TEM images show various shapes of anisotropic AuNPs (*e.g.,* plate-like and/or spherical particles) with a broad size distribution. The increase of temperature results in the decrease of particle size and narrows size distribution, whereas decrease in reaction temperature results in increase in particle size and broad size distribution with anisotropic AuNP nanostructures.

Thus, this paper highlights the privileged tris-triazole-PEG ligand (and presumably other tris-trz and tris-nitrogen ligands) over other triazole-type AuNP ligands for 4-NP reduction. These data demonstrate the successful design of this well-defined, new, green, and amphiphilic surface tris-triazole-PEG ligand. This study opens the route both towards investigation of various other NP stabilizers and ligands for NP surface catalysis and towards micellar-type NP catalysts.

Design and applications of an efficient amphiphilic "click" Cu^{I} catalyst in water

As mentioned above, CuAAC selectively yielding 1,4-disubstituted 1,2,3-triazoles has been applied to an enormous range of new syntheses and applications to macromolecules and nanomaterial science. The catalytic active Cu^{I} species was usually generated from the cheap and easy available mixture of $CuSO_4$ and sodium ascorbate (NaAsc), known as the Sharpless-Fokin catalyst. However, the CuAAC reaction rate is low if the catalyst is not present in high concentration and in the presence of activating ligand. For practical reaction processes, in most of the cases the Sharpless-Fokin catalyst is used in relatively large quantities in order to avoid the formation of the 1,5-isomer and to keep an acceptable reaction rate. The problem then remains to remove the copper, which limits this "click" chemistry in electronics and biomedicine. To overcome these difficulties, some ligands have been shown to considerably accelerate the reactions and reduce the catalyst amounts. Among them, nitrogen-based ligands such as polytriazoles and tris(2-aminoethyl)amine derivatives

(tren), have been found to be excellent, reducing the amount of Cu^{I} catalyst to the order of 1% or less. Recently it was reported that a recyclable dendritic nanoreactor containing intradendritic triazoles and the poly(*N*-isopropylacrylamide-*co*-*N*-vinylimidazole) polymer promoted CuAAC reactions in water and in *t*-BuOH/H_2O, respectively, down to the remarkable ppm level of Cu^{I} catalyst under the conditions of in situ Cu^{2+} reduction using NaAsc. With such low amounts of catalysts and exceptional efficiencies, CuAAC reactions in aqueous solution under mild reaction conditions effectively contributed to the pursuit of "green chemistry" with potential industrial applications.

Based on this tris-trz-PEG amphiphilic ligand, especially benefiting from the chelation effect, new efficient amphiphilic "click" Cu^{I} catalyst was designed by addition of $CuSO_4 \cdot 5H_2O$ under nitrogen to an aqueous solution containing the amphiphilic tris-trz-PEG ligand, then *in situ* reduction of the pre-catalyst PEG-tris-trz-Cu^{2+} to the PEG-tris-trz-Cu^{I} catalyst by dropwise addition of NaAsc (Figure 11).

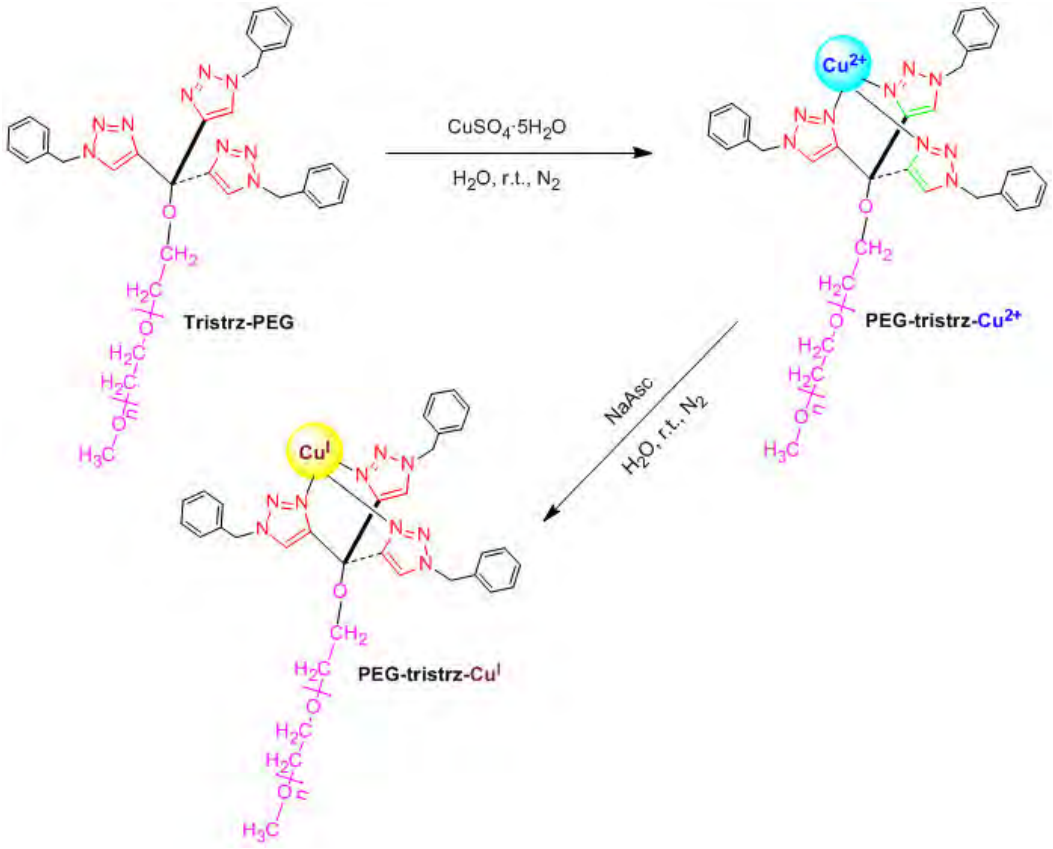

Figure 11. Synthesis of the PEG-tris-trz-Cu^{I} "click" catalyst.

This catalyst shows high activity for CuAAC "click" reaction in water at ambient temperature. Only ppm Cu^{I} were necessary to reach quantitative yields with TON up to 86000 and TOF 3600 h^{-1}. For the recycling of the catalyst: after the CuAAC reaction, The "click" products from the aqueous solution was extracted using cold diethyl ether (2×5 mL) while keeping the catalyst in the water phase. After charging another run of substrates, the water phase was directly injected by a syringe under N_2. External addition of NaAsc (10 equiv) was necessary to ensure keeping the catalytic Cu^{I} species active during catalysis. The amphiphilic tris-trz-PEG ligand is insoluble in cold diethyl ether, allowing the fully recyclability. The catalyst reused at least 6 times without change of ligand structure during the CuAAC reactions. Large-scale

syntheses were also successfully achieved with 93 % yield (Table 6).

Table 6: Product yield upon recycling 50 ppm catalyst in the reaction condition of 0.1 mmol benzyl azide, 0.105 mmol phenylacetylene and 1 mL water at 35℃.

Recycling number	1st	2nd	3rd	4th	5th	6th
Yield	95%	90%	83%	81%	75%	53%

To investigate the underlying reason(s) for this high efficiency in the CuAAC reactions in water using such low amounts of PEG-tris-trz-Cu^{I} catalyst. Cu^{I} stabilized by PEG 2000, monotrz-PEG and tris-trz-PEGwere compared with the original neat Cu^{I} ($CuSO_4$ + NaAsc, **A**) catalyst for the CuAAC of benzyl azide and phenylacetylene in water under identical conditions (Table 7).

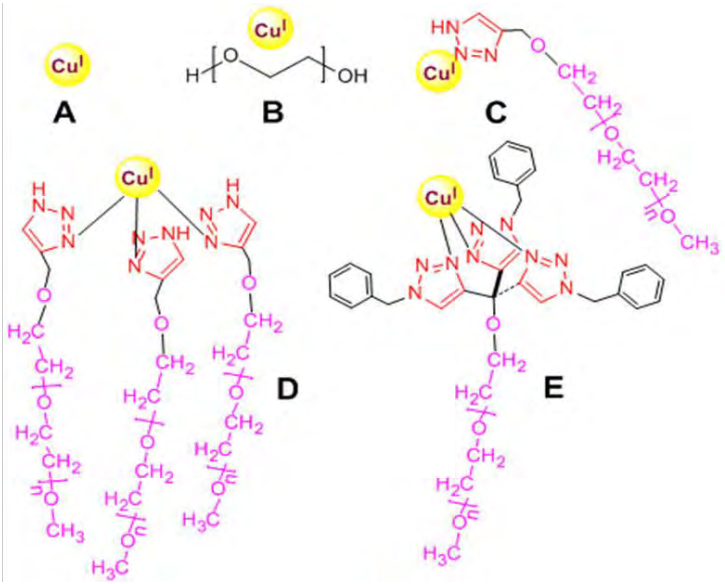

Table 7: Comparison between the crude yields (%) obtained with the Cu^I, PEG-Cu^I, PEG-mono-trz-Cu^I, and PEG-tris-trz-Cu^I catalysts in the CuAAC reaction between benzyl azide and phenylacetylene.

Amount / Catalysts	2000 ppm	200 ppm	100 ppm	50 ppm
Cu^I (**A**)	34.9	12.3	5	0
PEG-Cu^I (**B**)	40	12.5	5.6	2.9
1 PEG-mono-trz-Cu^I (**C**)	70.7	41	26.5	13.8
3 PEG-mono-trz-Cu^I (**D**)	91.4	79.4	66.7	34
PEG-tris-trz-Cu^I (**E**)	100	100	100	100

Thus, it is confirmed that the high efficiency of these click reactions catalyzed by very low amounts of PEG-tris-trz-Cu^I catalysts benefit from

(i) the chelation effect;

(ii) the amphiphilicity of the tris-trz-PEG ligand containing a tris-triazole tripod that increases the electron density on the metal center;

(iii) a PEG chain allowing homogeneous click reactions in water.

The general procedures of “click” reaction are: a glass vessel equipped with a magnetic stirring bar was charged with 0.1 mmol of organic azide and 0.105 mmol of alkyne under a nitrogen atmosphere. Catalytic amounts of catalyst were added into the

vessel under N_2, and degassed water was added in order to obtain 1 mL as the total volume of water. The reaction mixture was stirred during 20 h at 35 °C under N_2. After the reaction, the mixture was filtered and then extracted using CH_2Cl_2 (3× 10 mL). The organic layer was dried over Na_2SO_4 and filtered, and the solvent was removed *in vacuo* to give the corresponding 1,2,3-triazoles. The product was then purified by silica chromatography when necessary. The low level catalyst of PEG-tris-trz-Cu^I catalyst showed wide substrates scope in CuAAC reactions between various alkynes and organic azides in water (Figure 12), and excellent yields were generally obtained.

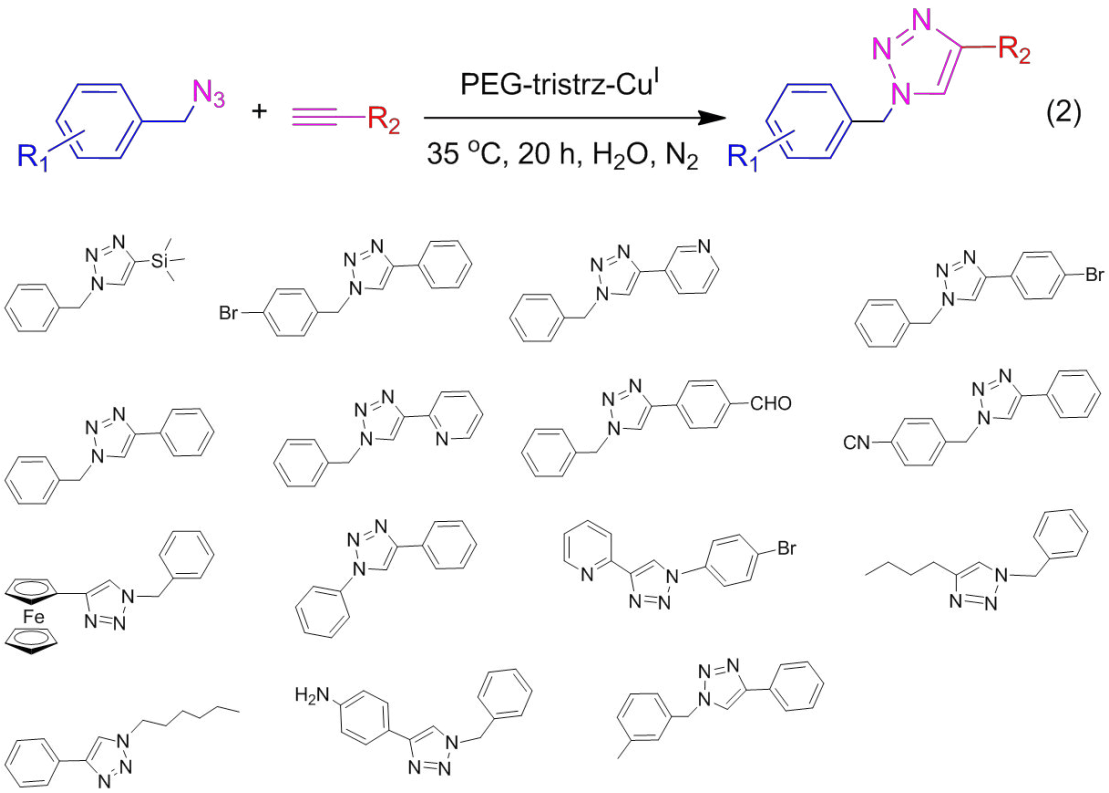

Figure 12. Substrate scope of CuAAC reactions between various azides and alkynes using the PEG-tris-trz-Cu^I catalyst.

Furthermore, the catalyst was applied to the efficient synthesis of various useful functional products with medicinal, catalytic, targeting, and labeling properties (Figure 13). For instance, 1-ethynylcyclohexanol has a simple structure, and it is known as an active metabolite of the old central nervous system depressant drug ethinamate. The click reaction with benzyl azide in excellent isolated yield (93%) was achieved using only 200 ppm at 35℃ for 20 h.

On the other hand, the PEG-tris-trz-Cu^{I} catalyst also allows click synthesis of 9-ferrocenyltriazole dendrimer and 9-pyridyltriazole dendrimer in excellent yields with 100 ppm Cu per azido branch of catalyst under ambient conditions in water. Taking the synthesis of 9-ferrocenyltriazole dendrimer as the example: A glass vessel equipped with a magnetic stirring bar was charged with nona-azido precursor (16.69 mg, 1 equiv.) and ethynylferrocene (22.1 mg, 1.05 equiv. per azido group) under argon atmosphere. The PEG-tris-trz-Cu^{I} catalyst (100 ppm per azido group) was added into the vessel under argon, and degassed water was added in order to obtain 1 mL as the total volume of water. The reaction mixture was stirred during 24 h at 40 °C, the light yellow solid formed sticked on the wall of the glass vessel and magnetic stirring bar. After the reaction, the glass vessel was washed twice with water and pentane respectively, and filtered. CH_2Cl_2 (30 mL) was then added to solubilize the dendrimer, the CH_2Cl_2 solution was then dried over Na_2SO_4 and filtered, and the solvent was removed *in vacuo* to yield the dendrimer.

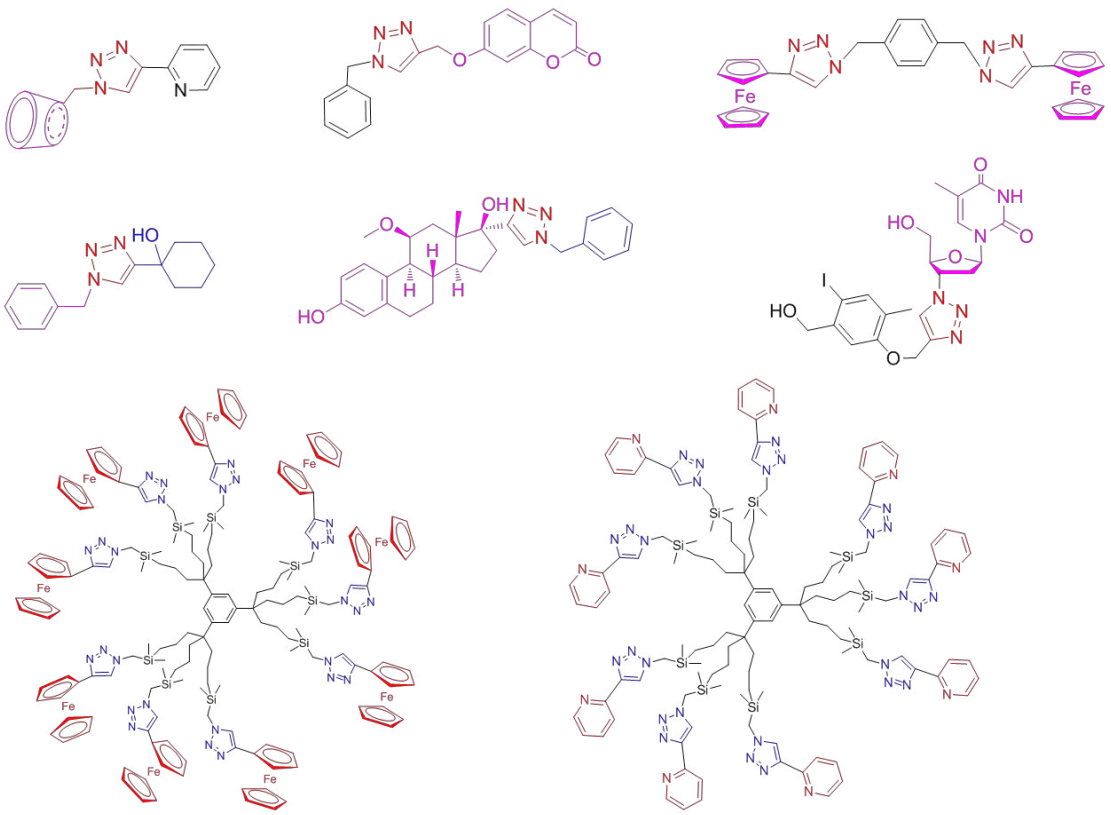

Figure 8. Application of the PEG-tris-trz-Cu^{I} catalyst to the synthesis of functional materials.

Thus, in this study, the family of nitrogen based ligands that accelerate the CuAAC reactions has been extended with the utilization of the amphiphilic tris-trz-PEG ligand. This recyclable ligand has now been shown to promote the conventional Sharpless-Fokin catalyst as a highly efficient Cu^{I} "click" catalyst in water for various organic syntheses. Comparative catalytic studies indicate that the tris-trz-PEG ligand is more efficient than the mono-trz-PEG ligand, and reduction of Cu^{II} to Cu^{I} is considerably slower with the former ligand than with later. These trends confirm the favorable effect of the chelation in tris-trz-PEG concerning the catalytic properties.

This study should contribute to the more effective synthesis of clicked compounds that are useful in current organic reactions and in various fields with the use of the copper catalyst in minute quantities down to industrially tolerable amounts.

Reference

1 P. Herves, M. Perez-Lorenzo, L. M. Liz-Marzàn, J. Dzubiella, Y. Lu, M. Ballauff, *Chem. Soc. Rev*. **2012**, *41*, 5577-5587

2 N. Pradhan, A. Pal, T. Pal, *Colloids Surf. A*, **2002**, *196*, 247-257.

3 a) Y. Mei, G. Sharma, Y. Lu, M. Drechsler, T. Irgang, R. Kempe, M. Ballauff, *Langmuir* **2005**, *21*, 12229–12234; b) S. Wunder, F. Polzer, Y. Lu, M. Ballauff, *J. Phys. Chem. C* **2010**, *114*, 8814–8820; c) S. Wunder, Y. Lu, M. Albrecht, M. Ballauff, *ACS Catal*. **2011**, *1*, 908-916; d) S. Gu, Y. Lu, J. Kaiser, M. Albrecht, M. Ballauff, *Phys. Chem. Chem. Phys.* **2015**, *17*, 28137-28143.

4 P. Zhao, X. Feng, D. Huang, G. Yang, D. Astruc, *Coord. Chem. Rev*. **2015**, *287*, 114-136.

Chapter 3

Efficient Heterogeneous Nanoparticles Catalysts Based on Graphene Supports

Introduction

This chapter concerns our approaches of the design of efficient nanocatalysts using graphene-based supports. Three sections (each containing a publication) are included in this chapter.

Section 3.2 demonstrates the synthesis, characterization of a recyclable RhAg nanocatalyst supported on reduced graphene oxide and its catalytic application as an efficient catalyst for 4-nitrophenol reduction in water. The design of ultra-fine, highly efficient and recyclable heterogeneous bimetallic nanoparticles catalysts is challenging. In this work, we report for the first time the preparation of ultrafine and monodispersed bimetallic RhAg nanoparticles that are uniformly supported on reduced graphene oxide (rGO) nanosheets (RhAg/rGO). The efficiencies of the RhAg/rGO catalysts are strongly dependent on the composition of Rh and Ag. The RhAg/rGO catalysts were characterized by various techniques including UV-vis., ICP-AES, TEM, HRTEM, STEM, EDX, and XPS, which are in collaborated with Drs. Roberto Ciganda, Luis Yate and Sergio Moya. The $RhAg_{0.5}$/rGO showed a remarkable reaction rate in 4-nitrophenol reduction. Moreover, the catalyst was recycled, and its amount was reduced to 100 ppm of $RhAg_{0.5}$/rGO while retaining an exceptional catalytic efficiency.

Section 3.3 shows the new nanocatalyst α-Fe_2O_3 nanocluster/graphene oxide (α-Fe_2O_3/GO) for efficient Suzuki–Miyaura coupling reactions in aqueous solution and reduction of 4-nitrophenol (4-NP) in water employing only ppm amounts of catalyst. The presence of the tristrz-PEG ligand not only insured formation of α-Fe_2O_3 but also quantitative deposition of α-Fe_2O_3 onto GO induced by supramolecular interactions. Moreover, the catalyst is recycled at least 4 times in good yields to the coupling products in the Suzuki–Miyaura coupling reactions.

Section 3.4 illustrates the syntheses and catalytic applications of graphene oxide-supported metal nanocatalysts for a variety of transition metals including both noble metals and biometals. The catalysts are synthesized using either exergonic or endergonic redox reactions between GO and the transition metal salts. These ultrafine,

surface-clean metal NPs on graphene oxide with good monodispersity show high efficiency in a varietry of water-based chemical reactions at ambient temperature. These reactions include 4-nitrophenol reduction by $NaBH_4$ (the standard test reaction), Sonogashira coupling, azide-alkyne 1,3-cycloaddition (click reaction) and dihydrogen production upon hydrolysis of ammonia-borane. Moreover, these efficient catalysts can also be recycled, as exemplified in the case of RhNPs/GO catalyzed hydrolysis of ammonia-borane for hydrogen production.

J Mater Sci

Chemical routes to materials

RhAg/rGO nanocatalyst: ligand-controlled synthesis and superior catalytic performances for the reduction of 4-nitrophenol

Changlong Wang[1,4], Roberto Ciganda[1,2], Luis Yate[3], Sergio Moya[3], Lionel Salmon[4], Jaime Ruiz[1], and Didier Astruc[1,*]

[1] *ISM, UMR CNRS No 5255, Univ. Bordeaux, 33405 Talence, France*
[2] *Facultad de Quimica, Universidad del Pais Vasco, Apdo 1072, 20080 San Sebastián, Spain*
[3] *Unidad Biosuperficies, CIC biomaGUNE, Paseo Miramon No. 182, Edif "C", 20009 Donostia-San Sebastián, Spain*
[4] *UPR CNRS No. 8241, Laboratoire de Chimie de Coordination, 31077 Toulouse, France*

Received: 27 February 2017
Accepted: 27 April 2017

ABSTRACT

The design of ultrafine, highly efficient and recyclable heterogeneous bimetallic nanoparticles catalysts is challenging. In this work, we report for the first time the preparation of ultrafine and monodispersed bimetallic RhAg nanoparticles that are uniformly supported on reduced graphene oxide (rGO) nanosheets (RhAg/rGO). A key is the presence of the tris(triazolyl)-polyethylene glycol (tristrz-PEG) ligand as a weak stabilizing agent. This amphiphilic tridentate ligand not only enables the formation of ultrafine RhAg NPs, but also allows quantitative fixation of the NPs onto the rGO, which avoids metal loss and further improves catalytic efficiency. The RhAg/rGO catalysts were characterized by various techniques including UV–Vis, ICP-AES, TEM, HRTEM, STEM, EDX and XPS. By varying the molar ratios of Rh to Ag, the highest catalytic activity in the reduction of 4-nitrophenol by $NaBH_4$ was obtained for $RhAg_{0.5}$/rGO with a remarkable reaction rate of $k_{app} = 14.8 \times 10^{-3}$ s^{-1} ($k_{nor} = 1415$ s^{-1} g^{-1}). Moreover, the catalyst was recycled, and its amount was reduced to 100 ppm of $RhAg_{0.5}$/rGO while retaining an exceptional catalytic efficiency. The present work contributes to the effective design of ultrafine bimetallic NPs/graphene-based nanocomposites and to the fabrication of very efficient and cost-effective catalysts.

Introduction

Noble bimetallic nanoparticles (NBNPs) have received considerable interest owing to their composition-dependent optical, electronic and catalytic properties and have been successfully applied to the homogeneous and heterogeneous catalysis of various organic and inorganic reactions [1–19]. The facile blending of two metals or the incorporation of two metals often enhances the catalytic activity and

Address correspondence to E-mail: d.astruc@ism.u-bordeaux.fr

DOI 10.1007/s10853-017-1158-7
Published online: 04 May 2017

regulates the selectivity. The resulting synergistic effect allows tuning the average binding energy of the NBNP surface and optimizes the charge density at specific active surface metal sites [20, 21]. As a consequence, NBNP catalysts are often more active than their monometallic counterparts, and the total catalytic amount of these very efficient NBNP catalysts is therefore minimized for practical applications. In this way, cost-effective catalysts are afforded via dilution of the efficient noble metals with other abundant metals.

Rhodium (Rh) has been reported as an efficient catalyst source in a wide range of processes [22], but it is scarce in earth and very expensive, while Ag is much more abundant and much less expensive than Rh. Ag is not industrially very useful in pure bulk form, and it is not a very efficient catalyst in its NP form, however. The blending of Rh and Ag NPs in bimetallic systems has thus been considered as a powerful means to further improve catalytic properties and at the same time to reduce the total amount of Rh. A difficulty along this line is that the construction of Rh/Ag bimetallic systems is not straightforward, due to the well-known immiscibility of these two metals. Indeed even at 2000 °C, the mixture of Ag and Rh does not produce a homogeneous solution, but only segregated clusters emerge out upon cooling. Such a feature has limited the potential applications of Rh/Ag bimetallic systems, and therefore, their chemistry and catalytic behavior have been less studied than those of many other bimetallic systems [23–25]. The emergence of nanoscience has brought about the possibility to overcome these problems by reducing the NP size to a very few nm, and small NPs have shown very different properties compared with the bulk form. In particular, the NP size allows solving the problem of the non-spontaneous miscibility [26–31]. For instance, recently Pal et al. elegantly established the synthesis of homogeneous Rh/Ag bimetallic NPs by a simple co-reduction process using hydrazine hydrate as reducing agent. Using this reagent, Rh/Ag bimetallic NPs were shown to be a very efficient catalyst for 4-nitrophenol (4-NP) reduction and decomposition of hydrogen peroxide. An ensemble effect was successfully proved by the enhanced catalytic activity that was obtained upon variation of the Ag/Rh ratios [32].

In the present work, we report for the first time the facile synthesis of various RhAg/rGO heterogeneous catalysts (rGO: reduced graphene oxide) with ultrafine NP size and their structural optimization and exceptional catalytic activity. The formation of RhAg bimetallic NPs with very small size (2–3 nm) was ensured using NP encapsulation by the tris(triazolyl)-polyethylene glycol (tristrz-PEG) ligand. This procedure allows the effective fixation of the small Rh/Ag NPs onto rGO through the supramolecular H-bonding interactions between the PEG termini of the tristrz-PEG ligand [33–35] and surface oxygen functional groups of rGO. The RhAg/rGO heterogeneous catalysts showed exceptional catalytic efficiencies in the 4-NP reduction by $NaBH_4$ in water at rt. Furthermore, due to the heterogeneity of the catalysts, they were easily recycled, and their long life and high reusability were demonstrated without significant decrease in the catalytic performance up to at least the fifth run.

Experimental section

General data

All solvents and chemicals were used as purchased, unless elsewhere noted. Milli-Q water (18.2 MΩ) was used for all the NP preparations. Prior to the synthesis, the Schlenk flask was washed with a solution of aqua regia ($HCl/HNO_3 = 3{:}1$, v/v) to remove traces of residual metal. UV–Vis absorption spectra were measured with Perkin-Elmer Lambda 19 UV–Vis spectrometer. The inductively coupled plasma optical emission spectroscopy (ICP-AES) analyses are achieved with a Varian ICP-AES 720ES. Transmission electron microscopy (TEM), high-resolution TEM (HRTEM) and scanning transmission electron microscopy (STEM)-coupled quantified energy-dispersive X-ray spectroscopy (EDX) were recorded at LCC, Toulouse. Size was calculated based on at least 100 NPs. X-ray photoelectron spectroscopy (XPS): System SPECS SAGE HR, X-Ray source: Mg Kα non-monochromatic, operated at 12.5 kV and 250 W. Take off angle was 90°, at $\sim 10^{-8}$ Torr. Pass energy for survey spectra is 30 and 15 eV for narrow scans. Analysis: spectra are calibrated to CC carbon 285 eV. Analysis consisted of Shirley background subtraction. Peaks are fitted with symmetrical Gaussian–Lorentzian (GL) line shapes. Sample is dispersed on silica substrate and evaporated prior to measurement.

Preparation procedures

GO Synthesis

GO was synthesized following a published procedure [36]. In short, 1 g of graphite powder was sonicated and stirred in an ice bath in the presence of 46 mL concentrated H_2SO_4 (Aldrich 99%) and 1 g of $NaNO_3$ (Aldrich 99%) for 30 min. Then, 6 g of $KMnO_4$ (Aldrich 99%) was very slowly added, and sonication was continued for another 30 min, after which the flask was removed and allowed to stir slowly overnight at 30 °C. Next, 50 mL of deionized H_2O was slowly added under nitrogen followed by 1 h of stirring. Finally, 300 mL of 3% H_2O_2 (Fisher, 30%) was dispensed into the flask, yielding a yellowish brown GO suspension. The as-prepared suspension was washed several times thoroughly with diluted HCl (3%) and deionized water via centrifugation, until the pH was neutral. After centrifugation, it was then sonicated and thereafter dried *in vacuo* at 60 °C overnight to obtain a GO powder.

Synthesis of the RhAg/rGO catalysts (Scheme 1)

Catalysts of RhAg/rGO with different molar ratios of Ag and Rh were synthesized in water at rt. Typically, different amounts of $AgNO_3$ and $Rh(NO_3)_3$ were added in the presence of the tristrz-PEG ligand (the Rh/Ag molar ratio is fixed for 0.002 mmol, and total metal precursors/ligand molar ratio = 1:1) to reach a total of 6 mL aqueous solution, and the mixture was stirred for 15 min. Then, a fresh aqueous solution of $NaBH_4$ (10 equiv. per total metal precursors, 1 mL) was added into the above mixture with magnetic stirring for 30 min, and GO was added and further stirred for 30 min to obtain uniformity. The mixture was then aged for 3 h, and the solid was separated, washed and dried at 60 °C overnight.

Catalytic reduction of 4-NP by $NaBH_4$ at 20 °C

The catalytic efficiencies of the catalysts RhAg/rGO catalysts were tested by the model reduction of 4-NP to 4-AP with excess of $NaBH_4$ that is fast, simple and well controlled. Generally, 4-NP (1 equiv.) was mixed with excess $NaBH_4$ (81 equiv.) in water under air at 20 °C. The color of the solution changed from light yellow to dark yellow due to the formation of the 4-nitrophenolate ion. Then, a solution containing the catalyst RhAg/rGO (0.2 mol%) was added into the mixture at 20 °C; the solution quickly lost its dark

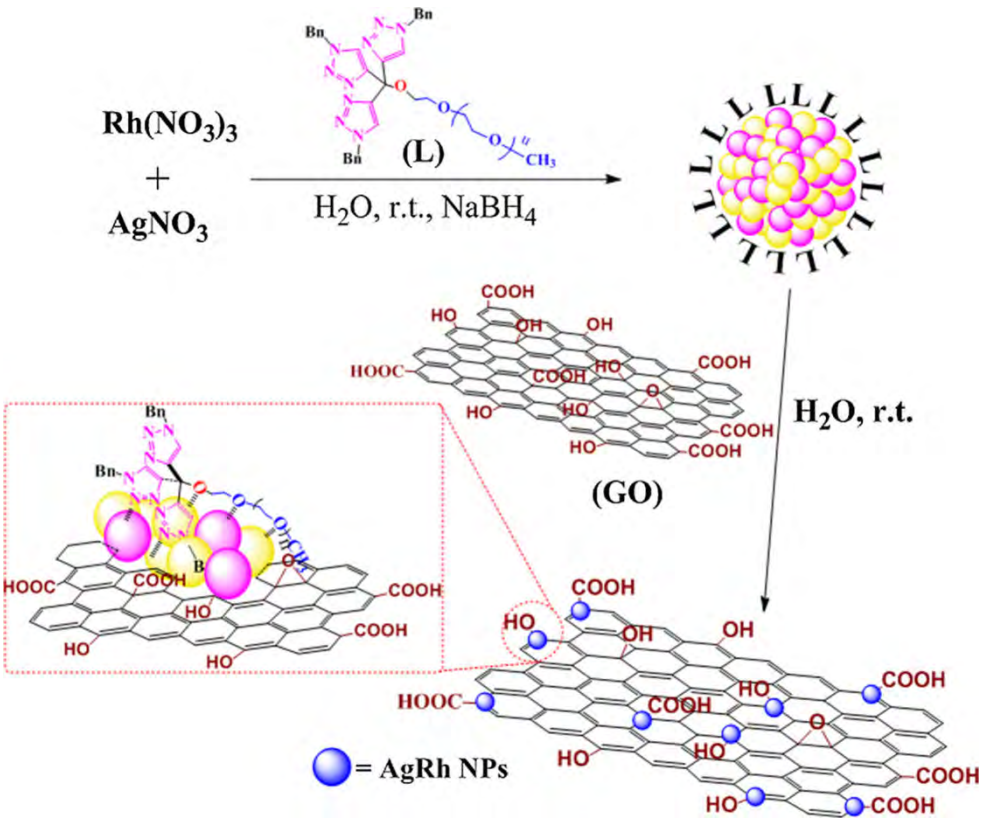

Scheme 1 Synthesis of the RhAg/rGO catalysts.

yellow color with time, and the progress of the reaction was quickly measured by UV–Vis spectroscopy in a scanning range of 250–500 nm (40 s for each run). For the recycling study, the catalyst was recovered by centrifugation, washed and re-dispersed in water. The reaction was then conducted following the above-mentioned procedure. Control experiments employing the Ag/rGO and Rh/rGO catalysts (0.2 mol% per nitrophenol) were also conducted for comparison.

Results and discussion

The GO powder was prepared according to a modified Hummer's method [36] followed by sonication treatment, and it was readily dispersed in water to form a light yellow suspension. The TEM image showed that the GO nanosheets consisted of several layered nanostructures (Fig. 1a).

The nanocatalyst construction started with the synthesis of AgNPs in aqueous solution in the presence of tristrz-PEG as the encapsulating ligand and involved reduction of Ag(I) by sodium borohydride [33]. The ligand-stabilized AgNPs presented a surface plasmon band (SPB) at 417 nm, and the AgNPs were monodispersed with a NP size of 2.3 nm.

After the synthesis, GO was directly added to the solution and further stirred for another 30 min, and meanwhile, GO was reduced by excess of $NaBH_4$ to rGO. The catalyst was then aged for 3 h, washed and dried, yielding the heterogeneous Ag/rGO catalyst (Scheme 1). The deposition process did not change the SPB and the size of AgNPs compared to the initial ligand-encapsulated AgNPs, resulting in the fixation of uniformed, monodispersed AgNPs onto rGO (Fig. S2). ICP-AES analysis indicated that >99% of the AgNPs were deposited onto the rGO.

We assume that the supramolecular H-bonding interactions between the PEG termini of the tristrz-PEG ligand and multiple surface oxygen functional groups, such as –COOH and –OH, of the rGO ensured this quantitative deposition process. The

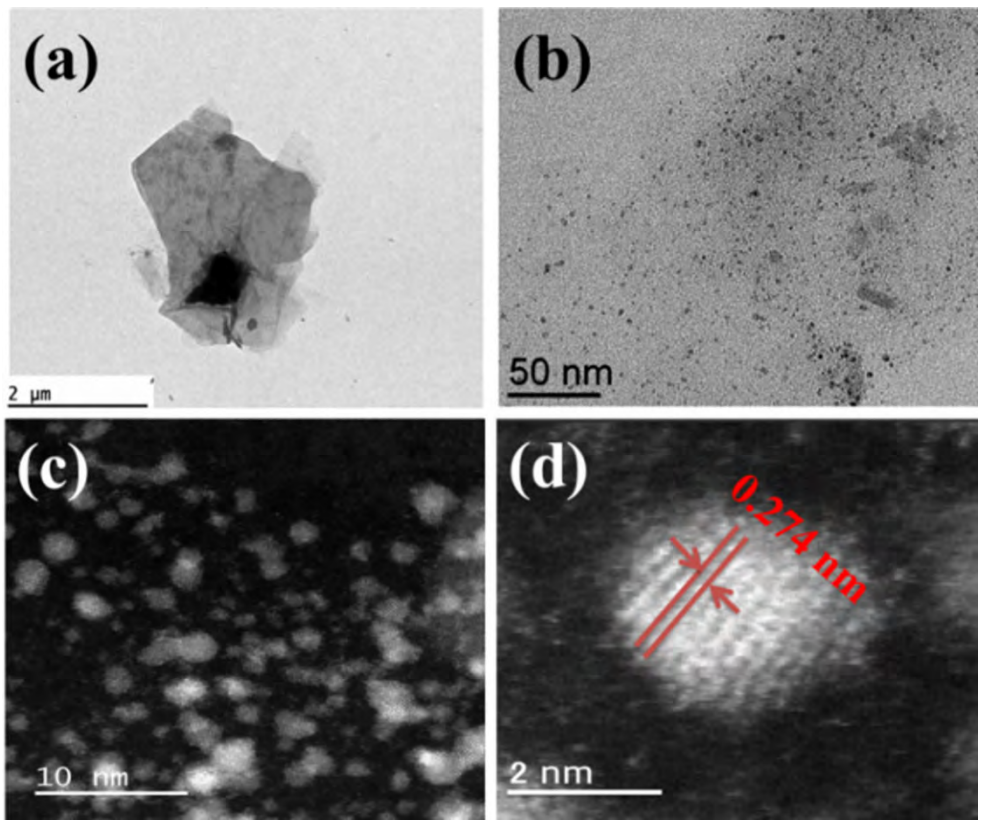

Figure 1 Typical TEM images of **a** GO and **b** $RhAg_{0.5}$/rGO; **c** and **d** are STEM *dark*-field image and HRTEM images of the $RhAg_{0.5}$/rGO catalyst at different magnification.

reduction of GO in the presence of a reductant especially in this case the $NaBH_4$ to rGO is well known, although the surface functional groups are also presented in rGO with some proportions upon reduction. Thus, the residual surface functional groups of rGO ensure this deposition process. The synergy with the triazole groups and PEG of tristrz-PEG ligand that also weekly interacted with the AgNP surface provides the effectiveness of small AgNP stabilization [33, 37] (Scheme 1). Rh/rGO was then prepared using the same method. The TEM image shows that the size of the RhNPs is 2.2 nm (Fig. S3).

We then further synthesized RhAg/rGO by dilution of Rh with Ag that changed the Rh to Ag molar ratios, with the aim to further increase the reaction efficiency and to reduce the total catalytic amount. Previously, we have shown that the tristrz-PEG ligand stabilized various transition metal NPs (TMNPs) with ultrafine sizes, which was attributed to the synergy between weak, but multidentate, surface coordination and the overall large bulk of the tristrz-PEG ligand [33]. Moreover, the surface weak ligand coordination and easy ligand substitution by substrates also benefit to the catalysts on the TMNPs surface. Now the utilization of this ligand has been extended to the synthesis of ultrafine NBNPs. With these various heterogeneous catalysts RhAg/rGO in hand, we first used UV–Vis spectroscopy to characterize the Rh/Ag bimetallic NPs (Fig. S1). Among all the samples, $RhAg_{0.5}$/rGO and $RhAg_1$/rGO represented the same and smallest SPB of 407 nm, while other samples showed larger SPB absorption wavelengths (Table 1). ICP-AES analysis indicates that, for instance in the $RhAg_{0.5}$/rGO catalyst, >99% of the RhAg NPs are deposited onto the rGO. Figures S4–S8 then show the representative TEM images of the synthesized catalysts RhAg/rGO with different Rh to Ag molar ratios. As shown in the TEM pictures, it is striking that monodispersed RhAg NPs are homogeneously dispersed on the surfaces of rGO. According to the results of the NP size distribution histogram, the average size of RhAg NP is in the range 2.2–3.0 nm (Table 1). The smallest size of RhAg NPs is observed with the $RhAg_{0.5}$/rGO sample, which is only 2.2 nm (Fig. 1b). Interestingly, we observe the formation of "particle on particle" by HRTEM and STEM dark-field image (Fig. 1c, and Figs. S9–S11). This might indicate that RhNPs are selectively linked to AgNPs, which may also suggest the formation of new active sites at the RhAg interface, and probably are beneficial for the catalytic reaction. On the other hand, a representative HRTEM image of alloyed $RhAg_{0.5}$ NPs also shows the (111) lattice fringe distance of 0.274 nm (Fig. 1d), indicating an increase of the interatomic separation distance for alloyed RhAg NPs. Although we have successfully shown the formation of bimetallic RhAg NPs by TEM, HRTEM and STEM, it is still difficult to obtain homogeneous alloyed RhAg NPs using this ligand encapsulation followed by $NaBH_4$ reduction method.

EDX analysis was conducted in order to investigate the elemental composition of the RhAg NPs, and the results are represented in Fig. S11 showing Rh, Ag, C and O signals that are provided by the $RhAg_{0.5}$/rGO sample. ICP-AES confirmed that the composition of the metals in this sample was associated with the Rh/Ag molar ratio of 2:1. For further characterization of the sample, high-resolution scanning transmission electron microscopy-coupled quantified energy-dispersive X-ray spectroscopy (HRSTEM-EDX) mapping of the $RhAg_{0.5}$/rGO sample was investigated (Fig. S12). Upon looking at the compositional maps of Rh, Ag, C and O, the presence of the RhAg NPs is clearly distinguished with the colors and the homogeneously monodispersed points.

Table 1 Properties of the synthesized catalysts RhAg/rGO and rate constants of 4-NP reduction by excess $NaBH_4$ at 20 °C

Catalysts	SPB (nm)	Size (nm)	k_{app} ($\times 10^{-3}$ s^{-1})	k_{nor} (s^{-1} g^{-1})
GO	–	–	–	–
Ag/rGO	417	2.3	1.43	106.9
Rh/rGO	–	2.2	6.1	727.1
$RhAg_{0.25}$/rGO	417	2.9	10.2	981.8
$RhAg_{0.5}$/rGO	407	2.2	14.8	1415.5
$RhAg_1$/rGO	407	2.3	12.9	1224.1
$RhAg_2$/rGO	416	2.8	10.6	998.1
$RhAg_4$/rGO	419	3.0	9.7	907.6

The exact oxidation states of the constituent metals in $RhAg_{0.5}$/rGO catalyst were checked by X-ray photoelectron spectroscopy (XPS). The Ag 3d core level XPS spectrum of the $RhAg_{0.5}$/rGO catalyst is shown in Fig. 2a. The Ag $3d_{5/2}$ and Ag $3d_{3/2}$ peaks confirm the binding energy (B. E.) values of 368.2 and 374.1 eV, respectively, with a difference of 5.9 eV that is assigned to the metallic state of Ag(0) in the $RhAg_{0.5}$/rGO system. Rh is partially oxidized, however, as the peaks at 308.8 and 313.3 eV correspond to $3d_{5/2}$ and $3d_{3/2}$ of Rh–O, respectively, whereas B. E. values at 306.7 and 311.4 eV are assigned to Rh $3d_{5/2}$ and Rh $3d_{3/2}$ of Rh(0), respectively (Fig. 2b). The surface oxide layers of Rh NPs play a critical role in determining the catalytic activity of metal catalysts [38, 39]. This partial oxidation is explained by the ultrasmall NPs size (2.2 nm) and the molar free energy of formation of metal oxides (−2.68 vs. −39 kcal mol^{-1} for Ag_2O and Rh_2O_3, respectively) [40]. These factors render the RhNPs relatively easily oxidizable. On the other hand, the higher ionization potential of Ag (7.56 eV) than that of Rh (7.46 eV) and the larger electronegativity of Rh (2.2) than that of Ag (1.9) also account for preventing complete Rh oxidation [32]. Thus, the oxidation of Ag in the catalyst $RhAg_{0.5}$/rGO was not observed, while Rh is partially oxidized, as authenticated by XPS analysis.

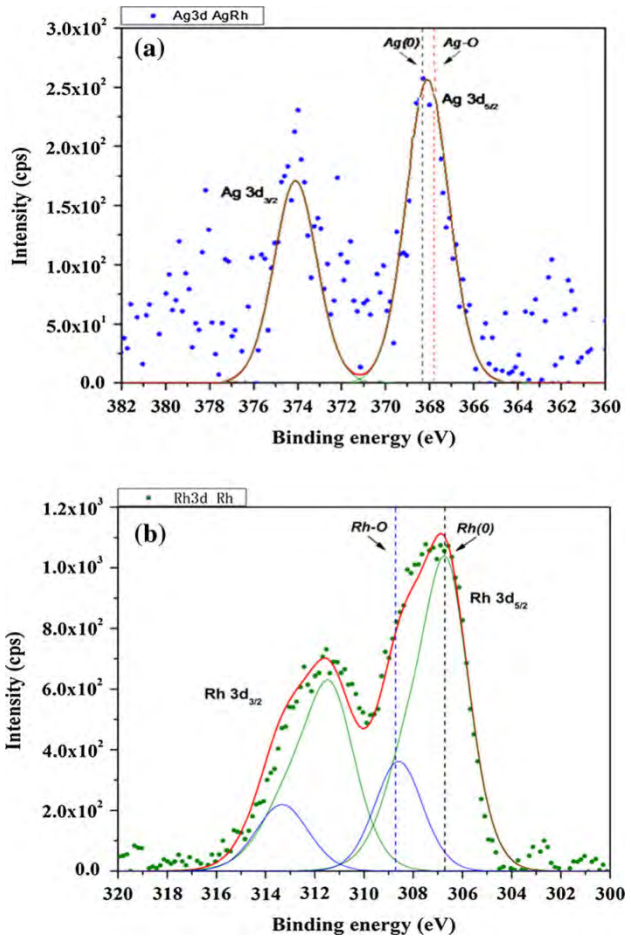

Figure 2 XPS spectra of **a** Ag 3d, and **b** Rh 3d over $RhAg_{0.5}$/rGO catalyst.

Catalytic properties of AgRh/rGO

The catalytic properties of these RhAg/rGO catalysts are explored here in the 4-NP reduction to 4-aminophenol (4-AP) by $NaBH_4$, a classic reaction for the scrutiny of the catalytic properties of transition metal NPs [41–53]. We first establish an energy-saving and environmentally friendly way, that is, the 4-NP reduction is conducted at 20 °C in water, instead of high temperature and/or organic solvents (See "Experimental" section). The 4-NP reduction by $NaBH_4$ to 4-AP was pioneered by Pal et al. in 2001, and detailed kinetic studies by Ballauff's group convincingly suggested the mechanism involving rearrangement of the substrate at the NP surface fitting the Langmuir–Hinshelwood (LH) model with an induction time caused by dynamic restructuring of the NP surface [45–53]. The 4-NP reduction reaction was easily monitored by UV–Vis spectroscopy using the intensity of the absorption band at 400 nm that corresponds to the decrease of the concentration (C_t) of the nitrophenolate anion with time along with the growth of a weak 4-AP band at 300 nm. C_0 is the initial 4-NP absorption. In the presence of the catalyst, this reaction is fitted with a pseudo-first-order kinetics with respect to 4-NP in the presence of excess $NaBH_4$, leading to the determination of the apparent kinetic rate constant, $k_{app} = -\ln(C_t/C_0)/t$, based on the regression of the slope from the logarithm plot [42–44, 54].

We first used the tristrz-PEG ligand-stabilized AgNPs to catalyze 4-NP reduction. The catalysis of the 4-NP reduction reaction by such AgNPs was not successful using only 0.2 mol% of catalyst, however, and with this catalyst, the reduction did not proceed even up to the tenth runs. Moreover, although we employed AgNPs with 2 mol% per 4-NP, induction time was observed with poor efficiency [33]. On the other hand, in the presence of Ag/rGO as catalyst, the reduction of the 4-NP occurred using the same amount of Ag/rGO catalyst (0.2 mol%) without induction time, with a

reaction rate $k_{app} = 1.43 \times 10^{-3}$ s^{-1}. The observed enhanced activity and the absence of induction time with the Ag/rGO catalyst are attributed to both the enhanced catalyst robustness and to the two-dimensional (2D) structure of rGO that facilitates 4-NP adsorption by π–π stacking interactions [55]. The 4-NP concentration near the Ag/rGO catalyst is optimized on the rGO surface, which accelerates the reduction process. The Rh/rGO (0.2 mol%) catalyzed reduction of 4-NP also proceeds readily without induction time, with an apparent rate constant $k_{app} = 6.1 \times 10^{-3}$ s^{-1}. A control experiment was also conducted in the presence of only GO as the catalyst, and reduction did not proceed even after 50 min.

Figures S13–S19 show the absorbance versus wavelength plots at different times for the reduction of 4-NP to 4-AP in the presence of the different catalysts $RhAg_{0.25}$/rGO, $RhAg_{0.5}$/rGO, $RhAg_1$/rGO, $RhAg_2$/rGO and $RhAg_4$/rGO, respectively. The absorbance peak at 400 nm disappeared faster after adding any of these bimetallic RhAg/rGO catalysts than with the mononuclear catalyst Rh/rGO, indicating a faster reaction activity of the bimetallic catalyst than their monometallic counterparts. As shown in Table 1, all the bimetallic catalysts RhAg NPs showed faster reaction rates than the monometallic NP catalysts, suggesting a favorable synergistic effect between Rh and Ag in the NPs. The so-called ensemble effect should be taken into account concerning the higher activities that have been observed among all the bimetallic RhAg systems. In these bimetallic catalysts, the surface Rh atoms are diluted by the surface Ag atoms, which cause charge redistribution and stabilization of the sole Rh atoms by Ag atoms, resulting in the isolation of more efficient catalyst sites [24, 32, 40]. The small Rh–Ag NP size and the Rh–Ag interfaces also generate other new active sites for the 4-NP reduction reaction. These factors result in the enhanced catalytic performance of bimetallic RhAg/rGO system compared to monometallic counterparts. For instance, blending Rh with 50% of Ag ($RhAg_{0.5}$/rGO) significantly enhances the reaction activity, k_{app} being 2.4 and 10.3 times larger than those of Rh/rGO and Ag/rGO counterparts, respectively. Among all the RhAg/rGO catalysts, $RhAg_{0.5}$/rGO showed the highest reaction rate, which is also associated with the smallest bimetallic RhAg NPs and SPB. Furthermore, the same catalyst $RhAg_{0.5}$/rGO synthesized under identical conditions in the absence of the tristrz-PEG ligand showed poor activity in 4-NP reduction ($k_{app=}1.17 \times 10^{-2}$ s^{-1}). This comparison highlighted the critical role of the tristrz-PEG ligand, as already demonstrated in a previous study [33]. Finally, the normalized rate constant (k_{nor}) that is associated with the amount of catalyst ($k_{nor} = k_{app}/m$) was also determined. The k_{app} value is very sensitive to various parameters, such as the concentrations of 4-NP and BH_4^- [43, 46, 49]. This normalized rate constant (k_{nor}) is generally used for the comparisons of the catalytic efficiency of 4-NP reduction using various heterogeneous catalysts, because the amount of catalyst is involved in the calculation.

The catalytic efficiencies of RhAg/rGO systems (Table 1) are advantageously compared with various recent studies from the literature listed in Table 2, a

Table 2 Comparison of the catalytic performances of RhAg/rGO with other noble bi- and trimetallic NP catalysts previously reported in the literature for the reduction of 4-NP by $NaBH_4$

Catalysts	$NaBH_4$ (equiv. per 4-NP)	k_{app} ($\times 10^{-3}$ s^{-1})	k_{nor} (s^{-1} g^{-1})
$RhAg_{0.5}$/rGO (This work)	81	14.8	1415
Pt–Au dendrites/rGO [56]	23809	3.8	926
PtAu-nanoflowers/rGO [57]	1429	12.4	826.7
Fe@Au-ATPGO [58]	100	1.4	400
$Pt_{55}Pd_{38}Bi_7$ nanowires [59]	33.7	4.3	286
AuPt@Au NCs/rGO [60]	1429	8.7	213
Ni@PtNi/rGO [61]	1000	4.5	257
Rh nanoparticles [62]	300	–	20.74
Rh/C-500 nanosheet [63]	1000	3.1	16.5
Ag@Au/graphene [64]	100	5.36	53.6
Ag@Pd/graphene [64]	100	8.67	86.7
Au–Pd/carbon spheres [65]	142.9	6.6	14.6
Ni–Ag@rGO [66]	114.3	89	16.24
Ag–Pt Nanowires [67]	142.9	6.93	11.55

large number of active NBNPs catalysts for the 4-NP reduction reactions being known. The k_{app} and k_{nor} values of $RhAg_{0.5}$/rGO are shown to be one of the best catalysts ever obtained when compared with the NBNPs catalysts reported in the literature for 4-NP reduction (Table 2). For instance, one of the best recent results were obtained by Feng's and Wang's group who reported 4-NP reduction by $NaBH_4$ catalyzed by Pt–Au nanodendrites supported on rGO with a remarkable reaction rate $k_{nor} = 926\ s^{-1}\ g^{-1}$ [56] and PtAu-nanoflowers/rGO with a reaction rate $k_{nor} = 826.7\ s^{-1}\ g^{-1}$ [57]. Other successful cases were that Fe@Au-ATPGO ($k_{nor} = 400\ s^{-1}\ g^{-1}$) reported by Gupta's group [58], $Pt_{55}Pd_{38}Bi_7$ nanowires ($k_{nor} = 286\ s^{-1}\ g^{-1}$) reported by Li's group [59] and AuPt@Au NCs/rGO ($k_{nor} = 213\ s^{-1}\ g^{-1}$) reported by Feng's group [60]. Therefore, in comparison the catalytic efficiency of the present RhAg/rGO catalytic system is most remarkable.

Based on these results, the mechanism for the 4-NP reduction by $NaBH_4$ in the presence of RhAg/rGO catalysts follows earlier suggestions involving BH_4^- adsorption onto the catalyst surface and transfer of active hydrogen species to the NP surface to form surface metal-hydride species [41–55, 59]. In addition, the presence of rGO mediates this process by increasing 4-NP absorption at the RhAg NP surface [55], and the RhAg NP surface is coordinated to the weak tristrz-PEG ligand that is readily substituted by substrates [33]. Consequently, the electron-rich Rh atom-coordinated hydrogen species is transferred to the nitro groups at the NP surface. Charge transfer within the Rh–Ag surface toward the Rh sites favors the hydride transfer to this substrate [60, 68]. It is also possible that excess BH_4^- transfers electrons [69, 70] to the bimetallic catalyst surface, still increasing the charge on the key active Rh–H site (Scheme 2).

The reusability of the $RhAg_{0.5}$/rGO catalyst was also investigated. As shown in Fig. 3a, the $RhAg_{0.5}$/rGO catalyst is reused at least five times without significant loss of reaction activity. In the fifth run, the rate constant for the 4-NP reaction was still $k_{app} = 12.1 \times 10^{-3}\ s^{-1}$, suggesting that the $RhAg_{0.5}$/rGO catalyst exhibits very good reusability in the reduction of 4-NP. This efficiency is also superior to that encountered in most of the cases using noble metal-based NP catalysts. Decreasing the total catalyst amount to an acceptable level with good reaction activity was also attempted. As shown in Fig. 3b, with 0.05 and 0.01 mol% $RhAg_{0.5}$/rGO catalyst, the reaction rate is $k_{app} = 8.2 \times 10^{-3}\ s^{-1}$ ($k_{nor} = 3140\ s^{-1}\ g^{-1}$) and $k_{app} = 5.3 \times 10^{-3}\ s^{-1}$ ($k_{nor} = 10140\ s^{-1}\ g^{-1}$), respectively, demonstrating the successful design of cost-effective RhAg/rGO catalytic system.

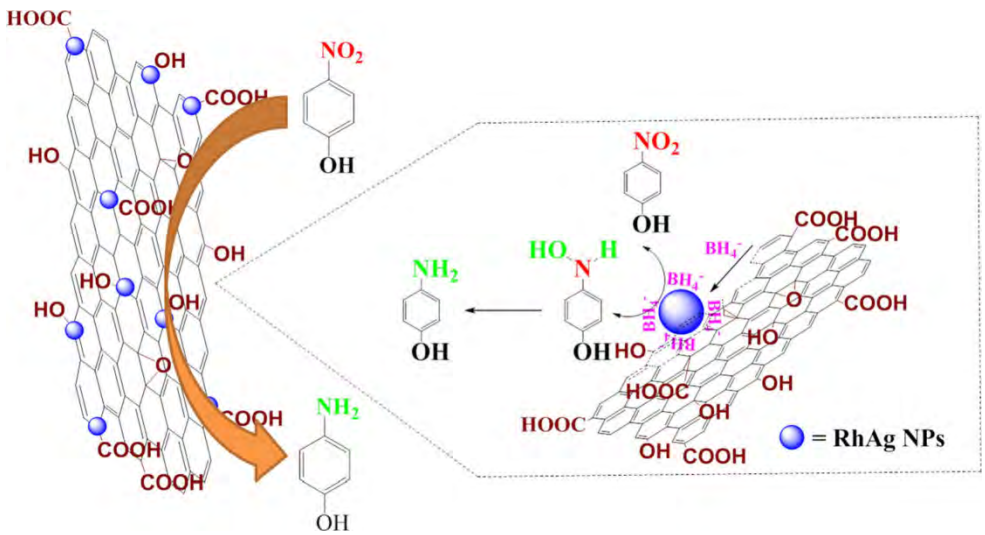

Scheme 2 Proposed mechanism for the 4-NP reduction by $NaBH_4$ in the presence of a RhAg/rGO catalyst.

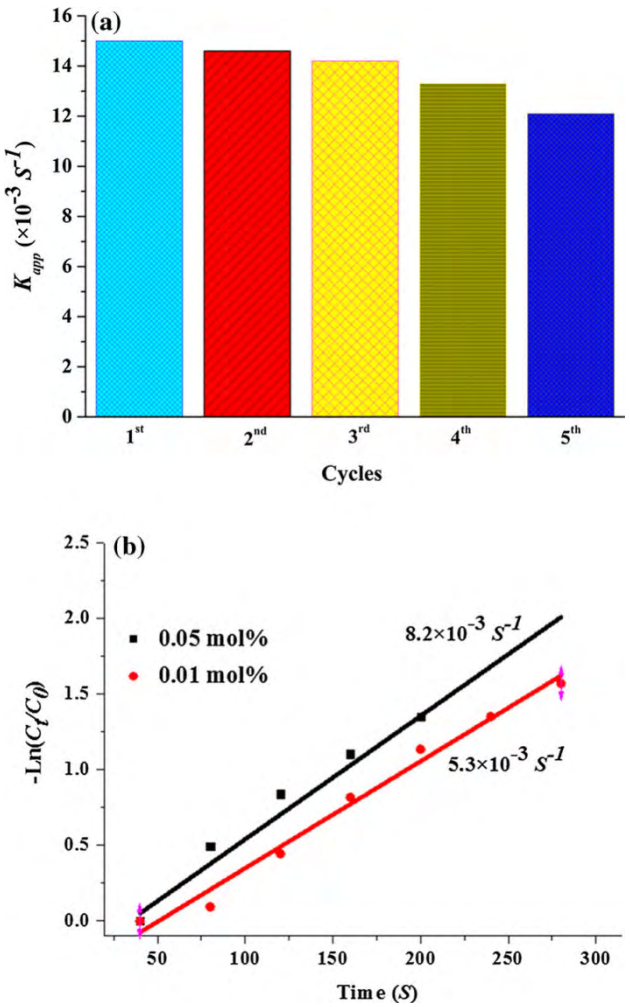

Figure 3 **a** Reusability of the $RhAg_{0.5}$/rGO catalyst for the 4-NP reduction by $NaBH_4$. **b** Plot of $-\ln(C_t/C_0)$ versus time for the reduction of 4-NP by $NaBH_4$ in the presence of 0.05 and 0.01% $RhAg_{0.5}$/rGO catalysts.

Conclusions

The facile synthesis of the heterogeneous catalyst RhAg/rGO with very narrow bimetallic RhAg NP size distribution and the exceptional catalyst activity for 4-NP reduction has been developed here for the first time. The presence of the tristrz-PEG ligand not only ensures ultrafine bimetallic NP formation, but also allows quantitative fixation of the RhAg NP onto the rGO surface. The bimetallic RhAg NPs involve a synergy between the two metals on rGO that improves the catalytic activity compared to both monometallic counterparts. Moreover, the catalyst exhibits very good reusability, and the catalyst amounts are largely decreased with high efficiency. The present work not only sheds a new light on the development of high-performance bimetallic NPs using appropriate supporting materials [71, 72], but also contributes to the design of very efficient, cost-effective catalysts for various current organic reactions.

Acknowledgements

Financial support from the China Scholarship Council (CSC) of the People's Republic of China (Grant to C.W.), the Universities of Bordeaux, Toulouse 3, the LCC (Toulouse) and the Centre National de la Recherche Scientifique (CNRS) is gratefully acknowledged.

Compliance with ethical standards

Conflict of interest The authors declare that they have no conflict of interest.

Electronic supplementary material: The online version of this article (doi:10.1007/s10853-017-1158-7) contains supplementary material, which is available to authorized users.

References

[1] Toshima N, Yonezawa T (1998) Bimetallic nanoparticles—novel materials for chemical and physical applications. New J Chem 122:1179–1201

[2] Sankar M, Dimitratos N, Miedziak PJ, Wells PP, Kiely CJ, Hutchings GJ (2012) Designing bimetallic catalysts for a green and sustainable future. Chem Soc Rev 41:8099–8139

[3] Wang D, Li Y (2011) Bimetallic nanocrystals: liquid-phase synthesis and catalytic applications. Adv Mater 23:1044–1060

[4] Liu X, Wang D, Li Y (2012) Synthesis and catalytic properties of bimetallic nanomaterials with various architectures. Nano Today 7:448–466

[5] Peng X, Pan Q, Rempel GL (2008) Bimetallic dendrimer-encapsulated nanoparticles as catalysts: a review of the research advances. Chem Soc Rev 37:1619–1628

[6] Wu B, Zheng N (2013) Surface and interface control of noble metal nanocrystals for catalytic and electrocatalytic applications. Nano Today 8:168–197

[7] Gawande MB, Goswami A, Asefa T, Guo H, Biradar AV, Peng D, Zboril R, Varma RS (2015) Core–shell nanoparticles: synthesis and applications in catalysis and electrocatalysis. Chem Soc Rev 44:7540–7590

[8] Crooks RM, Zhao MQ, Sun L, Chechik V, Yeung LK (2001) Dendrimer-encapsulated metal nanoparticles: synthesis, characterization, and applications to catalysis. Acc Chem Res 34:181–190

[9] Myers VS, Weir MG, Carino EV, Yancey DF, Pande S, Crooks RM (2011) Dendrimer-encapsulated nanoparticles: new synthetic and characterization methods and catalytic applications. Chem Sci 2:1632–1646

[10] Gao F, Goodman DW (2012) Pd–Au bimetallic catalysts: understanding alloy effects from planar models and (supported) nanoparticles. Chem Soc Rev 41:8009–8020

[11] Ferrando R, Jellinek J, Johnston RL (2008) Nanoalloys: from theory to applications of alloy clusters and nanoparticles. Chem Rev 106:845–910

[12] Hutchings GJ, Kiely CJ (2013) Strategies for the synthesis of supported gold palladium nanoparticles with controlled morphology and composition. Acc Chem Res 46:1759–1772

[13] Edwards JK, Freakley SJ, Carley AF, Kiely CJ, Hutchings GJ (2014) Strategies for designing supported gold–palladium bimetallic catalysts for the direct synthesis of hydrogen peroxide. Acc Chem Res 47:845–854

[14] Zhang L, Xie Z, Gong J (2016) Shape-controlled synthesis of Au–Pd bimetallic nanocrystals for catalytic applications. Chem Soc Rev 45:3916–3934

[15] Astruc D, Lu F, Ruiz J (2005) Nanoparticles as recyclable catalysts: the frontier between homogeneous and heterogeneous catalysis. Angew Chem Int Ed 44:7852–7872

[16] Zhang HJ, Watanabe T, Okumura M, Haruta M, Toshima N (2012) Catalytically highly active top gold atom on palladium nanocluster. Nat Mater 11:49–52

[17] Aita T, Kohyama M, Haruta M (2013) Electron microscopy study of gold nanoparticles deposited on transition metal oxides. Acc Chem Res 46:1773–1782

[18] Lopez-Sanchez JA, Dimitratos N, Hammond C, Brett GL, Kesavan L, White S, Miedziak P, Tiruvalam R, Jenkins RL, Carley AF, Knight D, Kiely CJ, Hutchings GJ (2011) Facile removal of stabilizer-ligands from supported gold nanoparticles. Nat Chem 3:551–556

[19] Sarina S, Zhu H, Jaatinen E, Xiao Q, Liu H, Jia J, Chen C, Zhao J (2013) Enhancing catalytic performance of palladium in gold and palladium alloy nanoparticles for organic synthesis reactions through visible light irradiation at ambient temperatures. J Am Chem Soc 135:5793–5801

[20] Jiang HL, Xu Q (2011) J Mater Chem 21:13705–13725

[21] Singh AK, Singh AK, Xu Q (2013) Synergistic catalysis over bimetallic alloy nanoparticles. ChemCatChem 5:652–676

[22] Yuan Y, Yan N, Dyson PJ (2012) Advances in the rational design of rhodium nanoparticle catalysts: control via manipulation of the nanoparticle core and stabilizer. ACS Catal 2:1057–1069

[23] Garcia S, Zhang L, Piburn GW, Henkelman G, Humphrey SM (2014) Microwave synthesis of classically immiscible rhodium–silver and rhodium–gold alloy nanoparticles: highly active hydrogenation catalysts. ACS Nano 8:11512–11521

[24] Yasukawa T, Miyamura H, Kobayashi S (2012) Polymer-incarcerated chiral Rh/Ag nanoparticles for asymmetric 1,4-addition reactions of arylboronic acids to enones: remarkable effects of bimetallic structure on activity and metal leaching. J Am Chem Soc 134:16963–16966

[25] Yasukawa T, Suzuki A, Miyamura H, Nishino K, Kobayashi S (2015) Chiral metal nanoparticle systems as heterogeneous catalysts beyond homogeneous metal complex catalysts for asymmetric addition of arylboronic acids to α, β-unsaturated carbonyl compounds. J Am Chem Soc 137:6616–6623

[26] Hirakawa K, Toshima N (2003) Ag/Rh bimetallic nanoparticles formed by self-assembly from Ag and Rh monometallic nanoparticles in solution. Chem Lett 32:8–79

[27] Toshima N, Kanemaru M, Shiraishi Y, Koga Y (2005) Spontaneous formation of core/shell bimetallic nanoparticles: a calorimetric study. J Phys Chem B 109:16326–16331

[28] Yang A, Sakata O, Kusada K, Yayama T, Yoshikawa H, Ishimoto T, Koyama M, Kobayashi H, Kitagawa H (2014) The valence band structure of Ag_xRh_{1-x} alloy nanoparticles. Appl Phys Lett 105:153109

[29] Kusada K, Yamauchi M, Kobayashi H, Kitagawa H, Kubota Y (2010) Hydrogen-storage properties of solid-solution alloys of immiscible neighboring elements with Pd. J Am Chem Soc 132:15896–15898

[30] Dai Y, Wang Y, Liu B, Yang Y (2015) Metallic nanocatalysis: an accelerating seamless integration with nanotechnology. Small 11:268–289

[31] Chen S, Thota S, Wang X, Zhao J (2016) From solid to core@shell to hollow Pt–Ag nanocrystals: thermally controlled surface segregation to enhance catalytic activity and durability. J Mater Chem A 4:9038–9043

[32] Roy A, Debnath B, Sahoo R, Chandrakumar KRS, Ray C, Jana J, Pal T (2016) Enhanced catalytic activity of Ag/Rh bimetallic nanomaterial: evidence of an ensemble effect. J Phys Chem C 120:5457–5467

[33] Wang C, Ciganda R, Salmon L, Gregurec D, Irigoyen J, Moya S, Ruiz J, Astruc D (2016) Highly efficient transition metal nanoparticle catalysts in aqueous solutions. Angew Chem Int Ed 55:3091–3095

[34] Wang C, Wang D, Yu S, Cornilleau T, Ruiz J, Salmon L, Astruc D (2016) Design and applications of an efficient amphiphilic "click" Cu^{I} catalyst in water. ACS Catal 6:5424–5431

[35] Özçubukçu S, Ozkal E, Jimeno C, Pericas MA (2009) A highly active catalyst for huisgen 1, 3-dipolar cycloadditions

based on the tris(triazolyl) methanol-Cu(I) structure. Org Lett 11:4680–4683

[36] Radich JG, Kamat PV (2013) Making graphene holey. gold-nanoparticle-mediated hydroxyl radical attack on reduced graphene oxide. ACS Nano 7:5546–5557

[37] Deraedt C, Wang D, Salmon L, Etienne L, Labrugère C, Ruiz J, Astruc D (2015) Robust, efficient, and recyclable catalysts from the impregnation of preformed dendrimers containing palladium nanoparticles on a magnetic support. ChemCatChem 7:303–308

[38] Kim SM, Qadir K, Seo B, Jeong HY, Joo SH, Terasaki O, Park JY (2013) Nature of Rh oxide on Rh nanoparticles and its effect on the catalytic activity of CO oxidation. Catal Lett 143:1153–1161

[39] Kim S, Qadir K, Jin S, Reddy AS, Seo B, Mun BS, Joo SH, Park JY (2012) Trend of catalytic activity of CO oxidation on Rh and Ru nanoparticles: role of surface oxide. Catal Today 185:131–137

[40] Prinz J, Gaspari R, Stöckl QS, Gille P, Armbrüster M, Brune H, Gröning O, Pignedoli CA, Passerone D, Widmer R (2014) Ensemble effect evidenced by CO adsorption on the 3-fold PdGa surfaces. J Phys Chem C 118:12260–12265

[41] Sau TK, Pal A, Pal T (2001) Size regime dependent catalysis by gold nanoparticles for the reduction of eosin. J Phys Chem B 105:9266–9272

[42] Pal AA, Pal T (2015) Nitroarene reduction: a trusted model reaction to test nanoparticle catalysts. Chem Commun 51:9410–9431

[43] Hervés P, Pérez-Lorenzo M, Liz-Marzán LM, Dzubiella J, Lu Y, Ballauff M (2012) Catalysis by metallic nanoparticles in aqueous solution: model reactions. Chem Soc Rev 41:5577–5587

[44] Zhao P, Feng X, Huang D, Yang G, Astruc D (2015) Basic concepts and recent advances in nitrophenol reduction by gold-and other transition metal nanoparticles. Coord Chem Rev 287:114–136

[45] Kuroda K, Ishida T, Haruta M (2009) Reduction of 4-nitrophenol to 4-aminophenol over Au nanoparticles deposited on PMMA. J Mol Catal A: Chem 298:7–11

[46] Wunder S, Polzer F, Lu Y, Ballauff M (2010) Kinetic analysis of catalytic reduction of 4-nitrophenol by metallic nanoparticles immobilized in spherical polyelectrolyte brushes. J Phys Chem C 114:8814–8820

[47] Saha S, Pal A, Kundu S, Basu S, Pal T (2010) Photochemical green synthesis of calcium-alginate-stabilized Ag and Au nanoparticles and their catalytic application to 4-nitrophenol reduction. Langmuir 26:2885–2893

[48] Wang SN, Zhang MC, Zhang WQ (2011) Yolk – shell catalyst of single Au nanoparticle encapsulated within hollow mesoporous silica microspheres. ACS Catal 1:207–211

[49] Wunder S, Lu Y, Albrecht M, Ballauff M (2011) Catalytic activity of faceted gold nanoparticles studied by a model reaction: evidence for substrate-induced surface restructuring. ACS Catal 1:908–916

[50] Li J, Liu CY, Liu Y (2012) Au/graphene hydrogel: synthesis, characterization and its use for catalytic reduction of 4-nitrophenol. J Mater Chem 22:8426–8430

[51] Zhang J, Han D, Zhang H, Chaker M, Zhao Y, Ma D (2012) In situ recyclable gold nanoparticles using CO_2-switchable polymers for catalytic reduction of 4-nitrophenol. Chem Commun 48:11510–11512

[52] Shivhare A, Ambrose SJ, Zhang H, Purves RW, Scott RWJ (2013) Stable and recyclable Au_{25} clusters for the reduction of 4-nitrophenol. Chem Commun 49:276–278

[53] Pachfule P, Kandambeth S, Dıaz D, Banerjee R (2014) Highly stable covalent organic framework–Au nanoparticles hybrids for enhanced activity for nitrophenol reduction. Chem Commun 50:3169–3171

[54] Gu S, Wunder S, Lu Y, Ballauff M (2014) Kinetic analysis of the catalytic reduction of 4-nitrophenol by metallic nanoparticles. J Phys Chem C 118:18618–18625

[55] Wu T, Zhang L, Gao J, Liu Y, Gao C, Yan J (2013) Fabrication of graphene oxide decorated with Au–Ag alloy nanoparticles and its superior catalytic performance for the reduction of 4-nitrophenol. J Mater Chem A 1:7384–7390

[56] Lv JJ, Wang AJ, Ma X, Xiang RY, Chen JR, Feng JJ (2015) One-pot synthesis of porous Pt–Au nanodendrites supported on reduced graphene oxide nanosheets toward catalytic reduction of 4-nitrophenol. J Mater Chem A 3:290–296

[57] Song P, He LL, Wang AJ, Mei LP, Zhong SX, Chen JR, Feng JJ (2015) Surfactant-free synthesis of reduced graphene oxide supported porous PtAu alloyed nanoflowers with improved catalytic activity. J Mater Chem A 3:5321–5327

[58] Gupta VK, Atar N, Yola ML, Ustundag Z, Uzun L (2014) A novel magnetic Fe@Au core–shell nanoparticles anchored graphene oxide recyclable nanocatalyst for the reduction of nitrophenol compounds. Water Res 48:210–217

[59] Shen YY, Sun Y, Zhou LN, Li YJ, Yeung ES (2014) Synthesis of ultrathin PtPdBi nanowire and its enhanced catalytic activity towards *p*-nitrophenol reduction. J Mater Chem A 2:2977–2984

[60] Liu Q, Xu Y, Wang A, Feng J (2015) One-step melamine-assisted synthesis of graphene-supported AuPt@Au nanocrystals for enhanced catalytic reduction of *p*-nitrophenol. RSC Adv 5:96028–96033

[61] Mei LP, Wang R, Song P, Feng JJ, Wang ZG, Chen JR, Wang AJ (2016) One-pot solvothermal synthesis of bimetallic yolk–shell Ni@PtNi nanocrystals supported on reduced graphene oxide and their excellent catalytic properties for *p*-nitrophenol reduction. New J Chem 40:2315–2320

[62] Lee Y, Jang S, Cho C-W, Bae J-S, Park S, Park KH (2013) Recyclable rhodium nanoparticles: green hydrothermal synthesis, characterization, and highly catalytic performance in reduction of nitroarenes. J Nanosci Nanotechnol 13:7477–7481

[63] Lin C, Wu G, Li H, Geng Y, Xie G, Yang J, Liu B, Jin J (2017) Nanoscale 9:1834–1839

[64] Liu CH, Chen XQ, Hu YF, Sham TK, Sun QJ, Chang JB, Gao X, Sun XH, Wang SD (2013) One-pot environmentally friendly approach toward highly catalytically active bimetal-nanoparticle-graphene hybrids. ACS Appl Mater Interfaces 5:5072–5079

[65] Tang S, Vongehr S, He G, Chen L, Meng X (2012) Highly catalytic spherical carbon nanocomposites allowing tunable activity via controllable Au–Pd doping. J Colloid Interface Sci 375:125–133

[66] Zhang L, Wu T, Xu X, Xia F, Na H, Liu Y, Qiu H, Wang W, Gao J (2015) Magnetic bimetallic nanoparticles supported reduced graphene oxide nanocomposite: fabrication, characterization and catalytic capability. J Alloy Compd 628:364–371

[67] Wang Y, Wang X, Sun B, Tang S, Meng X (2016) Concentration-dependent morphology control of Pt-coated-Ag nanowires and effects of bimetallic interfaces on catalytic activity. J Mater Sci Technol 32:41–47

[68] Lu W, Ning R, Qin X, Zhang Y, Chang G, Liu S, Luo Y, Sun X (2011) Synthesis of Au nanoparticles decorated graphene oxide nanosheets: noncovalent functionalization by TWEEN 20 in situ reduction of aqueous chloroaurate ions for hydrazine detection and catalytic reduction of 4-nitrophenol. J Hazard Mater 197:320–326

[69] Ciganda R, Li N, Deraedt C, Gatard S, Zhao P, Salmon L, Hernandez R, Ruiz J, Astruc D (2014) Gold nanoparticles as electron reservoir redox catalysts for 4-nitrophenol reduction: a strong stereoelectronic ligand influence. Chem Commun 50:10126–10129

[70] Deraedt C, Salmon L, Gatard S, Ciganda R, Hernandez R, Ruiz J, Astruc D (2014) Sodium borohydride stabilizes very active gold nanoparticle catalysts. Chem Commun 50:14194–14196

[71] Wang D, Astruc D (2017) The recent development of efficient Earth-abundant transition metal nanocatalysts. Chem Soc Rev 46:816–854

[72] Liu X, Astruc D (2017) From galvanic to anti-galvanic synthesis of bimetallic nanoparticles and applications to catalysis, sensing and materials science. Adv Mater. doi:10.1002/adma.201605305

ChemComm

COMMUNICATION

View Article Online
View Journal | View Issue

Cite this: *Chem. Commun.*, 2017, 53, 644

Received 18th October 2016,
Accepted 12th December 2016

DOI: 10.1039/c6cc08401j

www.rsc.org/chemcomm

An efficient parts-per-million α-Fe_2O_3 nanocluster/graphene oxide catalyst for Suzuki–Miyaura coupling reactions and 4-nitrophenol reduction in aqueous solution†

Changlong Wang,[ab] Lionel Salmon,[b] Roberto Ciganda,[ac] Luis Yate,[d] Sergio Moya,[d] Jaime Ruiz[a] and Didier Astruc*[a]

A new α-Fe_2O_3 nanocluster/graphene oxide catalyst is found to be efficient in parts-per-million for Suzuki–Miyaura coupling and 4-nitrophenol reduction in aqueous solution, and this catalyst is recycled at least 4 times in good yields.

Metal-catalyzed cross-coupling carbon–carbon (C–C) bond formation has significantly advanced organic synthesis.[1] In particular, Pd-catalyzed Suzuki–Miyaura (SM) coupling has been efficiently used in numerous procedures for the construction of C–C bonds.[2] Although chemists have successfully decreased the amounts of precious Pd catalyst in such reactions,[3] alternative methodologies to accomplish a similar catalytic SM coupling using ''green chemistry'', and especially cheap biometal catalysts (for instance Fe,[4] Ni,[5] or Cu,[6]) are highly encouraged. Nevertheless, well-defined alternative approaches most often result in the requirement of specific ligands, high catalyst loading, or hash reaction conditions and sometimes suffer from poor catalytic efficiency. Herein, we report a new heterogeneous catalytic system, α-Fe_2O_3 nanocluster/graphene oxide (α-Fe_2O_3/GO), **1**, for efficient SM coupling reactions in aqueous solution and reduction of 4-nitrophenol (4-NP) in water employing only ppm amounts of catalyst.

The synthesis of the new heterogeneous catalyst **1** is carried out in water. It first involves addition of an aqueous solution of $FeCl_3$ to the pre-solubilized amphiphilic tris(triazolyl)-polyethylene glycol (tris-trz-PEG)[7] ligand in water followed by reduction using NaOH. This pre-catalyst is then deposited on GO through supramolecular H-bonding interactions between the PEG termini of the tris-trz-PEG ligand and the functional groups of the GO support, followed by filtration and drying (Scheme S1, and ESI†). The Fe content was checked by inductively coupled plasma atomic emission spectroscopy (ICP-AES) analysis indicating that >99% of the α-Fe_2O_3 nanocluster was deposited onto GO.

The TEM images showed that α-Fe_2O_3 nanoclusters of only 1.8 nm in size were homogeneously deposited on the edge of the GO sheets (Fig. 1a and b). EDX analysis then showed the Fe, C, N, and O signals provided by the α-Fe_2O_3 nanocluster/GO sample (Fig. 1c). The phase structure of catalyst **1** was further characterized by HRTEM analysis showing a well-defined hexagonal shape and a lattice fringe spacing of 0.25 nm corresponding to the (110) crystallographic plane of the α-Fe_2O_3 crystal (Fig. 1d). The oxidation state of the Fe constituent in **1** was checked by X-ray photoelectron spectroscopy (XPS). The XPS survey spectrum (Fig. S2, ESI†) indicates that the sample contains C, O and Fe. In the C 1s spectrum, the peaks at 284.4, 286.4, 288.3 and 290.8 eV are attributed to the C–C, C–O, C═O, and O–C═O configurations, respectively.[8] The core level binding energies located at 726.4 and 712.3 eV are shown in the

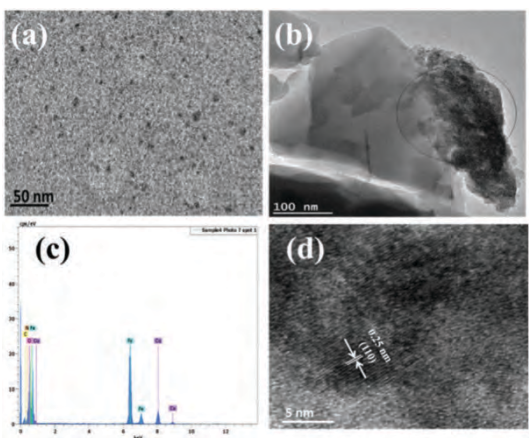

Fig. 1 (a and b) TEM images of the α-Fe_2O_3 nano-cluster/GO catalyst; (c) corresponding EXD analysis of the area in (b). (d) HRTEM image of α-Fe_2O_3 nanocluster/GO catalyst **1**.

[a] *ISM, UMR CNRS No. 5255, Univ. Bordeaux, 33405 Talence, France. E-mail: d.astruc@ism.u-bordeaux.fr*
[b] *Laboratoire de Chimie de Coordination, UPR CNRS No. 8241, 31077 Toulouse, France*
[c] *Facultad de Quimica, Universidad del Pais Vasco, Apdo 1072, 20080 San Sebastian, Spain*
[d] *CIC biomaGUNE, Unidad Biosuperficies, Paseo Miramon No. 182, Edif ''C'', 20009 Donostia-San Sebastian, Spain*

† Electronic supplementary information (ESI) available: Synthesis, characterization, and spectra of compounds. See DOI: 10.1039/c6cc08401j

Fe 2p spectrum, which correspond to the Fe $2p_{1/2}$ and Fe $2p_{3/2}$ core levels of α-Fe_2O_3, respectively.[9] Moreover, the shakeup satellite peak at about 719.0 eV,[10] a characteristic of the Fe^{3+} species, is also clearly seen.

Catalytic applications of the new catalyst **1** were first probed for the 4-NP reduction by $NaBH_4$ in water,[11] a trusted test reaction pioneered by Pal's group[11a] to explore the catalytic efficiency of nanoparticles surfaces. Indeed this reaction hardly proceeds in the absence of a metal catalyst.[11] In the presence of catalyst **1** in an aqueous solution containing 4-NP (1 equiv.) and $NaBH_4$ (81 equiv.), reduction proceeds with an induction time (t_0) of 1160 s (Fig. 2). This feature suggests the required activation and dynamic restructuring of the α-Fe_2O_3 nanocluster surface, as shown by Ballauff's group using AuNP and PdNP catalysts.[11d,g,h] Following the induction time, 4-NP reduction proceeds very well, with an apparent kinetic rate constant (k_{app}) of 4.17×10^{-4} s^{-1} (Fig. S3, ESI†). Given the addition of such a low amount of catalyst **1** (150 ppm per 4-NP), its catalytic efficiency is remarkable and even superior to the best noble metal nanoparticle catalysts. Control experiments conducted in the presence of GO alone indicated that the reaction did not proceed at all.

High-resolution UV-vis spectroscopy was used to monitor the reaction process by mixing α-Fe_2O_3/GO and $NaBH_4$ (Fig. S3 bottom, ESI†). The spectra did not change during the reaction, and no peaks at 352 nm and at 262 nm that corresponded to Fe(0) were observed, suggesting that Fe(0) is not involved in the reaction. To address the iron-leaching problem, we have conducted 4-NP reduction after the removal of the α-Fe_2O_3/GO catalyst by simple filtration. The yellow color of the reaction mixture did not change during 2 days, and the hot filtration test was negative (*vide infra*), suggesting that leaching of soluble Fe(0) species does not account for the reaction mechanism. It cannot be excluded that tiny amounts of Fe(0) are formed, however, and serve as a catalyst.[12]

Encouraged by the remarkable efficiency of **1** obtained in the 4-NP reaction, the catalytic performances have been further investigated in the Suzuki–Miyaura coupling reaction between bromobenzene and phenylboronic acid. This reaction was conducted at 80 °C under a nitrogen atmosphere for 24 h in the presence of 150 ppm mol% catalyst and K_2CO_3 as the base. Optimizations of the SM coupling reaction were first conducted by leaving the solvent as the only parameter. Solvent mixtures containing water and, as a co-solvent, DMF, ethylene glycol or EtOH were tested for this model reaction. The results showed that the presence of the H_2O/EtOH solution led to the best catalytic performance with a quantitative conversion and an 87% isolated yield. The amount of solvent is crucial in this SM reaction, as a larger amount of H_2O/EtOH solvent leads to a lack of conversion, while low amounts of solvent allow the reaction to proceed well (ESI†). These results indicate that the concentration of the substrates is crucial for this reaction.[1d]

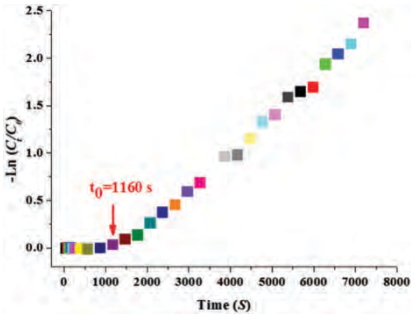

Fig. 2 Consumption rate of 4-NP: $-\ln(C_t/C_0)$ *vs.* time.

XPS was used to characterize the Fe oxidation state after the SM reaction, but no Fe(0) was found, indicating that EtOH does not reduce α-Fe_2O_3 under the present conditions (Fig. S12, ESI†).

In order to identify the actual active phase, ICP-AES analysis was conducted to exclude the possibility of trace Pd residues in **1**, because ppm levels of Pd are known to be sufficient for the catalysis of SM reactions. ICP-AES analysis showed that there was no residual Pd (or below the detection limit of 0.5 ppm) in **1**. Control experiments have also been conducted using either GO or α-Fe_2O_3 as the tentative catalyst for this model SM reaction, and no reaction occurred under these conditions. To investigate the homo- or heterogeneity of the α-Fe_2O_3 nanocluster/GO system, a hot filtration test was conducted. The standard SM reaction between bromobenzene and phenylboronic acid proceeds well in the presence of the catalyst, whereas the removal of the catalyst at half way inhibited the continuation of the reaction (Fig. S13, ESI†). Thus, the SM reaction by α-Fe_2O_3/GO occurs heterogeneously. It was also conducted in the presence of α-Fe_2O_3/active carbon for comparison, and this reaction occurred with poor yield (23%). Thus, it is concluded that **1** catalyzes the SM reaction, and the presence of GO enhances the catalyst efficiency. The high surface area of the GO support increases the concentration of substrates near the α-Fe_2O_3 catalyst and its efficiency.[13]

Given the optimized reaction conditions and high efficiency of catalyst **1**, the scope of the SM coupling reaction was examined with **1** (150 ppm) in a mixture of EtOH and H_2O under nitrogen atmosphere at 80 °C within 24 h (Table 1). A series of bromobenzene derivatives bearing various substituents were tested for the SM coupling reactions with phenylboronic acid under the optimized conditions.

Bromobenzene derivatives containing electron-withdrawing (NO_2, CHO, CH_3CO) and electron-donating (NH_2, CHO, CH_3) groups in the *para* position were suitable coupling partners, and the corresponding coupling products were all efficiently isolated with good yields (Table 1). No direct relationship between the yields and the electronic nature of the bromobenzene substituents was found, however. Substituted arylboronic acids were also investigated, and they reacted smoothly with bromobenzene to provide the desired products in good yields (entries 8 and 9). Comparison of catalyst **1** used in the present study with various available Pd catalysts for the SM reaction in aqueous solution from the literature (Table S1, ESI†) shows the advantages of the utilization of catalyst **1**. No coupling was obtained between bromobenzene and *n*-butylboronic acid, 1-bromopentane and phenylboronic acid, or 1-bromopentane and *n*-butylboronic acid, however.

The recyclability, a key issue in heterogeneous catalysis from both practical and environmental points of view, was also examined herein using a biphasic method. After the first reaction, diethyl

Table 1 Investigation of the substrate scope in the Suzuki–Miyaura reaction catalyzed by α-Fe_2O_3 nanocluster/GO[a]

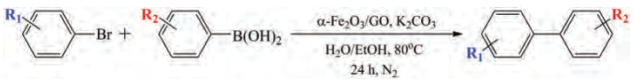

Entry	R_1	R_2	Conversion[b] (%)	Yield[c] (%)
1	H	H	100	87
2	4-NO_2	H	100	83.3
3	4-CHO	H	100	83
4	4-CH_3CO	H	100	84.5
5	4-NH_2	H	95	80
6	4-CH_3O	H	98	78
7	4-CH_3	H	90	75
8	H	2-CH_3	75	51
9	H	4-CH_3	98	82

[a] Reaction conditions: bromobenzene (0.2 mmol), phenylboronic acid (0.3 mmol), catalyst (150 ppm α-Fe_2O_3), K_2CO_3 (0.4 mmol), EtOH/H_2O (1 mL/1 mL), 80 °C, N_2, 24 h. [b] ^{1}H NMR conversion. [c] Yields of isolated products.

ether was added to extract the product while keeping the catalyst in the aqueous phase, followed by the charge of another run of substrates. In this way, the ppm amount of catalyst **1** for the SM coupling reactions was successfully recycled four times (ESI†), and therefore it is concluded that **1** is an excellent heterogeneous catalyst for the SM coupling reactions.

In conclusion, the heterogeneous system **1** is shown here to behave as a remarkable catalyst for both 4-NP reduction and Suzuki–Miyaura coupling reactions in aqueous solvents with only parts-per-million catalyst loading. The presence of the tris-trz-PEG ligand not only ensured the formation of α-Fe_2O_3 but also the quantitative deposition of α-Fe_2O_3 onto GO induced by supramolecular interactions. Moreover, recycling of the catalyst was also shown to be excellent. The mechanism of catalytic activation by α-Fe_2O_3/GO remains unclear in these two reactions, especially since no Fe(0) was detected. Also note that the lack of extension of the Suzuki–Miyaura reaction to alkyl bromides and alkylboronic acids is a limitation that must be taken into account in the mechanistic investigation of such catalytic systems.

Overall, the principles and results presented herein should significantly contribute to the development of "green chemistry" applications involving earth-abundant metal heterogeneous catalysts.

Financial support from the China Scholarship Council (CSC) of the People's Republic of China (grant to C. W.), the Universities of Bordeaux, Toulouse 3, the LCC (Toulouse), and the Centre National de la Recherche Scientifique (CNRS) is gratefully acknowledged.

Notes and references

1 (*a*) J. Hassan, M. Sévignon, C. Gozzi, E. Schulz and M. Lemaire, *Chem. Rev.*, 2002, **102**, 1359; (*b*) C. S. Yeung and Vy M. Dong, *Chem. Rev.*, 2011, **111**, 1215; (*c*) *New Trends in Cross-Coupling: Theory and Applications*, ed. T. Edicot, RSC Catalysis Series, London, 2014; (*d*) C. Deraedt and D. Astruc, *Acc. Chem. Res.*, 2014, **47**, 494.

2 (*a*) M. Lamblin, L. Nassar-Hardy, J. C. Hierso, E. Fouquet and F.-X. Felpin, *Adv. Synth. Catal.*, 2010, **352**, 33; (*b*) I. Favier, D. Madec, E. Teuma and M. Gomez, *Curr. Org. Chem.*, 2011, **15**, 3127; (*c*) A. J. J. Lennox and G. C. Lloyd-Jones, *Chem. Soc. Rev.*, 2014, **43**, 412; (*d*) Y. Wan, H. Wang, Q. Zhao, M. Klingstedt, O. Terasaki and D. Zhao, *J. Am. Chem. Soc.*, 2009, **131**, 4541; (*e*) S. Tanaka, T. Kaneko, N. Asao, Y. Yamamoto, M. Chen, W. Zhang and A. Inoue, *Chem. Commun.*, 2011, **47**, 5985; (*f*) Z. Li, S. Lin, L. Ji, Z. Zhang, X. Zhang and Y. Ding, *Catal. Sci. Technol.*, 2014, **4**, 1734; (*g*) C. M. A. Parlett, P. Keshwalla, S. G. Wainwright, D. W. Bruce, N. S. Hondow, K. Wilson and A. F. Lee, *ACS Catal.*, 2013, **3**, 2122.

3 (*a*) I. P. Beletskaya and A. V. Cheprakov, *Chem. Rev.*, 2000, **100**, 3009; (*b*) J. G. de Vries, *Dalton Trans.*, 2006, 421; (*c*) K. Okumara, T. Tomiyama, S. Okuda, H. Yoshida and M. Niwa, *J. Catal.*, 2010, **273**, 156; (*d*) C. Zhou, J. Wang, L. Li, R. Wang and M. A. Hong, *Green Chem.*, 2011, **13**, 2100; (*e*) Y. M. A. Yamada, S. M. Sarkar and Y. Uozumi, *J. Am. Chem. Soc.*, 2012, **134**, 3190.

4 (*a*) H. Firouzabadi, N. Iranpoor, M. Gholinejad and J. Hoseini, *Adv. Synth. Catal.*, 2011, **353**, 125; (*b*) L. Dong, J. Wen, S. Qin, N. Yang, H. Yang, Z. Su, X. Yu and C. Hu, *ACS Catal.*, 2012, **2**, 1829; (*c*) T. Hatakeyama, T. Hashimoto, K. K. A. D. S. Kathriarachchi, T. Zenmyo, H. Seike and M. Nakamura, *Angew. Chem., Int. Ed.*, 2012, **51**, 8834; (*d*) T. Hashimoto, T. Hatakeyama and M. Nakamura, *J. Org. Chem.*, 2012, **77**, 1168; (*e*) M. B. Gawande, Y. Monga, R. Zboril and R. K. Sharma, *Coord. Chem. Rev.*, 2015, **288**, 118; (*f*) P. Dohlert, M. Weidauer and S. Enthaler, *Chimia*, 2015, **69**, 327; (*g*) S. L. Daifuku, J. L. Kneebone, B. E. R. Snyder and M. L. Neidig, *J. Am. Chem. Soc.*, 2015, **137**, 11432; (*h*) M. Kataria, S. Pramanik, N. Kaur, M. Kumar and V. Bhalla, *Green Chem.*, 2016, **18**, 1495.

5 (*a*) S. Ge, and J. F Hartwig, *Angew. Chem., Int. Ed.*, 2012, **51**, 12837; (*b*) F. S. Han, *Chem. Soc. Rev.*, 2013, **42**, 5270; (*c*) L. M. Guard, G. W. Brudvig, N. Hazari and D. J. Vinyard, *Angew. Chem., Int. Ed.*, 2015, **54**, 13352; (*d*) S. Handa, E. D. Slack and B. H. Lipshutz, *Angew. Chem., Int. Ed.*, 2015, **54**, 11994; (*e*) N. A. Weires, E. L. Baker and N. K. Garg, *Nat. Chem.*, 2016, **8**, 75; (*f*) A. Ohtsuki, K. Yanagisawa, T. Furukawa, M. Tobisu and N. Chatani, *J. Org. Chem.*, 2016, **81**, 9409.

6 (*a*) M. B. Thathagar, J. Beckers and G. Rothenberg, *J. Am. Chem. Soc.*, 2002, **124**, 11858; (*b*) S. K. Gurung, S. Thapa, A. Kafle, D. A. Dickie and R. Giri, *Org. Lett.*, 2014, **16**, 1264; (*c*) Y. Sun, J. Yi, X. Lu, Z. Zhang, B. Xiao and Y. Fu, *Chem. Commun.*, 2014, **50**, 11060.

7 (*a*) S. Ozcubukcu, E. Ozkal, C. Jimeno and M. A. Pericas, *Org. Lett.*, 2009, **11**, 4680; (*b*) C. Wang, R. Ciganda, L. Salmon, D. Gregurec, J. Irigoyen, S. Moya, J. Ruiz and D. Astruc, *Angew. Chem., Int. Ed.*, 2016, **55**, 3091; (*c*) C. Wang, D. Wang, S. Yu, T. Cornilleau, J. Ruiz, L. Salmon and D. Astruc, *ACS Catal.*, 2016, **6**, 5424; (*d*) P. Etayo, C. Ayats and M. A. Pericàs, *Chem. Commun.*, 2016, **52**, 1997.

8 (*a*) S. C. Han, L. F. Hu, Z. Q. Liang, S. Wageh, A. A. Al-Ghamdi, Y. S. Chen and X. S. Fang, *Adv. Funct. Mater.*, 2014, **24**, 5719; (*b*) S. Liu, L. Zheng, P. Yu, S. Han and X. Fang, *Adv. Funct. Mater.*, 2016, **26**, 3331.

9 L. Q. Jing, Y. Cao, H. Q. Cui, J. R. Durrant, J. W. Tang, D. N. Liu and H. G. Fu, *Chem. Commun.*, 2012, **48**, 10775.

10 (*a*) Y. Yang, H. X. Ma, J. Zhuang and X. Wang, *Inorg. Chem.*, 2011, **50**, 10143; (*b*) S. Guo, G. Zhang, Y. Guo and J. C. Yu, *Carbon*, 2013, **60**, 437.

11 (*a*) T. K. Sau, A. Pal and T. Pal, *J. Phys. Chem. B*, 2001, **105**, 9266; (*b*) K. Esumi, R. Isono and T. Yoshimura, *Langmuir*, 2004, **20**, 237; (*c*) K. Kuroda, T. Ishida and M. Haruta, *J. Mol. Catal. A: Chem.*, 2009, **298**, 7; (*d*) S. Wunder, F. Polzer, Y. Lu and M. Ballauff, *J. Phys. Chem. C*, 2010, **114**, 8814; (*e*) S. Saha, A. Pal, S. Kundu, S. Basu and T. Pal, *Langmuir*, 2010, **26**, 2885; (*f*) S.-N. Wang, M.-C. Zhang and W. Q. Zhang, *ACS Catal.*, 2011, **1**, 207; (*g*) S. Wunder, Y. Lu, M. Albrecht and M. Ballauff, *ACS Catal.*, 2011, **1**, 908; (*h*) P. Herves, M. Perez-Lorenzo, L. M. Liz-Marzàn, J. Dzubiella, Y. Lu and M. Ballauff, *Chem. Soc. Rev.*, 2012, **41**, 5577; (*i*) J. Li, C.-Y. Liu and Y. Liu, *J. Mater. Chem.*, 2012, **22**, 8426; (*j*) J. Zhang, D. Han, H. Zhang, M. Chaker, Y. Zhao and D. Ma, *Chem. Commun.*, 2012, **48**, 11510; (*k*) A. Shivhare, S. J. Ambrose, H. Zhang, R. W. Purves and R. W. J. Scott, *Chem. Commun.*, 2013, **49**, 276; (*l*) P. Pachfule, S. Kandambeth, D. Diaz and R. Banerjee, *Chem. Commun.*, 2014, **50**, 3169; (*m*) T. Aditya, A. Pal and T. Pal, *Chem. Commun.*, 2015, **51**, 9410; (*n*) P. Zhao, X. Feng, D. Huang, G. Yang and D. Astruc, *Coord. Chem. Rev.*, 2015, **287**, 114.

12 S. Baea, S. Gimb, H. Kimb and K. Hanna, *Appl. Catal., B*, 2016, **182**, 541. In this article, it was reported that Fe(0) surface covered by magnetite (Fe_3O_4) layer underwent reduction by $NaBH_4$, producing small nanosized Fe(0) nanoparticles that catalysed 4-NP reduction to 4-aminophenol.

13 (*a*) T. Wu, L. Zhang, J. Gao, Y. Liu, C. Gao and J. Yan, *J. Mater. Chem. A*, 2013, **1**, 7384; (*b*) J.-J. Lv, A.-J. Wang, X. Ma, R.-Y. Xiang, J.-R. Chen and J.-J. Feng, *J. Mater. Chem. A*, 2015, **3**, 290; (*c*) P. Song, L.-L. He, A.-J. Wang, L.-P. Mei, S.-X. Zhong, J.-R. Chen and J.-J. Feng, *J. Mater. Chem. A*, 2015, **3**, 5321.

Redox Synthesis and high catalytic efficiency of transition-metal nanoparticle-graphene oxide nanocomposites

Changlong Wang, Roberto Ciganda, Luis Yate, Jimena Tuninetti, Victoria Shalabaeva, Lionel Salmon, Sergio Moya, Jaime Ruiz, Didier Astruc [*]

Dedication ((optional))

Abstract: *Although nanocatalysis is a promising area, increased efficiency and greenness are actively sought. Here we report the principle of the syntheses of graphene oxide (GO)-supported metal nanocatalysts (MNPs) for a variety of transition metals including both noble metals and biometal using either exergonic or endergonic redox reactions between GO and the transition metal salts. These new nanocatalysts are highly efficient in water at ambient temperature for 4-nitrophenol reduction (the test reaction), Sonogashira coupling, azide-alkyne 1,3-cycloaddition (click reaction) and dihydrogen production upon hydrolysis of ammonia-borane and recyclable.*

Nanocatalysis is a very promising area,[1] because high performance nanoparticles (NPs) may be efficiently designed in the absence of ligands that are often toxic, expensive, sensitive and/or of time-consuming synthesis. A variety of organic and inorganic nanocatalyst stabilizers have also been reported, but they usually damage the catalytic activity and may be difficult to remove.[2] Among heterogeneous catalyst supports, carbon materials have proven remarkable because of possible synergetic catalytic activation.[3] Carbon-supported NPs are usually obtained by metal cation reduction using various reductants, but catalysis may be marred by the reactant residue on the NP surface. Clean direct metal cation reduction by carbon materials has rarely been reported, however. Recently Dai's group utilized single-walled carbon nanotubes (SWNT) sidewall as reductant and stabilizer.[4] Redox-mediated nanocatalyst synthesis has also been demonstrated by Chen's group and Tang's group who utilized graphene oxide (GO) and reduced GO as redox mediator to provide efficient noble metal nanocatalysts with Pd and Au respectively.[5]

Here we report the general redox synthesis of green graphene-oxide-supported transition metal nanoparticle catalysts as a clean and most useful synthetic method of NP/GO catalyst avoiding the use of external reductant. This method applies here from noble metals for which the electron transfer from GO is exergonic, thus favorable, to first-raw biometals for which this redox process is endergonic but nevertheless accomplished owing to the fast follow-up NP formation. This concept is also extended to bimetallic NP-graphene oxide composites that include a noble metal and a biometal. It is very efficiently applied here to a variety of reactions in water at room temperature (rt) with remarkably low amounts of catalytic metals including 4-nitrophenol reduction (a reaction used as a test to optimize catalyst preparations), Sonogashira coupling, azide-alkyne 1,3-cycloaddition (click reaction) and dihydrogen production upon hydrolysis of ammonia-borane.

Rh NPs have not so far been generated by redox mediation with GO, but the oxidation potential of GO (0.48 V *vs.* SCE)[5a] and the redox potential of Rh^{3+}/Rh (0.76 V *vs.* SCE),[6] should in principle allow an exergonic primary electron transfer between GO and Rh^{3+}. Thus the redox-mediated synthesis of GO-stabilized RhNPs should be applicable for the production of a clean Rh-based nanocatalyst as our present results demonstrate.

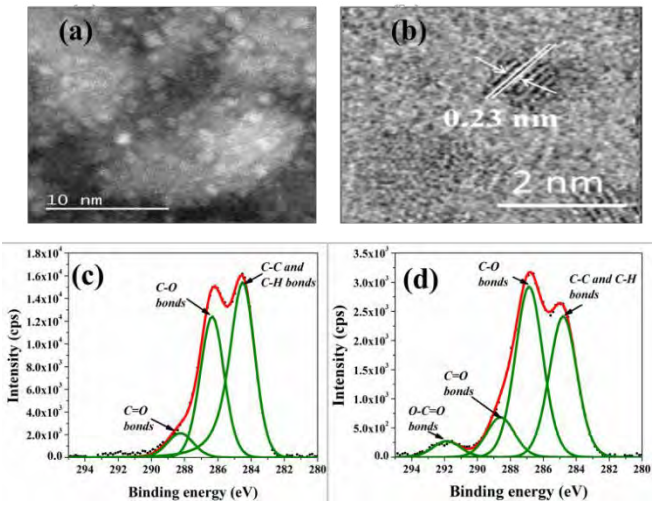

Figure 1. (a) STEM image and (b) HRTEM of the RhNPs/GO-45℃ nanocatalyst. XPS spectra of C1s on (c) GO and (d) RhNPs/GO-45℃ nanocatalyst.

First, GO was synthesized from commercial graphite using the modified Hummers method,[7] and transmission electron microscopy (TEM) images showed layered and flat structures (Figure S1), then sonication, and stirring formed a GO dispersion. Let us take the synthesis of RhNPs/GO nanocatalyst as the first example. RhNPs/GO was prepared by dropwise addition of an aqueous solution of $RhCl_3$ to the GO dispersion by syringe at 0°C followed by further stirring for another 30 min (SI). UV-vis. spectroscopy was used to monitor the reduction process with the rhodium *d-d* transition absorbance at 379 nm and 480 nm gradually decreasing with time, verifying the reduction

[*] C. Wang, R. Ciganda, Dr J. Ruiz, Prof. D. Astruc
ISM, UMR CNRS N° 5255, Univ. Bordeaux
33405 Talence Cedex, France
E-mail: d.astruc@ism.u-bordeaux1.fr

Drs C. Wang, V. Shalabaeva, L. Salmon
Laboratoire de Chimie de Coordination, UPR CNRS N° 8241
31077 Toulouse Cedex, France

Drs J.Tuninetti, L. Yate, S. Moya
CIC biomaGUNE, Unidad Biosuperficies,
Paseo Miramon No 182, Edif "C"
20009 Donostia-San Sebastian, Spain

[**] Financial support from the China Scholarship Council (CSC) of the People's Republic of China (grant to C.W.), the Universities of Bordeaux, Toulouse 3, Basque Country, and San Sebastian, the LCC (Toulouse), and the Centre National de la Recherche Scientifique (CNRS) is gratefully acknowledged.

of Rh^{3+} to Rh(0) by GO.[8] The reduction process was faster upon increasing the temperature. For instance the reduction of Rh^{3+} to Rh(0) by GO at 45℃ took only 1 min, whereas at 0℃ it required 30 min (Figure S4). The observed enhanced efficiency in the synthesis is attributed to an instantaneous nucleation process upon increasing the reaction temperature, resulting in reduced RhNP size (Table S1). Ostwald ripening takes place at higher temperature (> 45℃) following Rh atom nucleation, however, leading to the decrease in the number of Rh nuclei and to RhNP overgrowth.[6] Moreover after collecting by centrifugation, washing and redispersion in water, the nanocatalyst underwent a darker-to-lighter color change with increased temperatures, which is presumably related to the changes of RhNP size (Figure S5). Taken together, these phenomena indicate that the choice of the appropriate temperature in the synthesis optimizes the interaction between the RhNPs and the GO, a higher temperature weakening the GO anchoring ability and increasing the mobility of the Rh nuclei on the GO surface.[5,6,9]

Figure 1a shows the STEM image of RhNP/GO from the synthesis at 45℃. It is striking that the 1.8±0.3 nm RhNPs are fairly monodisperse on the GO surfaces. A high-resolution TEM (HRTEM) image (Figure 1b) of the RhNPs shows that the interplanar spacing of the particle lattice is 0.23 nm, corresponding to the (111) lattice spacing of face centered cubic Rh. X-ray photoelectron spectroscopy (XPS) was further recorded to investigate the surface nature of the RhNPs and GO. Comparison of the binding energy (B.E.) between the C1s spectra of GO and RhNP/GO clearly shows that after the reaction the peaks associated with the C–C bonds (B.E. = 284.6 eV) become predominant (Figure 1c), whereas the additional peak of C–O (B.E. = 286.6 eV) decreases during Rh^{3+} reduction (Figure 1d).[5a] The reducing nature of GO is due to the oxygenated functional groups attached to the hexagonal basal plane, further suggesting that these oxygenated functional groups (e.g. –OH, –COOH, epoxy) on the GO nanosheets play an important role of nanoparticles stabilizing ligands with the lone pairs of the oxygen atoms in the formation of RhNPs.[9] The B. E. values at 307.6 and 312.8 eV are assigned to Rh $3d_{5/2}$ and Rh $3d_{3/2}$ of Rh(0) respectively,[10] indicating the presence of metallic Rh (Figure S10). A *ca.*1 eV red shift of XPS peak of these very small RhNPs is observed and compared to bulk Rh, which is typical for very small metal NPs on a variety of support materials and is generally attributed to the reduced core-hole screening in metal clusters.[5b] Such a size-dependent alteration of electronic structures[5b] is seemingly concomitant with the enhanced catalytic properties (*vide infra*).

These results indicate that the high density of oxygen atom-containing functional groups on the GO surface interact with Rh atoms and therefore provide stabilization of RhNPs. A similar synthesis conducted under dark and only stirring in order to exclude the influence of light and power caused by the sonication showed no difference in the Rh^{3+} reduction to Rh(0) by GO. This confirms that the redox reaction between GO and Rh^{3+} accounts for the synthesis of RhNP/GO, as for the reaction proposed by Dai et al.[4] On the other hand, a galvanic reaction-like process in which the Rh reduction occurs on Rh nuclei by electrons transferred from GO may also be involved in the growth of the RhNPs after nucleation, accompanying GO oxidation.[5,11] The Raman spectra of the nanocatalyst RhNP/GO-45℃ showed no obvious change in the intensity ratio of I_D/I_G compared to pure GO, however (Figure S11), suggesting that the formation of RhNPs does not greatly reduce the size of the in-plane sp^2 domains of graphene.[4] Indeed, the XPS data suggest that the atomic content of Rh is only 1.9 %, which is too low to cause a large structural damage to GO sheets.

The catalysis of reduction by $NaBH_4$ of the pollutant 4-nitrophenol (4-NP) in water (Equation 1) to the useful dye 4-aminophenol was first probed; this is a trusted test reaction to further explore the catalytic efficiency of NP surfaces and optimize catalytic conditions.[12]

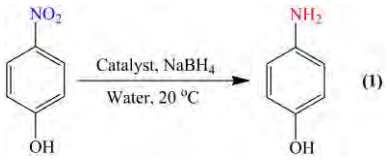

(1)

According to the reaction mechanism (see mechanistic details in the SI), the activation and dynamic restructuring of the NP surface are required, which eventually proceeds with an induction time if NP ligands are present.[13] Therefore, in the absence of surface restructuration if no ligand replacement is required, the 4-NP reduction catalyzed by surface-clean RhNP/GO would proceed with higher efficiency without induction time. The first attempt using 0.05 mol% catalyst in all the cases indicated that reduction was fast (in 40 s, the time for a complete scan) (SI), while control experiment showed the lack of any reactant conversion in the presence of only GO. Further decreasing the catalyst amount to 10 ppm (RhNPs per 4-NP) allows to easily monitor the reaction processes by UV-vis. spectroscopy, showing very fast 4-NP reduction without induction time (Table S1 and section 3).

The catalytic efficiencies were shown to undergo a volcano-type relationship with respect to RhNP/GO nanocatalysts synthesized at various temperatures. The catalyst RhNP/GO-45℃ showed the highest reaction rate, k_{app} = 11.8×10^{-3} s^{-1}, 1.65 times higher than that of RhNP/GO-0℃. The comparisons shown in Table S2 indicate that this catalyst showed the best efficiency ever obtained among various reported efficient catalysts. Remarkably, upon decreasing the total amount of RhNP/GO-45 ℃ to 1 ppm (RhNPs per 4-NP), high efficiency still remained, with k_{app} = 4.29×10^{-3} s^{-1} that is 1.4 times higher than the reaction rate obtained with 1 ppm of the catalyst RhNP/GO-0℃ under identical conditions. The remarkable efficiencies with exceptional low (ppm) amount of catalyst have so far never been reported and could be attributed to the ultrafine RhNP size and the very active surface-clean RhNPs. The presence of GO also increased the concentration of substrates near the surface Rh atoms,[14] benefiting to the catalytic efficiency.

With the efficient RhNP/GO-45℃nanocatalyst in hand, we then turned to another valuable reaction: the hydrolysis of ammonia-borane (AB) for H_2 generation. Owing to its high hydrogen content (19.6 wt%), high stability in the solid state and solution under ambient conditions, nontoxicity, and high solubility, AB has been considered as one of the leading contender in promising chemical H_2-storage materials.[15] Although many catalysts have been designed for the hydrolysis of AB, high-performance noble metal NPs still remain the most active catalysts for this reaction.[16] High catalyst loading of noble-metal catalyst and specific treatments are essential for the practical efficiency and sustainability, however. Herein we scrutinize the use of RhNP/GO-45℃ as a nanocatalyst for the hydrolysis of AB in water under air. This

provides one of the highest turnover frequencies (TOFs) for H_2 generation near or at ambient temperature with low catalyst amounts.

The reaction profile in the presence of various amounts of RhNP/GO-45℃ is shown in Figure S21. The nearly stoichiometric amounts of hydrogen release (3 equiv. H_2 per AB), indicate that hydrolysis of AB catalyzed by RhNP/GO-45℃ proceeds according to Equation (2):

$$n\,H_3NBH_3 + 2n\,H_2O \xrightarrow[H_2O,r.t.,\,Air]{Rh/GO\text{-}45\,^oC} n\,NH_4^+ + n\,BO_2^- + 3n\,H_2 \quad (2)$$

At the beginning of the reaction, the decay of AB producing H_2 was fast and linear as a function of the reaction time. Later on, it became slower especially under lower catalyst amounts. The hydrolysis of AB at rt (25±0.5℃) was completed within the shortest time (7.75 min) when the amount of RhNP/GO-45℃ was 0.15 mol%, providing a turnover frequency (TOF) of 258 mol_{H2} mol_{cat}^{-1} min^{-1}. The highest TOF was obtained with the optimum catalytic performance in the presence of 0.1 mol% catalyst for 9.5 min (TOF = 316 mol_{H2} mol $_{cat}^{-1}$ min^{-1}), while a further decrease of catalyst amount led to a longer reaction time and therefore the decrease of TOF values (Table S3). On the other hand, the uncatalyzed thermal reaction in the absence of catalyst showed negligible dehydrogenation of AB at the early stage of the reaction. The catalytic efficiencies obtained herein are comparable to the best previously reported performances achieved using several noble metal-based NP catalysts, showing the high efficiency of the present RhNP/GO system for hydrolysis of AB (Table S4).

Figure S21 demonstrates that the logarithmic plot of the calculated initial reaction rate *vs.* catalyst concentration has a slope of 1.03, indicating that the hydrolysis of AB catalyzed by RhNP/GO-45℃ follows a first-order kinetics with respect to catalyst concentration. The nearly horizontal line (slope of 0.042) indicates that the hydrolysis of AB catalyzed by RhNP/GO-45℃ is zero-order with respect to the AB concentration (Figure S22). This implies that AB activation is easy and thus rules out the possibility that the activation of AB in the rate-determining step (RDS). Furthermore, the activation energy (E_a) of hydrolysis of AB was determined to be approximately 21.4 kJ/mol (Figure S23 and calculations), one of the lowest E_a values compared to the literature (Table 3). Although the catalytic rates in the hydrolysis of AB catalyzed by RhNP/GO-45 ℃ is independent of the AB concentration, the kinetic isotope effects (KIEs)[17] were further investigated to shed light on the RDS of the reaction. Specifically in the hydrolysis of AB, the KIE value should tell if N−H or B−H or both bonds are broken or not during the RDS.[18-20]

The hydrolysis of the deuterated products of AB (see their synthesis in the SI) in the presence of RhNP/GO-45℃ results in slower reaction rates (Figure S27). A KIE of 1.33 was determined for deuteration at the boron site (NH_3BD_3), which indicates a similar dehydrogenation behavior to that of AB in H_2O. This shows the absence of large KIE for hydrolysis of AB deuterated at the boron site (NH_3BD_3). A larger KIE (2.57) was found for ND_3BH_3, suggesting that the O–H bond cleavage of H_2O might be in the RDS. This would be similar to the metal-catalyzed borohydride hydrolysis, in which half of the hydrogen comes from water.[21] Indeed, H_2O is activated by oxidative addition of a O-H bond on noble metal NP surfaces, forming adsorbed –OH and –H species. For instance, well-known precedents are found in the role of PtNPs as redox catalysts in water photo-splitting.[22] On the other hand, since the reaction rate is zero-order with respect to concentration of AB, H_2O dissociation alone as the RDS is not possible. Moreover, considering that the energy for the cleavage of the O-H bond in water (~493 kJ mol^{-1})[23a] is higher than those of B–N and B–H bond (~117 and ~430 kJ mol^{-1}, respectively),[24b] and the low energy barrier (E_a) obtained in the present hydrolysis reaction, the involvement of H_2O activation in the RDS of the hydrolysis is energetically favorable. Thus H_2O is most likely activated by an indirect O–H bond cleavage to form –H and –OH species promoted by AB in the presence of RhNP/GO-45℃.[19,20] Activation proceeds similarly in H_2O activation for $NaBH_4$ hydrolysis. We also suggest that the "hydridic" B-H hydrogen atom of AB forms a hydrogen bond with an "acidic" hydrogen atom of water in the ground state and that this B-Hδ⁻…Hδ⁺-O system undergoes oxidative addition followed by H_2 elimination on the Rh surface. Based on this understanding and experimental results, the hydrolysis of AB catalyzed by RhNPs/GO-45℃ in water is best presented overall as shown in Figure 2.

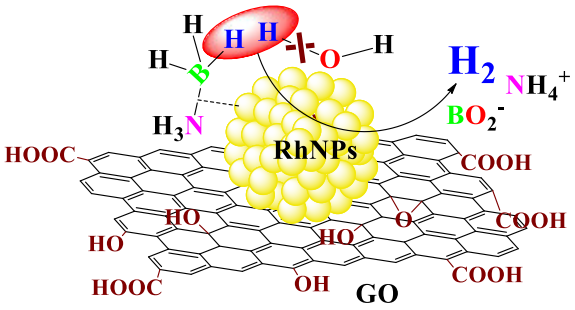

Figure 2. Proposed mechanism for the hydrolysis of AB by catalyzed by RhNP/GO-45℃.

The B–N bond in the AB is dissociated, since the NH_3 group does not participate in the hydrolysis.[16a] On the other hand, the presence of GO facilitates the adsorption of the reactant or desorption of products in water,[14] thus accelerating the overall process and improving the catalytic activity.

The general principle of transition-metal-GO nanocatalysts is extended to the synthesis of AuNPs/GO, PdNPs/GO, CuNPs/GO, and CuPd NPs/GO at 45℃ under identical conditions. In the case of AuNPs/GO, reduction of Au^{3+} by GO (Au^{3+}/Au^0 = 1.5 V *v.s* SHE) results in the high efficient AuNPs/GO nanocatalyst with AuNPs of 3.3 nm (Figure S28), as exemplified by the 0.05 mol% AuNPs/GO nanocatalyst catalyzed 4-NP reduction in water (Figure S29) without induction time and remarkable efficiency (k_{app} = 3.7×10^{-3} s^{-1}) compared to the recently reported values (Table S2).

Another challenging example is the synthesis of first raw metal NPs by reduction the metal precursors with GO, because the redox potential of $M^{2+/3+}/M(0)$ compared to the oxidation potential of GO makes the reaction endergonic. Upon heating at 45℃, however, Cu^{2+} reduction (Cu^{2+}/Cu^0=0.34 V *vs.* SHE) by GO proceeds due to the fast follow-up Cu atom aggregation that shifts the apparently unfavorable redox process. Thus the formation of CuNPs/GO in this way was confirmed by both UV-vis. spectroscopy and XPS. No SPB was observed due to the small CuNP size (3.0 nm), but the surface Cu(0) oxidation state is shown by XPS (Figure S31). On the other hand, 4-NP reduction is successfully achieved using 0.5% mol CuNPs/GO catalyst with no induction time and a high efficiency of 5.2×10^{-3} s^{-1} (k_{app}). The absence

of induction time in the 4-NP reduction suggests that activation and dynamic restructuring of the Cu(0) surface is not necessary due to the absence of molecular ligand. Note that even weakly stabilizing triazole-based ligand on CuNPs provoke the requirement of an induction time for 4-NP reduction.[24] The high efficiency of the CuNPs/GO nanocatalyst was also confirmed by the "click" reaction between benzyl azide and phenylacetylene, in which 93% isolated yield was achieved at 35 ℃ for 24 h using only 0.01 mol% of CuNPs (Equation 3); this is one of the lowest catalyst amounts among recent literature values.

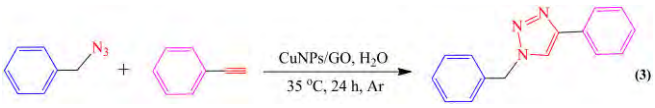

(3)

XPS suggests that the active Cu^{I} species is formed in the native oxide layer on the Cu surface through comproportionation of Cu^{0} and Cu^{II} (Figure S31).

Pd/Cu nanocatalysts have been successfully applied to Sonogashira coupling reactions, in which two cooperative catalytic cycles of Pd and Cu form the mechanism; thus an increased efficiency of Sonogashira coupling reaction is expected.[25] We assumed that the double reduction of equimolar amount of Pd^{2+} (Pd^{2+}/Pd^{0}=1.5 V *v.s* SHE) and Cu^{2+} by GO could result in a valuable heterogeneous catalyst for Sonogashira coupling reaction under hopefully very favorable conditions. Thus CuPd NPs/GO nanocatalyst prepared in this way was characterized by TEM and XPS. TEM showed the NP size is around 3.5 nm (Figure S35), while XPS suggested the molar ratio is Pd:Cu=1:1.35. Moreover, the CuPd NPs surface showed both the surface Cu(0) and the Cu^{2+} oxidation states of Cu (Figure S36), and the XPS peak $3d_{5/2}$ of Pd(0) located at 335.9 eV (Figure S37 and discussions). For comparison, CuNPs/GO and PdNPs/GO nanocatalysts were separately prepared and tested in the Sonogashira coupling between iodobenzene and phenylacetylene in water at room temperature (rt) for 24 h with 0.05 mol% metal loading. PdNPs/GO nanocatalyst with Pd size of 2.8 nm showed an acceptable 85 % conversion, while in the case of Cu NPs/GO nanocatalyst the conversion was less than 20%. Note that the result of PdNP/GO is already very good at rt, but with combined Cu and Pd, remarkably conversion was quantitative with 93% isolated yield in this Sonogashira coupling reaction (Equation 4). Therefore, synergistic CuPd NPs/GO nanocatalyst is an excellent catalyst for Sonogashira coupling in water at rt, i.e. under environmentally-friendly condition.

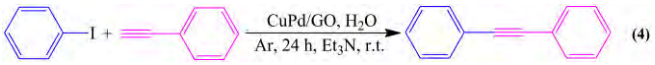

(4)

Finally, the reusability of the catalyst was studied using RhNP/GO-45℃ nanocatalyst in the hydrolysis of AB in water by continuous addition of a new proportion of AB aqueous solution when the previous run was completed. In this way RhNP/GO-45℃ was successfully recycled four times (Figure S40). Therefore it is an excellent catalyst for the hydrolysis reaction. The observed little decrease of activity in the fourth run is probably ascribed to the aggregation of RhNPs as shown by TEM image taken after recycling experiments (Figure S41). It is due to the slight deactivation effect of the hydrolysis product metaborate[15g,16a,16b,26] that accumulates during the hydrolysis and partly inhibits the catalytically active Rh surface atoms, and to the dilution of the reactant in water.

In summary, a simple, clean redox reaction between various transition metal cations and GO has been shown here to lead to the synthesis of ultrafine, surface-clean metal NPs on graphene oxide with good monodispersity. This method avoids the formation of reactant residues inhibiting the catalytic NP surface. The appropriate choice of temperature during the synthesis improves the reduction efficiency and enhances the interaction between the RhNPs and GO. Consequently, the nanocatalyst RhNP/GO without any other ligand shows exceptional efficiency in the 4-NP reduction down to 1 ppm metal level, and it is also very efficient for the hydrolysis of AB to produce H_2. The KIE studies allow the clarification of the RDS for AB hydrolysis. Moreover, this strategy also produces other excellent metal NP/GO catalysts for redox reactions in general, showing high efficiency in 4-NP reduction, Sonogashira coupling at rt, click reaction and hydrolysis of AB for hydrogen production with low amounts of catalytic metals. The activation of NP/G by GO as ligand recalls the efficient catalysis using oxides as ligands,[27] although the NP-GO interactions are of different nature here, of rather synergetic supramolecular type. The principles and clean and simple catalytic method presented herein could be extended to other transition-metal nanocatalysts and should contribute to the rational design of efficient nanocatalysts for a large variety of chemical reactions.

Conflict of interest

The authors declare no conflict of interest.

Keywords: transition-metal • nanoparticle • graphene oxide • redox reaction • catalysis

[1] a) A. Fihri, M. Bouhrara, B. Nekoueihahraki, J. M. Basset, V. Polhettiwar, *Chem. Soc. Rev.* **2011**, *40*, 5181-5203; b) L. M. Bronstein, Z. B. Shifrina, *Chem. Rev.* **2011**, *111*, 5301-5344; c) A. Balanta, C. Godart, C. Claver, *Chem. Soc. Rev.* **2011**, *40*, 4973-4985; d) E. Gross, J. H. -C. Liu, F. D. Toste, G. A. Somorjai, *Nat. Chem.* **2012**, *4*, 947-952; e) J. D. Scholden, B. C. Leal, J. Dupont, *ACS Catal.* **2012**, *2*, 184-200; f) M. Sankar, N. Dimitratos, P. J. Miedjack, P. P. Wells, C. J. Kiely, G. J. Hutchings, *Chem. Soc. Rev*. **2012**, *41*, 8099-8139; g) D. Astruc, *Nat. Chem.* **2012**, *4*, 255-267; h) M. Haruta, M. *Angew. Chem. Int. Ed.* **2014**, 53, 52-56; i) M. B. Gawande, A. Goswami, F.-X. Felpin, T. Asefa, X. X. Huang, R. Silva, X. X. Zou, R. Zboril, R. S. Varma, *Chem. Rev*. **2016**, 116, 3722; j) C. Amiens, D. Ciuculescu-Pradines, K. Philippot, *Coord. Chem. Rev.* **2016**, *308,* 409–432; k) Y. Xia, K. D. Gilroy, H.–C. Peng, X. Xia, *Angew. Chem. Int. Ed.* **2017**, 56, 60–95; l) D. Wang, D. Astruc, *Chem. Soc. Rev*. **2017**, *46,* 816-854; m) P. Liu, R. Qin, G. Fu, N. Zheng, *J. Am. Chem. Soc.* **2017**, *139*, 2122–2131.

[2] a) N. Toshima, T. Yomezawa, *New J. Chem.* **1998**, 22, 1179-1201; b) D. Astruc, F. Lu, J. Ruiz, *Angew. Chem., Int. Ed*. **2005**, *44*, 7852-7872; c) N. T. S. Phan, M. Van Der Sluys, C. W Jones, *Adv. Syn. Catal.* **2006**, *348*, 609-679; d) V. S. Myers, M. G. Weir, E. V. Carino, D. F. Yancey, S. Pande, R. M. Crooks, *Chem. Sci.* **2011**, *2*, 1632-1646; e) J. A. Lopez-Sanchez, N. Dimitratos, C. Hammond, G. L. Brett, L. Kesavan, S. White, P. Miedziak, R. Tiruvalam, R. L. Jenkins, A. F. Carley, D. Knight, C. J. Kiely, G. J. Hutchings, *Nat. Chem.* **2011**, *3*, 551-556; f) C. H. Cui, L. Gan, M. Heggen, S. Rudi, P. Strasser, *Nat. Mater.* **2013**, *12*, 765-771; g) G. Prieto, J. Zecevic, H. Friederich, K. P. de Jong, P. E. De Jongh, *Nat. Mater.* **2013**, *12*, 34-39; h) Z. Niu, Y. Li, *Chem. Mater.* **2014**, *26*, 72–83; h) K. Na, M. Choi, O. M. Yaghi, G. A. Somorjai, *Nano Lett.* **2014**, *14*, 5979-5983; i) J. K. Sun, W. W. Zhan, T. Akita, Q. Xu, *J. Am. Chem. Soc.* **2015**, *137*, 7063-7066.

[3] a) S. Navalon, A. Dhakshinamoorthy, M. Alvaro, H. Garcia, *Chem. Rev.* **2014**, *114*, 43, 5288-5301; b) D. R. Dreyer, A. D. Todd, C. W. Bielawski, *Chem. Soc. Rev.* **2014**, *114*, 6179-6212; c) X. B. Fan, G. L. Zhang, F. B. Zhang, *Chem. Soc. Rev.*

2015, *44*, 3023-3035; d) N. M. Julkapli, S. Bagheri, *Intern. J. Hydrogen Energy* **2015**, *40*, 948-979; e) S. Navalon, A. Dhakshinamoorthy, M. Alvaro, H. Garcia, *Coord. Chem. Rev.* **2016**, *312*, 99-148; f) C. Han, N. Zhang, Y. J. Xu, *Nano Today* **2016**, *11*, 351-372.

[4] H. C. Choi, M. Shim, S. Bangsaruntip, H. Dai, *J. Am. Chem. Soc.* **2002**, *124*, 9058-9059.

[5] a) X. Chen, G. Wu, J. Chen, X. Chen, Z. Xie, X. Wang, *J. Am. Chem. Soc.* **2011,** *133*, 3693-3695; b) H. Yin, H. Tang, D. Wang, Y. Gao, Z. Tang, *ACS Nano*. **2012**, *6*, 8288-8297.

[6] Y. Bia, G. Lu, *Chem. Commun.* **2008**, 6402-6404.

[7] J. G. Radich, P. V. Kamat, *ACS Nano* **2013**, *7*, 5546-5557.

[8] F. Durap, M. Zahmakıran, S. Özkar, *Appl. Catal. A: Gen.* **2009**, *369*, 53-59.

[9] a) P. R. Kannan, A. Swami, D. Srisathiyanarayanan, P. S. Shirude, R. Pasricha, A. B. Mandale, M. Sastry, *Langmuir* **2004**, *20*, 7825–7836; b) R. Pasricha, S. Gupta, A. K. Srivastava, *Small* **2009**, *5*, 2253–2259; c) F. Li, Y. Guo, Y. Liu, J. Yan, W. Wang, J. Gao, *Carbon* **2014**, *67*, 617-626.

[10] D. Özhava, S. Özkar *Appl. Catal. B: Environ.* **2016**, *181*, 716–726.

[11] Y. Qin, J. Li, Y. Kong, X. Li, Y. Tao, S. Li, Y. Wang, *Nanoscale* **2014**, *6*, 1281–1285.

[12] a) N. Pradhan, A. Pal, T. Pal, *Colloids Surf. A* **2002**, *196*, 247-257; b) T. Aditya, A. Pal, T. Pal, *Chem. Commun.* **2015**, *51*, 9410- 9431; c) P. Zhao, X. Feng, D. Huang, G. Yang, D. Astruc, *Coord. Chem. Rev*. **2015**, *287*, 114-136.

[13] a) S. Wunder, Y. Lu, M. Albrecht, M. Ballauff, *ACS Catal*. **2011**, *1*, 908-916; b) S. Gu, Y. Lu, J. Kaiser, M. Albrecht, M. Ballauff, *Phys. Chem. Chem. Phys.* **2015**, *17*, 28137-28143; c) Y. Lu, M. Ballauff, *Prog. Polym. Sci*. **2016**, *59*, 86-104.

[14] a) T. Wu, L. Zhang, J. Gao, Y. Liu, C. Gao, J. Yan, *J. Mater. Chem. A,* **2013**, *1*, 7384-7390; b) J. -J. Lv, A. -J. Wang, X. Ma, R. -Y. Xiang, J. -R. Chen, J. -J. Feng, *J. Mater. Chem. A* **2015**, *3*, 290-296; c) P. Song, L.-L. He, A. -J. Wang, L.-P. Mei, S. -X. Zhong, J. -R. Chen, J. -J. Feng, *J. Mater. Chem. A* **2015**, *3*, 5321-5327.

[15] a) Q. Xu, M. Chandra, *J. Power Sources*, **2006**, *163*, 364–370; b) M. Chandra, Q. Xu, *J. Power Sources*, **2007**, *168*, 135–142; c) F. H. Stephens, V. Pons, R. T. Baker, *Dalton Trans*. **2007**, 2613–2626; d) J. -M. Yan, X. -B. Zhang, S. Han, H. Shioyama, Q. Xu, *Angew. Chem., Int. Ed.*, **2008**, *47*, 2287–2289; e) C. W. Hamilton, R. T. Baker, A. Staubitz, I. Manners, *Chem. Soc. Rev.* **2009**, *38*, 279–293; f) H.-L. Jiang, S. K. Singh, J. -M. Yan, X. -B. Zhang, Q. Xu, *ChemSusChem*, **2010**, *3*, 541–549; g) O. Metin, V. Mazumder, S. Özkar, S. S. Sun, *J. Am. Chem. Soc.* **2010**, *132*, 1468-1469; h) A. Staubitz, A. P. M. Robertson, I. Manners, *Chem. Rev.* **2010**, *110*, 4079–4124; i) Q. L. Zhu, Q. Xu, *Energy Environ. Sci.* **2015**, *8*, 478–512; j) Q. –L. Zhu, Q. Xu, *Chem.* **2016**, *1*, 220-245.

[16] a) Q.–L. Zhu, J. Li, Q. Xu. *J. Am. Chem. Soc.* **2013**, *135*, 10210−10213; b) M. Rakap, *Appl. Catal. B: En.* **2015**, *163*, 129–134; c) W. -W. Zhan, Q. –L. Zhu, Q. Xu, *ACS Catal.* **2016**, *6*, 6892–6905; d) M. A. Khalily, H. Eren, S. Akbayrak, H. H. Susapto, N. Biyikli, S. Özkar, M. O. Guler, *Angew. Chem. Int. Ed.* **2016**, *55*, 12257 –12261; e) d) S. Akbayrak, Y. Tonbul, S. Özkar, *Appl. Catal. B: En.* **2016**, *198*, 162–170; f) K. Mori, K. Miyawaki, H. Yamashita, *ACS Catal.* **2016**, *6*, 3128–3135.

[17] a) K. C. Westaway, *J. Labelled Compd. Radiopharm.* **2007**, *50*, 989–1005; b) G. Guella, B. Patton, A. Miotello, *J. Phys. Chem. C,* **2007**, *111*, 18744–18750; c) E. M. Simmons, J. F. Hartwig, *Angew. Chem., Int. Ed.* **2012**, *51*, 3066–3072.

[18] Hydrolysis of AB by molecular catalysts: a) R. J. Keaton, J. M. Blacquiere, R. T. Baker, *J. Am. Chem. Soc.* **2007**, *129*, 1844–1845; b) P. Bhattacharya, J. A. Krause, H. Guan. *J. Am. Chem. Soc.* **2014**, *136*, 11153−11161; c) J. A. Buss, G. A. Edouard, C. Cheng, J. Shi, T. Agapie, *J. Am. Chem. Soc.* **2014**, *136*, 11272−11275.

[19] W. Chen, D. Li, Z. Wang, G. Qian, Z. Sui, X. Duan, X. Zhou, I. Yeboah, D. Chen, *AIChE J.* **2017**, *63*, 60–65.

[20] Z. Li, T. He, L. Liu, W. Chen, M. Zhang, G. Wu, P. Chen, *Chem. Sci.* **2017**, *8*, 781-788.

[21] B. H. Liu, Z. P. Li, *J. Power Sources* **2009**, *187*, 527–534.

[22] a) J. -M. Lehn, J. -P. Sauvage, *Nouv. J. Chim.* **1977**, *1*, 449–451; b) A. Hagfeldt, M. Grätzel, *Chem. Rev*. **1995**, *95*, 49–68.

[23] a) P. R. Rablen, *J. Am. Chem. Soc.* **1997**, *119*, 8350–8360; b) L. R. Peebles, P. Marshall, *J. Chem. Phys.* **2002**, *117*, 3132–3138.

[24] C. Wang, R. Ciganda, L. Salmon, D. Gregurec, J. Irigoyen, S. Moya, J. Ruiz, D. Astruc, *Angew. Chem., Int. Ed.,* **2016**, *55*, 3091-3095.

[25] a) R. Chinchilla, C. Nájera, *Chem. Rev.,* **2007**, *107*, 874−922; b) R. Chinchilla, C. Nájera, *Chem. Soc. Rev.,* **2011**, *40*, 5084–5121.

[26] W. Chen, J. Ji, X. Feng, X. Duan, G. Qian, P. Li, X. Zhou, D. Chen, W. Yuan, *J. Am. Chem. Soc.*, **2014**, *136*, 16736–16739.

[27] D. A. Pelletier, J.-M. Basset, *Acc. Chem. Res*. **2016**, *49*, 664-677.

Entry for the Table of Contents (Please choose one layout)

Layout 1:

COMMUNICATION

Text for Table of Contents

New graphene oxide supported metal nano- catalysts synthesized using redox reactions are highly efficient in water at ambient temperature for 4-nitrophenol reduction, Sonogashira coupling, azide-alkyne 1,3-cycloaddition and dihydrogen production upon hydrolysis of ammonia-borane and recyclable.

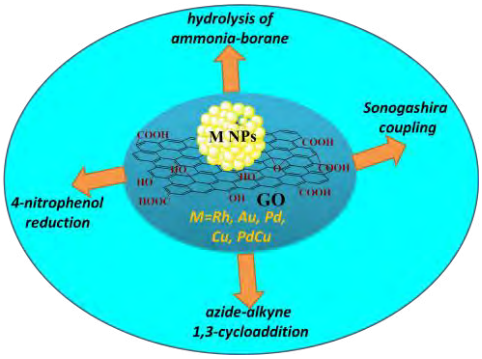

Synthesis and high catalytic efficiency of transition-metal nanoparticle-graphene oxide nanocomposites

Changlong Wang, Roberto Ciganda, Luis Yate, Jimena Tuninetti, Victoria Shalabaeva, Lionel Salmon, Sergio Moya, Jaime Ruiz, Didier Astruc

Summary

In this chapter, we mainly contribute to the rational design of nanoparticles catalysts supported on graphene based nanomaterials as efficient catalysts for a variety of chemical reactions including 4-nitrophenol reduction, Suzuki-Miyaura reaction, Sonogashira coupling, azide-alkyne 1,3-cycloaddition, and hydrolysis of ammonia-borane for hydrogen generation.

RhAg/rGO nanocatalyst: ligand-controlled synthesis and superior catalytic performances for the reduction of 4-nitrophenol

The first paper reports the preparation of ultrafine and monodispersed bimetallic RhAg nanoparticles (NPs) that are uniformly supported on reduced graphene oxide nanosheets (RhAg/rGO).

The nanocatalyst construction started with the synthesis of NPs in aqueous solution in the presence of tristrz-PEG as the encapsulating ligand and involved reduction by sodium borohydride. GO was directly added to the solution and further stirred for another 30 min, and meanwhile GO was reduced by excess of $NaBH_4$ to rGO. The catalyst was then aged for 3 h, washed and dried, yielding the heterogeneous RhAg/rGO catalysts (Figure 1).

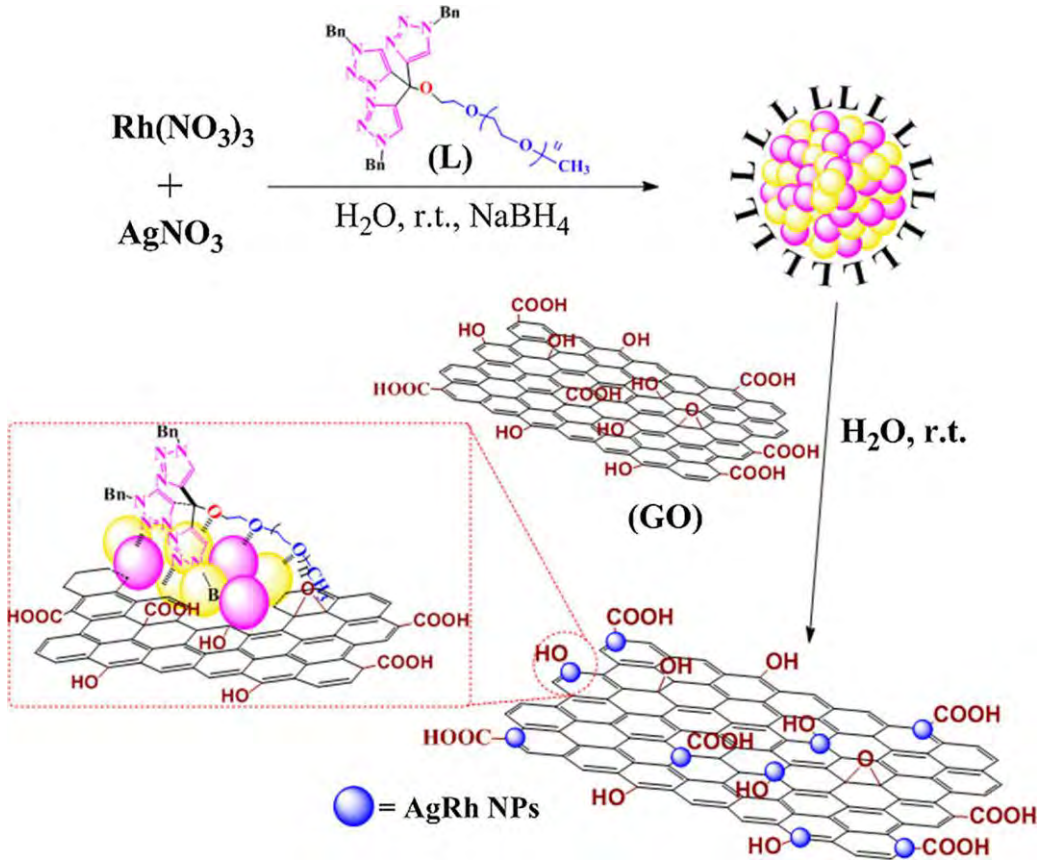

Figure 1. Synthesis of the RhAg/rGO catalysts.

The supramolecular H-bonding interactions between the PEG termini of the tristrz-PEG ligand and multiple surface oxygen functional groups, such as –COOH and –OH, of the rGO ensured the quantitative deposition process. The synergy with the triazole groups and PEG of tristrz-PEG ligand that also weekly interacted with the RhAgNP surface provide the effectiveness of small NP stabilization. The RhAg/rGO catalysts were characterized by various techniques including UV-vis., ICP-AES, TEM, HRTEM, STEM, EDX, and XPS. The bimetallic RhAg NPs involve a synergy between the two metals on rGO that improves the catalytic activity compared to both

monometallic counterparts. By varying the Rh/Ag molar ratios, the highest catalytic activity in the reduction of 4-nitrophenol by $NaBH_4$ was obtained for $RhAg_{0.5}$/rGO with a remarkable reaction rate of $k_{app} = 14.8 \times 10^{-3}\ s^{-1}$ ($k_{nor} = 1415\ s^{-1}\ g^{-1}$, Figure 2).

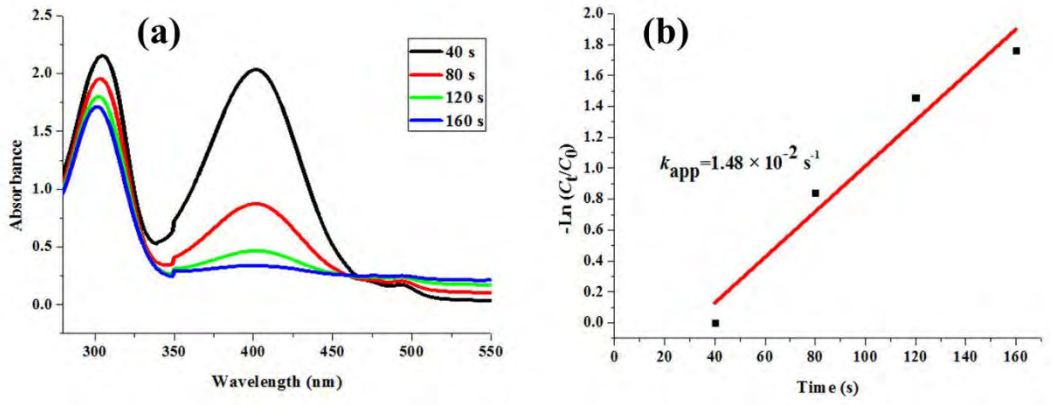

Figure 2. (a) UV-vis. spectra of the 4-NP reduction by $NaBH_4$ catalyzed by $RhAg_{0.5}$/rGO (top); (b) consumption rate of 4-NP: -ln(C_t/C_0) *vs.* reaction time .

The mechanism for the 4-NP reduction by $NaBH_4$ in the presence of RhAg/rGO catalyst follows earlier suggestions involving BH_4^- adsorption onto the catalyst surface and transfer of active hydrogen species to the NP surface to form surface metal-hydride species. The presence of rGO mediates this process by increasing 4-NP absorption at the RhAg NP surface, and the RhAg NP surface is coordinated to the weak tristrz-PEG ligand that is readily substituted by substrates. Consequently, the electron-rich Rh atom-coordinated hydrogen species is transferred to the nitro groups at the NP surface. Charge transfer within the Rh-Ag surface towards the Rh sites favors the hydride transfer to this substrate. It is also possible that excess BH_4^-

transfers electrons to the bimetallic catalyst surface, still increasing the charge on the key active Rh-H site (Figure 3).

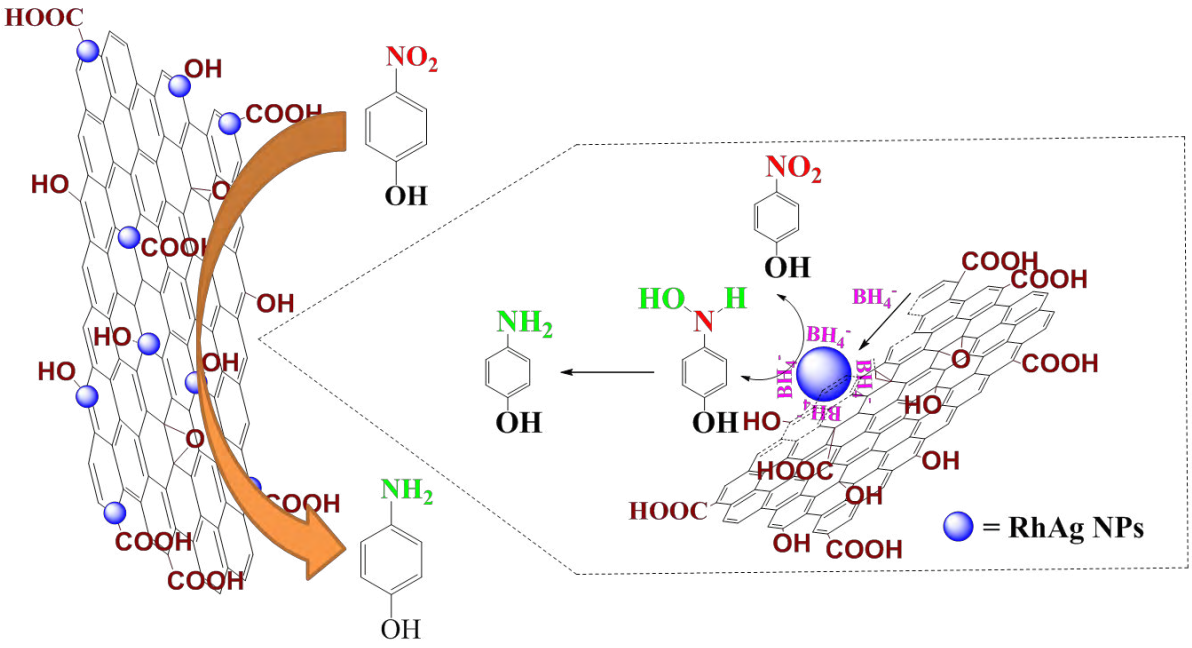

Figure 3. Proposed mechanism for the 4-NP reduction by $NaBH_4$ in the presence of a RhAg/rGO catalyst.

The reusability of the $RhAg_{0.5}$/rGO catalyst was also investigated, and the $RhAg_{0.5}$/rGO catalyst is reused at least five times without significant loss of reaction activity. In the fifth run, the rate constant for the 4-NP reaction was still k_{app} = 12.1 $\times 10^{-3}$ s^{-1}, suggesting that the $RhAg_{0.5}$/rGO catalyst exhibits very good reusability in the reduction of 4-NP (Table 1). This efficiency is also superior to that encountered in most of the cases using noble metal based NP catalysts. Decreasing the total catalyst

amount to an acceptable level with good reaction activity was also attempted. With 0.05 mol% and 0.01 mol% $RhAg_{0.5}$/rGO catalyst, the reaction rate is $k_{app} = 8.2 \times 10^{-3}$ s^{-1} ($k_{nor} = 3140$ s^{-1} g^{-1}) and $k_{app} = 5.3 \times 10^{-3}$ s^{-1} ($k_{nor} = 10140$ s^{-1} g^{-1}), respectively, demonstrating the successful design of cost-effective RhAg/rGO catalytic system (Figure 4). The work not only sheds a new light on the development of high performance bimetallic NPs using appropriate supporting materials, but also contributes to the design of very efficient, cost-effective catalysts for various current organic reactions.

Table 1. Recycling results of the 4-NP reduction using $RhAg_{0.5}$/rGO as the catalyst.

Catalytic runs	1	2	3	4	5
k_{app} ($\times 10^{-3}$ s^{-1})	14.8	14.6	14.2	13.3	12.1

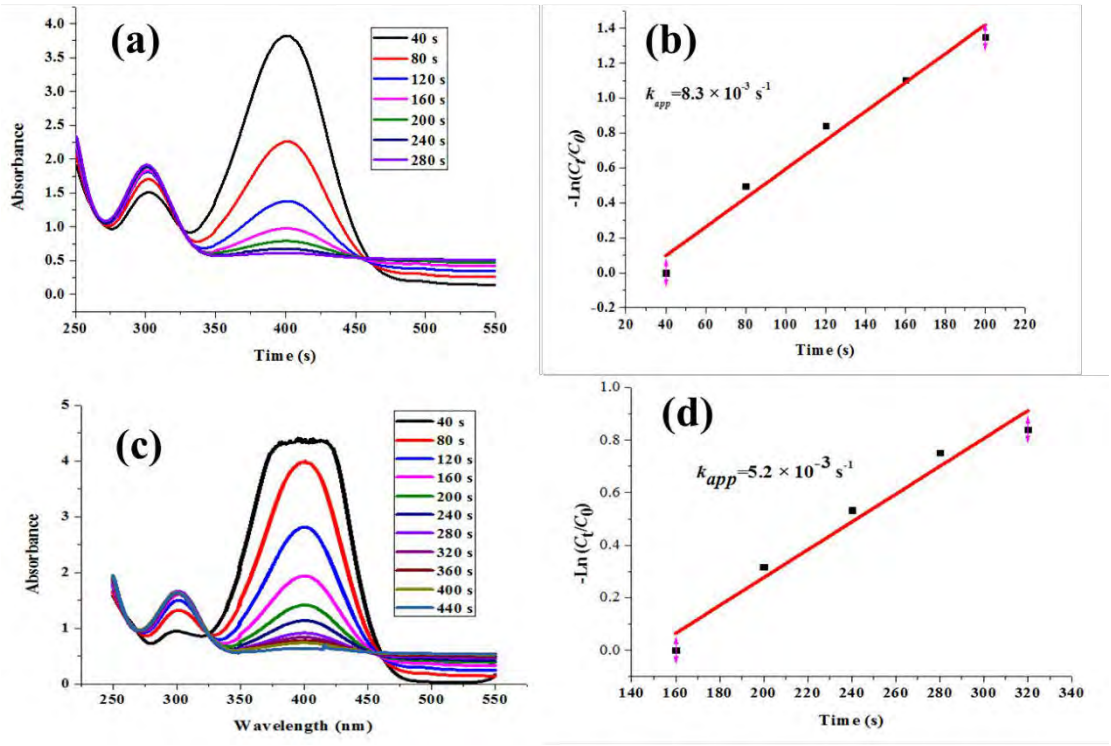

Figure 4. (a) UV-vis. spectra of the 4-NP reduction by $NaBH_4$ catalyzed by 0.05 mol% $RhAg_{0.5}$/rGO; (b) consumption rate of 4-NP: -ln(C_t/C_0) *vs.* reaction time; (c) UV-vis. spectra of the 4-NP reduction by $NaBH_4$ catalyzed by 0.01 mol% $RhAg_{0.5}$/rGO; (d) consumption rate of 4-NP: -ln(C_t/C_0) *vs.* reaction time. C_t value represents the absorbance at 400 nm that corresponds to the nitrophenolate anion decreases with time along with the growth of a weak 4-AP band at 300 nm. C_0 value represents the absorbance at 400 nm that corresponds to the nitrophenolate anion at the beginning of the reaction.

Efficient parts-per-million α-Fe_2O_3 nanocluster/graphene oxide catalyst for Suzuki–Miyaura coupling reactions and 4-nitrophenol reduction in aqueous solution

Secondly, the supramolecular H-bonding interactions between the PEG termini of the tris-trz-PEG ligand and the functional groups of the graphene oxide (GO) support enable the design of new heterogeneous α-Fe_2O_3 nanocluster/GO catalysts. First, ligand stabilized α-Fe_2O_3 nanoclusters of only 1.8 nm size were synthesized, and GO was then directly injected, and the catalyst was aged for 3 hours. The catalyst was then collected and dried *in vacuo* at 50 ℃ overnight to yield the catalyst (Figure 5).

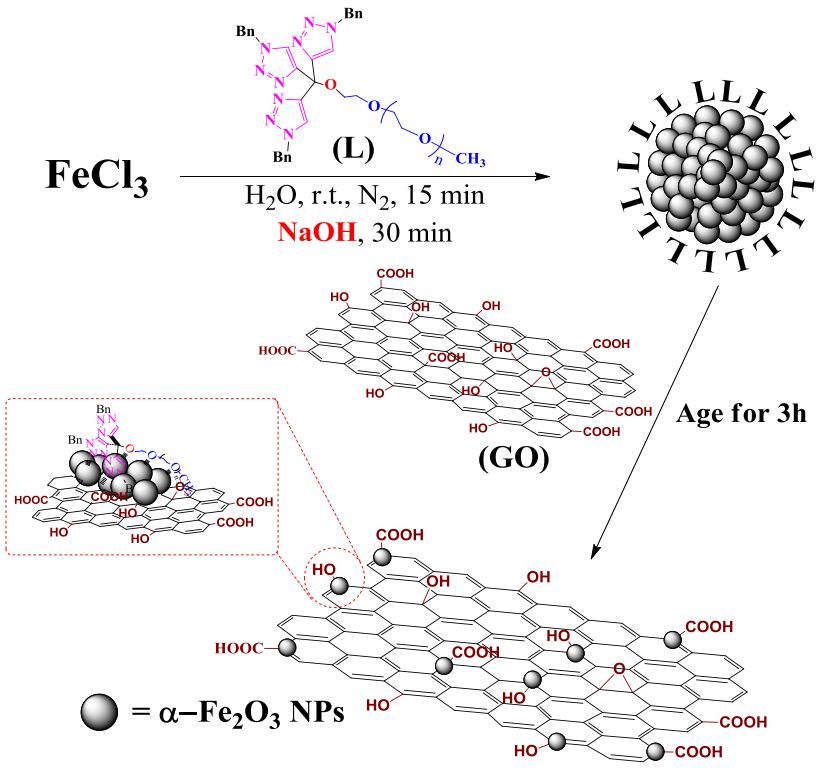

Figure 5. Synthesis of the catalyst α-Fe_2O_3/graphene oxide, **1**.

XPS showed the core level binding energies located at 726.4 and 712.3 eV are shown in the Fe 2p spectrum, which correspond to Fe $2p_{1/2}$ and Fe $2p_{3/2}$ core level of the α-Fe_2O_3, respectively. Moreover the shakeup satellite peak at about 719.0 eV also

suggested the presence of Fe^{3+} species (Figure 6).

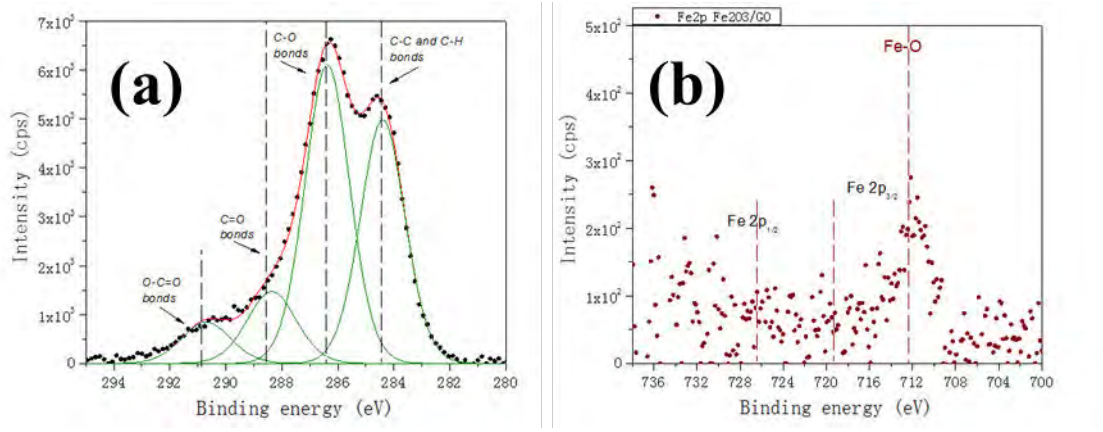

Figure 6. XPS of the catalyst **1**. C 1s spectrum (a) and Fe2p (b).

Catalytic applications of the catalyst were first probed for the 4-NP reduction by $NaBH_4$ in water, showing high efficiency with an apparent kinetic rate constant (k_{app}) of $4.17\times10^{-4}\ s^{-1}$ (Figure 7).

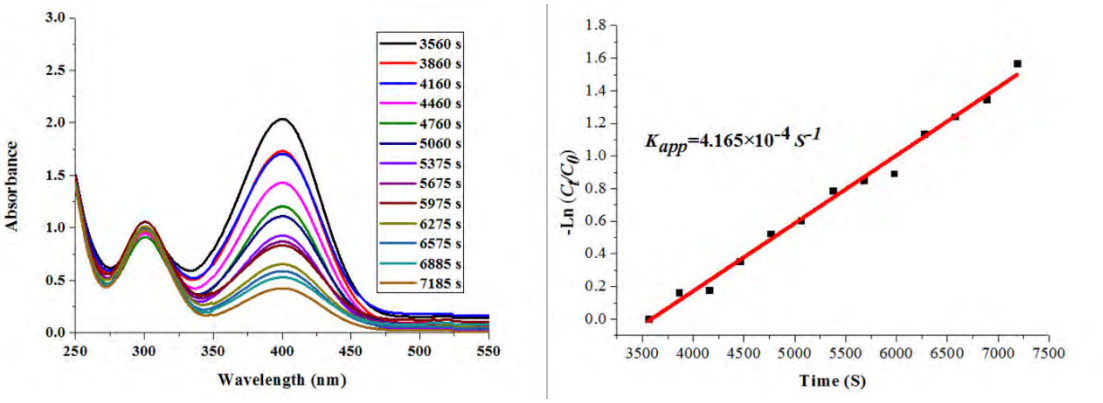

Figure 7. UV-vis. spectra for the 4-NP reduction by $NaBH_4$ catalyzed by **1** (left); consumption rate of 4-NP: $-\ln(C_t/C_0)$ *vs.* time (right).

Furthermore, α-Fe_2O_3 nanocluster/GO catalysts also showed high efficiency towards

Suzuki-Miyaura reaction with only parts per million (ppm) amount of metal loading. We first optimized the reaction condition by leaving the solvent as the only parameter. Solvent mixtures containing water and, as co-solvent, DMF, ethylene glycol or EtOH were tested for this model reaction. The results showed that the presence of the H_2O/EtOH solution led to the best catalytic performance with a quantitative conversion and a 87% isolated yield (Table 2).

Table 2. Optimization of the Suzuki–Miyaura coupling reactions.[a]

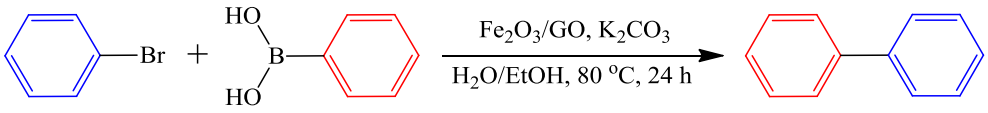

Catalyst	Solvent	Conversion	Yield
α-Fe_2O_3/GO	H_2O/DMF （1mL：1 mL)	0	0
α-Fe_2O_3/GO	H_2O/ethylene glycol (1mL:1 mL)	0	0
α-Fe_2O_3/GO	H_2O/EtOH (1:1, 2 mL)	100%	87%
α-Fe_2O_3/GO	H_2O/EtOH (1:1, 20 mL)	0	0
GO	H_2O/EtOH (1:1, 2 mL)	0 (1^{st}); 0 (2^{nd}); 0 (3^{rd}).	0
α-Fe_2O_3	H_2O/EtOH (1:1, 2 mL)	0	0

[a] Reaction condition: bromobenzene (0.2 mmol), phenylboronic acid (0.3 mmol),

catalyst (150 ppm α-Fe_2O_3), K_2CO_3 (0.4 mmol), 80℃, N_2, 24 h.

The procedures for Suzuki–Miyaura coupling reactions are : A dry Schlenk flask was charged with K_2CO_3 (2 equiv.), phenylboronic acid (1.5 equiv.), and bromobenzene (1 equiv.). The catalyst **1** was then successively added, and the solvents H_2O and EtOH were added in order to make a total of 2 mL of solvent (volume ratio of H_2O/EtOH: 1/1). The suspension was then allowed to stir under N_2 for 24 hours at 80℃. After the reaction, the Schlenk flask was cooled to r.t., the mixture was extracted three times with diethyl ether (Et_2O, 3 × 10 mL), the organic phase was dried over Na_2SO_4, and the solvent was removed *in vacuo*. In parallel, the reaction was checked using TLC in only petroleum ether as eluent. The crude product was checked by ^1H NMR in order to calculate the conversion. The purification by flash chromatography column was conducted with silica gel as the stationary phase and petroleum ether as the mobile phase.

The Suzuki-Miyaura reactions by α-Fe_2O_3 nanocluster/GO catalyst showed broad substrates scope. Bromobenzene derivatives containing electron-withdrawing (NO_2, CHO, CH_3CO) and electron-donating (NH_2, OCH_3, CH_3) groups in *para* position were suitable coupling partners, and the corresponding coupling products were all efficiently isolated with good yields (Table 3).

Table 3. Investigation of the substrate scope in the Suzuki-Miyaura reaction catalyzed by α-Fe_2O_3 nanocluster/GO.[a]

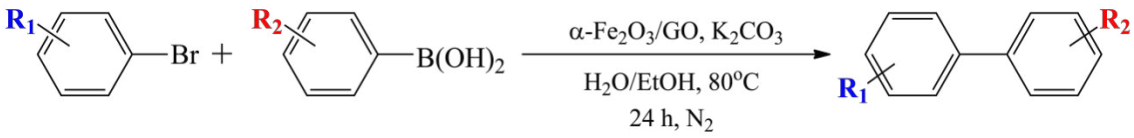

Entry	R_1	R_2	Conversion[b]	Yield[c]
1	H	H	100%	87%
2	4-NO_2	H	100%	83.3%
3	4-CHO	H	100%	83%
4	4-CH_3CO	H	100%	84.5%
5	4-NH_2	H	95%	80%
6	4-CH_3O	H	98%	78%
7	4-CH_3	H	90%	75%
8	H	2-CH_3	75%	51%
9	H	4-CH_3	98%	82%

[a] Reaction condition: bromobenzene (0.2 mmol), phenylboronic acid (0.3 mmol), catalyst (150 ppm α-Fe_2O_3), K_2CO_3 (0.4 mmol), EtOH/H_2O (1 mL/1 mL), 80℃, N_2, 24 h; [b] ^{1}H NMR conversion; [c] yields of isolated product.

To prove the heterogeneity of the Suzuki-Miyaura reaction by α-Fe_2O_3/GO, hot filtration test was conducted. The standard Suzuki-Miyaura reaction between bromobenzene and phenylboronic acid proceeded well in the presence of the catalyst, whereas removal of the catalyst at half way inhibited continuation of the reaction

(Figure 8). Moreover, no residual Pd was found in the α-Fe_2O_3 nanocluster/GO catalysts. Catalyst also can be recovered and reused four times without significantly loss of catalytically active NPs and activities.

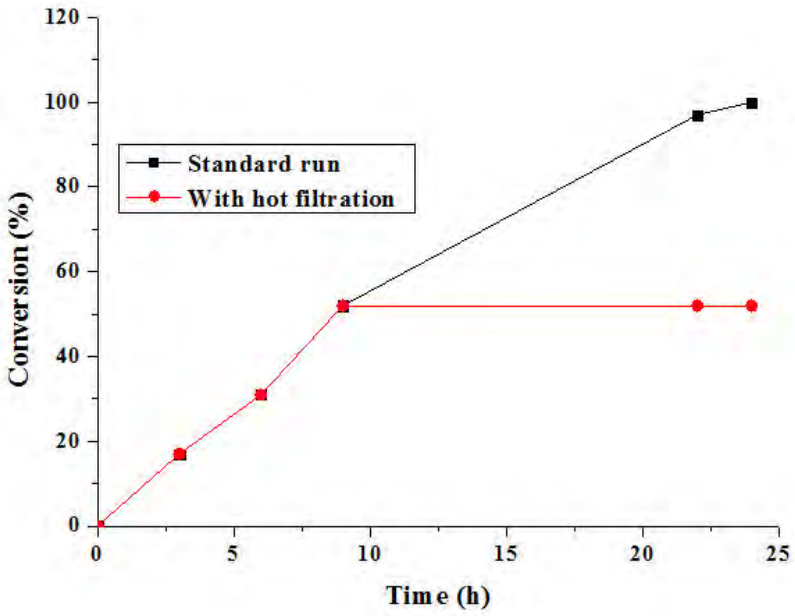

Figure 8. Hot filtration test of the standard Suzuki reaction in the presence of α-Fe_2O_3/graphene oxide catalyst.

In summary, the principles and results presented in this work should significantly contribute developing the ‘‘Green Chemistry” applications involving earth-abundant metal heterogeneous catalysts.

Redox Synthesis and high catalytic efficiency of transition-metal nanoparticle-graphene oxide nanocomposites

Nanocatalysis is a very promising area, because high performance nanoparticles (NPs) may be efficiently designed in the absence of ligands that are often toxic, expensive, sensitive and/or of time-consuming synthesis. A variety of organic and inorganic nanocatalyst stabilizers have also been reported, but they usually damage the catalytic activity and may be difficult to remove. Facing this problem, we report highly efficient ligand-free nanocatalysts synthesis based on the redox reaction between transition-metal cations and GO providing transition metal NP/GO nanocatalysts and their use in water under ambient conditions for a variety of reactions.

We generalized the concept of "redox mediated synthesis" on the GO-supported metal nanocatalysts. This means that GO is used as an electron-reservoir nanomaterial that transfers electrons and eventually oxo ligands to the metals of the NPs. This recalls Basset's strategies using inorganic oxide materials as ligands of early transition metal-based molecular catalysts, although the binding is considerably stronger in the latter case. Both noble metals and biometals using either exergonic or endergonic redox reactions between GO and the transition metal salts have been used in our general approach.

The general procedure for the synthesis of transition-metal nanoparticle-graphene oxide nanocomposites are (taking the synthesis of RhNP/GO as example, Figure 9): 45 mg of graphene oxide was dispersed in 100 mL of water to obtain a yellow colored solution with ultrasonic treatment. Then, 6 mL of this GO solution was taken and injected into a Schlenk flask with continuous stirring at the given temperature in an oil bath. The temperature of the GO solution is controlled by an external thermometer.

When the given temperature was reached, a 1 mL aqueous solution of metal precursors was then added dropwise. The mixture was allowed to further stir for 30 min, and the resulting catalyst was collected by centrifugation and washed with water, and then re-dispersed in water.

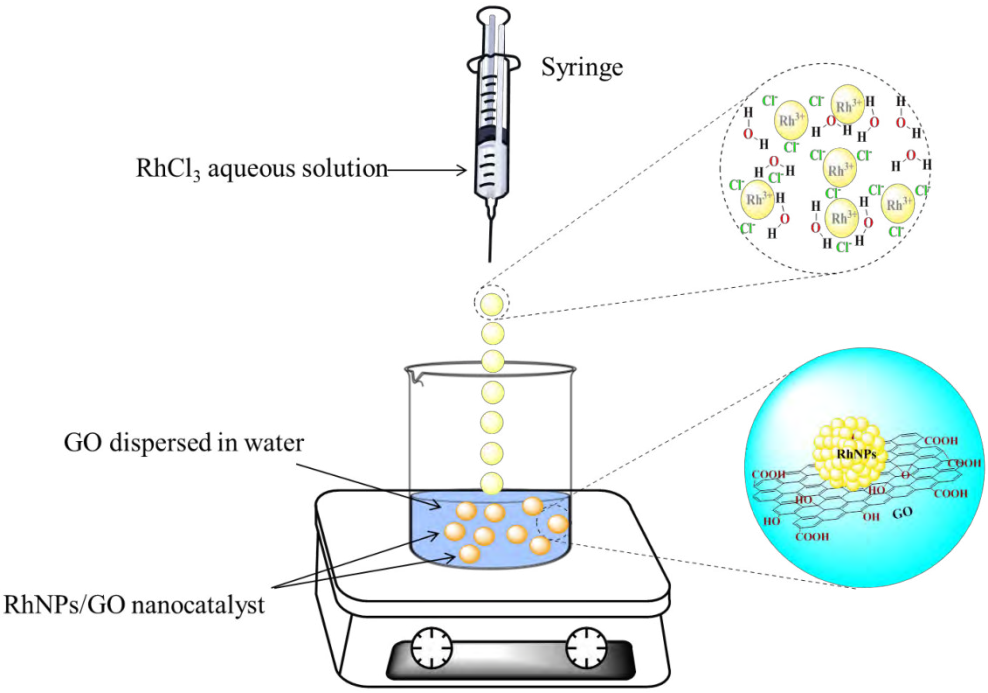

Figure 9. Synthesis of the nanocatalyst RhNPs/GO.

The reducing nature of GO is due to the oxygenated functional groups attached to the hexagonal basal plane, further suggesting that these oxygenated functional groups (e.g. –OH, –COOH, epoxy) on the GO nanosheets play an important role of NPs stabilizing ligands with the lone pairs of the oxygen atoms in the formation of NPs. The ultrafine, surface-clean metal NPs are formed on GO with good monodispersity. These new nanocatalysts are highly efficient in water at ambient temperature. The high efficiencies and recyabilities of the nanocatalysts were exemplified in

4-nitrophenol reduction by RhNP/GO, AuNP/GO and CuNP/GO, Sonogashira coupling by CuNP/GO, PdNP/GO, and PdCuNP/GO, azide-alkyne 1,3-cycloaddition by CuNP/GO, and hydrolysis of ammonia-borane for hydrogen generation by RhNP/GO catalyst (Figure 10).

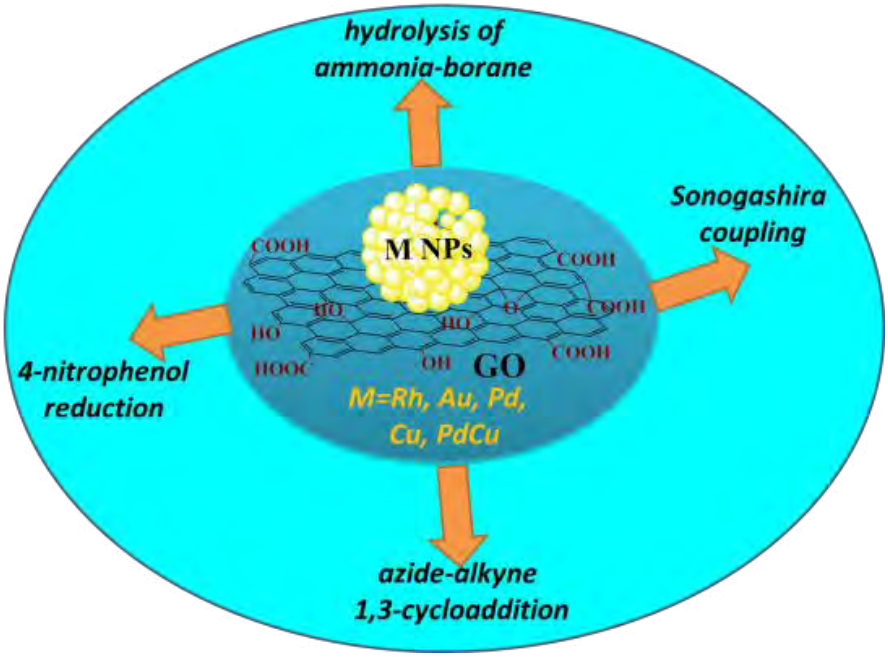

Figure 10. Transition metal NP/GO nanocatalysts in water under ambient conditions show excellent efficiencies for 4-nitrophenol reduction, the hydrolysis of ammonia-borane (AB) for H_2 generation the Sonogashira reaction and the click reaction.

In the case of RhNP/GO catalyzed 4-nitrophenol reduction, the catalytic efficiencies were shown to undergo a volcano-type relationship with respect to RhNP/GO nanocatalysts synthesized at various temperatures. The catalyst RhNP/GO-45℃

showed the highest reaction rate, k_{app} = 11.8×10^{-3} s^{-1}. Remarkably, upon decreasing the total amount of RhNP/GO-45℃ to 1 ppm (RhNPs per 4-NP), high efficiency still remained, with k_{app} = 4.29×10^{-3} s^{-1} that is 1.4 times higher than the reaction rate obtained with 1 ppm of the catalyst RhNP/GO-0℃ under identical conditions (Figure 11). The remarkable efficiencies with exceptional low (ppm) amount of catalyst have so far never been reported and could be attributed to the ultrafine RhNP size and the very active surface-clean RhNPs. The presence of GO also increased the concentration of substrates near the surface Rh atoms, benefiting to the catalytic efficiency.

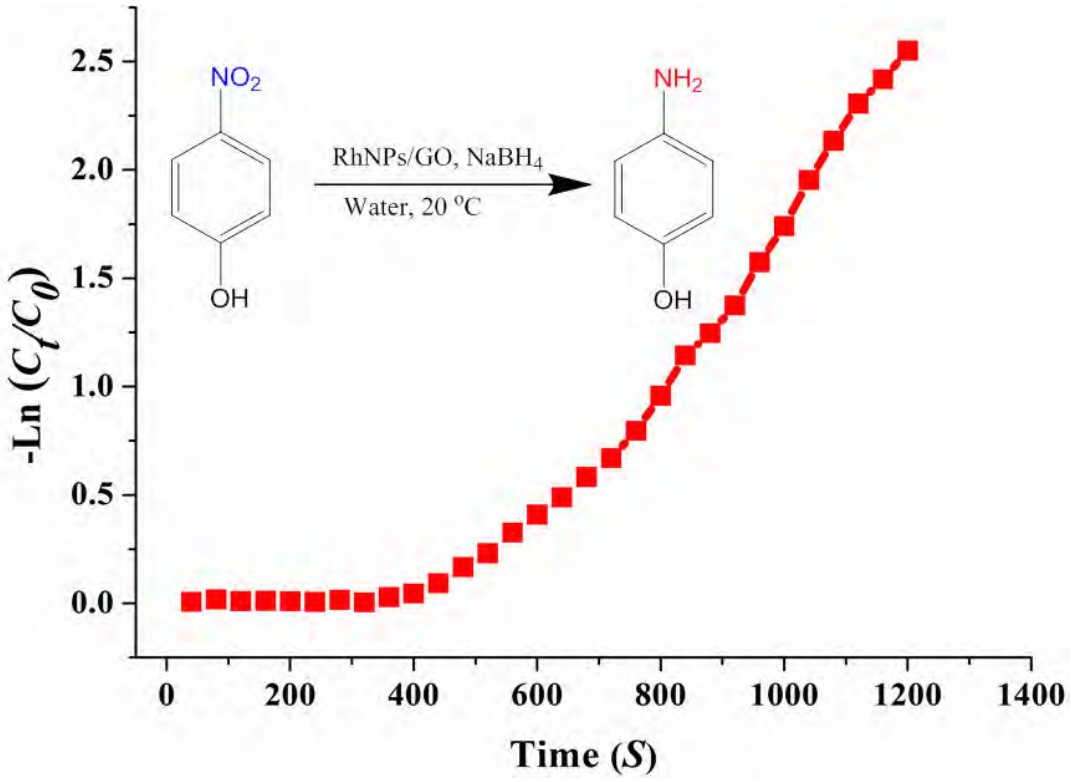

Figure 11. Consumption rate of 4-NP in the presence of 1 ppm of the nanocatalyst RhNP/GO-45℃: -ln(C_t/C_0) *vs.* reaction time.

The efficient RhNP/GO-45℃nanocatalyst was also tested for the hydrolysis of AB for hydrogen generation (Scheme 1). The highest TOF was obtained with the optimum catalytic performance in the presence of 0.1 mol% catalyst for 9.5 min (TOF = 316 mol_{H2} mol $_{cat}^{-1}$ min^{-1}), showing the high efficiency of the present RhNP/GO system for hydrolysis of AB (Table 4).

$$n\ H_3NBH_3 + 2n\ H_2O \xrightarrow[H_2O,\ air,\ r.t.]{Rh/GO\text{-}45\ ^oC} n\ NH_4 + n\ BO_2^- + 3n\ H_2 \quad \textbf{(1)}$$

Table 4. Performances of the catalyst RhNPs/GO-45℃ for the hydrolysis of AB with various catalytic amounts.

Catalyst amount	Maximum H_2/AB ratio	Completion time (min)	TOF (mol_{H2} / $mol_{catalyst}$ · min
0.15 mol%	3	7.75 min	258.1
0.10 mol%	3	9.5 min	315.8
0.05 mol%	3	24 min	250.0
0.02 mol%	3	112 min	133.9

The logarithmic plot of the calculated initial reaction rate *vs*. catalyst concentration has a slope of 1.03 (Figure 12a), indicating that the hydrolysis of AB catalyzed by RhNP/GO-45℃ follows a first-order kinetics with respect to catalyst concentration.

The nearly horizontal line (slope of 0.042) indicates that the hydrolysis of AB catalyzed by RhNP/GO-45℃ is zero-order with respect to the AB concentration (Figure 12b). Furthermore, the activation energy (E_a) of hydrolysis of AB was determined to be approximately 21.4 kJ/mol (Figure 12c).

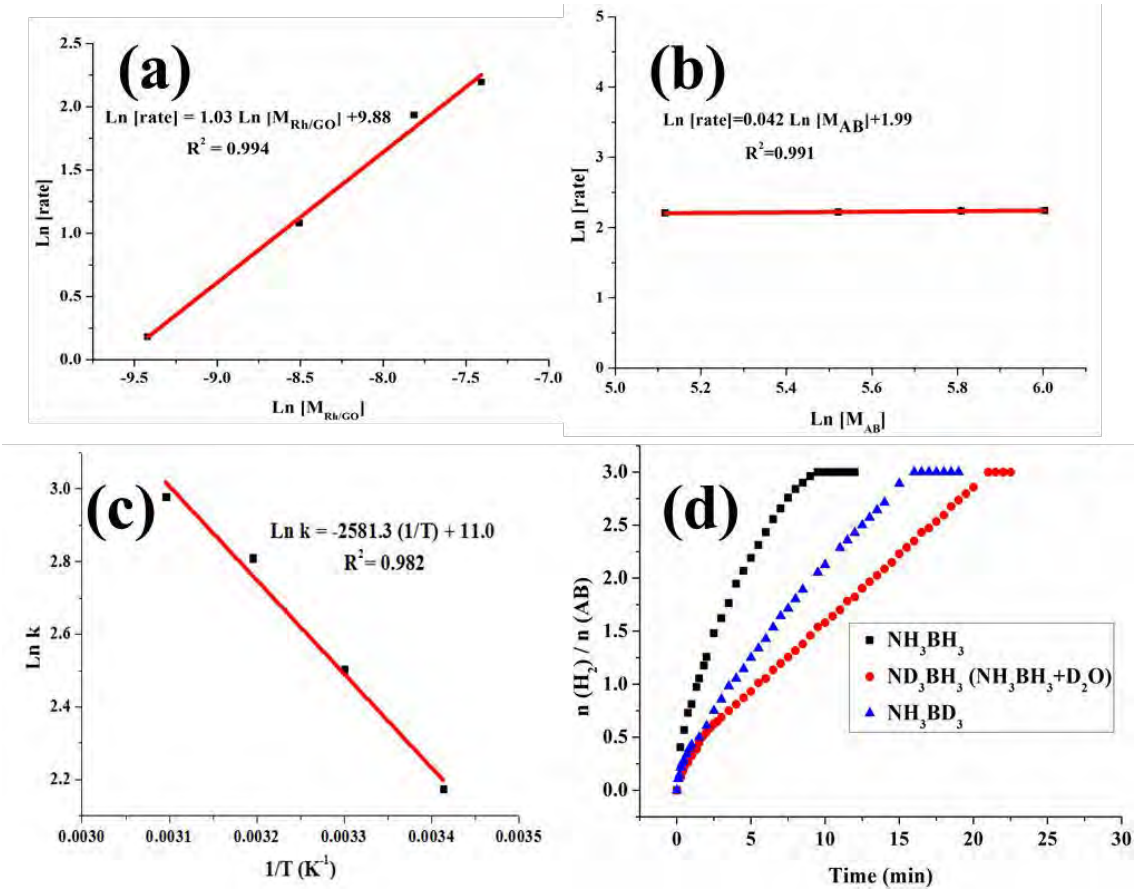

Figure 12. (a) The plot of hydrogen generation rate *vs.* the concentration of RhNPs/GO-45℃ both in natural logarithmic scale; (b) The plot of hydrogen generation rate *vs.* the concentration of AB both in natural logarithmic scale; (c) Arrhenius plots obtained from the kinetic data; (d) Hydrogen evolution from NH_3BH_3, ND_3BH_3, and NH_3BD_3 catalyzed by 0.1 mol% RhNP/GO-45℃.

The detailed mechanism was explored by especially the kinetic isotope effects (KIEs) (Figure 12d). Thus, in this reaction, H_2O is most likely activated by an indirect O–H bond cleavage to form –H and –OH species promoted by AB in the presence of RhNP/GO-45 ℃. Activation proceeds similarly in H_2O activation for $NaBH_4$ hydrolysis. We also suggest that the "hydridic" B-H hydrogen atom of AB forms a hydrogen bond with an "acidic" hydrogen atom of water in the ground state and that this B-Hδ^-…Hδ^+-O system undergoes oxidative addition followed by H_2 elimination on the Rh surface. The B–N bond in the AB is dissociated, since the NH_3 group does not participate in the hydrolysis (Figure 13). On the other hand, the presence of GO facilitates the adsorption of the reactant or desorption of products in water, thus accelerating the overall process and improving the catalytic activity.

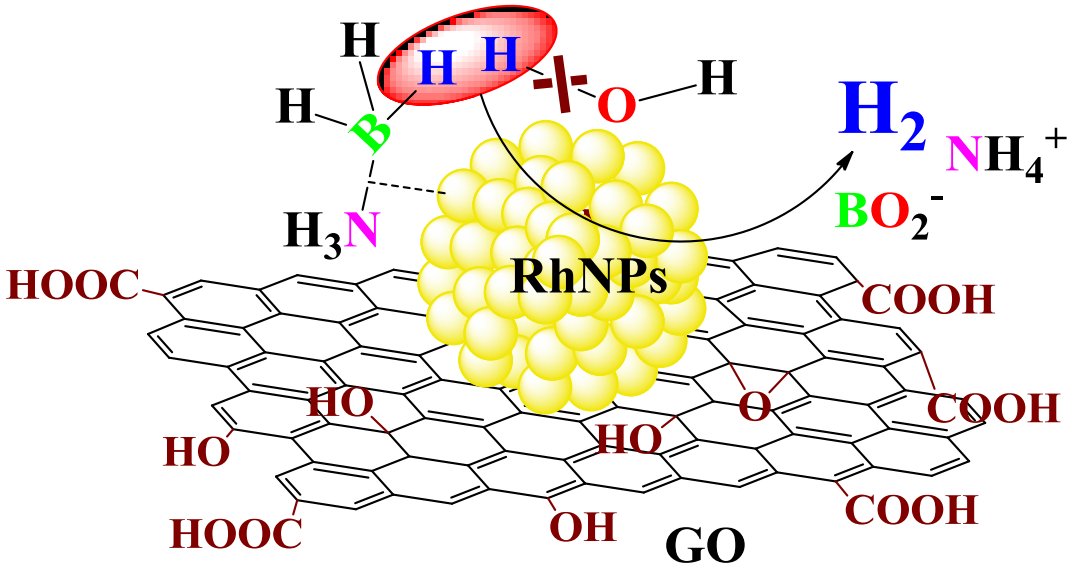

Figure 13. Proposed mechanism for the hydrolysis of AB by catalyzed by RhNP/GO-45℃.

The reusability of the catalyst was also studied, which was successfully recycled four times (Figure 14). The observed little decrease of activity in the fourth run is probably ascribed to the aggregation of RhNPs as shown by TEM image taken after recycling experiments. It is due to the deactivation effect of the hydrolysis product metaborate[6-8] that accumulates during the hydrolysis and inhibits the catalytically active Rh surface atoms, and to the diluted reactant in water.

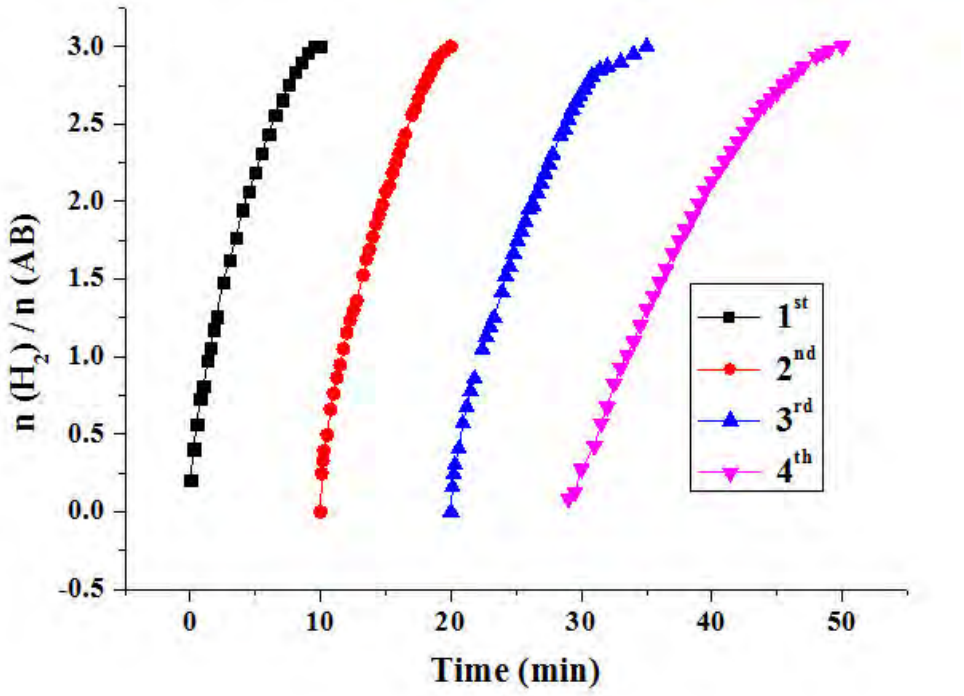

Figure 14. Time plots of the catalytic dehydrogenation of AB by the nanocatalyst RhNPs/GO-45℃ for the reusability test.

The general principle of transition-metal-GO nanocatalysts is extended to the synthesis of AuNPs/GO, PdNPs/GO, CuNPs/GO, and CuPd NPs/GO at 45℃ under identical conditions. In the case of AuNPs/GO, reduction of Au^{3+} by GO (Au^{3+}/Au^{0} =

1.5 V *v.s* SHE) results in the high efficient AuNPs/GO nanocatalyst with AuNPs of 3.3 nm , as exemplified by the 0.05 mol% AuNPs/GO nanocatalyst catalyzed 4-NP reduction in water without induction time and remarkable efficiency (k_{app} = 3.7×10^{-3} s^{-1}, Figure 13).

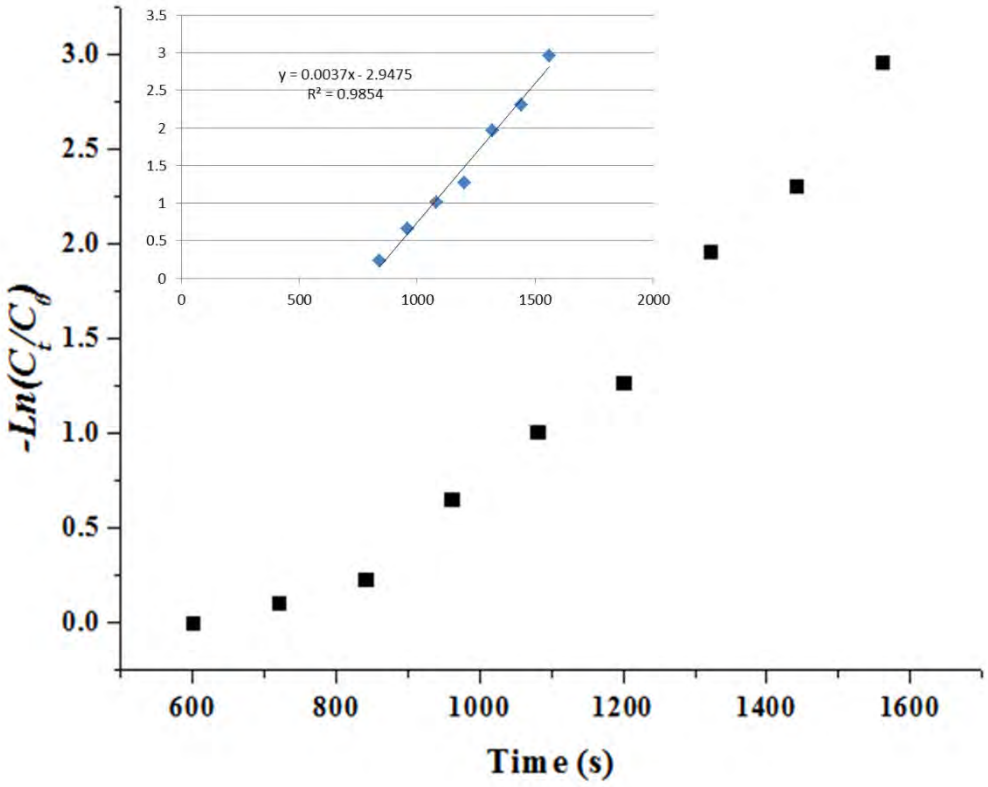

Figure 13. 4-NP reduction catalyzed by 0.05mol% AuNPs/GO nnaocatalyst: Consumption rate of 4-NP: -ln(C_t/C_0) *vs.* reaction time.

More challenging, the synthesis of first raw metal NPs by reduction the metal precursors with GO was also proved successful. 4-NP reduction is successfully achieved using 0.5% mol CuNPs/GO catalyst with no induction time and a high efficiency of 5.2×10^{-3} s^{-1} (k_{app}). The absence of induction time in the 4-NP reduction

suggests that activation and dynamic restructuring of the Cu(0) surface is not necessary due to the absence of molecular ligand. The high efficiency of the CuNPs/GO nanocatalyst was also confirmed by the "click" reaction between benzyl azide and phenylacetylene (Scheme 2, Figure 14). The procedures for the azide-alkyne cycloaddition reactions are: A glass vessel equipped with a magnetic stir bar was charged with 0.1 mmol of benzyl azide and 0.105 mmol of phenylacetylene under Ar. The catalyst was added into the vessel under Ar, and water was added in order to obtain a given volume of aqueous solution (1 mL). The reaction mixture was then stirred for 24 h at 35 °C under Ar. After the reaction, 5 mL water was added and the final product was extracted from water with CH_2Cl_2 (3 × 5 mL). The organic layer was dried over Na_2SO_4 and filtered, and the solvent was removed *in vacuo* to give the 1-benzyl-4-phenyl-1H-[1,2,3]triazole.

When using only 0.01 mol% of CuNPs for the "click" reaction between benzyl azide and phenylacetylene, 93% isolated yield was achieved at 35 ℃ for 24 h; this is one of the lowest catalyst amounts among recent literature values. XPS suggested that the active Cu^{I} species is formed in the native oxide layer on the Cu surface through comproportionation of Cu^{0} and Cu^{II} (Figure 15).

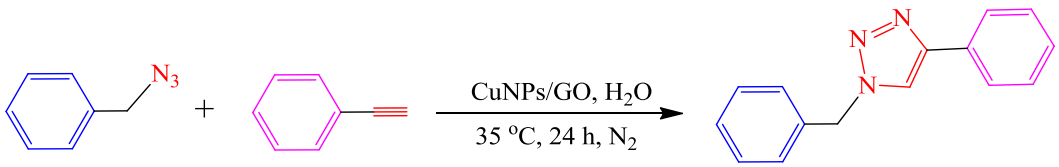

(2)

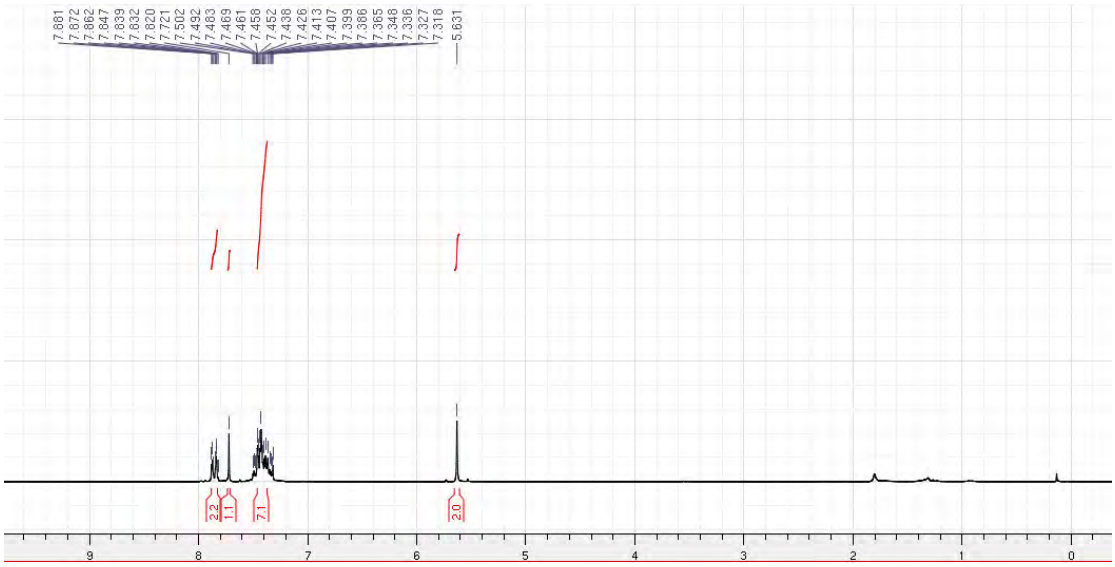

Figure 15. ^{1}H NMR spectrum of 1-benzyl-4-phenyl-1H-[1,2,3]triazole.

^{1}H NMR (300 MHz, $CDCl_3$) δ_{ppm}: 7.84-7.79 (m, 2H), 7.67 (s, 1H), 7.41-7.67 (m, 7H), 5.59 (s, 2H).

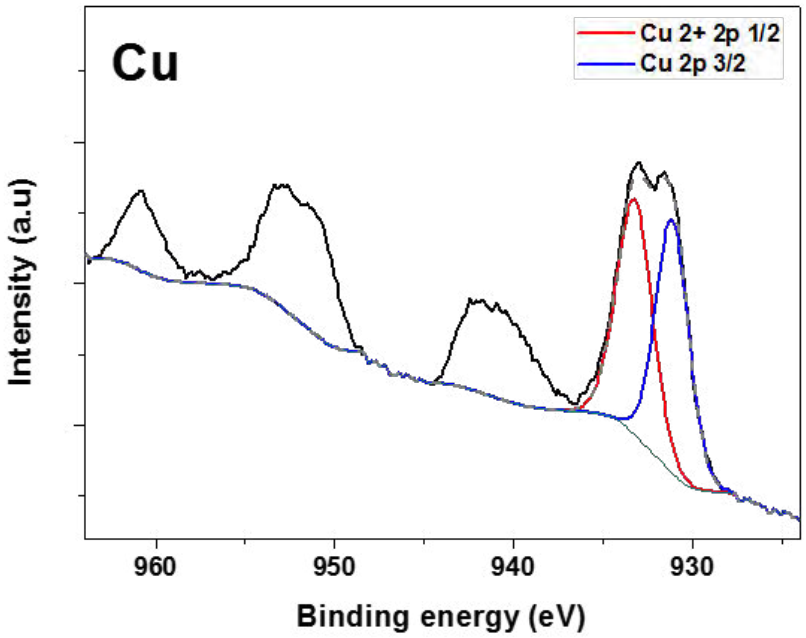

Figure 14. X-ray photoelectron spectroscopy of Cu 2p. In sample Cu/GO both species are almost in the same proportion (51.9% Cu^{2+} and 48.1% in Cu^{0}).

Moreover, double reduction of equimolar amount of Pd^{2+} and Cu^{2+} by GO result in a valuable heterogeneous CuPd NPs/GO nanocatalyst for Sonogashira coupling reaction in water at room temperature. Procedures for the Sonogashira reaction are: A dry Schlenk flask equipped with a magnetic stir bar was charged with alkyne (0.6 mmol), iodobenzene (0.5 mmol), and triethylamine (1.5 mmol) under Ar. Catalyst (0.05 mol%) was then added under Ar, and water was then added in order to obtain a given volume of aqueous solution (2 mL). The mixture was allowed to stir for 24 h at room temperature. After the reaction, 3 mL water was added and the aqueous phase was extracted three times with 5 mL Et_2O. The organic phase was dried over Na_2SO_4, and the solvent was removed in vacuo. In parallel, the reaction was checked using TLC with petroleum ether as the eluent and ^1H NMR spectroscopy. Purification by flash chromatography was conducted with silica gel as the stationary phase and petroleum ether as the mobile phase.

Synergistic CuPd NPs/GO nanocatalyst is an excellent catalyst for Sonogashira coupling in water at rt, i.e. under environmentally-friendly conditions, showing remarkably quantitative conversion with 93% isolated yield in this Sonogashira coupling reaction (Scheme 3 and Figure 15). This work shows a promising way to the rational design of efficient nanocatalysts for a large variety of chemical reactions.

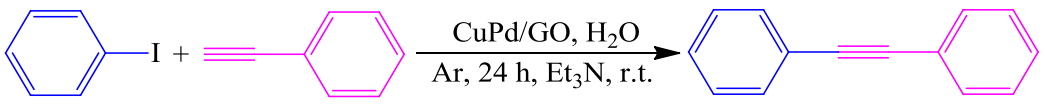

(3)

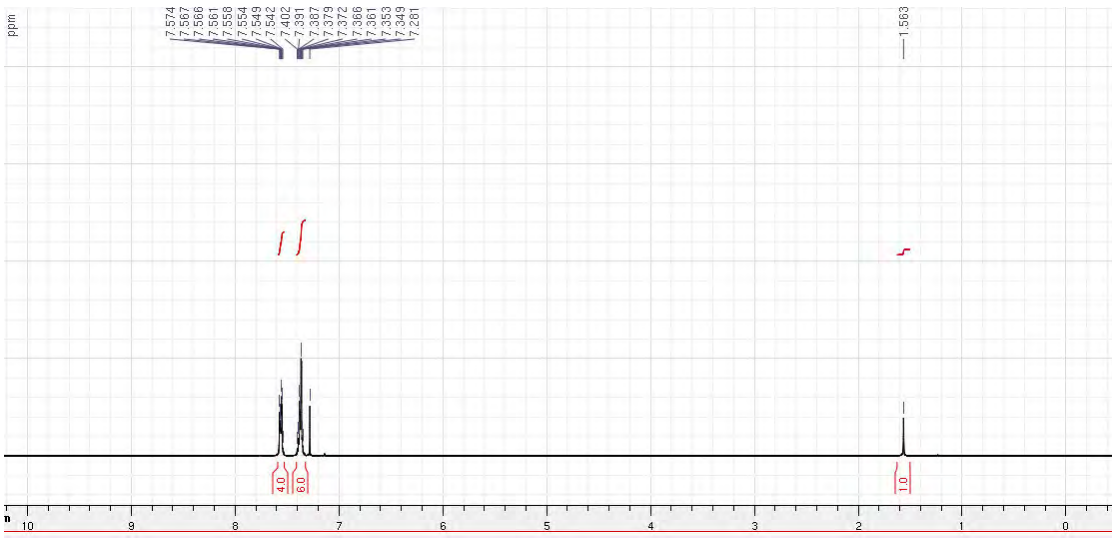

Figure 15. ^{1}H NMR spectrum of diphenylacetylene ($CDCl_3$ 400 MHz) δ_{ppm}: 7.34-7.40 (m, 6H), 7.54-7.57 (m, 4H).

Thus in this study, we presented that a simple redox reaction between various transition metal cations and GO has been shown here to lead to the synthesis of ultrafine, surface-clean metal NPs on GO with good monodispersity. The appropriate choice of temperature during the synthesis improved the reduction efficiency and enhanced the interaction between the RhNPs and GO. Consequently, the nanocatalysts showed exceptional efficiency in the 4-NP reduction, hydrolysis of AB to produce H_2, Sonogashira coupling at room temperature, "click" reaction and hydrolysis of AB for hydrogen production with low amounts of catalytic metals. The principles and catalytic method presented herein could be extended to other transition-metal nanocatalysts and should contribute to the rational design of efficient nanocatalysts for a large variety of chemical reactions.

Chapter 4

Metal Organic Frameworks Stabilize Efficient Non-noble Metal Nanoparticles Catalysis

Introduction

Metal organic frameworks (MOFs) are emerging and outstanding porous nanomaterials, that advantageous compare with other conventional inorganic supports.[1] Catalytically active transition-metal nanoparticles (MNPs) are confined in and stabilized by MOFs within their frameworks to control the nucleation and growth of nanoparticles, which prevents the aggregation of MNPs and prolongs their stabilities.[2] Moreover, the high specific MOF surface areas and tunable pore sizes ensure the good dispersion of MNPs. This allows exposing active sites and facilitate the accessibility of substrates to the active NPs surface by reducing diffusion resistance. On the other hand, the direct use of nanoconfinement effect by MOFs provides a facile method to prepare ligand-free and ultrafine NPs/MOFs nanocatalysts, which is significant but also crucial for the design of highly efficient heterogeneous catalysts.

This chapter highlights the synthesis, characterization and catalytic function of the highly dispersed ligand-free biometal NPs /zeolitic imidazolate framework (ZIF-8; $[Zn(MeIM)_2]_n$) nanocatalysts, especially with effort to further improve the catalytic activity of nanocatalyts by understandings the mechanistic aspects of the hydrolysis reaction. We show the high efficiency of highly dispersed ligand-free Ni NPs/ZIF-8 nanocatalyst inspired from the mechanistic studies in the hydrolysis of AB in water. We also discover the ion effect in this reaction allowing a remarkable improvement of the catalytic performance and controlled release of hydrogen.

References

[1] a) J. Y. Lee, O. K. Farha, J. Roberts, K. A. Scheidt, S. T. Nguyen, J. T. Hupp, *Chem. Soc. Rev.,* **2009**, *38*, 1450-1459; b) J. Liu, L. Chen, H. Cui, J. Zhang, L. Zhang, C. –Y. Su, *Chem. Soc. Rev.,* **2014***, 43,* 6011-6061; c) A. H. Chughtai, N. Ahmad, H. A. Younus, A. Laypkov, F. Verpoort, *Chem. Soc. Rev.,* **2015**, *44*, 6804-6849.

[2] a) A. Dhakshinamoorthy, H. Garcia, *Chem. Soc. Rev.,* **2012**, *41*, 5262-5284; b) G. Lu, S. Li, Z. Guo, O. K. Farha, B. G. Hauser, X. Qi, Y. Wang, X. Wang, S. Han, X.

Liu, J. S. DuChene, H. Zhang, Q. Zhang, X. Chen, J. Ma, S. C. J. Loo, W. D. Wei, Y. Yang, J. T. Hupp, F. Huo, *Nat. Chem.,* **2012**, *4*, 310–316; c) K. M. Choi, K. Na, G. A. Somorjai, O. M. Yaghi, *J. Am. Chem. Soc*. **2015**, *137*, 7810-7816; d) K. Na, M. Choi, O. M. Yaghi, G. A. Somorjai, *Nano Lett.* **2014**, *14*, 5979-5983; e) B. Rungtaweevoranit, J. Baek, J. R. Araujo, B. S. Archanjo, K. M. Choi, O. M. Yaghi, G. A. Somorjai, *Nano Lett.*, **2016**, *16*, 7645–7649; f) H.-L. Jiang, B. Liu, T. Akita, M. Haruta, H. Sakurai, Q. Xu, *J. Am. Chem. Soc.*, **2009**, *131*, 11302–11303; g) A. Aijaz, A. Karkamkar, Y. J. Choi, N. Tsumori, E. Rönnebro, T. Autrey, H. Shioyama, Q. Xu, *J. Am. Chem. Soc.*, **2012**, *134*, 13926–13929; h) B. An, J. Zhang, K. Cheng, P. Ji, C. Wang, W. Lin, *J. Am. Chem. Soc.*, **2017**, *139*, 3834–3840.

Hydrolysis of ammonia-borane over Ni/ZIF-8 nanocatalyst: high efficiency, mechanism and controlled hydrogen release

*Changlong Wang,[§,‖] Jimena Tuninetti,[♯] Zhao Wang,[♩] Chen Zhang,[§] Roberto Ciganda,[‖] Lionel Salmon,[§] Sergio Moya,[♯] Jaime Ruiz,[‖] Didier Astruc[‖,]**

[§] *Laboratoire de Chimie de Coordination, UPR CNRS 8241, 31077 Toulouse Cedex, France*

[‖] *ISM, UMR CNRS N° 5255, Univ. Bordeaux, 33405 Talence Cedex, France*

[♯] *CIC biomaGUNE, Unidad Biosuperficies, Paseo Miramon No 182, Edif "C", 20009 Donostia-San Sebastian, Spain*

[♩] *Sorbonne Universités, UPMC Univ Paris 06, UMR CNRS 7197, Laboratoire de Réactivité de Surface, 4 Place Jussieu, Tour 43-33, 3ème étage, Case 178, F-75252 Paris, France*

Abstract

Non-noble metal nanoparticles are notoriously difficult to prepare and stabilize with appropriate dispersion, which in turn severely limits their catalytic functions. Here using zeolitic imidazolate framework (ZIF-8) as MOF template, catalytically remarkably efficient ligand-free first-row late transition-metal nanoparticles are prepared and compared. Upon scrutiny of the catalytic principles in the hydrolysis of

ammonia-borane, the highest total turnover frequency among these first-row late transition metals is achieved for the templated Ni nanoparticles with 85.7 $mol_{H2} \cdot mol_{cat}^{-1} \cdot min^{-1}$ at room temperature, which overtakes performances of previous non-noble metal nanoparticles systems, and is even better than some noble metal nanoparticles systems. Mechanistic studies especially using kinetic isotope effects show that cleavage by oxidative addition of an O–H bond in H_2O is the rate determining steps in this reaction. Inspired by these mechanistic studies, an attractive and effective "on-off" control of hydrogen production is further proposed.

Introduction

Catalytic hydrogen generation from hydrogen storage materials is considered as a convenient, inexpensive, and effective approach to address the energy and environmental concern.[1-4] Among various chemical hydrogen storage materials, ammonia-borane (AB) has a high hydrogen content (19.6 wt%), high stability in the solid state and solution under ambient conditions, nontoxicity, and high solubility. Therefore it is considered as one of the most leading contender in promising chemical hydrogen-storage materials for various applications.[5-15]

Until now, effective catalysts for hydrolysis of AB are typically based on expensive and rare noble metal nanocatalysts (e.g., Rh, Pt, Ru). Considerable efforts have been devoted to the design of high-performance noble metal-free nanocatalysts,[16-25] On the other hand, the hydrolysis of AB under mild conditions by cheap and earth-abundant

first row metal nanoparticles (Fe, Co, Ni and Cu, "BM") with practical efficiency and sustainability remains extremely challenging, largely due to their labile nature, complex mechanistic manifolds and low catalytic efficiencies.[26]

Supported nanoparticle (NP) catalysts have shown remarkable catalytic efficiencies. It has also been found, however, that the activities were significantly influenced or/and eventually determined by the NP supports.[27-37] In this regard, metal organic frameworks (MOFs) are outstanding emerging porous nanomaterials that are advantageous compared to other conventional inorganic supports.[38-43] MOFs allow confining and stabilizing catalytically active metal NPs within their frameworks, which controls the nucleation and growth of NPs, thus preventing their aggregation and prolonging their stabilities.[44-51] Moreover, the high specific surface areas and tunable pore sizes ensured good NP dispersion, which allows exposing active sites and facilitates the accessibility of substrates to the active NP surface by reducing diffusion resistance.[44-51] On the other hand, the direct use of nanoconfinement effect by MOFs provides a facile method to prepare ligand-free and ultrafine NP/MOF nanocatalysts, which is significant but also crucial for the design of highly efficient heterogeneous catalysts. However, the comparison of the catalytic efficiencies of BMNPs using the same MOF template have not yet been disclosed.

In addition to the rational design of new nanocatalysts, insights to the mechanistic aspects of the hydrolysis reaction would be essential for the enhancement of the catalytic efficiencies of the BMNPs/MOFs nanocatalysts. The details of the reaction process of AB hydrolysis over BMNPs/MOFs nanocatalysts again have rarely been

experimentally examined, however. In order to address these challenging issues, we now report the synthesis, characterization and catalytic functions of the BMNPs/zeolitic imidazolate framework (ZIF-8; $[Zn(MeIM)_2]_n$) nanocatalysts, especially with efforts to further improve the catalytic activity by understanding the mechanistic aspects of the hydrolysis reaction. First, the supporting nanomaterial of ZIF-8 is synthesized and characterized. Then we highlight the efficiency of Ni NPs/ZIF-8 nanocatalyst by comparing the catalytic activities of first-row late transition-metals NPs/ZIF-8 catalysts in the hydrolysis of AB in water under mild conditions. Subsequently we scrutinize the catalytic behavior of Ni NPs/ZIF-8 nanocatalysts for the hydrolysis of AB in water, the mechanistic aspects of this reaction using kinetic isotope effects (KIEs), and an anion effect for the control of hydrogen release. The catalytic activity of the nanocatalyst Ni NPs/ZIF-8 surpassed all the non-noble metal NP systems for the hydrolysis of AB.

Result and discussion

Synthesis and characterizations of the nanocatalysts: The ZIF-8 nanoparticles[52] are first rapidly synthesized in water using a modified method (SI).[53] Transmission electron microscope (TEM) image indicates that the ZIF-8 NPs are nanocrystals with sharp hexagonal facets, and the average size of ZIF-8 NPs is around 75 nm (Figure S1). Powder X-ray diffraction (PXRD) proves the pure phase of ZIF-8 nanomaterial (Figure S2). ZIF-8 NPs show a type I isotherm in the N_2 adsorption measurement. The

presence of micropores results in volume increase adsorbed at very low relative pressures, whereas a second uptake at a high relative pressure indicates the existence of textural meso/macroporosity formed by the packing of NPs (Figure S3). The Brunauer-Emmett-Teller (BET) surface area of ZIF-8 NPs is 1663.3 $m^2 g^{-1}$. Refluxing the ZIF-8 NPs in either methanol or water during one day does not change the framework structure, as evidenced from the unchanged PXRD patterns (Figure S2), showing the thermal and chemical stabilities of ZIF-8 NPs.[52,53]

The nanocatalysts BMNPs/ZIF-8 are prepared using the deposition-precipitation (DP) method with fast reduction by $NaBH_4$, then collected by centrifugation followed by washing and drying *in vacuo* (Scheme 1 and SI). These nanomaterials are clearly distinguished by their colors (compare the photographs in Figure S4); for instance Ni NPs/ZIF-8 appears grey, whereas Cu NPs/ZIF-8 is completely black. No diffractions are detected for Ni NP species from PXRD patterns after reduction in Ni NPs/ZIF-8 compared to ZIF-8 NPs, which indicates that Ni loadings are too low or Ni NPs are too small.[49,54] The metal loading is determined by inductively coupled plasma-optical emission spectroscopy (ICP-AES); for instance the Ni loading in Ni NPs/ZIF-8 is 2.2 wt%. The metal oxidation state is then identified by X-Ray photoelectron spectroscopy (XPS). Binding energies (B.E.) of 1021.4 and 1044.5 eV are observed for the $2p_{3/2}$ and $2p_{1/2}$ levels of the Zn^{2+} ion in the ZIF-8 framework, respectively (Figure S5). Moreover the well-defined peaks with B.E. of 852.2 and 870.1 eV are detected for the $2p_{3/2}$ and $2p_{1/2}$ levels (Figure S6), respectively, of metallic Ni^0 in the Ni NPs.[17,21]

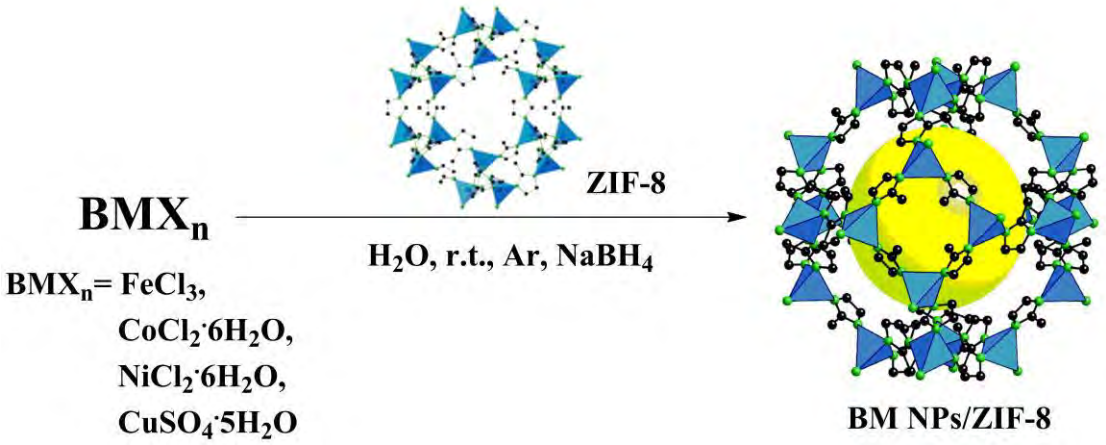

Scheme 1. Preparations of the nanocatalysts BMNP/ZIF-8.

Interestingly, after the deposition of the BMNPs, the nanocatalysts BMNPs/ZIF-8 become more spherical, as exemplified by NiNPs/ZIF-8 (Figures 1a and 1b). The measurements of the NP size by TEM encounters problems, however, probably due to their small sizes and lack of contrast over ZIF-8 framework. In order to release the BMNPs from the nanocatalysts BMNPs/ZIF-8 for direct TEM characterization, the ZIF-8 framework was then digested using a solution of ethylenediaminetetraacetic acid (EDTA)[55] in the presence of poly(vinylpyrrolidone) (PVP, Mw = 10,000) to stabilize the ultrasmall NPs. In this way the sizes of the BMNPs are successfully measured by TEM (Table 1). The size of the released NiNPs is 2.7 nm, and other size distributions of FeNPs, CoNPs, and CuNPs are shown in Table 1 and in the SI (Figures S7-S10). On the other hand, nitrogen sorption experiments of the nanocatalysts show type I shape and considerable decrease of pore volume and BET surface areas (Table 1 and Figure S3). This indicates blocking of the windows of the ZIF-8 framework cavities by highly dispersed NPs within the locally distorted

environment or/and the location of NPs at the surface; the latter was also shown by TEM in Figure 1b, for instance for NiNPs/ZIF-8.

Table 1. Physical properties and catalytic efficiencies of the nanocatalysts.

Sample	Size[a] (nm)	BET surface area ($m^2\ g^{-1}$)	Pore volume ($cm^3\ g^{-1}$)	TOF[b] ($mol_{H2} \cdot mol_{cat}^{-1} \cdot min^{-1}$)
ZIF-8	75±3	1663.3	0.6614	--
FeNPs/ZIF-8	3.0±0.4	1313.3	0.4491	2.5
CoNPs/ZIF-8	2.9±0.3	1313.8	0.4539	19.4
NiNPs/ZIF-8	2.7±0.3	1324.3	0.4255	35.3/85.7[c]
CuNPs/ZIF-8	3.2±0.4	1367.3	0.4110	5.6

[a] TEM size. [b] Hydrolysis of AB in water at room temperature (25 ± 0.5°C), TOF = mol_{H2} released / ($mol_{catalyst}$ × reaction $time_{(min)}$). [c] TOF is obtained in the presence of 0.3M NaOH.

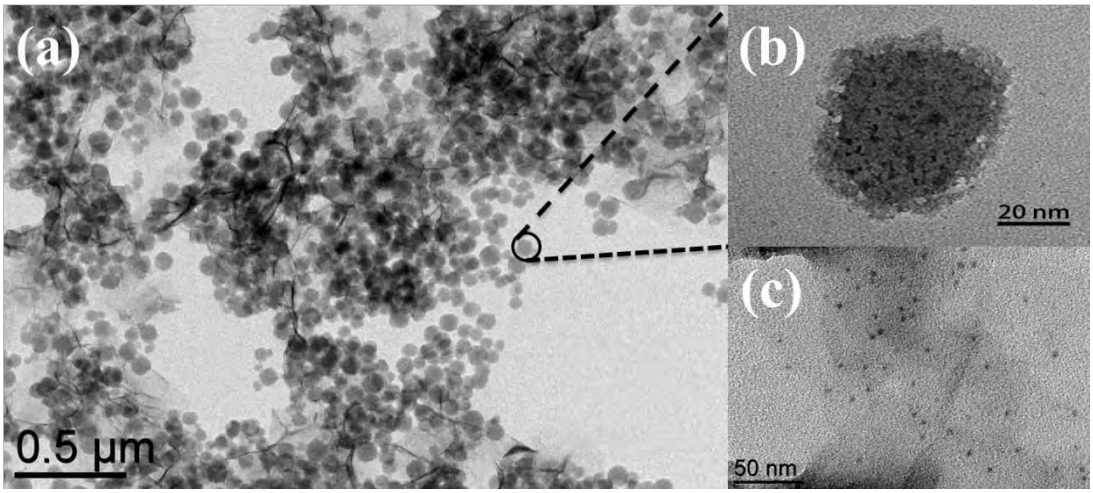

Figure 1. TEM images of NiNPs/ZIF-8: (a) at 500 nm scale. (b) at 20 nm scale. (c) NiNPs in NiNPs/ZIF-8 after digestion using EDTA and capping with PVP.

High efficiency of NiNPs/ZIF-8 in the hydrolysis of AB and mechanistic studies. The catalytic performances of the BMNPs/ZIF-8 are evaluated for the hydrolysis of AB reaction in water. Hydrolysis of AB starts in water by employing 3 mol% of the various late transition metal nanocatalysts BMNPs/ZIF-8 (measured by ICP-AES). The reaction profile in the presence of the nanocatalysts BMNPs/ZIF-8 is shown in Figure S11. The volumes of gas collected represent nearly 3 equiv. H_2 per AB with no detectable NH_3 (SI),[56] indicating that hydrolysis of AB catalyzed by the nanocatalyst BMNPs/ZIF-8 proceeds according to Equation (1):

$$H_3NBH_3 + 2\,H_2O \xrightarrow[\text{r.t., } H_2O]{\text{BMNPs/ZIF-8 nanocatalysts}} NH_4^+ + BO_2^- + 3\,H_2 \qquad (1)$$

This comparison demonstrates the best activity of NiNPs/ZIF-8 in terms of turn over

frequency (TOF) among the four nanocatalysts BMNPs/ZIF-8 (Table 1 and Figure S11). Therefore the catalytic system NiNPs/ZIF-8 was chosen for further studies.

Figure S12 shows the logarithmic plot of the hydrogen generation rate *vs*. concentration of NiNPs/ZIF-8; the slope is 0.98, indicating that the hydrolysis of AB catalyzed by NiNPs/ZIF-8 is first-order with respect to the catalyst concentration. On the other hand hydrolysis of AB catalyzed by NiNPs/ZIF-8 is zero-order with respect to the AB concentration, as a nearly horizontal line (slope of 0.086) is observed (Figure S13). This implies that under the present reaction conditions, AB is easily activated, and thus the possibility of the activation of AB in the rate-determining step (RDS) is ruled out. This also is in accordance with the KIE results (*vide infra*). The activation energy (E_a) of AB hydrolysis, determined by measuring the time dependence of H_2 generation at various temperatures, is approximately 42.7 kJ/mol (Figure S14 and calculation). This value also is lower than those found for several known noble metal-based nanocatalysts (Table S1).

Although the catalytic rates in the hydrolysis of AB catalyzed by NiNPs/ZIF-8 is independent of the AB concentration, the KIE[57-59] was further investigated in order to shed light on the RDS of hydrolysis of AB catalyzed by NiNPs/ZIF-8. Indeed in this reaction the KIE value should tell if N−H or B−H or both bonds are broken during the RDS.[16,60-63]

The hydrolysis of the deuterated products of AB (for their synthesis, see S.I.) in the presence of NiNPs/ZIF-8 shows slower reaction rates (Figure S17). A KIE of 1.33 is determined for deuteration at the boron site (NH_3BD_3), indicating a similar

dehydrogenation behavior to that of AB in H_2O. This indicates that the absence of large KIE for hydrolysis of AB deuterated at the boron site (NH_3BD_3). On the other hand, the KIE value of 2.49 is calculated according to the H_2 generation rates in ND_3BH_3 (NH_3BH_3–D_2O system), suggesting that the O–H bond cleavage of H_2O might be in the RDS. This would be similar to the metal-catalyzed borohydride hydrolysis, in which half of the hydrogen comes from water.[64] Previously, it has been suggested that the water activation by means of oxidative addition of a O-H bond on noble metal NP surfaces easily occurs, forming adsorbed –OH and –H species. For instance Pt NPs have been known as the redox catalyst for water photo-splitting.[65,66] That Ni is the best metal found here for the hydrolysis reaction among those four first-row late transition metals is in accord with oxidative addition of water as the RDS, because Ni(0) is known by far the best first-row metal catalyst of reactions involving oxidative addition.[67] In addition the involvement of water activation in the RDS may be partially explained by the higher O-H bond energy (～493 kJ mol^{-1})[68] than that of B–N and B–H bond (～117 and ～430 kJ mol^{-1}, respectively).[69] Thus it is mostly likely that the water molecule is activated by an indirect O–H bond cleavage to form –H and –OH species promoted by AB in the presence of the nanocatalyst NiNPs/ZIF-8. Since the NH_3 group does not participate in the hydrolysis, the B–N bond dissociates in AB, followed by H_2 release (Figure 2).

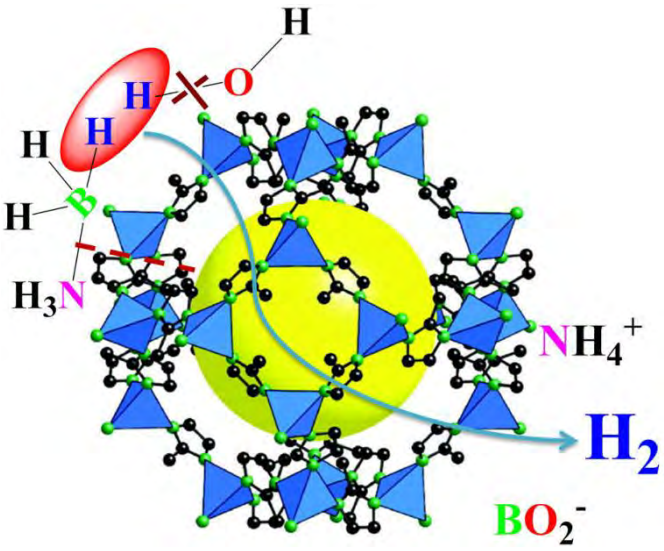

Figure 2. Proposed mechanism for the hydrolysis of AB catalyzed by NiNPs/ZIF-8.

Remarkable improvement of the catalytic performance by ion effect allowing the controlled release of hydrogen. From the mechanistic studies, it can be assumed that if OH^- is directly adsorbed on the surface of the Ni nanocatalyst, a bifunctional catalyst with both H and OH adsorptions should be highly expected to provoke the surface reaction. Thus the presence of surface OH^- should be of great value for the enhancement of the catalytic activity. To verify this hypothesis, various concentrations of NaOH (0.1-0.4 M), a conventional OH^- provider in aqueous solution, were separately added to the reaction media that only contained NiNPs/ZIF-8. After stirring for 30 min, the aqueous solution of AB was added, and the catalytic activities were examined. Surprisingly, as shown in Figure S18, the H_2 generation rates greatly improved as compared to the one in the absence of NaOH. The H_2 generation rates first increased with the increased NaOH concentrations (0.1-0.3 M), then decreased with higher NaOH concentration (0.4 M). It is suggested that the accumulation of too

much OH^- beyond the optimum level (0.3 M) could significantly reduce the beneficial effect, resulting in the decrease of the H_2 generation rate. The highest reaction rate in term of TOF is 85.7 $mol_{H2}\cdot mol_{cat\text{-}1}\cdot\ min^{-1}$ with 0.3 M NaOH, showing the best activity among all the non-noble metal NP systems. This is even more efficient than noble metal NPs systems (Table S1); for instance the utilization of commercial 40 wt % Pt/C catalyst only had a TOF of 55.56 $mol_{H2}\cdot molcat^{-1}\cdot\ min^{-1}$. Control experiment shows that the addition of NaOH has no effect on AB in aqueous solution in the absence of catalyst, as no H_2 release is observed, as also confirmed by the ^1H and ^{11}B NMR spectra.[70] On the other hand, other bases such as Na_2CO_3 and $NaHCO_3$ have no influence or slow down the H_2 generation rate (SI).

In parallel the hydrolysis reaction was also conducted under identical conditions, except that NaOH was replaced by HCl (0.3 M solution for the final concentration), and it was surprisingly found that there was no hydrogen release. Thus in the present study, the contribution from OH^- predominated. The influence of OH^- and H^+ disclosed here is different from the very recent work involving AB hydrolysis by single Rh atoms/VO_2 nanorods, which showed positive correlation between the H^+ concentration and the reaction rate.[71]

Density functional theory (DFT) calculations on the interaction of H and OH with (111) metal Ni surface suggested that H forms an essentially covalent bond with the metal, whereas OH forms a largely ionic bond.[72] The weaker covalent interaction and a stronger Pauli repulsion of the OH with the metal *d* electrons result in the preference of binding molecular hydroxyl to Ni surface rather than H.[73,74] Moreover, Ni is more

oxophilic than Pt, so that it can better promote surface OH adsorption than Pt.[75] To confirm this, XPS is re-called to measure the surface binding energy of Ni 2p upon treatment with NaOH. As shown in Figure S23, upon treatment with NaOH, the binding energy at 855.6 eV that associates with $Ni(OH)_2$ species[76] becomes predominant, verifying the coordination of OH group to the Ni surface. On the other hand, a *ca.* 0.76 eV Ni 2p binding energy downshift was also observed. Thus upon coordination of OH group to the Ni surface, the OH adsorbates donate electrons to the Ni surface. This results in an increased electron density around the Ni surface, which facilitates the interaction with the reactant, AB. The E_a of AB hydrolysis in the presence 0.3 M NaOH was considerably decreased to 28.0 kJ/mol (Figure S24). Therefore the overall reaction activity is significantly improved.

The reason for the switch off of hydrogen generation possibly comes from two aspects. One of them is the negative effect of H^+ on the self-ionization of water that suppresses the OH^- formation and occupation of OH^- absorption sites on the NiNP surface. The other one is the ion effect, because Cl^- ligands are known to limit the catalytic activity of NPs by strongly bonding to NPs surface, which inhibits access to the surface active sites. We thus first conducted the initial reaction by adding NaCl solution (0.3 M), and found that the H_2 generation rate was slower than that without NaCl solution. H_2 was released smoothly, however, with a TOF of 16.67 $mol_{H2}\cdot mol_{cat}^{-1}\cdot min^{-1}$ (Figure S25). This result suggests the possible ion effect in the reaction. To confirm this ion effect, other aqueous solutions of for instance NaI, $NaBF_4$, NaBr, NaF, and Na_2SO_4 were then added to the reaction media with final

concentration of 0.3 M (SI). The H_2 generation rates were considerably slowed down compared with the initial reaction preformed with only NiNPs/ZIF-8, and the TOFs were 10.3, 13.7, 16.2, 18.5 and 21.4 $mol_{H2}\cdot mol_{cat}^{-1}\cdot min^{-1}$ for NaI, $NaBF_4$, NaBr, NaF and Na_2SO_4, respectively. Interestingly, the catalytic activities follow the order: SO_4^{2-} > F^- > Cl^- > Br^- > I^-, which also follows the direct Hofmeister series. Significant ion effects occurred and showed correlations with the catalytic activities obtained in the hydrolysis of AB reaction, a characteristic fingerprint of the Hofmeister effects. It is suggested that H^+ plays a very negative effect in the hydrolysis reaction. On the other hand, ions such as Cl^-, F^-, Br^- et al present in the solution prefer to bind to the surface active sites of NiNPs, leaving less active surface sites available to OH^- generated from water activation in the RDS of hydrolysis. Thus the negative synergistic effects switched off the hydrogen release. Therefore here we establish for the first time that the anion effect tuned hydrolysis of AB catalyzed by the nanocatalyst NiNPs/ZIF-8 in water, allowing the hydrogen generation to reversibly turn "off" and "on". This property is of great practical importance for on-board hydrogen applications under ambient conditions (*vide infra*).

The "on-off" control of hydrogen generation is achieved by addition of an equimolar amount of aqueous solution of HCl and NaOH to the reaction media (Figure 3). Through the studies above, OH^- facilitates the hydrolysis reaction, while H^+ and Cl^- play negative roles in the hydrolysis of AB. At the beginning of the hydrolysis reaction, H_2 generation can be completely stopped by adding 0.3 M HCl solution, and the H_2 generation is released again by adding the same NaOH molarity. In this way,

the H_2 generation is controlled. In addition, in each "on-off" cycle, a gradual decrease in the H_2 generation is also observed. Indeed the poisoning effect of H^+ dominates the switch off of the H_2 generation. The subsequent addition of NaOH neutralizes the HCl solution, however. The effect of NaCl production (from NaOH + HCl) was also observed in the medium, also considerably slowing down the H_2 generation (*vide supra*).

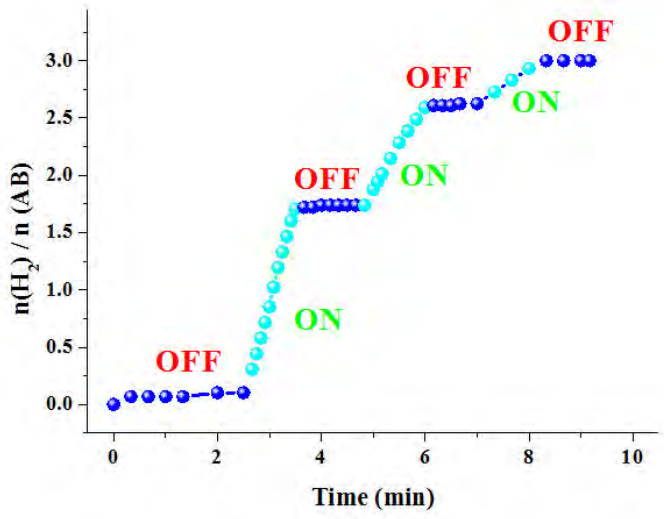

Figure 3. "On-off" control of H_2 production in the AB hydrolysis in water.

Finally, we examined the reusability of the nanocatalyst NiNPs/ZIF-8, which is a critical issue for further practical applications. The reusability tests were conducted under the present conditions by continuous addition of a new proportion of AB aqueous solution when the previous run was completed. As shown in Figure 4, the activity of NiNPs/ZIF-8 is essentially retained until the fifth runs, where a slight drop

in reaction rate is observed. The nanocatalyst was then characterized after the fifth runs by PXRD and TEM techniques, PXRD showing the unchanged nanostructure (Figure S30), while TEM showed the increase of NiNP size (Figure S31). Thus the decrease in the activity is ascribed to the diluted reactant in water, the deactivation effect of the hydrolysis product metaborate,[77-79] and to the increased NiNP size, especially for NPs at the surface of ZIF-8.

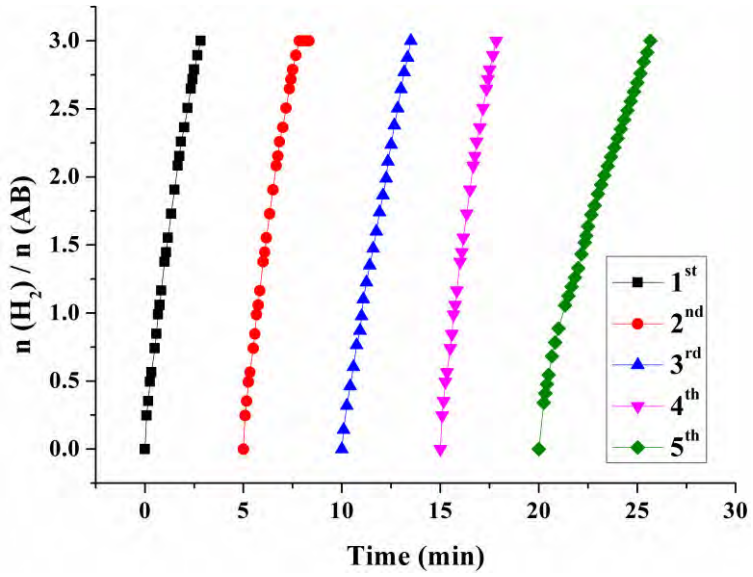

Figure 4. Plots of volume of H_2 *vs.* time for the hydrolysis of AB catalyzed by the 3% NiNPs/ZIF-8 during the reusability test.

Concluding remarks. In summary, highly dispersed ligand-free Fe NPs, Co NPs, Ni NPs and Cu NPs have been successfully synthesized using ZIF-8 as nanocatalyst template, and the highest catalytic activity for hydrogen generation upon hydrolysis of AB is shown to be that of NiNPs/ZIF-8 showing a TOF value of 85.7 $mol_{H2}{\cdot}mol_{cat}^{-1}{\cdot}min^{-1}$. This represents the best TOF value ever reported for noble

metal-free catalysts. Detailed mechanistic investigations, especially KIE measurements, show that the RDS for AB hydrolysis is the cleavage of an O–H bond in H_2O by means of oxidative addition of such a bond on Ni NP surfaces. Inspired by this approach, we further disclosed the ion effect in this reaction, which allowed a remarkable improvement of the catalytic performance and the controlled release of hydrogen. The principles and results obtained here may not only provide insights into the rational design of highly efficient non-noble metal-based nanocatalysts, but also demonstrate a promising step towards the application of chemical hydrogen storage materials in a fuel-cell-based hydrogen economy.

ASSOCIATED CONTENT

Supporting Information. Syntheses and characterization of the nanocatalysts. ^{1}H NMR spectra of the products. Profiles of hydrolysis of the AB hydrolysis reactions. This material is available free of charge via the Internet at http://pubs.acs.org.

AUTHOR INFORMATION

Corresponding Author

*Author to whom correspondence should be addressed.

E-mail: didier.astruc@u-bordeaux.fr

Notes

The authors declare no competing financial interest.

ACKNOWLEDGMENT

Record of an XPS spectrum of Ni-ZIF-8 nanomaterial from and helpful discussion with Luis Yate (CIC biomaGUNE) and financial support from the China Scholarship Council (CSC) of the People's Republic of China (grant to C.W.), the Universities of Toulouse 3 and Bordeaux, the Centre National de la Recherche Scientifique (CNRS), and CIC biomaGUNE (FP7-PEOPLE-IRSES- HIGRAPHEN Project ID: 612704) are gratefully acknowledged.

REFERENCES

1 Armaroli, N.; Balzani, V. *ChemSusChem* **2011**, *4*, 21–36.

2 Yang, J.; Sudik, A.; Wolverton, C.; Siegel, D. J. *Chem. Soc. Rev.* **2010**, *39*, 656–675.

3 Li, Z.; Xu, Q. *Acc. Chem. Res.* **2017**, *50*, 449–1458.

4 He, T.; Pachfule, P.; Wu, H.; Xu, Q.; Chen, P. *Nat. Rev. Mater.* **2016**, *1*, 16059.

5 Chandra, M.; Xu Q. *J. Power Sources* **2006**, *156*, 190-194.

6 Hamilton, C. W.; Baker, R. T.; Staubitz, A.; Manners, I. *Chem. Soc. Rev.* **2009**, *38*, 279–293.

7 Staubitz, A.; Robertson, A. P. M.; Manners, I. *Chem. Rev.* **2010**, *110*, 4079–4124.

8 Zhu, Q. L.; Xu, Q. *Energy Environ. Sci.* **2015**, *8*, 478–512.

9 Rossin, A.; Peruzzini, M. *Chem. Rev.* **2016**, *116*, 8848-8872.

10 Zhu, Q. –L.; Xu, Q. *Chem* **2016**, *1*, 220-245.

11 Zhan, W. -W.; Zhu, Q. –L.; Xu, Q. *ACS Catal.* **2016**, *6*, 6892–6905.

12 Akbayrak, S.; Özkar S. In *Hydrogen Production Technologies,* pp. 207-230, *Sankir, M. and Sankir*, *N. D.; ed.;* Wiley-VCH: Weinheim, Germany, **2017**.

13 Yang, Q. H.; Xu, Q.; Yu, S. H.; Jiang, H. L. *Angew.Chem., Int .Ed.* **2016**, *55,* 3685-3689.

14 Khalily, M. A.; Eren, H.; Akbayrak, S.; Susapto, H. H.; Biyikli, N.; Özkar, S.; Guler, M. O. *Angew. Chem. Int. Ed.* **2016**, *55*, 12257 –12261.

15 J. –X. Kang, T. –W. Chen, D. –F. Zhang, L. Guo, *Nano Energy* **2016**, 23, 145–152.

16 Li, Z.; He, T.; Liu, L.; Chen, W.; Zhang, M.; Wu, G.; Chen, P. *Chem. Sci.* **2017**, *8*, 781-788.

17 Mahyari, M.; Shaabani, A. *J. Mater. Chem. A,* **2014**, *2*, 16652–16659.

18 Yu, C.; Fu, J.; Muzzio, M.; Shen, T.; Su, D.; Zhu, J.; Sun, S. *Chem. Mater.*, **2017**, *29*, 1413–1418.

19 Zhou, L.; Meng, J.; Li, P.; Tao, Z.; Mai, L.; Chen, J. *Mater. Horiz.*, **2017**, *4*, 268-273.

20 Bulut, A.; Yurderi, M.; Ertas, I. E.; Celebi, M.; Kaya, M.; Zahmakiran, M. *Appl. Catal. B: En.* **2016**, *180*, 121–129.

21 Yin, H.; Kuwahara, Y.; Mori, K.; Cheng, H.; Wen, M.; Yamashita, H. *J. Mater. Chem. A* **2017**, *5*, 8946-8953.

22 Liu, P.; Gu, X.; Kang, K.; Zhang, H.; Cheng, J.; Su, H. *ACS Appl. Mater.*

Interfaces **2017**, *9*, 10759–10767.

23 Zhang, H.; Gu, X.; Liu, P.; Song, J.; Cheng, J.; Su, H. *J. Mater. Chem. A* **2017**, *5*, 2288-2296.

24 Tang, C.; Xie, L.; Wang, K.; Du, G.; Asiri, A. M.; Luo, Y.; Sun, X. *J. Mater. Chem. A* **2016**, *4*, 12407-12410.

25 Feng, K.; Zhong, J.; Zhao, B.; Zhang, H.; Xu, L.; Sun, X.; Lee, S. -T. *Angew. Chem., Int. Ed.* **2016**, *55*, 11950-11954.

26 Wang, D.; Astruc, D. *Chem. Soc. Rev.* **2017**, *46*, 816-854.

27 Yang, Q.; Xu, Q.; Jiang, H.–L. *Chem. Soc. Rev.* **2017**, DOI: 10.1039/C6CS00724D.

28 Astruc, D.; Lu, F.; Ruiz, J. *Angew. Chem., Int. Ed*. **2005**, *44*, 7852-7872.

29 Navalon, S.; Dhakshinamoorthy, A.; Alvaro, M.; Garcia, H. *Coord. Chem. Rev.* **2016**, *312,* 99–148.

30 Fihri, A.; Bouhrara, M.; Nekoueihahraki, B.; Basset, J. M.; Polhettiwar, V. *Chem. Soc. Rev.* **2011**, *40*, 5181-5203.

31 Gross, E.; Liu, J. H. -C.; Toste, F. D.; Somorjai, G. A. *Nat. Chem*. **2012**, *4*, 947-952.

32 Bai, C.; Liu, M. *Nano Today* **2012**, *7*, 258-281.

33 Scholden, J. D.; Leal, B. C.; Dupont, J. *ACS Catal.* **2012**, *2*, 184-200.

34 Sankar, M.; Dimitratos, N.; Miedjack, P. J.; Wells, P. P.; Kiely, C. J.; Hutchings, G. J. *Chem. Soc. Rev*. **2012**, *41*, 8099-8139.

35 Haruta, M. *Angew. Chem. Int. Ed.* **2014**, *53*, 52-56.

36 Amiens, C.; Ciuculescu-Pradines, D.; Philippot, K. *Coord. Chem. Rev.* **2016**, *308,*

409-432.

37 Xia, Y.; Gilroy, K. D.; Peng, H.–C.; Xia, X. *Angew. Chem.*, *Int. Ed.* **2017**, *56*, 60-95.

38 Lee, J.Y.; Farha, O. K.; Roberts, J.; Scheidt, K. A.; Nguyen, S. T.; Hupp, J. T. *Chem. Soc. Rev.* **2009**, *38*, 1450-1459.

39 Farrusseng, D.; Aguado, S.; Pinel, C. *Angew. Chem., Int. Ed.* **2009**, *48*, 7502-7513.

40 Zeng, L.; Guo, X.; He, C.; Duan, C. *ACS Catal.* **2016**, *6*, 7935–7947.

41 Liu, J.; Chen, L.; Cui, H.; Zhang, J.; Zhang, L.; Su, C. –Y. *Chem. Soc. Rev.* **2014***, 43,* 6011-6061.

42 Chughtai, A. H.; Ahmad, N.; Younus, H. A.; Laypkov, A.; Verpoort, F. *Chem. Soc. Rev.* **2015**, *44*, 6804-6849.

43 Dhakshinamoorthy, A.; Garcia, H. *Chem. Soc. Rev.* **2012**, *41*, 5262-5284.

44 Lu, G.; Li, S.; Guo, Z.; Farha, O. K.; Hauser, B. G.; Qi, X.; Wang, Y.; Wang, X.; Han, S.; Liu, X.; DuChene, J. S.; Zhang, H.; Zhang, Q.; Chen, X.; Ma, J.; Loo, S. C. J.; Wei, W. D.; Yang, Y.; Hupp, J. T.; Huo, F. *Nat. Chem.* **2012**, *4*, 310–316.

45 Choi, K. M.; Na, K.; Somorjai, G. A.; Yaghi, O. M. *J. Am. Chem. Soc*. **2015**, *137*, 7810-7816.

46 Na, K.; Choi, M.; Yaghi, O. M.; Somorjai, G. A. *Nano Lett.* **2014**, *14*, 5979-5983.

47 Rungtaweevoranit, B.; Baek, J.; Araujo, J. R.; Archanjo, B. S.; Choi, K. M.; Yaghi, O. M.; Somorjai, G. A. *Nano Lett.* **2016**, *16*, 7645–7649.

48 Aijaz, A.; Karkamkar, A.; Choi, Y. J.; Tsumori, N.; Rönnebro, E.; Autrey, T.; Shioyama, H.; Xu, Q. *J. Am. Chem. Soc.* **2012**, *134*, 13926–13929.

49 Zhao, M.; Yuan, K.; Wang, Y.; Li, G.; Guo, J.; Gu, L.; Hu, W.; Zhao, H.; Tang, Z. *Nature* **2016**, *539*, 76–80.

50 An, B.; Zhang, J.; Cheng, K.; Ji, P.; Wang, C.; Lin, W. *J. Am. Chem. Soc.* **2017**, *139*, 3834–3840.

51 Choi, K. M.; Kim, D.; Rungtaweevoranit, B.; Trickett, C. A.; Barmanbek, J. T. D.; Alshammari, A. S.; Yang, P.; Yaghi, O. M. *J. Am. Chem. Soc.* **2017**, *139*, 356–362.

52 Park, K. S.; Ni, Z.; Cote, A. P.; Choi, J. Y.; Huang, R.; Uribe-Romo, F. J.; Chae, H. K.; O'Keeffe, M.; Yaghi, O. M. *Proc. Natl. Acad. Sci. U.S.A.* **2006**, *103*, 10186–10191.

53 Pan, Y.; Liu, Y.; Zeng, G.; Zhao, L.; Lai, Z. *Chem. Commun.* **2011**, *47*, 2071–2073.

54 Yurderi, M.; Bulut, A.; Zahmakiran, M.; Gülcan, M.; Özkar, S. *Appl. Catal. B: Environ.* **2014**, *160*, 534–541.

55 Lu, G.; Hupp, J. T. *J. Am. Chem. Soc.* **2010**, *132*, 7832–7833.

56 Metin, Ö.; Mazumder, V.; Özkar, S.; Sun, S. *J. Am. Chem. Soc.* **2010**, *132*, 1468-1469.

57 Westaway, K. C. *J. Labelled Compd. Radiopharm.* **2007**, *50*, 989–1005.

58 Guella, G.; Patton, B.; Miotello, A. *J. Phys. Chem. C* **2007**, *111*, 18744–18750.

59 Simmons, E. M.; Hartwig, J. F. *Angew. Chem., Int. Ed.* **2012**, *51*, 3066–3072.

60 Keaton, R. J.; Blacquiere, J. M.; Baker, R. T. *J. Am. Chem. Soc.* **2007**, *129*, 1844–1845.

61 Bhattacharya, P.; Krause, J. A.; Guan, H. *J. Am. Chem. Soc.* **2014**, *136*, 11153−11161.

62 Buss, J. A.; Edouard, G. A.; Cheng, C.; Shi, J.; Agapie, T. *J. Am. Chem. Soc.* **2014**, *136*, 11272−11275.

63 Chen, W.; Li, D.; Wang, Z.; Qian, G.; Sui, Z.; Duan, X.; Zhou, X.; Yeboah, I.; Chen, D. *AIChE J.* **2017**, *63*, 60–65.

64 Liu, B. H.; Li, Z. P. *J. Power Sources* **2009**, *187*, 527–534.

65 Lehn, J. -M.; Sauvage, J. -P. *Nouv. J. Chim.* **1977**, *1*, 449–451.

66 Hagfeldt, A.; Grätzel, M. *Chem. Rev.* **1995**, *95*, 49–68.

67 Astruc, D. *Organometallic chemistry and catalysis;* Springer: Berlin, New York, **2007**.

68 Rablen, P. R. *J. Am. Chem. Soc.* **1997**, *119*, 8350–8360.

69 Peebles, L. R.; Marshall, P. *J. Chem. Phys.* **2002**, *117*, 3132–3138.

70 Fu, Z.-C.; Xu, Y.; Chan, S. L.-F.; Wang, W.-W.; Li, F.; Liang, F.; Chen, Y.; Lin, Z.-S.; Fu, W.-F.; Che, C.-M. *Chem. Commun.* **2017**, *53*, 705-708.

71 Wang, L.; Li, H.; Zhang, W.; Zhao, X.; Qiu, J.; Li, A.; Zheng, X.; Hu, Z.; Si, R.; Zeng, J. *Angew. Chem., Int. Ed.* **2017**, *56*, 4712 –4718.

72 Koper, M. T. M.; van Santen, R. A. *J. Electroanal. Chem.* **1999**, *472*,126–136.

73 Gómez, E. del V.; Amaya-Roncancio, S.; Avalle, L. B.; Linares, D. H.; Gimenez, M. C. *Appl. Sur. Sci.* **2017**, *420*, 1–8.

74 Bengaard, H. S.; Nørskov, J. K.; Sehested, J.; Clausen, B. S.; Nielsen, L. P.; Molenbroek, A. M.; Rostrup-Nielsen, J. R. *J. Catal.* **2002**, *209*, 365–384.

75 Wang, C.; Chi, M.; Wang, G.; van der Vliet, D.; Li, D.; More, K.; Wang, H.-H.; Schlueter, J. A.; Markovic, N. M.; Stamenkovic, V. R. *Adv. Funct. Mater.* **2011**, *21*,

147−152.

76 Grosvenor, A. P.; Biesinger, M. C.; St.C. Smart, R.; McIntyre, N. S. *Surf. Sci.* **2006**, *600*, 1771-1779.

77 Zhu, Q. –L.; Li, J.; Xu. Q. *J. Am. Chem. Soc.* **2013**, *135*, 10210−10213.

78 Rakap, M. *Appl. Catal. B: En.* **2015**, *163*, 129–134.

79 Chen, W.; Ji, J.; Feng, X.; Duan, X.; Qian, G.; Li, P.; Zhou, X.; Chen, D.; Yuan, W. *J. Am. Chem. Soc.* **2014**, *136*, 16736–16739.

TOC

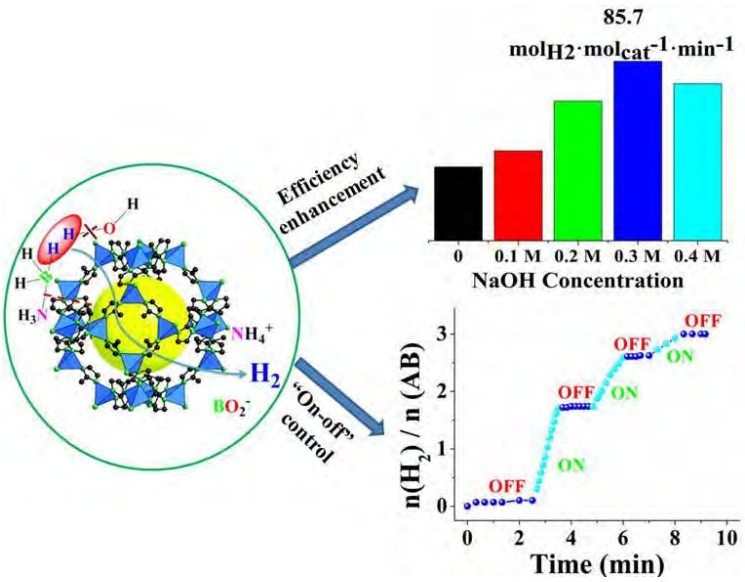

Summary

Non-noble metal nanoparticles (NPs) are notoriously difficult to prepare and stabilize with appropriate dispersion, which in turn severely limits their catalytic functions. The fourth chapter we contributed to the utilization of metal organic framework-stabilized/supported biometal NPs catalysts in the hydrolysis of ammonia-borane (AB) reaction.

Hydrolysis of ammonia-borane over Ni/ZIF-8 nanocatalyst: high efficiency, mechanism and controlled hydrogen release

In this paper, we firstly rapidly synthesized the zeolitic imidazolate framework (ZIF-8; $[Zn(MeIM)_2]_n$) in water with 88%yield in average based on the amount of Zn^{2+}. Procedures for the preparation of the ZIF-8 NPs with 75 nm are: In a typical synthesis, 2-methylimidazole is dissolved in 80 mL water, and stirring at 35 ℃ to form a homogeneous solution. Then, an aqueous solution of $Zn(NO_3)_2 \cdot 6H_2O$ dissolved in 9 mL water was rapidly injected into an aqueous solution. The molar ratio of Zn^{2+} : 2-methylimidazole : H_2O is 1 : 70 : 1238. The mixture was stirred for 2 min, and the product was collected by centrifugation and washed by water. The ZIF-8 NPs were then dried at 60 ℃ *in vacuo* overnight.

The ZIF-8 NPs showed high Brunauer-Emmett-Teller (BET) surface area (1663.3 $m^2 g^{-1}$), and good thermal and chemical stabilities (Figure 1).

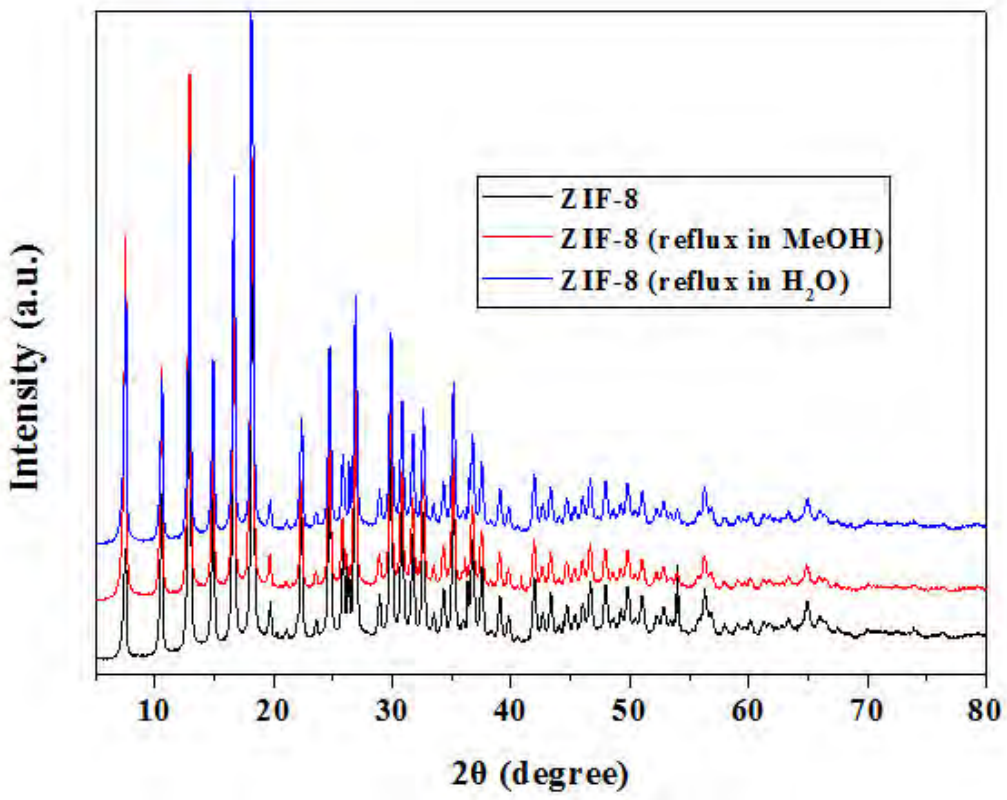

Figure 1. PXRD patterns of as-synthesized ZIF-8 NPs and ZIF-8 NPs refluxing in water or methanol one day.

The ZIF-8 stabilized biometal NPs were then synthesized as follows (Figure 2): a Schlenk flask is charged with 100 mg ZIF-8 NPs under argon. Then 5 mL water is injected, and the mixture is allowed to stir for 30 min. The metal precursor dissolved in 1 mL water is injected. This mixture is stirred continuously at room temperature for 2 h. Then, 1 mL aqueous solution of fresh prepared $NaBH_4$ (10 equiv per metal) is quickly added. The mixture is allowed to further stir for another 30 min, and the resulting nanocatalyst is collected by centrifugation and washed with water, and then dried at 60 ℃*in vacuo* overnight.

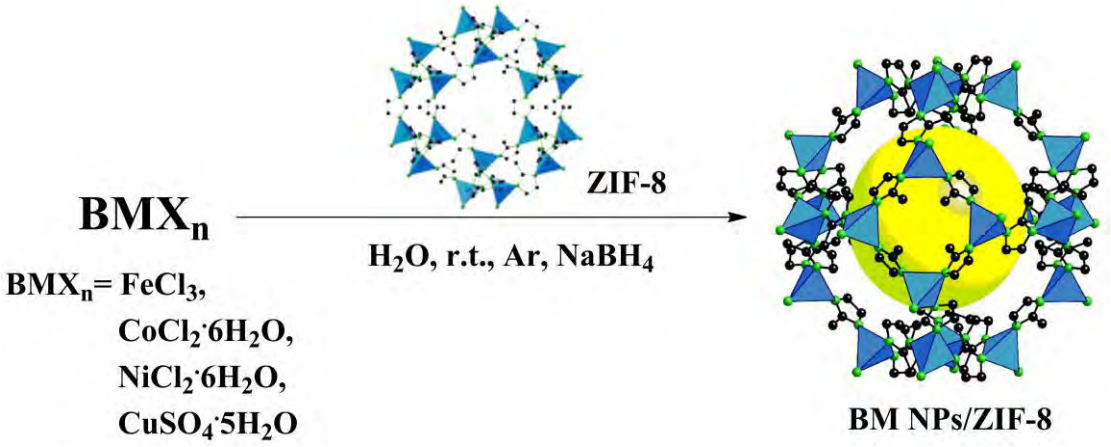

Figure 2. Preparations of the nanocatalyst BMNP/ZIF-8.

The measurements of the NP size by TEM using a solution of ethylenediaminetetraacetic acid (EDTA) to digest the ZIF-8 framework, and using poly(vinylpyrrolidone) (PVP, Mw = 10,000) to stabilize the ultrasmall NPs. The size of the released NiNPs is 2.7 nm, and other size of FeNPs, CoNPs, and CuNPs are 3.0, 2.9, and 3.2 nm, respectively (Figure 3).

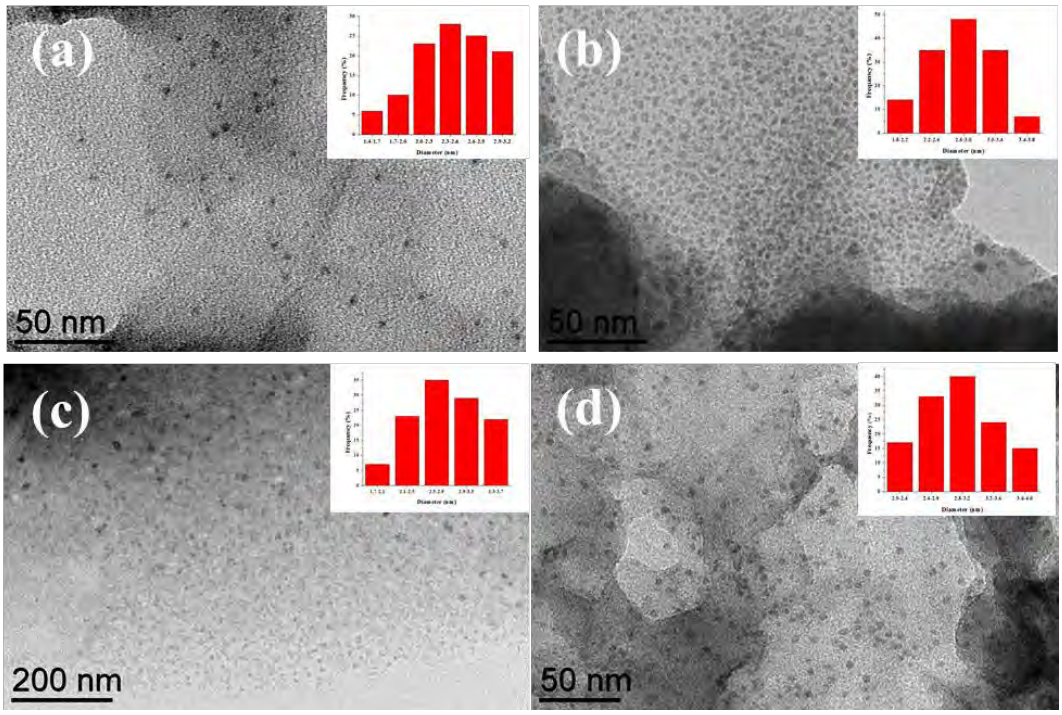

Figure 3. Size distributions of the NPs after digestion of nanocatalysts with EDTA, and nanoparticles capping with PVP: (a) NiNPs; (b) FeNPs; (c) CoNPs; (d) CuNPs.

Nitrogen sorption experiments of the nanocatalysts show type I shape and considerable decrease of pore volume and BET surface areas (Figure 4). This indicates blocking of the windows of the ZIF-8 framework cavities by highly dispersed NP occupations within the locally distorted environment or/and the location of NPs at the surface.

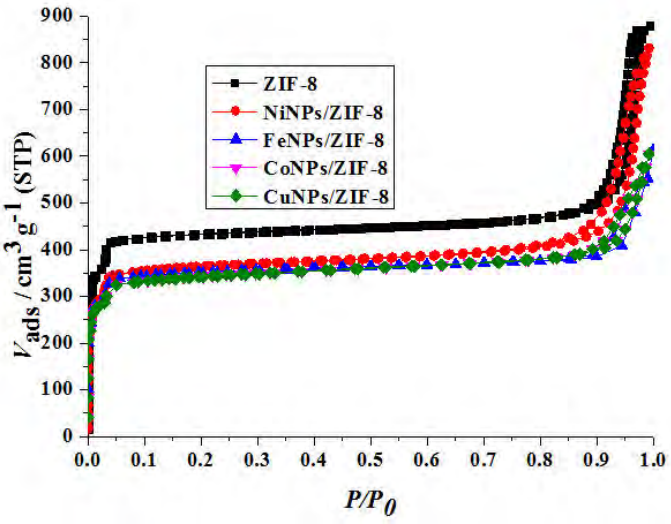

Figure 4. Nitrogen adsorption–desorption isotherms of ZIF-8 and BMNPs/ZIF-8 nanocatalsyts.

We compared their efficiencies in the hydrolysis of AB reaction, showing the best efficiency of NiNPs/ZIF-8 nanocatalyst in term of turnover frequency in this reaction (Figure 5).

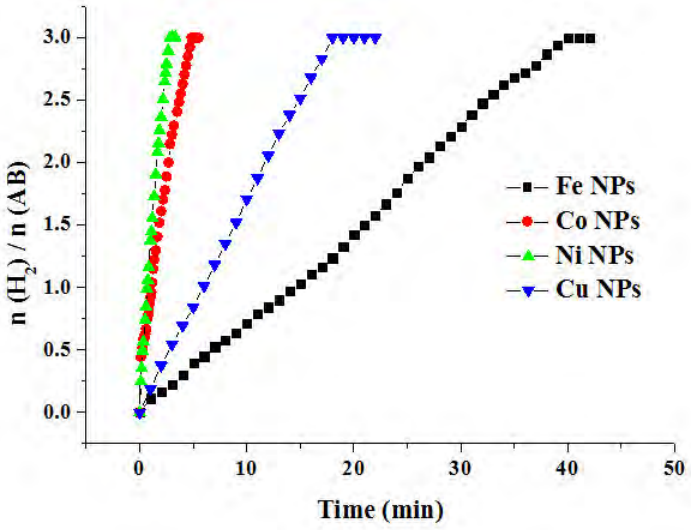

Figure 5. Comparison of the Hydrogen evolution from NH_3BH_3 in H_2O in water in the presence of 3 mol% of BM NPs/ZIF-8 nanocatalysts.

Therefore the catalytic system NiNPs/ZIF-8 was chosen for further studies. Figure 6a shows the logarithmic plot of the hydrogen generation rate *vs*. concentration of NiNPs/ZIF-8; the slope is 0.98, indicating that the hydrolysis of AB catalyzed by NiNPs/ZIF-8 is first-order with respect to the catalyst concentration. On the other hand hydrolysis of AB catalyzed by NiNPs/ZIF-8 is zero-order with respect to the AB concentration, as a nearly horizontal line (slope of 0.086) is observed (Figure 6b). This implies that under the present reaction conditions, AB is easily activated, and thus the possibility of the activation of AB in the rate-determining step (RDS) is ruled out. This also is in accordance with the KIE results. The activation energy (E_a) of AB hydrolysis, determined by measuring the time dependence of H_2 generation at various temperatures, is approximately 42.7 kJ/mol (Figure 7c).

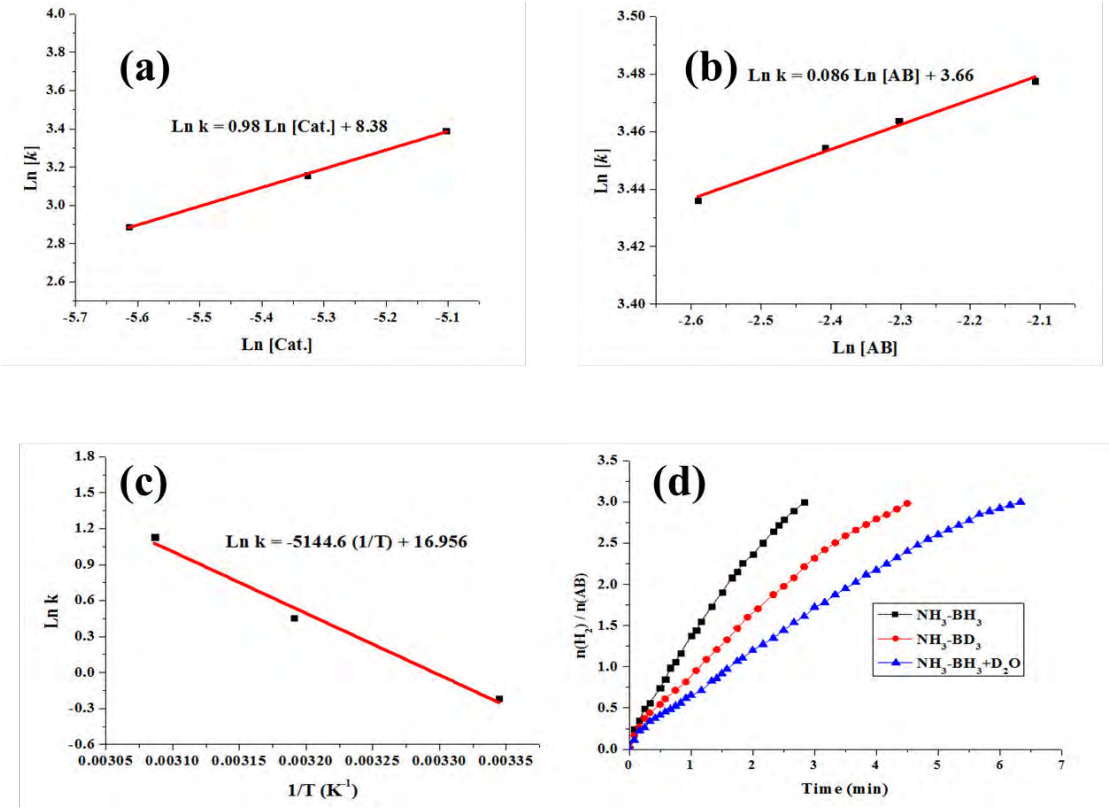

Figure 7. (a) The plot of hydrogen generation rate versus the concentration of Ni NPs/ZIF-8 nanocatalyst both in natural logarithmic scale; (b) the plot of hydrogen generation rate versus the concentration of AB both in natural logarithmic scale; (c) Arrhenius plots obtained from the kinetic data; (d) Hydrogen evolution from NH_3BH_3, ND_3BH_3, and NH_3BD_3 catalyzed by 3 mol% Ni NPs/ZIF-8 nanocatalyst.

By detailed mechanistic investigations, especially by investigating the rate-determining step in this reaction by kinetic isotope effects using NiNPs/ZIF-8 nanocatalyst (Figure 7d), we proposed that the water molecule is activated by an indirect O–H bond cleavage to form –H and –OH species promoted by AB in the presence of the nanocatalyst NiNPs/ZIF-8. Due to the NH_3 group does not participate in the hydrolysis, the B–N bond then dissociates in AB, followed by H_2 release.

We then assumed that if OH^- is directly adsorbed on the surface of the Ni nanocatalyst, a bifunctional catalyst with both H and OH adsorptions should be highly desired to provoke the surface reaction. Indeed, H_2 generation rates greatly improved as compared to the one in the absence of NaOH (Figure 8), while the addition of HCl creased the reaction.

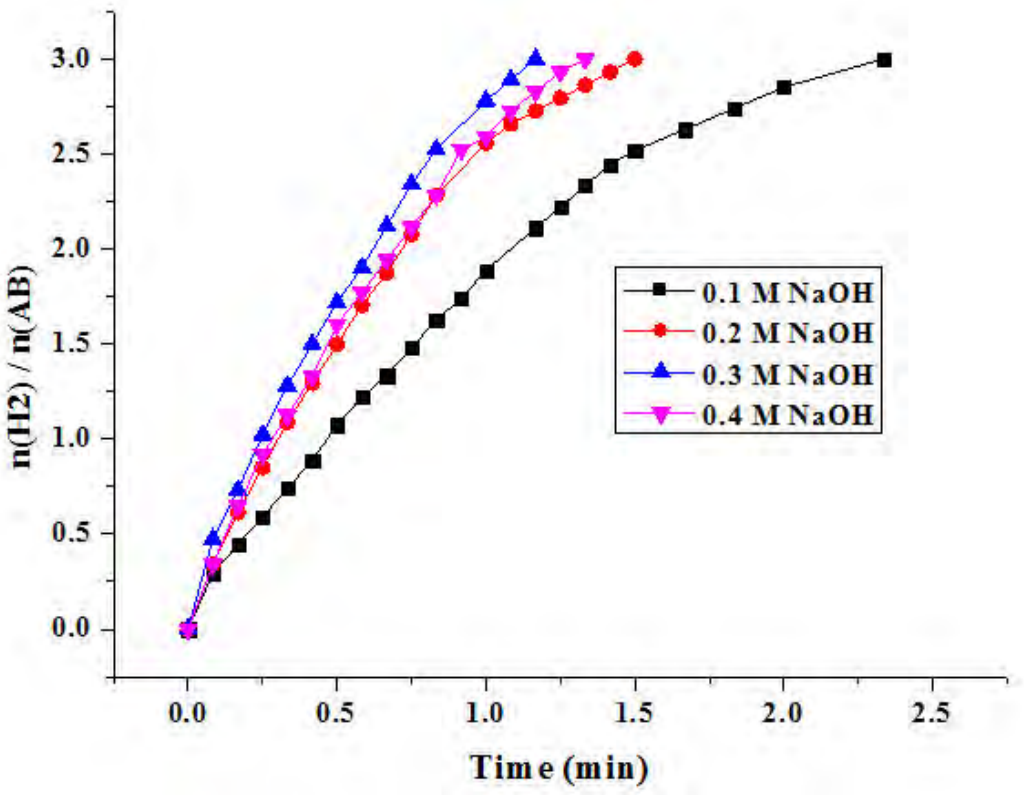

Figure 8. Hydrogen evolution from NH_3BH_3 by 3 mol% Ni NPs/ZIF-8 nanocatalyst in the presence of 0.1-0.4 M NaOH.

The reason for the switch off of hydrogen generation comes from two aspects. One is the negative effect of H^+ on the self-ionization of water that suppressed the OH^- formation and occupation of OH^- absorption sites on the NiNP surface. The other is the ion effect, because Cl^- ligands are known to limit the catalytic activity of NPs by

strongly bonding to NPs surface, which inhibits access to the surface active sites. By detailed studies, we then firstly disclosed that the "on-off" control of hydrogen generation by addition of an equimolar amount of aqueous solution of HCl and NaOH to the reaction media, which is of great practical importance for on-board hydrogen applications under ambient conditions (Figure 9).

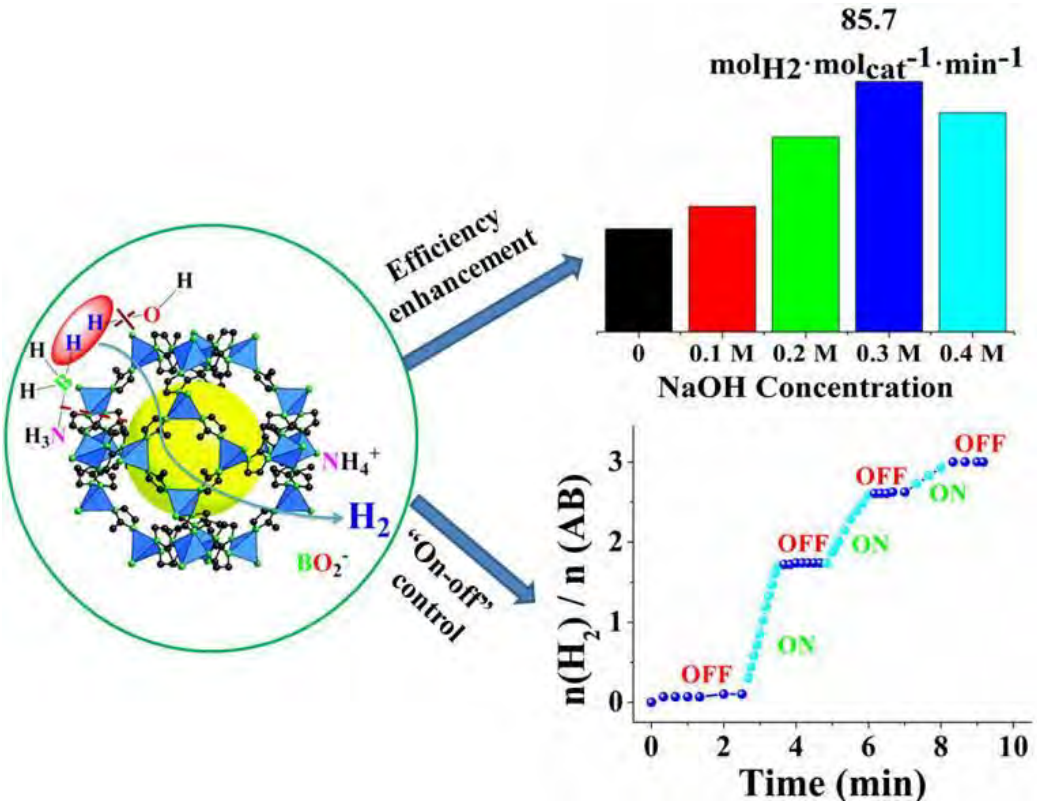

Figure 9. Enhancing the catalytic efficiency of nanocatalyst NiNPs/ZIF-8 in hydrolysis of AB by mechanistic studies, and the controlled hydrogen release.

Furthermore, we examined the reusability of the nanocatalyst NiNPs/ZIF-8 in the hydrolysis of AB in water. The activity of the NiNPs/ZIF-8 nanocatalyst is essentially retained until the fifth runs. The nanocatalyst was then characterized after the fifth runs by PXRD and TEM techniques, PXRD showing the unchanged nanostructure

(Figure 10a), while TEM showed the increase of NiNP size (Figure 10b). The decrease of the catalytic activity was due to the diluted reactant in water, the deactivation effect of the hydrolysis product metaborate, and to the increased NiNP size, especially for NPs at the surface of ZIF-8.

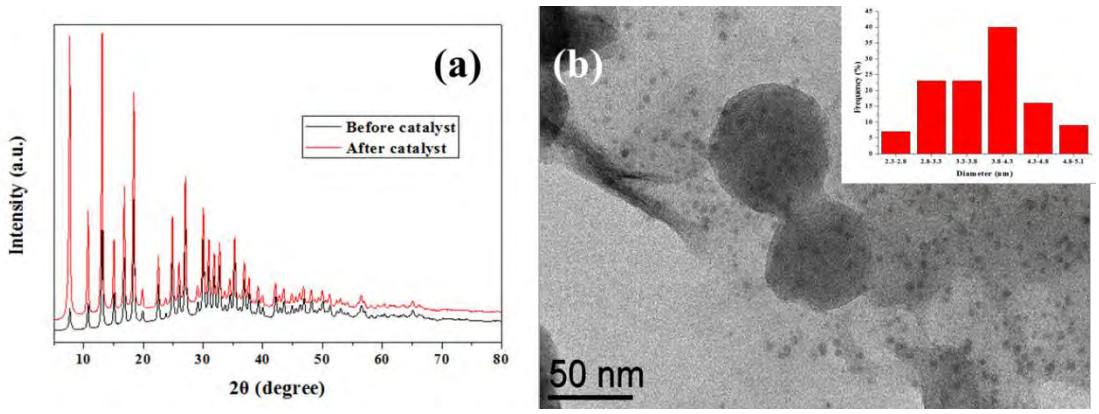

Figure 10. (a) PXRD patterns of as-synthesized NiNPs/ZIF-8 NPs before and after the catalytic reaction; (b) TEM image and size distribution of the Ni NPs (3.8±0.5 nm) after digestion of nanocatalysts with EDTA, and nanoparticles capping with PVP .

Thus, the principles and results here may not only provide insights into the rational design of high efficient non-noble metal based nanocatalysts, but also demonstrate a promising step towards the application of chemical hydrogen storage materials in a fuel-cell-based hydrogen economy.

Conclusions and Perspectives

In this thesis, our investigations have concerned the design, characterization and catalytic applications of transition metal-based nanomaterials, specifically focusing on two aspects:

(i) the design, synthesis and catalytic application of the amphiphilic ligand-stabilized late transition-metal nanoparticle catalysts;

(ii) the design, synthesis and catalytic properties of heterogeneous transition metal nanoparticle catalysts based on graphene and metal organic framework supports.

First, in a review of metal-catalyzed azide-alkyne cycloaddition reactions with catalysts based on various transition metals, we emphasized the significance of this particular reaction by state of the art of the mechanistic studies, and figure out the recent developments, breakthroughs, trends and challenges in this area. Based on this review article and the extension of our previous work, we proposed a new concept based on the design of amphiphilic ligand that mimics the functions of dendrimers to stabilize efficient transition-metal nanoparticles catalysts. This tris(triazolyl)-polyethylene glycol (tris-trz-PEG) amphiphilic ligand is specifically synthesized by the copper-catalyzed alkyne-azide cycloaddition forming the tris-triazole group that is later linked to a PEG 2000 chain through a Williamson reaction. We compared the efficiencies of amphiphilic ligand-transition metal nanoparticles in the 4-nitrophenol reduction reaction, and selected the most efficient four NPs, namely AuNPs, PdNPs, RuNPs, and CuNPs. The later three were then utilized for their well-known reactions such as the Suzuki-Miyaura reaction, transfer hydrogenation and azide-alkyne cycloaddition reaction. These nanocatalysts are surprisingly efficient with only parts-per-million (ppm) metal loadings, and recyclable. It has then been shown that the weak surface ligand coordination and easy ligand substitution by substrates played a critical role in determining the high efficiencies of the nanocatalysts. On the other hand, we demonstrated the influence of the triazole denticity on the stabilization of

AuNPs in the 4-NP reduction by $NaBH_4$ in water, and also compared the efficiencies of utilization of tris-trz-PEG with commercial polyethylene glycol 2000 (PEG) and polyvinylpyrrolidone (PVP) in the AuNP stabilization and catalysis. Furthermore, benefiting from the chelation effect, the amphiphilicity of the tris-trz-PEG ligand containing a tris-triazole tripod that increases the electron density on the metal center, and a PEG chain allowing homogeneous "click" reactions in water, an efficient amphiphilic "click" Cu^I catalyst in water is designed. This catalyst shows high activity for CuAAC "click" reaction in water at ambient temperature with catalyst loading at only ppm levels for the synthesis of various useful functional products with medicinal, catalytic, targeting, and labeling properties. Furthermore, the catalyst was recycled at least six times without change of ligand structure during the CuAAC reactions. This study contributes to the more effective synthesis of "click" compounds with multiple functions under minute quantity of Cu^I catalyst under green conditions.

Heterogeneous catalysts have many advantages over homogeneous ones, such as easy catalyst separation and recovery, regeneration, and use. Benefiting from the utilization of the tris-trz-PEG ligand, the NPs are formed with ultrafine size and therefore enable efficient catalysts. Tris-trz-PEG ligand-stabilized bimetallic RhAg nanoparticles and the α-Fe_2O_3 nanocluster are supported on reduced graphene oxide and graphene oxide, respectively. The synergtic effect of bimetallic RhAg NPs on rGO is shown to be more efficient than monometallic counterparts. The catalyst was recycled, and its amount was reduced to ppm level while retaining an exceptional catalytic efficiency in the 4-nitropheol reduction by $NaBH_4$ in water at room temperature. On the other hand, with the α-Fe_2O_3 nanocluster/GO nanocatalyst, high efficiencies were achieved in 4-nitropheol reduction and Suzuki-Miyaura reaction. The catalyst is also recoverable and can be reused without significantly loss of catalytically active NPs and activities. Furthermore, we have generalized the concept of "redox mediated synthesis" on the graphene oxide (GO)-supported metal nanocatalysts. This means that graphene oxide is used as an electron-reservoir nanomaterials that transfers electrons and eventually oxo ligands to the metals of the NPs. This recalls Basset's strategies using inorganic oxide materials as ligands of

early transition metal-basec molecular catalysts, although the binding is considerably stronger in the latter case. Both noble metals and biometals using either exergonic or endergonic redox reactions between GO and the transition metal salts have been used is our general approch. The ultrafine, surface-clean metal NPs are formed on graphene oxide with good monodispersity. These new nanocatalysts are highly efficient in water at ambient temperature. The high efficiencies and recyabilities of the nanocatalysts were exemplified in 4-nitrophenol reduction by RhNP/GO, AuNP/GO and CuNP/GO, Sonogashira coupling by CuNP/GO, PdNP/GO, and PdCuNP/GO, azide-alkyne 1,3-cycloaddition by CuNP/GO, and hydrolysis of ammonia-borane for hydrogen generation by RhNP/GO catalyst. This work shows a promising way to the rational design of efficient nanocatalysts for a large variety of chemical reactions.

Furthermore, the following work contributed to the utilization of metal organic framework-stabilized/supported non-noble metal NPs catalysts in the hydrolysis of ammonia-borane reaction. We showed the best efficiency of NiNPs/ZIF-8 nanocatalyst in term of turnover frequency in this reaction over the noble metal-free catalysts, an important achievement in terms or green chemistry and cost saving. By detailed mechanistic investigations, especially by investigating the rate-determining step in this reaction, remarkable improvement of the catalytic performance and the controlled release of hydrogen are obtained. The principles and results here may not only provide insights into the rational design of high efficient non-noble metal based nanocatalysts, but also demonstrate a promising step towards the application of chemical hydrogen storage materials in a fuel-cell-based hydrogen economy.

In sum, this thesis has led to advances in development of current knowledge on the design, characterization, and catalytic applications of transition metal-based nanomaterials. The incessant search for new avenues on efficient transition-metal nanocatalysts benefits from the advantages of ligand design and supports, has led to the advent of the constructions of novel and efficient transition-metal based nanocatalysts. The effectiveness of ligand design using “click” chemistry has involved the formation of triazole ligands that mildly stabilized ultrafine nanoparticles that are efficient nanocatalysts. Heterogeneous nanocatalysts based on graphene based

and metal organic framework supports are thus promising in a variety of chemical reactions, especially taking the synthetic effect, support effect and reusability into account. Thus the design of new nanocatalysts based on transition metal nanomaterials are shown here as a promising research direction due to the increasing demands of development of sustainable and green chemistry.

The NP shape, size, morphology, composition, and the supports are the key parameters in the determination and enhancement of their functionality and potential applications in catalysts. Thus insights into the synthesis and characterizations of new nanocatalysts as well as the implementations by theoretical calculations will shed new light on the effective catalyst designs.

In spite of the rapid growth of utilization of transition metal-based nanomaterials as catalysts, problems and challenges are still remained. While theoretical and computational studies have provided insight to reactions, general chemical reactions still require considerable theoretical modeling to predict the most adequate nanocatalysts in order to achieve the best catalytic performance. *In-situ* characterizations would be of great value to characterize nanocatalysts and follow the chemical reactions, and to experimentally understand insights provided by theoretical calculations. Efforts in this direction should be considerable developed.

Extension of the scope of the field by exploring novel and efficient transition metal-based nanocatalysts for more and general chemical reactions is also required. For instance the exploration of new multifunctional nanocatalysts including the design of new bi- and trimetallic nanocomposites, core-shell nanocatalysts is necessary for organic synthesis under harsh conditions. Moreover, considerable efforts should also be devoted to the design of highly efficient earth-abundant transition metal nanocatalysts (Fe, Co, Ni and Cu) for various modern chemical reactions under ambient, green conditions. Furthermore, the activity, selectivity, and recyclability, instability of these nanocatalysts and the leaching of NPs are problems that need be critically addressed. Optimistically one may anticipate that with the increasing attentions paid to the subject, the challenges and problems will be overcome in due course.

Changlong WANG- List of PhD Publications

(1) **Changlong Wang**, Roberto Ciganda, Lionel Salmon, Danijela Gregurec, Joseba Irigoyen, Sergio Moya, Jaime Ruiz and Didier Astruc, Highly efficient transition metal nanoparticle catalysts in aqueous solutions, *Angewandte Chemie International Edition.* **2016**, *55* (9), 3091-3095. ***(Highly cited paper)***

(2) **Changlong Wang** and Didier Astruc, Nanogold plasmonic photocatalysis for organic synthesis and clean energy conversion, *Chemical Society Reviews.* **2014**, *43* (20), 7188-7216. ***(Highly cited paper). Ne figurera pas dans la thèse***

(3) **Changlong Wang**, Djamila Ikhlef, Samia Kahlal, Jean-Yves Saillard, Didier Astruc, Metal-catalyzed azide-zlkyne "Click" reactions: mechanistic overview and recent Trends, *Coordination Chemistry Reviews.* **2016**, *316*, 1-20. ***(Highly cited paper)***.

(4) **Changlong Wang**, Dong Wang, Shilin Yu, Thomas Cornilleau, Jaime Ruiz, Lionel Salmon and Didier Astruc, Design and applications of an efficient amphiphilic "click" Cu^{I} catalyst in water, *ACS Catalysts.* **2016**, *6* (8), 5424–5431.

(5) **Changlong Wang**, Lionel Salmon, Roberto Ciganda, Luis Yate, Sergio Moya, Jaime Ruiz, Didier Astruc, Efficient parts-per-million *a*-Fe_2O_3 nanocluster/graphene oxide catalyst for Suzuki–Miyaura coupling reactions and 4-nitrophenol reduction in aqueous solution, *Chemical Communications*, **2017**, *53*, 644-646.

(6) **Changlong Wang**, Lionel Salmon, Qian Li, María Echeverría Igartua, Sergio Moya, Roberto Ciganda, Jaime Ruiz and Didier Astruc, From mono to tris-1,2,3-triazole-stabilized gold nanoparticles and their compared catalytic efficiency in 4-nitrophenol reduction, *Inorganic Chemistry*, **2016**, *55* (13), 6776–6780.

(7) **Changlong Wang**, Roberto Ciganda, Luis Yate, Sergio Moya, Lionel Salmon, Jaime Ruiz and Didier Astruc, RhAg/rGO nanocatalyst: ligand-controlled synthesis and superior catalytic performances for the reduction of 4-nitrophenol, *Journal of Materials Science*, **2017**, *52*, 9465-9476.

(8) Fangyu Fu, Angel Martinez, **Changlong Wang**, Roberto Ciganda, Luis Yate, Ane Escobar, Sergio Moya, Eric Fouquet, Jaime Ruiz and Didier Astruc, Exposure to air boosts CuAAC reactions catalyzed by PEG-stabilized Cu nanoparticles, *Chemical Communications*, **2017**, *53*, 5384-5387. ***Ne figurera pas dans la thèse***

(9) Djamila Ikhlef, **Changlong Wang,** Samia Kahlal, Boubekeur Maouche, Didier Astruc, Jean-Yves Saillard, Computational and Theoretical Chemistry, **2015**, *1073*, 131–138. ***Ne figurera pas dans la thèse***

(10) Roberto Ciganda, Joseba Irigoyen, Danijela Gregurec, Ricardo Hernández, Sergio Moya, **Changlong Wang**, Jaime Ruiz, Didier Astruc. Liquid–Liquid Interfacial Electron Transfer from Ferrocene to Gold (III): An Ultrasimple and Ultrafast Gold Nanoparticle Synthesis in Water under Ambient Conditions. *Inorganic Chemistry*, **2016**, 55, 6361–6363. ***Ne figurera pas dans la thèse***

Publications à soumettre

(11) **Changlong Wang**, Roberto Ciganda, Luis Yate, Jimena Tuninetti, Victoria Shalabaeva, Lionel Salmon, Sergio Moya, Jaime Ruiz, Didier Astruc, *Synthesis and high catalytic efficiency of transition-metal nanoparticle-graphene oxide nanocomposites. A soumettre à Angew. Chem. en juin 2017*

(12) **Changlong Wang**, Chen Zhang, Zhao Wang, Roberto Ciganda, Luis Yate, Lionel Salmon, Sergio Moya, Jaime Ruiz, Didier Astruc, *Hydrolysis of ammonia-borane over Ni/ZIF-8 nanocatalyst: high efficiency, ion effect and controlled hydrogen release. A soumettre à JACS en juillet 2017*

Nanomatériaux à base d'éléments de transition tardifs en catalyse

Résumé:

Les nanosciences et nanotechnologies impliquent de travailler avec des matériaux de taille nanométrique avec l'exploration, la caractérisation et l'application de nanomatériaux structurés. Ce domaine a connu beaucoup de succès et est devenu un champ de recherches émergent dans lequel des études significatives ont révolutionné les familles des systèmes nanométriques.[1] Les promesses et possibilités de travaux sont très vastes. Par exemple, les nano machines transformeront la médecine pour la recherche contre le cancer ou pour la délivrance ciblée de médicaments.[2] Les nanomatériaux ont suscité un grand intérêt pour leurs applications en optique, électronique et mécanique et, parmi ces applications, la nano catalyse se trouve en bonne place. En effet, les nano catalyseurs[3] offrent des débouchés dans les domaines des synthèses de médicaments, des conversions d'énergie, de la décontamination pour l'environnement et de la chimie verte pour la production en chimie fine.

Les catalyseurs homogènes sont solubilisés dans les milieux réactionnels et bénéficient d'une grande efficacité, sont très sélectifs et connaissent des utilisations industrielles, mais ils souffrent du manque de leur récupération et de leur réutilisation, ainsi que de leur stabilité thermique très limitée.[4] Par opposition, les catalyseurs hétérogènes bénéficient de leur facilité de récupération à partir des milieux réactionnels et de la possibilité de leur utilisation à haute température. En revanche, ils souffrent de problèmes de sélectivité et de la difficulté des explorations mécanistiques. D'autre part, la catalyse verte qui fait partie intégrante des grands principes de la chimie verte constitue un objectif privilégié des processus chimiques actuels. Les éléments de cette catalyse verte comprennent idéalement des coût de préparation peu

élevés, des activités élevées, de bonnes sélectivités, de hautes sélectivités, des stabilités importantes, un recouvrement efficace et une bonne recyclabilité. Les catalyseurs verts devraient efficacement catalyser les réactions dans des solvants “verts” (par exemple sans solvant, dans l’eau ou dans l’éthanol). Finalement la définition et les applications des catalyseurs verts ne sont pas seulement une tâche de grande importance économique et environnementale pour la science de la catalyse, mais elle doit également se préoccuper de la contamination par les métaux dans les produits de réaction.

La nano catalyse se définit comme la catalyse utilisant les nanoparticules (NP) métalliques.[3] Les nanoparticules actives catalytiquement ont des tailles comprises entre de l’ordre du nanomètre (nm) et plusieurs dizaines ou centaines de nanomètres (contenant de quelques dizaines à quelques milliers d’atomes). Elles ont un rapport surface sur volume élevé et un grand pourcentage d'atomes de surface, c'est-à-dire de façon prédominante des atomes de surface sur les coins et les arêtes. Depuis approximativement le début des années 1990, ce domaine de la catalyse a acquis son Independence. Il est habituellement appelé catalyse colloïdale ou catalyse semi-hétérogène car on lui attribuait alors de constituer un pont entre la catalyse homogène et la catalyse hétérogène. De cette façon, la nano catalyse combine les aspects positifs de la catalyse homogène avec une haute activité catalytique et une bonne sélectivité, ainsi que la possibilité d’ études mécanistiques permettant des améliorations des catalyseurs de même qu’une bonne recyclabilité.[4]

Dans ce contexte, les nanomatériaux à base d’éléments de transition sont d’un intérêt particulier pour l’utilisation de nano catalyseurs.[5,6] Les nanomatériaux hétérogènes à base d’éléments de transition contiennent les entités catalytiquement actives qui conduisent à l’activation des substrats et les réactions catalytiques procèdent sur les surfaces des matériaux

supportés conduisant à l'efficacité et à la sélectivité. De façon à obtenir des nanoparticules catalytiquement actives nanométriques, les tailles des nanoparticules doivent être réduites à quelques dizaines à quelques milliers d'atomes. C'est la raison pour laquelle les nanoparticules à base d'éléments de transition tardifs ont la nécessité d'être stabilisés par des dendrimères, polymères, liquides ioniques et supports inorganiques solides tels que la silice, l'alumine, la zircone, le carbone sous ses différentes formes, etc. Dans les faits, les stabilisants jouent un rôle crucial et ont une influence sur les propriétés catalytiques.[7] Par exemple, certains ligands fortement coordonnants (thiolates, phosphines, oxydes de phosphine, etc.) inhibent les sites catalytiquement actifs de la surface du catalyseur, ce qui conduit à des effets catalytiques négatifs se développant sur la surface des nanoparticules. Par conséquent, les ligands "verts" qui impliquent une stabilisation douce dans l'eau et sont facilement déplaçables par les substrats de la surface catalytique en procurant éventuellement un nombre accru de sites catalytiquement actifs sont particulièrement recherchés afin d'améliorer les efficacités catalytiques. Effectivement, la synthèse rationnelle de catalyseurs à base de nanoparticules sans ligands, ultrafines et efficaces constitue actuellement un défi notable.

Avant la présente thèse de PhD, notre groupe de recherche a examiné l'efficacité des dendrimères en tant que supports des nanoparticules à base d'éléments de transition tardifs et templates pour des réactions catalytiques homogènes et hétérogènes.[8] Nous avons étendu le principe de la catalyse à l'aide de template dendritiques de nanoparticules métalliques à la nano catalyse induite par des ligands, en particulier à des nanomatériaux à base de ligand amphiphile triazole (click) dans le but d'améliorer les efficacités catalytiques. Par conséquent, la présente thèse de PhD implique le design et l'application de nanomatériaux à base d'éléments de transition tardifs en tant que nouveaux nano catalyseurs pour une variété de réactions chimiques avec un objectif de nano-ingénierie de la taille et de l'environnement de

façon à améliorer l'activité catalytique, la stabilité des nano catalyseurs, leur recouvrement et à décroître la charge de catalyseur.

Dans le premier chapitre, un article de revue écrit en collaboration entre notre groupe et le groupe du Professeur Jean-Yves Saillard de l'Université de Rennes sur les aspects théoriques et les recherches récentes concernant la catalyse de réactions "click", en fait la principale de ces réactions, c'est-à-dire la cycloaddition1-3 de type Huisgen entre un alcyne et un azoture catalysée par le cuivre (en abrégé anglais CuAAC), mais aussi par une variété d'autres éléments de transition et lanthanides (Cu, Ru, Ag, Au, Ir, Ni, Zn, Ln) (en abrégé anglais MAAC), (Figure 1).[9] Ces réactions MAAC sont parmi les plus utilisées des réactions en chimie "verte", et sont les plus fréquemment utilisées des diverses réactions dites "click". D'abord développées par le groupe de Sharpless et par celui de Meldal en 2002 avec Cu(I)[10], ces réactions ont ensuite été étendues par Fokin à des catalyseurs au Ru(II) en 2005, puis à beaucoup d'autres éléments de transition catalytiques. Des mécanismes variés basés sur des calculs théoriques et des résultats expérimentaux comprenant la caractérisations d'intermédiaires réactionnels et optimisations de paramètres de réactions qui sont intimement connectés ont été proposés pour les diverses réactions MAAC catalysées par ces composés métalliques. Les objectifs sont l'optimisation des conditions réactionnelles et des catalyseurs, la simplification des procédures, leur application dans l'industrie et la diminution des quantités de catalyseurs employées.

Depuis 2012, de nouvelles tendances sont apparues souvent représentant à la fois des découvertes incisives pour de nouvelles applications et de nouveaux défis mécanistiques. Ces avancées récentes doivent inspirer les chimistes théoriciens pour rationaliser les mécanismes de nouvelles voies catalytiques.

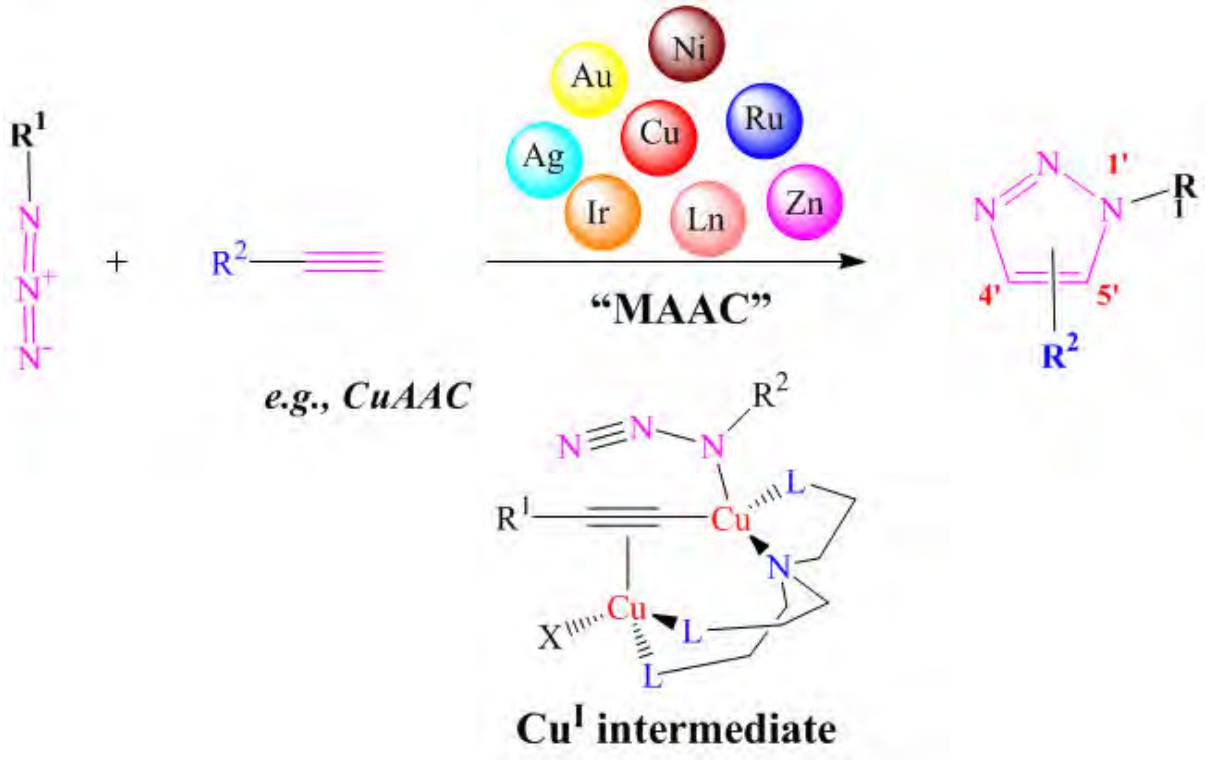

Figure 1. Réactions de cycloaddition 1-3 des alcynes avec les azotures catalysées par des composés des éléments de transition.

Dans le second chapitre est proposé un nouveau concept basé sur le design de ligands amphiphiles qui miment les fonctions des dendrimères amphiphiles en stabilisant des nanoparticules des éléments de transition variés. Ces ligands amphiphiles sont le tris (triazolyl)-polyéthylène glycol (en abrégé anglais: tris-trz-PEG) contenant trois ligands cycles triazole (c'est-à-dire "clickés") et une chaine polyéthylène glycol (PEG 2000). Ils sont synthétisés par réaction "click" CuAAC et réaction de Williamson. Les nanoparticules des éléments de transition sont synthétisées en présence du ligand amphiphile par réduction des cations métalliques précurseurs par $NaBH_4$ (Figure 2).

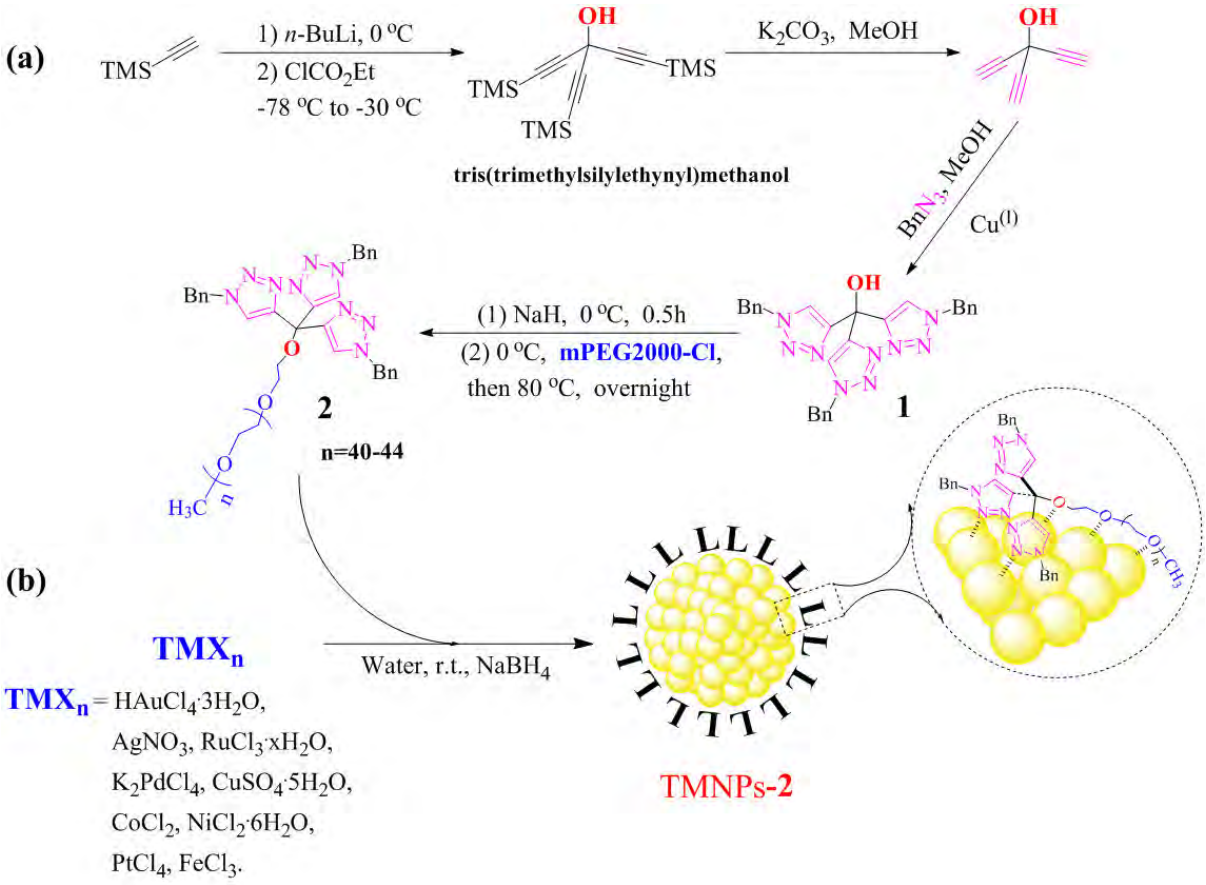

Figure 2. a) Synthèse du nouveau ligand amphiphile **2**. b) Synthèse des nanoparticules des éléments de transition (en abrégé anglais TMNP-**2**).

Nous avons comparé les efficacités des catalyseurs à base de nanoparticules d'éléments de transition tardifs pour la catalyse de réduction du 4-nitrophénol et sélectionné les nanoparticules des quatre éléments les plus actifs, c'est-à-dire les nanoparticules d'or, de palladium, de ruthénium et de cuivre (en abrégé anglais: AuNPs, PdNPs, RuNPs, et CuNPs). Les trois derniers ont été utilisés pour leur efficacité bien connue en catalyse de la réaction de Suzuki-Myaura, la réaction de transfert d'hydrogénation et la réaction "click" entre les acétyléniques et les alcynes respectivement. Ces catalyseurs sont étonnamment efficaces avec seulement quelques parties par million (ppm) de métal, et recyclables. Par exemple, les CuNPs testées pour la réaction "click" entre l'azoture de benzyle et le phénylacétylène, ont

été trouvées extrêmement efficaces. Cette réaction est effectivement achevée quantitativement à 35°C en 24 heures avec seulement 20 ppm de Cu à partir de CuNP-2, ce qui conduit à un nombre de turnover (TON) de 28000 et une fréquence de turnover (TOF) of 1170 h^{-1}, ce qui constitue l'un des tous meilleurs résultats jamais obtenus avec des CuNPs comme catalyseur. De surcroît, les expériences de recyclage utilisant 100 ppm de CuNPs ont procuré un rendement supérieur à 80% pendant les quatre dernières expériences de recyclage, ce qui montre la bonne stabilité du catalyseur. Nous avons utilisé la spectroscopie photo électronique de rayons X (XPS) pour rechercher la nature de l'espèce effectivement active du catalyseur et observé que l'espèce active du catalyseur était une espèce de Cu(I). Il est inévitable que la surface des CuNPs soit oxydée par l'oxygène de l'air et, par conséquent, Cu(I) est formé à la surface de Cu par comproportionation entre Cu(0) et Cu(II), même si l'on prend garde d'éviter l'air . Des études ultérieures ont montré que la faible coordination des ligands et leur substitution facile par les substrats jouait un rôle crucial dans la grande efficacité des nano catalyseurs.[11]

D'autre part, nous avons également comparé la stabilisation des AuNPs par des triazoles mono-, bis- et tridentates et l'influence de cette denticité sur la réduction du 4-nitrophénol (4-NP) par $NaBH_4$ dans l'eau et aussi inclus la comparaison avec un polyéthylène glycol courant (PEG 2000) ainsi qu'avec les AuNPs stabilisées par le poly(vinylpyrrolidone) (PVP) (Figure 3 et Tableau 1). Ces résultats démontrent la réussite du design de ce nouveau ligand "vert" amphiphile bien défini. Cette étude ouvre la voie vers la recherche d'autres stabilisants variés pour la catalyse de surface à l'aide de nanoparticules et vers des catalyseurs nano particulaires de type micellaire.

Tableau 1: Réduction du 4-nitrophénol en 4-aminophénol par $NaBH_4$ catalysée par des nanoparticules d'or AuNP-**L** variées à 20°C.[a]

AuNP-**L**	Bande de plasmon de surface [SPB (nm)]	Taille (nm)[c]	Temps d'induction (*s*)	K_{app} [d] ($\times 10^{-3}$ S^{-1})
AuNP-**1**[b]	-- (--)	**--**	0	5.2 (3.5)
AuNP-**2**[b]	527 (537)	7.3±0.5 (9.5±0.7)	0	2.6 (2.3)
AuNP-**3**[b]	527	8.3±0.5	0	18.4
AuNP-**4**[b]	515 (524)	3.1±0.3 (5.8±0.4)	0	24.9 (20.9)
AuNP-**5**	515	2.9±0.3	0	43.7
AuNP-**6**	495	2.2±0.4	40	15.2
AuNP-**5-THT**	556	14.5±1	0	17.5
AuNP-**5-0℃**	538	3.4±0.7	40	13.3

[a] Conditions: 4-NP (1 équiv.), $NaBH_4$ (81 équiv.) et catalyseurs AuNP-**L** (0.2 mol%). [b] Résultats donnés avec 3 trz par AuNP; résultats entre parenthèses utilisant 1 trz par AuNP. [c] Taille du coeur (MET) des AuNP-**L**. [d] Constante de vitesse.

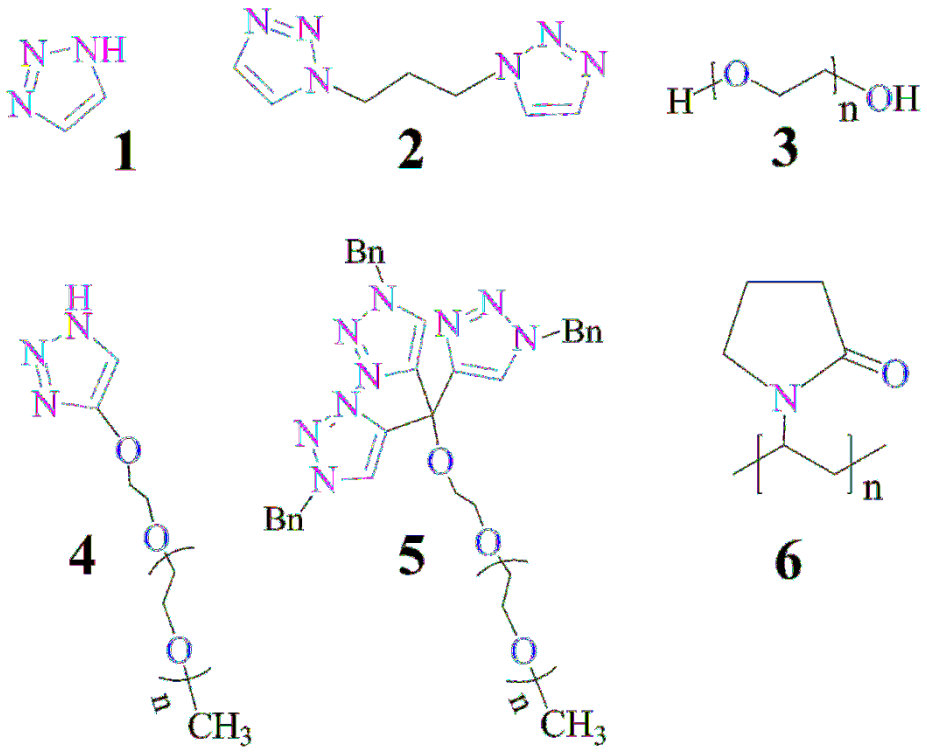

Figure 3. Ligands utilisés pour la stabilisation de nanoparticules d'or: **1** 1.2.3, triazole; **2** bis-triazole; **3** PEG 2000; **4** mono-triazole-PEG; **5** tris-triazole-PEG; **6** PVP (masse moléculaire Mw = 10.000).

Sur la base de ce ligand, en bénéficiant en particulier de l'effet chélatant, l'amphiphilie du ligand tris-trz-PEG contenant un tripode tris-triazole accroît la densité électronique sur le centre métallique. La chaine PEG permet, à l'aide de CuNPs, la catalyse homogène des réactions "click" dans l'eau et contribue à procurer au ligand sa nature amphiphile (Figure 4). Ce catalyseur montre une grande activité pour la réaction "click" dans l'eau à température ambiante avec une charge en catalyseur de seulement quelques ppm pour la synthèse de produits d'intérêt médicinal, catalytique, de ciblage et de marquage. Cette étude contribue à la

synthèse plus efficace de composes “clickés” comportant de multiples fonctions avec des quantités très minimes de catalyseur de Cu(I) dans des conditions “vertes”.[12]

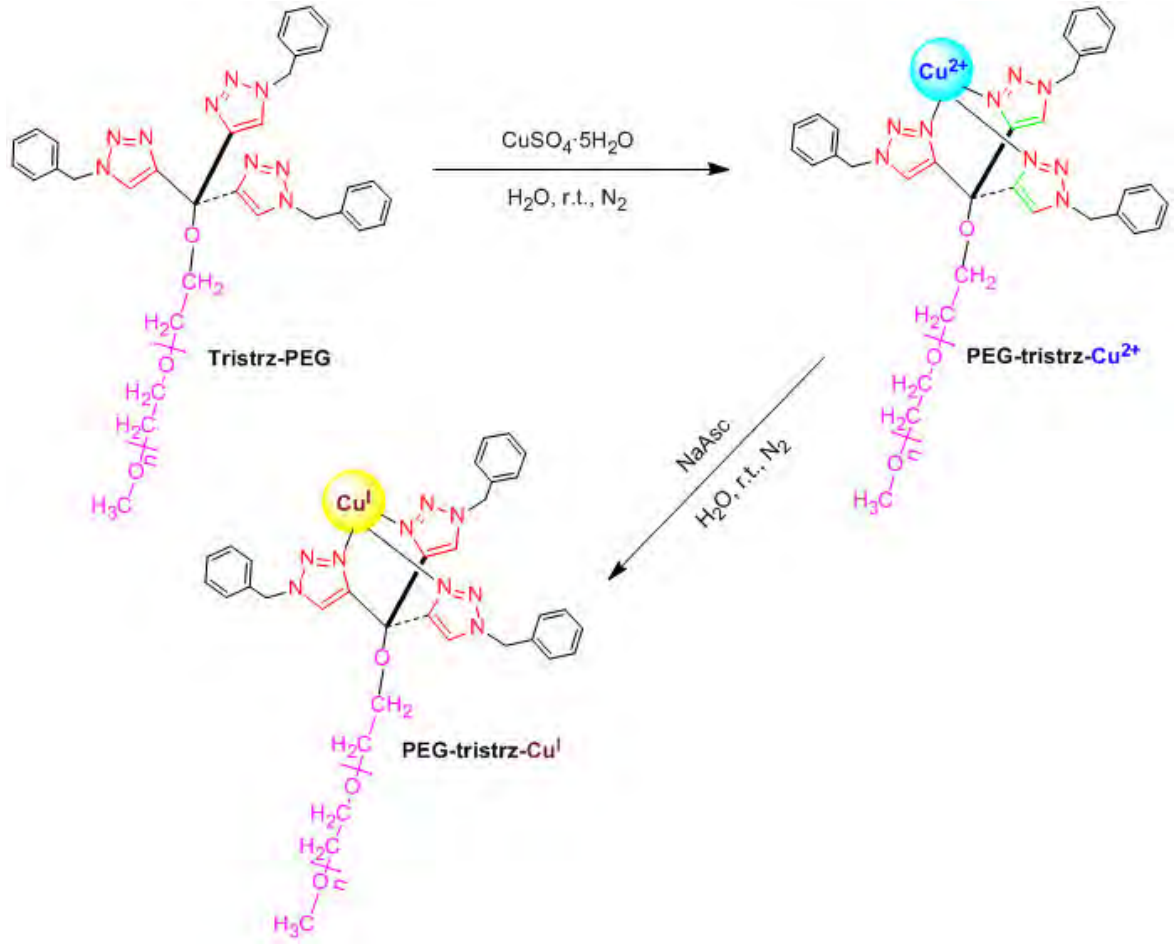

Figure 4 Synthèse du catalyseur “click” PEG-tris-trz-Cu^{I} .

Pour comprendre les raisons de cette très haute efficacité catalytique du catalyseur dans les réactions CuAAC dans l’eau utilisant de si faibles quantités de catalyseur, les catalyseurs Cu(I)- mono-, bis- et tris-triazole ont été comparés avec le catalyseur original Cu(I) obtenu par le groupe de Sharpless à partir de $CuSO_4$ + ascorbate de sodium pour la réaction de l’azoture de benzyle avec le phénylacétylène dans l’eau dans des conditions identiques. Il se confirme que la grande efficacité des réactions “click” catalysées par une très faible quantité

de catalyseur PEG-tris-trz-Cu^{I} bénéficie de l'effet chélate, de l'amphiphilie du ligand et de la chaîne PEG facilitant les réactions dans l'eau. Cette étude contribue à la synthèse plus efficace de produits "clickés" qui sont utiles en synthèse organique ainsi que dans différents domaines utilisant le Cu(I) ainsi que pour une application industrielle limitant fortement les quantités de Cu introduites.

Le troisième chapitre traite de la préparation de nanoparticules bimétalliques ultrafines Rh-Ag mono dispersées qui sont uniformément supportées sur des nano-feuillets d'oxyde de graphène réduit (RhAg/rGO, Figure 5). Les nanoparticules Rh-Ag font intervenir une synergie électronique entre les deux métaux sur l'oxyde de graphène réduit qui améliore l'activité catalytique entre les deux métaux par comparaison avec les deux nanoparticules de chaque métal prises séparément. En faisant varier le rapport Rh/Ag, nous avons pu montrer que la meilleure activité catalytique se trouve au niveau de $RhAg_{0.5}$/rGO pour la réduction du 4-nitrophénol. La réutilisation a également été examinée, et le catalyseur $RhAg_{0.5}$/rGO a pu être réutilisé cinq fois sans perte significative d'activité dans cette réaction. Lors de la cinquième réutilisation, la constante de vitesse pour la réduction du 4-nitrophénol par $NaBH_4$ est encore de $k_{app} = 12.1 \times 10^{-3}\ s^{-1}$, ce qui suggère que le catalyseur $RhAg_{0.5}$/rGO montre une très bonne possibilité de recyclage pour cette réaction. Cette efficacité catalytique est également supérieure à celle rencontrée pour la plupart des catalyseurs à base de nanoparticules d'éléments de transition du groupe des métaux nobles. La décroissance de la quantité totale de catalyseur de réaction a également été examinée. Avec 0,05 mol% et 0,01 mol% du catalyseur $RhAg_{0.5}$/rGO, la vitesse de réaction est $k_{app} = 8.2 \times 10^{-3}\ s^{-1}$ ($k_{nor} = 3140\ s^{-1}\ g^{-1}$) et $k_{app} = 5.3 \times 10^{-3}\ s^{-1}$ ($k_{nor} = 10140\ s^{-1}\ g^{-1}$), respectivement, démontrant le succès du design du catalyseur $RhAg_{0.5}$/rGO.[13]

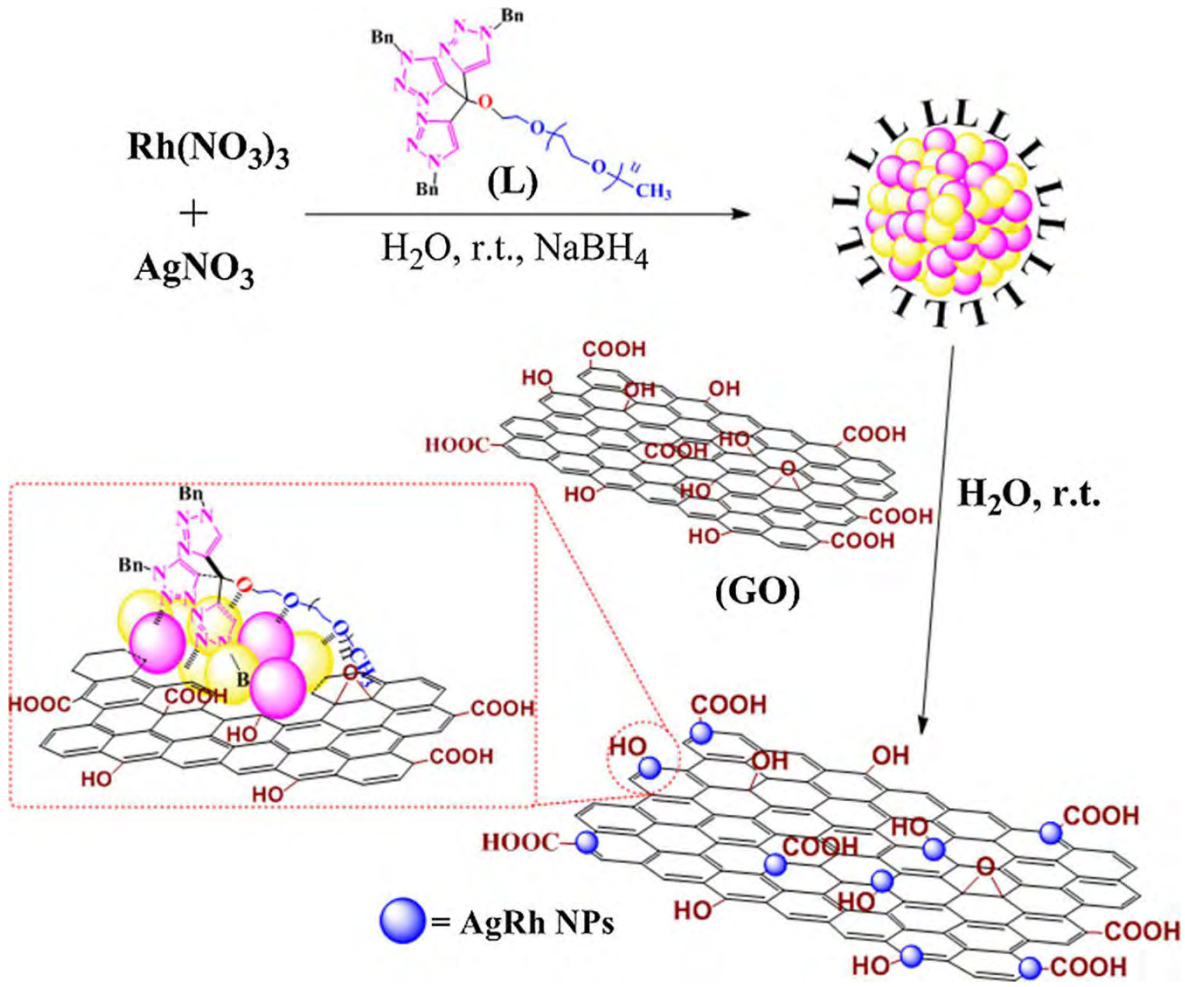

Figure 5. Synthèse du catalyseur RhAg/rGO.

Ensuite, les interactions supramoléculaires impliquant des liaisons hydrogène entre le polyéthylène glycol terminal du ligand tris-trz-PEG et les groupements fonctionnels de l'oxyde de graphène en tant que support permettent d'envisager un nouveau catalyseur hétérogène α-Fe_2O_3 nano cluster/GO. Les nano clusters α-Fe_2O_3/GO dont la taille est seulement de 1.8 nm ont été déposés de façon homogène sur les bords des nano-feuillets d'oxyde de graphène. La spectroscopie XPS a montré que les énergies de liaison au niveau du coeur sont de 726.4 and 712.3 eV dans la région 2p du fer, ce qui correspond à Fe $2p_{1/2}$ and Fe $2p_{3/2}$ de α-Fe_2O_3, respectivement. De plus, les pics satellites situés vers 719.0 eV ont aussi suggéré la présence d'espèces du Fe(III). Les applications catalytiques de ce nouveau

matériau ont été démontrées pour la réduction du 4-nitrophénol par $NaBH_4$ dans l'eau, indiquant une haute efficacité. De plus, ce catalyseur a également montré un grande efficacité pour la réaction de Suzuki-Miyaura avec seulement quelques ppm de charge de métal. La catalyse de la réaction de Suzuki-Miyaura par le nano cluster α-Fe_2O_3/GO a montré son efficacité pour une grande variété de substrats. Les dérivés du bromobenzène contenant les groupements électro-accepteurs (NO_2, CHO, CH_3CO) et électro-donneurs en position para se sont avérés de bon partenaires de réaction, et les produits de couplage correspondants ont été isolés efficacement avec de bons rendements.

Le test de filtration à chaud a suggéré que la réaction de Suzuki-Miyaura catalysée par le nano-cluster α-Fe_2O_3/GO procède de façon hétérogène, car la réaction standard Suzuki-Miyaura entre le bromobenzène et l'acide phénylboronique procède bien en présence du catalyseur, alors que l'enlèvement de ce catalyseur à mi- réaction inhibe complètement la poursuite de la réaction. De plus, aucun résidu de palladium n'a été trouvé dans le catalyseur α-Fe_2O_3/GO. Le catalyseur peut aussi être récupéré et recyclé quatre fois sans perte significative de nanoparticules ni d'activité catalytique.[14]

De hautes efficacités ont été trouvées pour une variété de réactions avec des nano-catalyseurs synthétisés par réaction redox entre des sels de cations de métaux de transition et l'oxyde de graphène conduisant à la production de nanoparticules métalliques supportées sur support oxyde de graphène. Nous avons généralisé ce concept de synthèse induite par voie redox sur support oxyde de graphène. Ceci signifie que l'oxyde de graphène est utilisé comme nanomatériau réservoir d'électrons qui transfère des électrons et éventuellement des ligands oxo vers les nanoparticules ou leurs précurseurs cationiques. Ceci rappelle les stratégies de Basset utilisant les oxydes inorganiques comme ligands de catalyseurs moléculaires des

premiers éléments de transition, bien que les énergies de liaison métal-ligand soient considérablement plus élevées dans ce dernier cas. Nos réactions redox entre les cations métalliques et l'oxyde de graphène ont impliqué aussi bien des cations de métaux nobles que des cations de bio métaux, les réactions pouvant être soit exergoniques, soit endergoniques. Dans ce dernier cas, elles sont quand même rendues possibles par l'agrégation des atomes formés qui pousse la réaction redox défavorable. Des nanoparticules métalliques ultrafines à la surface propre sont formées sur support oxyde de graphène avec une bonne monodispersité. Ces nouveaux catalyseurs sont hautement efficaces dans l'eau à température ambiante. Les hautes efficacités et recyclabilité des nano-catalyseurs sont démontrées, par exemple pour la réduction du 4-nitrophénol par $NaBH_4$ avec, pour catalyseurs de cette famille, RhNP/GO, AuNP/GO et CuNP/GO, pour la réaction de Sonogashira avec CuNP/GO, PdNP/GO, et PdCuNP/GO, pour la réaction CuAAC avec CuNP/GO et pour l'hydrolyse de l'amine-borane générant l'hydrogène moléculaire avec RhNP/GO (Figure 6).[15]

Dans le cas de la réaction d'hydrolyse de l'amine-borane pour la génération d'hydrogène catalysée par RhNP/GO-45°C, des études mécanistiques détaillées suggèrent que la molécule de H_2O est probablement activée par coupure indirecte de la liaison O-H pour former des espèces adsorbée –H et –OH sous l'influence de l'amine-borane. La synthèse et l'utilisation comme catalyseurs efficaces des nanoparticules des éléments de transition tardifs de la première ligne (bio métaux) constitue un défi très notable et cette méthode s'est aussi avérée productive à cet effet. La catalyse de réduction du 4-nitrophénol par $NaBH_4$ par de telles nanoparticules de Cu en utilisant 0.5% mol CuNPs/GO, ne nécessitant aucun temps d'induction avec une constante de vitesse remarquable de 5.2×10^{-3} s^{-1} (k_{app}). Ces performances sont de toute évidence dues à l'absence de nécessité de restructuration de la surface en l'absence de ligand. La haute efficacité de CuNPs/GO est aussi confirmée par le

succès de la réaction “click” CuAAC entre le phénylacétylène et l’azoture de benzyle avec un rendement de 93% en 24h avec seulement 0.01 mol% de CuNPs, ce qui constitue l’un des tout meilleurs résultats jamais obtenus avec des nanoparticules de cuivre dans la littérature récente. Par ailleurs, la réduction biélectronique de Pd(II) et Cu(II) par l’oxyde de graphène conduit à un nano-catalyseur hétérogène CuPd NPs/GO qui est efficace pour la réaction de couplage de Sonogashira Cette approche ainsi que les résultats très positifs obtenus sont prometteurs pour la mise au point de catalyseurs de ce type pour une multitude d’autres réactions.

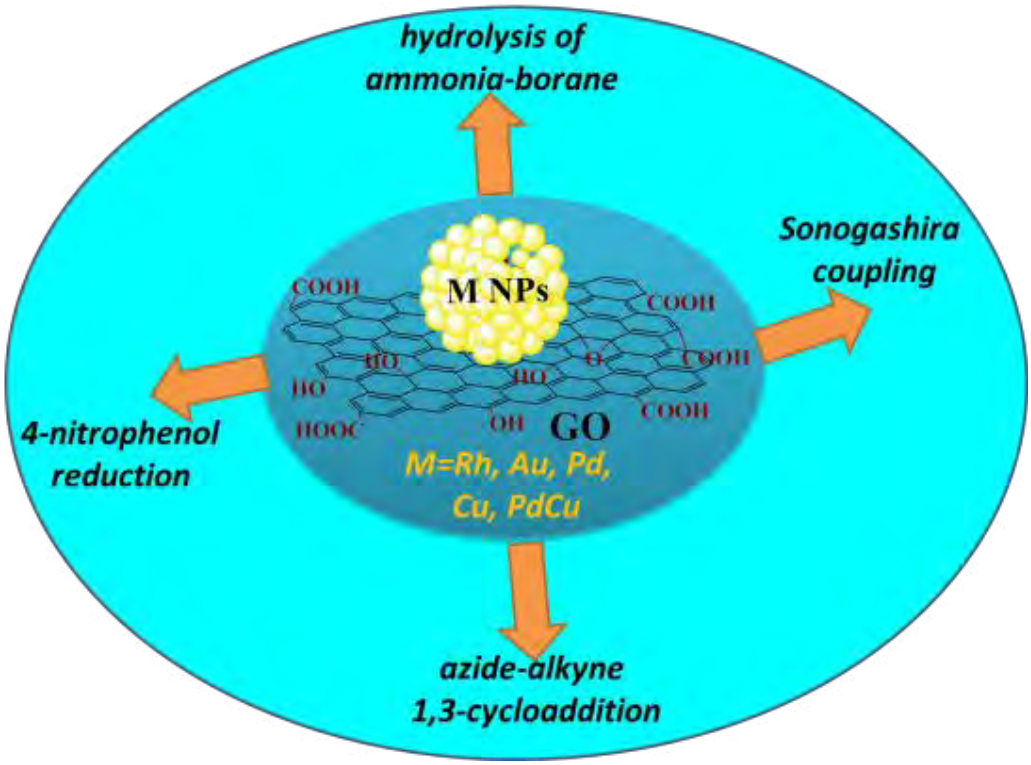

Figure 6. Nano catalyseurs à base de nanoparticules de métaux de transition supportés sur oxyde de graphène montrant d’excellentes efficacités à température ambiante pour la réduction du 4-nitrophénol par $NaBH_4$ en 4-aminophénol, l’hydrolyse de l’ammoniac-borane avec génération de H_2, la réaction de Sonogashira et la réaction “click”.

Le quatrième chapitre constitue une contribution à la catalyse par les nanoparticules bimétalliques stabilisées par les "molecular organic frameworks" (MOFs, réseaux moléculaires organiques) pour l'hydrolyse de l'amine borane avec dégagement d'hydrogène. Tout d'abord, nous avons synthétisé les nanoparticules bimétalliques stabilisées par ZIF-8 et comparé leurs efficacités pour l'hydrolyse de l'amine borane. Nous avons montré que la meilleure efficacité est celle du nano catalyseur NiNPs/ZIF-8 pour le nombre fréquence de turnover qui surpasse ceux obtenus avec des catalyseurs à bas de métaux nobles, ce qui constitue un résultat remarquable en termes de chimie "verte" et de coût.[16]

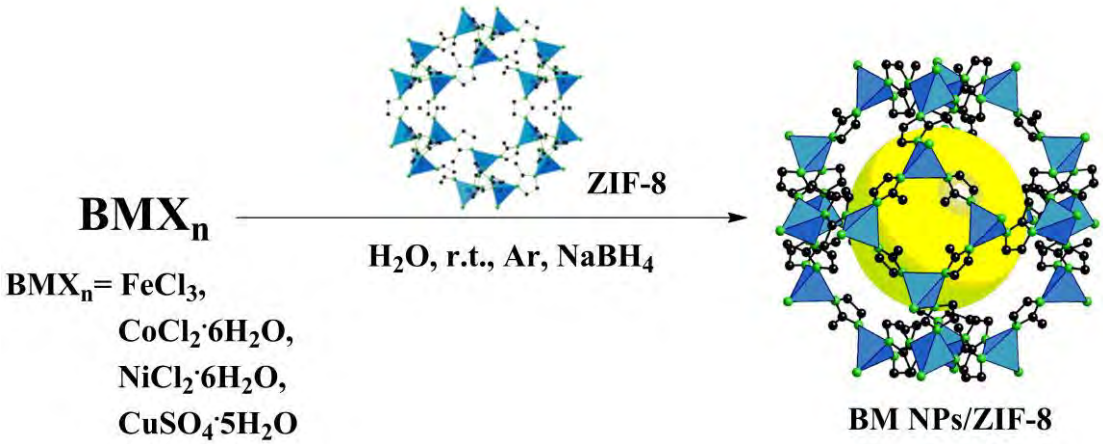

Figure 7. Préparation des nano catalyseurs BMNP/ZIF-8.

A l'aide d'études mécanistiques détaillées, en particulier par la recherche de l'étape cinétiquement déterminante de cette réaction à l'aide des effets isotopiques cinétiques, nous avons proposé que la molécule d'eau est active par coupure indirecte de la liaison O-H pour former des espèces –H et –OH adsorbées favorisées par l'amine-borane en présence du nano catalyseur NiNP/ZIF-8. Etant donné que le groupement NH_3 ne participe pas à l'hydrolyse, c'est la liaison B-N qui est coupée dans l'amine-borane, suivi du départ de H_2. Nous avons alors assumé que si OH^- est directement adsorbé sur la surface du nano catalyseur au nickel,

un catalyseur bifonctionnel avec adsorption de H et OH à la fois doit conduire à la réaction à la surface du catalyseur. En fait, la vitesse de génération de H_2 augmente beaucoup par rapport à celle observée en absence de NaOH, alors que l'addition de HCl provoque au contraire l'arrêt de la réaction. Les raisons de l'arrêt de la génération d'hydrogène sont de deux sortes. L'une d'entre elles est l'effet négatif de H^+ sur l'auto-ionisation de l'eau qui supprime la formation de OH^- et l'occupation des sites –OH à la surface des nanoparticules de nickel. L'autre est l'effet ionique car les ligands Cl- sont connus pour limiter l'activité catalytique des nanoparticules en se liant fortement à la surface, ce qui inhibe l'accès aux sites de surface. Par des expériences détaillées, nous avons découvert le contrôle "on-off" de la génération d'hydrogène par addition d'une quantité équivalente de solution aqueuse de HCl et de NaOH au milieu, ce qui est d'un grand intérêt pratique pour la génération de H_2 dans des conditions ambiantes.

Nous avons également examiné la réutilisation du nano catalyseur NiNPs/ZIF-8 pour l'hydrolyse de l'amine-borane dans l'eau. Cette activité du catalyseur NiNPs/ZIF-8 pour l'hydrolyse de l'amine-borane dans l'eau est essentiellement conservé jusqu'au cinquième recyclage. Les principes et résultats apportent non seulement une vision de la mise au point rationnelle d'un catalyseur hautement efficace basé sur des métaux de transition non nobles, mais ils démontrent une étape prometteuse vers des matériaux de type piles à combustible destinés au stockage de l'hydrogène.

A la fin de la thèse, les conclusions et perspectives résument les progrès résultant de la recherche conduite durant cette thèse concernant la mise au point et l'application des nano catalyseurs à base d'éléments de transition tardifs pour diverses réactions chimiques. Ensuite, des perspectives sont dégagées, indiquant que le développement de nouveaux catalyseurs

hétérogènes, par exemple l'exploration de catalyseurs bimétalliques et de catalyseurs basés sur les métaux abondants sur la terre (en particulier les "bio-métaux") devrait constituer une direction de recherche primordiale.

En résumé, cette thèse a conduit à l'avancée du développement de l'état des connaissances concernant la mise au point, la caractérisation et les applications catalytiques de nanomatériaux catalytiques basés sur les éléments de transition tardifs. La recherche incessante de nouvelles possibilités d'améliorations des nanomatériaux basés sur les éléments de transition tardifs bénéficie de l'avantage du design de nouveaux ligands et supports et a conduit à la construction de nouveaux nano catalyseurs basés sur les éléments de transition tardifs. L'efficacité du design de ligand utilisant la chimie "click" a impliqué la formation de ligands triazoles qui stabilisent de façon douce et optimale la surface de nanoparticules qui sont d'excellents nano-catalyseurs.

Les catalyseurs hétérogènes basés sur le graphène et les réseaux moléculaires organiques sont très prometteurs pour une variété de réactions chimiques, en particulier prenant en compte l'effet synthétique, l'effet de support et la réutilisation. Par conséquent, la mise au point de nouveaux nano-catalyseurs à base de matériaux comprenant des nanoparticules de métaux de transition tardifs apparait ici comme une direction de recherche prometteuse en raison de la demande croissante de chimie durable et verte.

Références

[1] a) G. M. Whitesides, *Small.* **2005**, *1*, 172-179; b) *Concepts of Nanochemistry*, ed. L. Cademartiri, G. A. Ozin, Wiley-VCH, Weinheim, **2009**, p. 5; c) M. V. Kovalenko, L. Manna, A. Cabot, Z. Hens, D. V. Talapin, C. R. Kagan, V. I. Kiminov, A. L. Rogach, P. Reiss, D. J. Milliron, *ACS Nano* **2015**, *2*, 1012-1057.

[2] *The Nobel Prize in Chemistry 2016–Advanced Information. Nobelprize.org. Nobel Media AB 2014. Web. October 6, 2016,*

http://www.nobelprize.org/nobel_prizes/chemistry/laureates/2016/advanced.html.

[3] a) *Nanoparticles and Catalysis*, rédacteur : D. Astruc, Wiley-VCH, **2008**; b) *Modern Surface Organometallic Chemistry*, rédacteur : J.-M. Basset, R. Psaro, D. Roberto and R. Ugo, Wiley-VCH, Weiheim, **2009**; c) A. Fihri, M. Bouhrara, B. Nekoueishahraki, J.-M. Basset, V. Polshettiwar, *Chem. Soc. Rev.,* **2011**, *40*, 5181-5203; d) *Nanomaterials in Catalysis*, rédacteur: P. Serp and K. Philippot, Wiley-VCH, **2013**; e) S. Zhang, L. Nguyen, Y. Zhu, S. Zhan, C.-K. Tsung, F. Tao, *Acc. Chem. Res.,* **2013**, *46*, 1731-1739.

[4] a) D. Astruc. *Organometallic Chemistry and Catalysis*, Springer, Berlin, **2007**; b) D. Astruc, *Chimie organométallique et catalyse*. EDP Science, Les Ullis, **2013**.

[5] a) R. A. Sheldon, I. Arends, U. Hanefeld, *Green Chemistry and Catalysis*. Wiley-VCH, Weinheim, Germany, **2007**; b) *Handbook of Heterogeneous Catalysis*, rédacteurs : G. Ertl, H. Knozinger et J. Weitkamp, Wiley-VCH, Weinheim, **1997**; c) A. Suzuki, dans *Modern Arene Chemistry*, rédacteur: D. Astruc. Wiley-VCH, Weinheim, **2002**; d) G. A. Somorjai, *Introduction to Surface Chemistry and Catalysis*. Wiley, New York, **1994**.

[6] a) L. D. Pachón, G. Rothenberg, *Appl. Org. Chem.,* **2008**, *22*, 288-299; b) N. Yan, C. Xiao, Y. Kou, *Coord. Chem. Rev.,* **2010**, *254*, 1179-1218; c) J. D. A. Pelletier, J.-M. Basset, *Acc. Chem. Res*. **2016**, *49*, 664-677.

[7] a) N. Toshima, T. Yonezawa, *New J. Chem.* **1998**, *22*, 1179-1201; b) J. Durand, E. Teuma, M. Gomez, *Eur. J. Inorg. Chem*. **2008**, 3577-3586; c) V. S. Myers, M. G. Weir, E. V. Carino, D. F. Yancey, S. Pande, R. M. Crooks, *Chem. Sci.* **2011**, *2*, 1632-1646.

[8] a) D. Astruc, *Nat. Chem*. **2012**, *4*, 255-267; b) C. N. Pinaud, D. Astruc, *J. Am. Chem. Soc*. **2014**, *136*, 12092–12098; c) D. Wang, J. Ruiz, D. Astruc, *Acc. Chem. Res*. **2015**, *48*, 1871-1880.

[9] C. Wang, D. Ikhlef, S. Kahlal, J. Y. Saillard, D. Astruc, *Coord. Chem. Rev.,* **2016**, *316*, 1–20.

[10] a) M. Meldal, C. W. Tornoe, *Chem. Rev*. **2008**, *108*, 2952-3015; b) J. E. Hein, V. V. Fokin, *Chem. Soc. Rev*. **2010**, *39*, 1302-1315; c) M. Rodriguez-Rodriguez, P. Llanes, C. Pradel, M. A. Pericas, M. Gomez, *Chem. Eur. J*. **2016**, *22*, 18247-18253.

[11] C. Wang, R. Ciganda, L. Salmon, D. Gregurec, J. Irigoyen, S. Moya, J. Ruiz, D. Astruc, *Angew. Chem., Int. Ed*. **2016**, *55*, 3091-3095.

[12] C. Wang, D. Wang, S. Yu, T. Cornilleau, J. Ruiz, L. Salmon, D. Astruc, *ACS Catal*. **2016**, *6*, 5424–5431.

[13] C. Wang, R. Ciganda, L. Yate, S. Moya, L. Salmon, J. Ruiz, D. Astruc, *J. Mater. Sci.* **2017**, 52, 9465-9476.

[14] C. Wang, L. Salmon, R. Ciganda, L. Yates, S. Moya, J. Ruiz, D. Astruc, *Chem. Commun*. **2017**, ***53***, 644 – 646.

[15] C. Wang, R. Ciganda, L. Yate, J. Tuninetti, V. Shalabaeva, L. Salmon, S. Moya, J. Ruiz, D. Astruc, soumis à publication.

[16] C. Wang, C. Zhang, Z. Wang, R. Ciganda, L. Yate, L. Salmon, S. Moya, J. Ruiz, D. Astruc, soumis à publication.

Nanomatériaux à base de métaux de transition pour la catalyse

Résumé: La nanocatalyse à base de métaux de transition constitue un domaine prometteur pour lequel l'efficacité accrue, le caractère de chimie verte et le recyclage sont activement recherchés. Dans cet esprit, cette thèse a été dédiée à la synthèse, la caractérisation et les applications catalytiques de nouveaux nanomatériaux à base de métaux de transition.

D'une part, en catalyse homogène colloïdale, des nanoparticules de métaux de transition stabilisées par des ligands amphiphiles ont procuré d'excellentes performances catalytiques en terme d'activité, stabilité et recyclabilité pour la réduction du nitro-4-phénol, le couplage de Suzuki-Miyaura, le transfert d'hydrogéné et la cyclo-addition entre un alcyne et un azoture dans l'eau.

D'autre part, en catalyse hétérogène, le design, la synthèse et les applications catalytiques de nano-catalyseurs basés sur les supports de type graphène ou architectures moléculaires organiques ont également été conduits. Leurs excellentes propriétés catalytiques ont été démontrées pour la réduction du nitro-4-phénol, le couplage de Sonogashira, la cyclo-addition des alcynes avec les azotures et l'hydrolyse d'ammonia-borane avec génération d'hydrogène dans l'eau dans les conditions ambiantes.

Mots-clés : métaux de transition, nanomatériaux, catalyse, ligand amphiphile, graphène, MOF

Transition Metal Nanomaterials in Catalysis

Abstract: Transition metal nanocatalysis is a promising area, where increased efficiency, greenness and reusability are actively sought. In this spirit, the thesis has been devoted to the synthesis, characterization and catalytic applications of new transition metal nanomaterials. Amphiphilic ligand stabilized transition metal nanoparticles catalysts have provided excellent catalytic performances in terms of activity, stability and recyclability in the 4-nitrophenol reduction, Suzuki-Miyaura coupling, transfer hydrogenation and alkyne-azide cycloaddition reactions with low amounts of metal loadings. Moreover, an efficient amphiphilic "click" Cu^{I} catalyst was also designed for part-per-million levels of alkyne-azide cycloaddition reaction in water.

The design, synthesis and catalytic application of heterogeneous nanocatalysts based on graphene and metal organic framework supports have also been carried out, and their excellent catalytic properties in 4-nitrophenol reduction, Sonogashira coupling, alkyne-azide cycloaddition and hydrolysis of ammonia-borane for hydrogen generation in water under ambient conditions have been disclosed.

Keywords: Transition metal, nanomaterials, catalysis, amphiphilic ligand, support, green chemistry, graphene, MOF